Characterizing Novel Genetic and Environmental Pathways in Epithelial Development

Nishanthi Mathiyalagan

M.Sc.

A thesis submitted in total fulfilment of the requirements for the degree of

Doctor of Philosophy

Department of Physiology, Anatomy and Microbiology

School of Life Sciences

College of Science, Health and Engineering

La Trobe University

Victoria, Australia

November 2021

Statement of Authorship

This thesis includes work by the author that has been published or submitted for publication as described in the text. Except where reference is made in the text of the thesis, this thesis contains no material published elsewhere or extracted in whole or in part from a thesis accepted for the award of any other degree or diploma. No other persons' work has been used without due acknowledgement in the main text of the thesis. This thesis has not been submitted for the award of any degree or diploma in any other tertiary institution.

Nishanthi Mathiyalagan

4th November 2021

Table of contents

List of figures

List of tables

Abstract

The maintenance of viable epithelia is essential during both embryonic development and for adult life and relies on the complex synergies of multiple genetic and molecular pathways. The highly conserved ***Grainyhead-like (Grhl)*** transcription factors (TFs), are among the most critical genes required for epithelial establishment. Specifically, family member *Grhl3* is essential in the homeostatic maintenance of numerous epithelia including skin, craniofacial primordia, bladder, and intestine, and therefore delineating the specific function and genetic pathways regulated by this TF holds significant therapeutic promise for several human congenital and adult-onset epithelial diseases.

Our group has generated several *grhl3*-CRISPR knockout lines in zebrafish. Characterization of these fish lines (**Chapter 3**), and particularly identifying and characterising novel key downstream target genes that are directly regulated by *grhl3* has been critical to understand the nature of *grhl3*-dependent molecular networks in epithelial homeostasis.

Two major approaches were used to identify the putative target genes of *Grhl3*. Firstly, the promoters of all mammalian genes were aligned to search for the presence of a conserved *grhl* binding site (AACCGGTT). Secondly, meta-analysis of 41 published *grh* and *Grhl* RNA-SEQ/microarray datasets was performed, to generate a list of the most-differentially regulated genes following *grhl3* mis-expression in primary epithelia and cell lines (**Chapter 4**).

I have characterized the expression (using real time PCR) of the differentially regulated genes of *grhl* in the *grhl3*-deficient zebrafish embryos to verify the reliability of bioinformatics approaches used to identify the target genes of *grhl*. Furthermore, rescue experiments with full length mRNA have been performed to determine whether the phenotypic loss of *grhl3* can be compensated by the expression of predicted target genes. Additionally, knockout/knockdown-based experiments of differentially regulated *grhl3*-genes following *grhl* abrogated function was performed to determine their role and interaction with *grhl3* in epithelial homeostasis (**Chapter 5**).

Lastly, the identification of both genetic and environmental factors that interact with abrogated *Grhl* function in epithelial establishment and homeostasis is critical since epithelial disease caused by *Grhl*-deficiency is significantly influenced by environmental

factors such as smoking, alcohol and nutritional imbalance (esp. folate, retinoic acid [RA] and zinc deficiency). Our *grhl3*$^{-/-}$ zebrafish line is a robust model system to understand the effect of various chemicals. I have particularly tried to understand the effect of polyphenols, vitamins, and minerals to determine whether they may rescue epithelial defects observed in the *grhl3*$^{-/-}$ embryos (**Chapter 6**). Doing this will help us determine the compounds that may play an integral role in epithelial formation.

Overall, this work identifies the putative target genes of *grhl3* and environmental factors that influence the phenotypes of *grhl3*$^{-/-}$ embryos. Determining the targets of *grhl3* help elucidate the molecular mechanisms involved in various epithelial and developmental processes. This is critical to understand the aetiology of epithelial birth defects including neural tube defects (NTDs), cleft palate, Van der Woude Syndrome, ectodermal dysplasia, and many others. Finally, identifying environmental factors that rescue the *grhl3* phenotypes indicate the possibility of using these factors for the prevention of epithelial birth defects in humans.

Acknowledgments

This PhD would have been impossible without the support of these amazing people, and I once again extend my heartfelt thanks to everyone for all they have done. Lastly, I express my gratitude to La Trobe University for providing me with the Full Fee Research Scholarship and Postgraduate Research Scholarship to pursue this research.

Publications arising from this work

Publications resulting from work in this thesis

- Mathiyalagan, N., L. B. Miles, P. J. Anderson, T. Wilanowski, B. L. Grills, S. J. McDonald, M. C. Keightley, A. Charzynska, M. Dabrowski and S. Dworkin (2019). "Meta-Analysis of Grainyhead-Like Dependent Transcriptional Networks: A Roadmap for Identifying Novel Conserved Genetic Pathways." <u>Genes</u> **10** (11): 876.

  *-Awarded the **Higher Degree Research student publication prize** for the best research publication of 2019 by the Department of Physiology, Anatomy and Microbiology, La Trobe University, Australia.*

- Mathiyalagan N and Dworkin S^ "Wholemount In-situ Hybridisation (WISH) in zebrafish embryos to analyse craniofacial development", in "*Craniofacial Development: Methods and Protocols*", Springer-Nature, in press, October 2021.

Other Publications indirectly related to work in this thesis

- Phatak, M., S. Kulkarni, L. B. Miles, N. Anjum, S. Dworkin and M. Sonawane (2021). "Grhl3 promotes retention of epidermal cells under endocytic stress to maintain epidermal architecture in zebrafish." <u>PLoS Genetics</u> **17**(9): e1009823.

  -My work on myovb-grhl3 interaction was acknowledged.

Conference presentations

Oral presentations

Australian and New Zealand Zebrafish Meeting (Jan 2020)

Yara Valley Estate, Australia

Title: Role of grhl3 gene regulatory network in epithelial development

Flash talks

1-minute 'Flash talk'

International Zebrafish Conference (June 2019)

Suzhou, China

Awarded a travel award to attend this conference.

3 Minute Thesis (3MT) competition (July 2019)

School of Life Sciences

La Trobe University, Melbourne, Australia

3 minutes 'Science Bites Talk'

Physiology, Anatomy Microbiology (PAM) Research Symposium (Dec 2018)

La Trobe University, Melbourne, Australia.

3 minutes 'Lightning Talk'

La Trobe Institute for Molecular Science (LIMS) Research Symposium (Nov 2018)

La Trobe University, Melbourne, Australia.

Poster presentations

Physiology, Anatomy Microbiology (PAM) Research Symposium (Dec 2019)

La Trobe University, Melbourne, Australia.

Title: Role of grhl3 gene regulatory network in epithelial development

12th Victorian Cell and Developmental Biology Meeting (Dec 2019)

La Trobe University, Melbourne, Australia.

Title: Role of grhl3 gene regulatory network in epithelial development

International Zebrafish Conference (June 2019)

Suzhou, China

Title: *Characterizing novel genetic and environmental pathways in epithelial development*

11th Victorian Cell and Developmental Biology Meeting (Dec 2018)

Monash University, Melbourne, Australia.

Title: Characterizing novel genetic and environmental pathways in epithelial development

Physiology, Anatomy Microbiology (PAM) Research Symposium (Dec 2018)

La Trobe University, Melbourne, Australia.

Title: Characterizing novel genetic and environmental pathways in epithelial development

<u>**Video presentations**</u>

Visualize Your Thesis Competition (July 2019)

La Trobe University, Australia.

Title: Characterizing novel genetic and environmental pathways in epithelial development

Disruptions due to COVID-19

A number of experiments integral for my research could not be done owing to the COVID-19 pandemic, and some of these are listed here:

- I had raised and genotyped several zebrafish CRISPR knockout lines during early November 2019, and these were still breeding efficiently at the beginning of February 2020. However, with the lockdown commencing at the end of March 2020, all my experiments came to a standstill for the next 3.5 months owing to prohibition of on campus access from March-June 2020 for all non-essential work.

- When I was allowed back into the lab to do essential experiments in July 2020, several of my fish lines were old, and their breeding efficiency was severely affected, causing unnecessary delays in my experiments, while these lines were re-established. Moreover, the significant delays in my project led to me abandoning analyses of a new CRISPR-line (*klhdc8a* knockout line) we had generated.

- I was unable to perform in-situ hybridization (other than for a very small number of probes), complete histological analysis of intestine (to finalise the analyses presented here), apoptosis/proliferation quantitation of neural crest cell production in the pharyngeal arches and immunohistochemistry for epithelial markers (particularly in the intestine) as they were considered non-essential as per strict La Trobe University guidelines for campus access in much of 2020.

- I had substantial difficulty procuring some of the chemicals/apparatus for my experiments (particularly, RNAse A and CoStar Netwells for in situ hybridisation) as they were shipped from overseas and took several months to reach us, thereby severely impacting my work.

- I was granted full time access to do my experiments between October 2020 and May 2021. However, owing to family circumstances, I was compelled to return home after this time, and no further experimental work was possible.

- Lastly, my ability to attend both national and international conferences (other than in an online capacity) was eliminated from March 2020 onwards, resulting in reduced abilities to both showcase my work and learn from others' advances in the field.

Abbreviations

%	Percent
±	Plus, or Minus
°C	Degrees Celsius
µg	Micrograms(S)
µl	Microliter(S)
µm	Micrometre(S)
µM	Micromolar
BMP	Bone Morphogenetic Protein
bp	Base pairs
BSA	Bovine Serum Albumin
CE	Convergent Extension
ChIP SEQ	Chromatin Immunoprecipitation Sequencing
CL/P	Cleft Lip/Palate
cldn	Claudin
CRISPR	Clustered Regularly Interspaced Short Palindromic Repeats
ct	Curly tail
DAPI	4',6-Diamidino-2-Phenylindole, Dihydrochloride
Ddc	Dopa decarboxylase
DNA	Deoxyribonucleic Acid
dpf	Days post fertilization
EGFP	Enhanced Green Fluorescent Protein
EGFR	Epidermal Growth Factor Receptor
EMSA	Electrophoretic Mobility Shift Assay
EMT	Epithelial Mesenchymal Transition
Eng2a	Engrailed 2a

ERK	Extracellular Regulated Kinase
et al	Et alia (and others)
EVL	Enveloping Layer
FL	Full-Length
g	Gram(S)
GEI	Gene-Environment Interactions
gldc	Glycine decarboxylase
GO	Gene Ontology
grh	Grainyhead
Grhl	Grainyhead-like
GRN	Gene Regulatory Network
Hcy	Homocysteine
hpf	Hours post fertilization
HYB	Hybridization
KD	Knockdown
LB	Luria-Bertani
MC	Meckel's Cartilage
MCS	Multiple Cloning Site
MHB	Midbrain-Hindbrain Boundary
min	Minutes
mM	Millimolar
MO	Morpholino
mRNA	Messenger ribonucleic acid
n	Number of samples
NCC	Neural Crest Cells
ns	Not statistically significant
NTDs	Neural Tube-Like Defects

Ovol1	Ovo like transcriptional repressor 1
PCP	Planar Cell Polarity
PCR	Polymerase Chain Reaction
PFA	Para Formaldehyde
PNP	Posterior Neuropore
Pvrl4	Poliovirus receptor-related 4
RA	Retinoic Acid
RNA-SEQ	RNA Sequencing
ROS	Reactive Oxygen Species
rpm	Revolutions per minute
RSV	Resveratrol
RT-qPCR	Real-Time Quantitative PCR
SD	Standard Deviation
sec	Seconds
SNP	Single Nucleotide Polymorphism
Spec1	Small protein effector 1 of cdc42
SSC	Squamous Cell Carcinoma
Tbc1d2	Tbc1 domain family, member 2
TF	Transcription Factor
TGF	Transforming Growth Factor
Tgm	Transglutaminase
Tmem54	Transmembrane Protein 54
TUNEL	Terminal Deoxynucleotidyl Transferase DUTP Nick End Labeling
WT	Wild-Type
ZO	Zona Occludens
α	Alpha
β	Beta

Chapter 1: Introduction

1.1 Epithelia and epithelial development

1.1.1 Definition, types, and characteristics

Epithelia, tissue composed of one or more layers of cells, line the external and internal surfaces of the body and organs forming a protective barrier against invading micro-organisms, carcinogens, and other environmental insults (Presland and Jurevic 2002). Besides acting as the first line of defence, epithelia play an integral role in the transport of essential factors (such as hormones, nutrients, and fluids) via the process of diffusion and transcellular transport. Furthermore, they are involved in secretory roles in glands and organs such as intestine and pancreas (Ganz 2002). Owing to the numerous functions they possess, epithelia have undergone structural specialisations in different parts of the body and ultimately, perform critical regulatory functions that maintain tissue and organ homeostasis.

Epithelia are classified broadly as simple, pseudostratified, and stratified, based on the number of cell layers (Samuelson 2007). Simple epithelia such as in the linings of lung alveoli, pleural cavity, and endothelium, comprise a single layer of epithelial cells, forming direct contact with the basement membrane. They are particularly involved in functions such as absorption and filtration. Complex epithelia (also known as stratified epithelia) such as those in the linings of pharynx and buccal cavity, are multilayered, and present where body linings must endure mechanical or chemical insults. Protection is one of the vital functions of stratified epithelia owing to their tensile strength and durability. Lastly, pseudostratified columnar epithelia, lining the trachea and upper respiratory tract, comprise a single layer of cells with the cell nuclei being positioned at different levels creating an illusion of them being stratified.

Simple and complex epithelia are further classified histologically based on the shape of the cells that comprise it, i.e., squamous (flattened and scale-like), cuboidal (cube-like) or columnar (Samuelson 2007) (Figure 1.1).

Figure 1.1 Classification of epithelial tissue based on cell shape and number of cell layers.

1.1.2 Origin and structure

Epithelial tissue originates from all the three major germinal layers: ectoderm (e.g., epidermis); mesoderm (e.g., lining of gastrointestinal tract) and endoderm (e.g., inner linings of body cavities). Once established, epithelial cells adhere to the basement membrane/basal lamina, a specialized extracellular matrix which partitions the epithelia from the underlying tissue. Epithelial cells are highly polarized with the apical (facing the lumen of organ or external environment) and basal surfaces (facing the basal lamina) showing differences in function and structure. These epithelial cells are held tightly against one another by specialised cell-cell adhesive junctions namely gap junctions, desmosomes, tight junctions, and adherens junctions to form a highly organized structure (Figure 1.2).

- *Gap junctions*

Gap junctions, also known as macula communicans, or communicating junctions, are specialized intercellular channels that allows direct diffusion of ions and small molecules between adjacent cells (Goodenough and Paul 2009). Gap junctions are composed of transmembrane proteins called connexins and a group of six connexins form a connexon. Connexons of two adjacent cells align to form a continuous channel, allowing diffusion of small molecules between the cells (Evans and Martin 2002).

- *Tight junctions*

Tight junctions, also known as zonula occludens, are cell-cell adhesion complexes that form intercellular barriers between epithelial cells. This is critical to demarcate the tissue

spaces and allow selective diffusion of ions and solutes across the epithelium (paracellular transport)(Balda and Matter 1998).

Tight junctions are composed predominantly of claudins and other transmembrane proteins including occludins, tricellulins, and junctional adhesion molecules (JAMs). The interaction between claudin and transmembrane proteins is strengthened with the help of adaptor proteins such as ZO (zonula occludens) proteins, cingulin, PAR3, PAR6 and MUPP1 (Fanning, Jameson et al. 1998, D'Atri and Citi 2001). In addition, signalling molecules such as Rho GTPases, Rho effectors, aPKC regulate the establishment and disassembly of tight junctions (Citi, Guerrera et al. 2014).

- *Anchoring junctions*

<u>Adherens junctions (AJs)</u> : Adherens junctions, also known as zonula adherens, are primarily involved in the development and maintenance of epithelial and endothelial barriers (Niessen 2007). Furthermore, adherens junctions play a crucial role in the mechanical stability of keratinocytes, ensure proper epidermal cohesion, and regulate intercellular signalling events (Vasioukhin, Bauer et al. 2001). They lie just below tight junctions and are characterized by two juxtaposing membranes, separated by ~20 nm.

The two basic adhesive units that comprise AJs are the nectin-afadin complex and the classical cadherin-catenin complex (Niessen 2007). The ultimate strength and adhesive specificity of the AJs is reliant on the cell-specific expression of cadherins and nectins (Niessen 2007).

<u>Desmosomes and hemidesmosomes:</u> Desmosomes, also known as macula adherens, are intercellular junctions forming a tight network between cytoskeletal intermediate filaments of adjacent cells. Formation of this tight mesh-like network ensures the ability to resist mechanical stress (Garrod and Chidgey 2008). Transmembrane glycoproteins composed of cadherin group of proteins are essential to strengthen the strong adhesion established between epithelial cells and the 2 families of desmosomal cadherins primarily involved in cell adhesion (2017) are Desmogleins and Desmocollins.

Although hemidesmosomes appear morphologically similar to desmosomes, differences are seen in terms of function and composition. Instead of forming a network between adjacent epithelial cells, hemidesmosomes form a connection between the basal surface of epithelial cells and the underlying basal lamina (basement membrane)(Borradori and

Sonnenberg 1999). They are composed of integrin proteins to mediate adhesion in place of cadherins (Borradori and Sonnenberg 1999).

By means of these cell-cell junctions (gap, tight and anchoring cell junctions), the cells interact closely to form a highly organized epithelium.

1. Tight junction
2. Adherans junction
3. Desmosomes
4. Gap junctions
5. Hemidesmosomes

Extracellular matrix
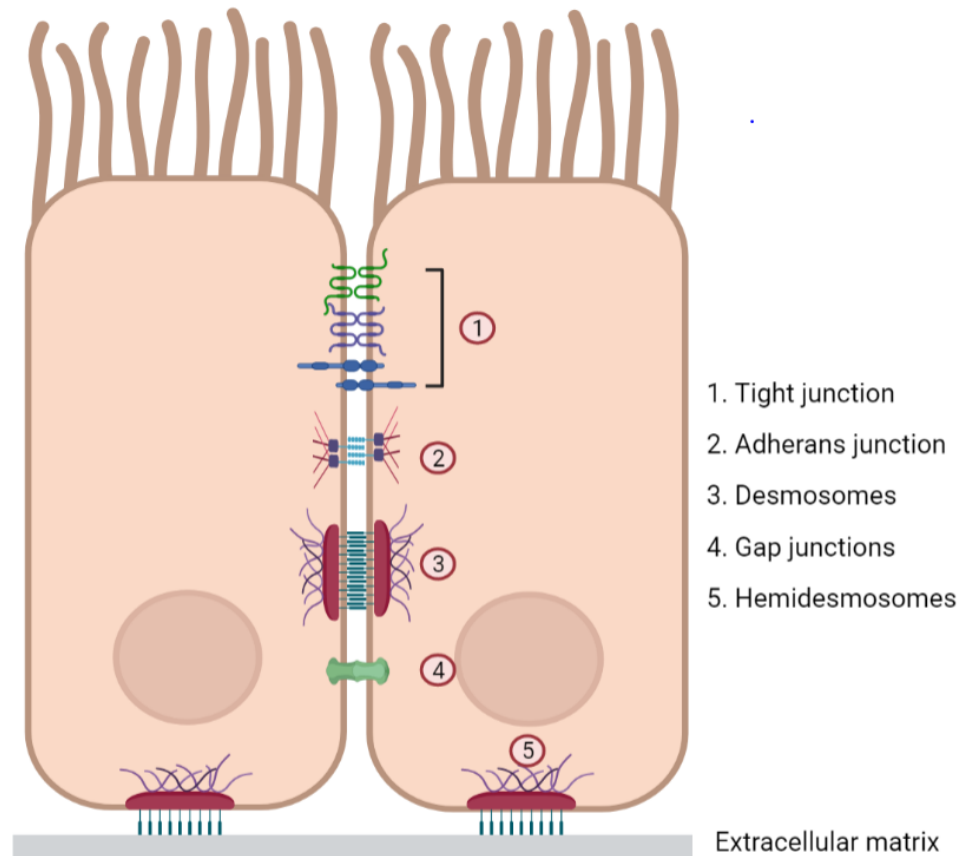
Figure 1.2 Types of cell-cell junctions.

1.1.3 Significance of understanding epithelial development

Understanding epithelial development is essential, as defective epithelial formation during embryogenesis contributes to congenital anomalies such as cleft palate and spina bifida, which are reported to be among the most common and debilitating birth defects (Wilson 1977). In addition, poor epithelial establishment greatly predisposes individuals to adult-onset pathologies such as skin diseases, pathogenic infections, and cancers of epithelial origin. Therefore, understanding the normal process by which epithelia develop is likely to uncover novel insights in the treatment of both congenital disorders, as well as improving outcomes for adult patients with diseases of epithelial origin.

Congenital anomalies, one of the leading causes of mortality and morbidity, account for approximately 3.3 million children under the age of 5 dying every year, and an estimated 3.2 million children suffering a disabled state throughout their life (Christianson, Howson et al. 2006). The World Health Organisation (WHO) defines congenital anomalies as "structural or functional anomalies that occur during intrauterine life and that can be identified prenatally, at birth, or sometimes later in infancy". A substantial number of congenital anomalies result from impaired or defective epithelial development/establishment. For example, birth defects such as cleft palate are caused due to the aberrant periderm formation (a thin layer that is formed from palatal epithelium, and overlies it), and neural tube defects (NTDs) arise due to failure of closure of neural folds as a result of either defective formation of neuroepithelium, or aberrant formation of adjacent surface ectodermal epithelium. Therefore, an understanding of the development of complex epithelia is necessary to understand the aetiology of epithelial defects.

1.1.4 Key signalling and genetic pathways in epithelial development

Epithelial cells are continuously lost or damaged throughout life and there is a continuous need to replace them. This process of maintaining a constant population of cells is referred to as tissue homeostasis and is brought about by the continuous division of epithelial stem cells.

To maintain the population of epithelial cells, stem cells must have an inexhaustible capacity to differentiate and self-renew; these processes are closely regulated by several signalling pathways. One of the significant pathways controlling the specification and maintenance of stem cells is the *Wnt* signalling pathway (Reya and Clevers 2005), the deregulation of which is associated with cancers of epithelial origin. Likewise, the *Notch* signalling pathway regulates the stem cell to differentiate to drive lineage specification (Artavanis-Tsakonas, Rand et al. 1999). Both the pathways are highly conserved across the eukaryotic kingdom. Although *Notch* and *Wnt* signalling pathways have been well understood in epithelial stem cells, other pathways such as the Bone Morphogenetic Protein (BMP) and Sonic hedgehog (*Shh*) networks have also been identified to play a vital role in maintaining the population of epithelial cells. BMPs have been identified to govern activation and differentiation of stem cells (Botchkarev, Botchkareva et al. 2001, Andl, Ahn et al. 2004, Sancho, Batlle et al. 2004), while *Shh* plays a significant role in regulating the proliferation of epithelial cells (Beachy, Karhadkar et al. 2004, Madison,

Braunstein et al. 2005). These pathways closely interact to maintain epithelial cell populations and identifying further genetic pathways that similarly contribute to epithelial fidelity and homeostasis is a key hallmark of research into epithelial development.

These well-established signal transduction pathways regulate numerous genes in epithelial homeostasis. To identify the genes involved in epithelial development, two major approaches have generally been used. Firstly, epithelial phenotypes are qualitatively described following abrogation of gene function, either via naturally occurring mutations in humans or targeted genetic deletion in animal models. Secondly, large-scale molecular analysis (e.g., RNA-SEQ, Chromatin-Immunoprecipitation [ChIP]-SEQ) comprehensively characterise the genetic landscape at defined stages of epithelial formation. These approaches have identified numerous crucial genes for epithelial development, of which the "Grainyhead-like" family of transcription factors (*Grhl*) is considered to be one of the critical drivers in epithelial development (Bray and Kafatos 1991, Wilanowski, Tuckfield et al. 2002, Ting, Wilanowski et al. 2003, Auden, Caddy et al. 2006, Lin, Tsai et al. 2011, Miles, Darido et al. 2017). The following section describes the current state of knowledge pertaining to *Grhl*-involvement in epithelial development.

1.2 Grainyhead-like transcription factors: Critical genes in epithelial development

The *Grhl* family of transcription factors, vertebrate orthologues of the ancient *Drosophila* gene *grainyhead* (*grh*), act as key players in the development and repair of epithelial barriers. Initially discovered in the fruit-fly model *Drosophila melanogaster*, they drive numerous functions, including the formation of cuticle, closure of the skin, hair formation and orientation of the fly wing, and formation of the fly head skeleton (Bray and Kafatos 1991). Similarly, *ceGrh*, the *C. elegans* orthologue of *grh* is critical for maintaining the structural integrity of the cuticle.

In mammals, *grh* is sub-functionalized into three orthologues, namely *Grhl1*, *Grhl2* and *Grhl3* (Wilanowski, Tuckfield et al. 2002, Ting, Wilanowski et al. 2003, Auden, Caddy et al. 2006), and these orthologues are highly conserved transcription factors integral in the establishment of epithelia (Table 1.1). The wide range of functions regulated by *grh*/*Grhl* TFs in epithelial development include neural tube closure and axial patterning (Ting, Wilanowski et al. 2003, Rifat, Parekh et al. 2010), neuroblast proliferation and apoptosis

(Almeida and Bray 2005, Cenci and Gould 2005), wound healing (Caddy, Wilanowski et al. 2010), and craniofacial development and palatal fusion in vertebrates (Dworkin, Simkin et al. 2014, Peyrard-Janvid, Leslie et al. 2014, Leslie, Liu et al. 2016). This incredible functional diversity is brought about largely by the binding of *Grhl* to the cis-regulatory elements (such as promoter or an enhancer element), thereby driving the expression of critical genes during early embryonic development and tissue homeostasis. Downstream target genes, together with others that comprise the gene regulatory network involving *Grhl3* that drive epithelial barrier formation will be described in detail in sections 1.4, 1.5, 1.6 and 1.7.

1.2.1 Molecular structure

The highly conserved protein domain of both *grh* and the vertebrate *Grhl* orthologues, comprises a DNA binding domain, transactivation domain, and dimerization domain (Miles, Dworkin et al. 2017). Present at the N-terminal is the transactivation domain, primarily responsible for the transcriptional activation of the protein. The DNA binding domain present at the central region of the protein binds to the highly conserved sequence AACCGGTT. The DNA binding domain along with the dimerization domain located at the C-terminal of the *Grhl* protein plays key role in dimer formation with other *Grhl* proteins (Uv, Thompson et al. 1994, Kudryavtseva, Sugihara et al. 2003, Ting, Wilanowski et al. 2003). In *Drosophila Grh* protein, ERK phosophorylation sites are present at the N-terminal and have been identified to play an integral role during later development for the activation of epidermal repair genes during epithelial barrier repair following tissue damage (Kim and McGinnis 2011). Similarly, putative ERK phosophorylation sites have also been discovered in the mammalian *Grhl* factors. The formation of a functional *Grhl3* protein comprising these domains is critical to drive the molecular networks involved in epithelial formation.

1.2.2 Conservation and expression

Grhl/grh loss-of-function has been described in numerous species. Loss of *ceGrh* causes cuticular defects, strikingly comparable to the phenotypes of *grh* mutant fruit flies (Venkatesan, McManus et al. 2003). Likewise, in *Xenopus laevis*, *XGrhl1* is crucial for ectodermal development, and the dominant negative form of *XGrhl1* results in poor formation of epidermis, partly due to the lowered expression of XK81A1 keratin gene (Tao, Kuliyev et al. 2005). In zebrafish, *grhl2* is further sub-functionalized (*grhl2a* and

grhl2b). g*rhl2b* regulate patterning of the brain and otic vesicle (Han, Mu et al. 2011, Dworkin, Darido et al. 2012), whereas *grhl1* and *grhl3* play a significant role in epithelial development (Janicke, Renisch et al. 2010, Miles, Darido et al. 2017). Interestingly, GRH is also expressed in fungi – organisms devoid of epidermal tissues. GRH in *Neurospora crassa*, an ascomycete fungus is essential for remodelling of the cell wall and lack of GRH results in defective remodelling of cell wall causing poor dispersal of conidial spores (Paré, Kim et al. 2012). This clearly shows that the function of *grh/Grhl* is highly conserved across the eukaryotic kingdom over 700 million years of evolution (Bray and Kafatos 1991, Wilanowski, Tuckfield et al. 2002, Ting, Wilanowski et al. 2003, Venkatesan, McManus et al. 2003, Tao, Kuliyev et al. 2005, Auden, Caddy et al. 2006, Lin, Tsai et al. 2011, Paré, Kim et al. 2012, Miles, Darido et al. 2017)(Table 1.1).

1.2.3 *Grhl* orthologues

- *Grhl1*

In mammals, *Grhl1* is crucial for the anchorage of the hair to the skin and formation of epithelial barrier. Mice lacking *Grhl1* display abnormal coat growth, defective hair anchorage, and thickening of the epidermis on the palmoplantar surfaces of their paws (Rickman, Simrak et al. 1999, Hunt, Rickman et al. 2001).

Defective barrier formation in mice causes increased susceptibility to chemically induced skin tumor development. The *Grhl1*$^{-/-}$ mouse, when subjected to a chemical carcinogenesis protocol, showed the growth of squamous cell carcinoma (SSC) tumours, affirming its role as a significant tumour suppressor in the SSC of the skin (Mlacki, Darido et al. 2014). Likewise, GRHL1 acts as tumour suppressor in neuroblastoma, an early childhood cancer arising from the neural crest cells (Fabian, Lodrini et al. 2014). Therefore, the expression of *Grhl1* during early developmental stages is critical for intact barrier formation and consequently, in preventing barrier defects and cancers of epithelial origin.

- *Grhl2*

Grhl2 is vital for closure of a number of embryonic tissues and absence of this gene in mice leads to cranial neural tube defects (exencephaly), cleft face, and defects in the closure of body wall (thoracoabdominoschisis) and kidney defects (Pyrgaki, Liu et al.

2011). *Grhl2* is a key regulator in the growth of maxillary processes and embryonic mice lacking *Grhl2* displayed fully penetrant split face formation associated with cranioschisis (Pyrgaki, Liu et al. 2011), and fully penetrant spina bifida. Furthermore, *Grhl2* deficient mice (ENU-generated *Grhl2^Nisw* mice) exhibited cleft face and complete exencephaly of the hindbrain, midbrain, and forebrain. In zebrafish as well, loss of *grhl2b* was associated with poor establishment and morphogenesis of midbrain-hindbrain boundary (MHB) at 21 hours post-fertilization (hpf). This was further accompanied by impaired ventricle development and neural cell death in the midbrain and hindbrain areas (Dworkin, Darido et al. 2012). Lastly, *Grhl2*-deficient mice exhibited thoracoabdominoschisis, a condition where the organs within the thorax and abdomen are exposed to the uterine environment, caused due to failed body wall closure (Pyrgaki, Liu et al. 2011).

Besides its expression in the maxillary processes, *Grhl2* is also highly expressed in the ureteric buds, nephric duct and collecting duct epithelia of developing kidney in mice. Mice lacking *Grhl2* exhibited poor luminal expansion of the nephric duct and deformed epithelial barrier formation in the collecting duct (Aue, Hinze et al. 2015). About 8.8% of *Grhl2*-knockdown (KD) mice showed unilateral agenesis of the kidney (attributed to defects in the epithelium of the nephric duct), while remaining animals exhibited no developmental defects in urogenital systems (Hinze, Ruffert et al. 2018). Lastly, the poor barrier formation in collecting duct in the medullary part of kidney resulted in compromised osmoregulation between the hypertonic interstitium and lumen of the kidneys (Kurbel, Dodig et al. 2002). This caused difficulty to concentrate the urine under thirsting conditions and consequently led to increased urinary output, comparable to patients suffering from diabetes insipidus (Devuyst 2012).

In humans, GRHL2 recessive missense mutation causes a condition called ectodermal dysplasia, primarily affecting children. Children with ectodermal dysplasia exhibit hypodontia (developmental absence of one or more teeth), palmoplantar keratoderma (thickening of the skin on the palms of the hands and soles of the feet), hyperpigmentation of the oral cavity and dysphagia (difficulty in swallowing), caused as a result of poor barrier formation (Petrof, Nanda et al. 2014). Furthermore, examination of keratinocytes isolated from patients with GRHL2 mutation showed that they displayed altered cell morphology and failed to form intact cell junctions, further signifying the importance of GRHL2 in the establishment of epithelial barriers (Petrof, Nanda et al. 2014).

Additionally, poor expression of GRHL2 has been predominantly seen in breast, ovarian, gastric, and cervical cancers (Cieply, Farris et al. 2013, Werner, Frey et al. 2013, Xiang, Fu et al. 2013, Chung, Tan et al. 2016, Xiang, Fu et al. 2017). Downregulation of GRHL2 leads to a reduction in the expression of E-cadherin. This consequently results in an increased rate of epithelial mesenchymal transition (EMT) resulting in epithelial cancers (Werth, Walentin et al. 2010).

GRHL2 also acts an excellent genetic marker for prognosis of other cancer types such as hepatocellular carcinoma (HCC) (Tanaka, Kanai et al. 2008), clear cell renal carcinoma (ccRCC) (Butz, Szabó et al. 2014), and prostate cancer (Danila, Anand et al. 2014). Therefore, it is critical to further investigate the role of GRHL2 in these cancer types and understand the GRHL2 mediated transcriptional networks involved in oncogenesis.

- *Grhl3*

Grhl3 is essential for the formation of the epithelial barrier and for driving wound healing following epithelial damage (Caddy, Wilanowski et al. 2010, Gordon, Zeller et al. 2014). Loss of *Grhl3* in vertebrates causes a wide array of epithelial defects; the clefting disorder Van der Woude Syndrome (Butali, Mossey et al. 2014, Peyrard-Janvid, Leslie et al. 2014, Mangold, Bohmer et al. 2016, Wang, Sun et al. 2016), non-syndromic palatal clefts (Eshete, 2018), spina bifida (Ting, Wilanowski et al. 2003, De Castro, Hirst et al. 2018), kidney/bladder diseases (Yu, Mannik et al. 2009), impaired eyelid closure (Yu, Bhandari et al. 2008), cancers of epithelial origin (Darido, Georgy et al. 2011, Panis, Pizzatti et al. 2013, Xu, Liu et al. 2014) and skin barrier defects (Ting, Caddy et al. 2005, Bhandari, Gordon et al. 2013). A detailed description of the *Grhl3* associated epithelial birth defects and diseases are discussed in the next section.

1.3 *Grhl3* associated epithelial birth defects and diseases

1.3.1 Craniofacial abnormalities

In humans, approximately 70% of cleft lip/palate (CL/P) cases are non-syndromic, caused due to the interaction of multiple genetic and environmental factors, while the remaining 30% cases are syndromic, due to chromosomal aberration or monogenic causes. Approximately 70% Van der Woude syndrome (syndromic) cases are caused as a result of mutation of IRF6 (interferon regulatory factor 6), a regulator of GRHL3 (Peyrard-Janvid, Leslie et al. 2014), while non-syndromic cleft lip/palate are caused by dominant GRHL3 mutations (Mangold, Böhmer et al. 2016). Therefore, it is critical to understand the role of GRHL3 in craniofacial development in order to comprehend the aetiology of orofacial abnormalities.

In mouse, an interaction of oral periderm, a supra-epithelial structure formed temporarily during the mid-gestation embryonic stage, along with the endoderm- and ectoderm-derived epithelia and neural crest cells (NCCs) underlie craniofacial morphogenesis and patterning (Dworkin, Boglev et al. 2016). A defect in any of these, especially the oral periderm is responsible for craniofacial deformities in mouse (Peyrard-Janvid, Leslie et al. 2014, Richardson, Hammond et al. 2014). *Grhl3* is crucial for the formation of periderm, and a mutation in *Grhl3* leads to craniofacial abnormalities (Peyrard-Janvid, Leslie et al. 2014), clearly signifying the importance of *Grhl3* in the orofacial development of mouse.

In zebrafish, *grhl3* is primarily expressed in the medial endoderm and developing endodermal pouches of the pharynx, from 16 hpf until 96 hpf (Dworkin, Simkin et al. 2014). Antisense oligonucleotide (morpholino; MO) mediated knockdown of *grhl3* resulted in facial defects with a severely reduced craniofacial skeleton, particularly in the lower jaw. The underlying cause of craniofacial deformities in *grhl3* morphants is attributed to the apoptosis of NCC cells that normally populate the pharyngeal arches (Dworkin, Simkin et al. 2014). Furthermore, it is hypothesized that the NCC defects induced in *grhl3* morphants are primarily due to aberrations within the pharyngeal endoderm microenvironment, signifying the importance of establishment of pharyngeal endoderm during jaw formation (Piotrowski and Nüsslein-Volhard 2000).

To conclude, loss of *Grhl3* contributes to craniofacial deformities in humans, mouse, and zebrafish, suggesting that the *Grhl3* function in craniofacial formation is highly conserved across vertebrates.

1.3.2 Neural tube defects

Closure of the neural tube is accomplished by bending of the neural plate to form bilateral neural folds, which later fuse along the rostra-caudal extent of the embryonic body axis (Greene and Copp 2014). The closure process is driven largely by the neuroepithelium, along with overlying surface ectoderm present at the leading edge of the neural folds. Failure of neural tube closure is often associated with several congenital abnormalities, commonly referred to as neural tube defects (NTDs).

Grhl3, primarily expressed in the surface ectoderm adjoining the neuroepithelium, gut endoderm and caudo-lateral epiblast (Gustavsson, Greene et al. 2007, De Castro, Hirst et al. 2018), is one of the critical genes involved in the closure of neural folds along the entire length of the body axis (Ting, Wilanowski et al. 2003, Ting, Wilanowski et al. 2003, Gustavsson, Greene et al. 2007, De Castro, Hirst et al. 2018). Embryonic mice deficient in *Grhl3* displayed thoracolumbosacral spina bifida and curled tail, with 2% of the embryos also showing exencephaly (Ting, Wilanowski et al. 2003). During gestation, the neural plate furrowed normally, however, neural fold elevation was absent, and the neural epithelium remained convex in *Grhl3*^{-/-} mice. Thus, complete loss of *Grhl3* causes failure of posterior neuropore (PNP) closure, resulting in spina bifida (Ting, Wilanowski et al. 2003).

In zebrafish, morpholino (MO)-mediated knockdown of *grhl3* resulted in defects analogous to mammalian NTDs, including shortening of axis and curved tail at 96 hpf (Miles, Darido et al. 2017) very similar to the posterior spinal cord neural tube defects observed in mice lacking *Grhl3* (Ting, Wilanowski et al. 2003). Additionally, MHB folding, and morphogenesis was severely disrupted following *grhl3* loss at 24 hpf (Miles, Darido et al. 2017). *GRHL3* mutation in humans was also found to be associated with spina bifida (Lemay, De Marco et al. 2017), demonstrating the high degree of *GRHL3* conservation in neural tube closure across vertebrates.

- ▪ *Curly tail mice*

An excellent mouse model system to understand the pathogenesis of NTDs is the *curly tail (ct)* mouse, caused due to a single nucleotide polymorphism (SNP) in a putative *Grhl3* enhancer, located ~21 kb upstream of the transcriptional start-site (TSS) of *Grhl3* (Gustavsson, Greene et al. 2007). The phenotypes commonly seen in these mice include exencephaly (~3% of embryos), spina bifida (10%) and a curled tail (50%)(Gruneberg 1954). The phenotypes of *curly tail* mice were strikingly similar to the NTDs observed in *Grhl3*$^{-/-}$ mice. Along with failed closure of the posterior neural tube, decreased proliferation of cells in the ventral bud of embryos was observed at 21 to 25 somite stage in the *ct* mouse (Copp, Brook et al. 1988, Peeters, Schutte et al. 1998). Similar studies done to understand the pathogenesis of NTDs in *Grhl3*$^{-/-}$ mice showed reduction of proliferating cells in the ventral bud, particularly in the hindgut endoderm (Gustavsson, Greene et al. 2007), suggesting a close association between the pathogenesis of NTDs observed in *ct* and *Grhl3*$^{-/-}$ mice.

Likewise, several parallels have been drawn between NTDs occurring in *ct* mice and that of humans. Some of the resemblances include the elevation of alpha-fetoprotein (AFP) levels in both amniotic fluid (Adinolfi, Beck et al. 1976) and maternal serum (Jensen, Andersen et al. 1991), high frequency of exencephaly in female foetuses (Seller and Perkins-Cole 1987), association with polyhydramnios and hydrocephaly (Embury, Seller et al. 1979) and multifactorial inheritance (Neumann, Frankel et al. 1994). Owing to these similarities, the *curly tail* mouse has become a valuable model system to understand the pathogenesis of NTDs in humans (van Straaten and Copp 2001).

In addition to the genetic contribution of reduced Grhl3 activity, the phenotype of the ct mouse was found to be influenced by environmental factors. For example, the, penetrance of spina bifida (Ting, Wilanowski et al. 2003) is exacerbated/alleviated by several factors including folic acid, retinoic acid, tobacco smoke, mitomycin C, temperature, hydroxyurea, and inositol (Seller, Embury et al. 1979, Seller and Perkins 1982, Seller and Perkins 1983, Seller and Perkins 1986, Seller and Perkins-Cole 1987, Greene, Leung et al. 2017). Therefore, the Grhl3 ct mouse can act as an ideal model system to understand novel gene-environment interactions (GEI) involved in epithelial development. Decoding the GEI interactions is critical to understand the pathogenesis of epithelial defects, and to

understand the environmental influences on genetically-sensitised individuals in the context of congenital and adult epithelial disease (detailed in section 1.7).

1.3.3 Failed eyelid closure

The leading edge of the developing eyelid and wounds shows extensive expression of *Grhl3* (Yu, Bhandari et al. 2008). Mice lacking *Grhl3* display delayed eyelid closure and understanding this open-eye phenotype is of interest to investigate the role of *Grhl* in closure of epithelial structures (Yu, Bhandari et al. 2008). Defective eyelid fusion occurs mainly due to the poor formation of the leading edge of the eyelid, poor F-actin polymerization, severe reduction of migrating keratinocytes along the leading edge followed by poor filopodia formation (Yu, Bhandari et al. 2008). In vertebrates, the movement of keratinocytes to the leading edge of the eye is regulated by the signalling cascade involving *Grhl3*, acting upstream of the *TGFa* in the epidermal growth factor receptor (EGFR/ERK) pathway (Yu, Bhandari et al. 2008). Perturbed signalling of this pathway was the underlying source of the eye-open at birth (EOB) phenotype (failure of closure of eyelids) in *Grhl3$^{-/-}$/Lmo4$^{-/-}$* mice (Hislop, Caddy et al. 2008). Additionally, *Grhl3* also interacts with the planar cell pathway (PCP) (involved in wound repair) (Caddy, Wilanowski et al. 2010) to drive eyelid closure (Kibar, Vogan et al. 2001, Curtin, Quint et al. 2003, Lu, Borchers et al. 2004). Therefore, genetic interaction of *Grhl3* with the EGFR/ERK and PCP pathway is critical to drive eyelid closure in vertebrates.

1.3.4 Kidney/bladder diseases

Establishment of barriers across the tubular epithelium of nephrons and collecting ducts during kidney organogenesis is crucial to perform functions of osmoregulation and urine osmolality. The urothelium, impermeable epithelial barrier lining the lower part of the bladder, pelvis, and renal ureter, is essentially made up of three cell layers namely, basal, intermediate and superficial (umbrella) cells (Negrete, Lavelle et al. 1996). *Grhl3* is critical for terminal differentiation of the urothelial cells and mice lacking *Grhl3* displayed impaired differentiation of the umbrella cells, causing defective formation of epithelial barrier (Yu, Mannik et al. 2009). However, in humans, no renal or urinogenital defects have been identified so far due to GRHL3 mutation.

1.3.5 Cancers of epithelial origin

GRHL3 is an excellent tumour suppressor of SSC (squamous cell carcinoma), much like GRHL1 (Darido, Georgy et al. 2011). Loss of *Grhl3* in the adult epidermis of mice invokes loss of expression of phosphatase and tensin homolog (PTEN), a tumour suppressor and a critical target of *Grhl3* (Darido, Georgy et al. 2011). *Pten* loss in the epidermis induces SCC by activating the PI3K/AKT/mTOR signalling cascade (Darido, Georgy et al. 2011). Human skin and head-and-neck SSC showed reduced expression of GRHL3 and PTEN and an elevated expression of miR-21, a proto-oncogenic microRNA targeting the two tumour suppressors (Darido, Georgy et al. 2011). Hence, normalized expression of GRHL3 is critical for the suppression of SSC.

GRHL3 acts an excellent cancer biomarker for the prognosis of breast cancers (Panis, Pizzatti et al. 2013, Xu, Liu et al. 2014). In breast cancers, TGF-β evokes downregulation of GRHL3 and HNF4A (hepatocyte nuclear factor 4 alpha) and activation of transcription factors of the ZEB, Snail and Twist families. This results in inhibition of E-cad transcription, thereby driving epithelial to mesenchymal transition (EMT)(Alotaibi, Basilicata et al. 2015). Thus, maintaining the expression of GRHL3 is critical for the repression of epithelial cancers such as SCC and breast cancer.

1.3.6 Skin barrier defects

Grhl3 is extensively expressed in the epidermis from E10.5 to adulthood in mice, and although *Grhl1* and *Grhl3* showed similar expression patterns from E15.5, they have non-overlapping and non-redundant functions in epithelial barrier formation (Boglev, Wilanowski et al. 2011). Mice lacking *Grhl3* showed perturbed skin barrier function and defective wound healing as mentioned previosusly in section 1.2.2 (Ting, Caddy et al. 2005). Furthermore, *Grhl3$^{-/-}$* mice showed reduced expression of Transglutaminase 1 (Tgase1), a key enzyme involved in the crosslinking of the structural components of the epidermis. Mice deficient in *Grhl3* also displayed defective lipid processing and abnormal lamellar lipid architecture. Furthermore, lamellar ichthyosis, a genetic skin disorder often characterized by large scales and variable redness is caused due to mutations in TGASE1 (Huber, Rettler et al. 1995, Russell, DiGiovanna et al. 1995), regulated by GRHL3, clearly indicating the significance of GRHL3 in lipid synthesis. Additionally, loss of GRHL3 in the skin triggers an inflammatory response leading to secretion of thymus and

activation-regulated chemokine (TARC) by keratinocytes to generate a hyperproliferative response, and disturb the normal differentiation of epidermis (Goldie 2018). Thus, to summarise, GRHL3 is essential for keratinocyte differentiation and lipid synthesis; vital processes involved in epithelial differentiation.

In humans, RNA profiling has revealed an upregulation of microRNA 21 (miR-21) in *GRHL3*$^{-/-}$ skin (Bhandari, Gordon et al. 2013). miR-21 was often upregulated in diseased skin conditions including psoriasis, and atopic dermatitis, suggesting a close link between *GRHL3* and pathogenesis of skin diseases (Bhandari, Gordon et al. 2013).

Table 1.1 Morphological consequences as a result of *Grhl* mutations across various species (Modified and adapted from Miles et.al 2017).

Grhl orthologue	Mutation	Morphological consequence	Reference
Drosophila			
grh	Null mutant	Defects in epidermal structures and head skeleton	(Bray and Kafatos, 1991)
		Defects in wound healing	(Mace et al., 2005)
C.elegans			
ce-Grh	RNA interference	Defects in cuticle formation and embryonic lethality	(Venkatesan, McManus et al., 2003)
Xenopus			
XGrhl1	dominant negative mutation	Defective epidermal differentiation	(Tao, Kuliyev et al. 2005)
Zebrafish			
grhl1	Morpholino	No discernible defects	(Janicke et al., 2010)
		Inner ear defects	(Liu et al., 2015)
grhl2a	Null mutant	Impaired otic development: Hearing and balance defects	(Han et al., 2011)
grhl2b	Morpholino	Midbrain-hindbrain patterning defects	(Dworkin et al., 2012)
grhl3	Morpholino	Craniofacial defects	(Dworkin et al., 2014)
		Midbrain-hindbrain patterning defects; curved tail	(Miles, Darido et al. 2017)
	Null mutant	Embryonic rupture at epiboly stage	(Miles, Darido et al. 2017)
Mice			
Grhl1	Null mutant	Viable and fertile	
		Hair anchorage defects	(Wilanowski et al., 2008)
		Higher susceptibility to develop Squamous cell carcinoma (SCC)	(Darido et al., 2011, Mlacki et al., 2014)
		Epidermal barrier disruption	(Mlacki et al., 2014)
Grhl2	Null mutant (lethal)	Neural tube defects	(Rifat et al., 2010)
		Failed cranial neural tube closure, split face, lumbo-sacral spina bifida, abdominoschsis	
		Cranial neural tube defects	(Brouns et al., 2011)
		Changes in tight junction components	(Senga et al., 2012)
		Cleft face and maxilla	
		Forebrain defects	(Menke et al., 2015)
Grhl3	Null mutant (lethal)	Neural tube defects	(Rifat et al., 2010)
		Barrier defects	(Dworkin et al., 2011, Ting et al., 2005b)
		- Changes in extracellular lipids	
		- Downregulation of adhesion molecules	(Yu et al., 2006)
		Impaired wound healing	(Ting et al., 2005a, Ting et al., 2005b)
Humans			
GRHL2	Frameshift in exon 13	Progressive autosomal dominant hearing loss	(Peters et al., 2002, Van Laer et al., 2008)
	SNP	Susceptibility to age related hearing impairment (ARHI)	(Van Laer et al., 2008)
	Missense mutations in exon 9 and 11	Autosomal recessive ectodermal dysplasia syndrome	(Petrof et al., 2014)
	SNP	Protection from sudden sensorineural hearing loss	(Lin et al., 2016)
	SNP	Protection from noise induced hearing loss	(Li et al., 2013)
GRHL3	Missense mutations and truncations	Van der Woude syndrome	(Peyrard-Janvid et al., 2014)
	SNP	Cleft Palate (increased risk)	(Leslie et al., 2016)
	Missense mutations	Non-syndromic Cleft Palate	(Mangold et al., 2016)
Neurospora			
grhl	Null mutations and deletion mutations	Defect in cell wall remodelling	(Paré, Kim et al. 2012)

1.4 *Grhl* co-factors

Drosophila studies have found that *grh* is constitutively bound to the promoter of target genes, with subsequent *grh*-dependent activation/repression closely regulated by the recruitment and decruitment of specific co-factors (Nevil, Bondra et al. 2017). This work indicates a previously under-appreciated mechanism of *grh*-mediated transcription and suggests that the identification and characterisation of co-factors that synergise with *grh* in mediating transactivation or repression may be as important as identifying specific target genes to which *grh/Grhl* factors bind (Nevil, Bondra et al. 2017).

Grhl co-factors are proteins that interact and enhance the *Grhl* DNA binding specificity. Of the numerous *Grhl* co-factors identified so far, planar cell polarity (PCP) genes have been found to be among the most critical co-factors for epithelial formation. Genes involved in the PCP pathway i.e., *Vangl2* (the vertebrate orthologue of Drosophila *vgo)*, *Celsr1* (cadherin EGF LAG seven-pass G type receptor 1), *PTK7* (protein tyrosine kinase 7 (inactive)) and *Scrb1* (scavenger receptor class B member 1)(Caddy, Wilanowski et al. 2010) closely interact with *Grhl3* during neural tube closure, and wound healing in mice. Besides the PCP genes, a close regulation between *Lmo4* (LIM-only domain protein) and *Grhl3* has been identified during cranial neural tube closure (Yu, Lin et al. 2006) in mice. Likewise, both *Grhl2* and *Grhl3* genes play co-operative roles in midbrain hindbrain closure, as the compound heterozygotes ($Grhl2^{+/-}/Grhl3^{+/-}$) display exencephaly comparable to the $Grhl3^{-/-}$ mice. Moreover, $Grhl2^{+/-}/Grhl3^{+/-}$ showed fully penetrant thoraco-lumbo-sacral SB and exencephaly very similar to $Grhl3^{-/-}$ mice (Pyrgaki, Liu et al. 2011). Similarly, MO-mediated knockdown of both *grhl2b* and *grhl3* in zebrafish embryos showed convergence extension-mediated axial patterning defects and MHB defects (Dworkin, Darido et al. 2012, Miles, Darido et al. 2017), suggesting that *grhl* factors may hetero-dimerise in fish, as they are thought to do in mammals.

Furthermore, it has been identified that both *Grhl2* and *Grhl3* play co-operative roles in eyelid fusion much like in neural tube closure and wound repair (Boglev, Wilanowski et al. 2011). A similar co-operative relationship in eyelid fusion has also been identified between *Grhl3* and *Lmo4*. This indicates similarities in the genetic pathways between *Grhl3* mediated neural tube closure, wound healing, and eyelid fusion (Hislop, Caddy et al. 2008).

1.5 Enhancers of *Grhl*

An enhancer element is a non-coding genomic DNA that typically lies either well upstream of the transcriptional start site (TSS), or within an intron, and allows binding of other proteins, to activate transcription. Several studies have identified a role for enhancers in the regulation of *Grhl* signalling. A putative enhancer element that regulates *Grhl3* expression was first discovered ~21 kb upstream of the *Grhl3* TSS; mutations in this element underpin NTDs in the *Grhl3* hypomorphic *curly tail* mice (Gustavsson, Greene et al. 2007, Uslu, Petretich et al. 2014). Another enhancer element – *mm1419* in the *Grhl2* proximal promoter region, weakly drove the expression of *Grhl2* along the midbrain-hindbrain boundary at E11.5 (de Vries, Carpinelli et al. 2020). This is significant, as loss of *Grhl2* typically leads to complete impairment of neurulation at this region (Pyrgaki, Liu et al. 2011, Menke, Cionni et al. 2015), although the specific role of *mm1419* is yet to be formally investigated. Thus, regulation of *Grhl2* and *Grhl3* transcription by enhancer elements appears to be an important mechanism involved in neurulation in vertebrates.

Enhancer elements have been found to play significant role in craniofacial development (Gordon, Tan et al. 2009). A novel 2.4 kb enhancer element located ~34 kb upstream of the *Grhl2* TSS (termed *mm1286*) is known to drive reporter gene expression in a spatiotemporal pattern closely resembling that of endogenous *Grhl2* in craniofacial primordia (de Vries, Carpinelli et al. 2020). *mm1286* interacts with *Grhl2* to drive palatal closure in mice and the absence of this genomic element results in significant predisposition to cleft palate at birth (de Vries, Carpinelli et al. 2020). This suggests that *mm1286* is a critical enhancer element of *Grhl2* to drive craniofacial formation in mice.

Identifying the proteins that bind to these enhancers to drive expression of *Grhl2* shapes as a key direction to identifying novel upstream regulators of this gene family.

1.6 Upstream regulators of *Grhl*

Numerous target genes of *Grhl* have been discovered so far, however very little is known about how this epithelial transcription factor is regulated. In order to understand how *Grhl* is regulated, it is crucial to identify its upstream regulators i.e., proteins that bind to both the *Grhl* promoter and enhancers, thereby activating *Grhl*-dependent transcription. A description of the key upstream regulators of *Grhl* that drive various epithelial processes

(ERK, *fgf8,irf6, p53* and *klf5)*(Auden, Caddy et al. 2006, Brynczka, Labhart et al. 2007, Bell, Zhang et al. 2011, Kim and McGinnis 2011, Dworkin, Darido et al. 2012, Peyrard-Janvid, Leslie et al. 2014) is presented below.

Grhl is well-known for its role in epithelial barrier formation and repair of epithelial barrier following injury. Studies have shown that post translational modification of GRH by ERK (extracellular signal-regulated kinase) phosphorylation is critical for driving the wound-dependent expression of GRH target genes and for the activation of *Dopa decarboxylase (Ddc)* and *misshapen (msn)* epidermal wound enhancers (Kim and McGinnis 2011). Likewise, *Grhl3*, comprises putative ERK phosphorylation sites on the N terminal domain and mice lacking *Grhl3* exhibit defects in both skin barrier formation and wound-induced repair (Ting, Caddy et al. 2005), suggesting that ERK phosphorylation of GRH might be an evolutionarily conserved process in epidermal wound repair (Kim and McGinnis 2011). Besides wound healing, *Grhl3* acts downstream of *Klf5,* a transcriptional factor that regulates the formation of the urothelial barrier. *Klf5* activates *Grhl3* by binding directly to the *Grhl3* promoter region, in turn regulating the expression of cell adhesion genes including *cldn 5, 6, 8, 9* and *11* and *occludin* for the establishment of an effective urothelial barrier (Bell, Zhang et al. 2011). Thus, *Grhl3* mediated barrier formation and wound healing is brought about by the close interaction of *Grhl3* and its upstream regulators.

The tumour suppressor p53 has also been found to facilitate neural tube closure via the regulation of *Grhl3* expression (Brynczka, Labhart et al. 2007) and the absence of p53 causes exencephaly comparable to that of *Grhl3* null mice (Sah, Attardi et al. 1995). Likewise, in zebrafish, *fgf8* appears to act upstream of *grhl2b*, together driving expression of downstream *grhl2b* targets, namely *spec1* and *eng2a,* to bring about the patterning and morphogenesis of the MHB (Dworkin, Darido et al. 2012).

In palatal development, *Grhl3* is believed to be regulated by *Irf6.* Absence of *Irf6* in mice causes rigid, inflexible epidermis along with cleft palate arising as a result of defective establishment of periderm (Ingraham, Kinoshita et al. 2006), much like that seen in the *Grhl3*^{-/-} mice (Ting, Wilanowski et al. 2003). In zebrafish, *irf6* is extensively expressed in pharyngeal pouches (Ben, Jabs et al. 2005) and plays an integral role in the development of enveloping layer (EVL) much like *grhl3* (de la Garza, Schleiffarth et al. 2013). Loss of *irf6* in zebrafish embryos causes poor EVL formation. This phenotype was rescued by

overexpressing *grhl3*, thereby demonstrating the significance of *grhl3* as a key player in *irf6* dependent pathway in EVL formation (de la Garza, Schleiffarth et al. 2013).

To conclude, upstream regulators of *Grhl* regulate the transcriptional activity of *Grhl* in barrier formation, neural tube closure and palatal development. Therefore, elucidating the upstream genomic landscape governing *Grhl* will help us understand how *Grhl* is regulated in various developmental processes.

1.7 Downstream target genes of *Grhl*

As a highly conserved family of transcription factors, *Grhl* family members bind to the promoters of numerous target genes (Table 1.2) to drive epithelial establishment. Therefore, identifying the genetic networks involved in *grhl*-dependent epithelial closure will help us understand the molecular and cellular pathogenesis of several epithelial defects/diseases.

In *Drosophila*, *grh* is essential for regulating the neuronal expression of *Dopa decarboxylase* (*Ddc*). The expression of this gene is critical for cross-linking of protein/lipids in the cuticle, the absence of which causes cuticular defects (Bray and Kafatos 1991). Likewise, in mammals, Transglutaminase 1 and 5 (*Tgm1 and Tgm5*), key enzymes involved in the crosslinking of the structural components of the epidermis analogous to the *Ddc* in *Drosophila*, were identified to be excellent targets of *Grhl3* in barrier formation. Embryonic mice lacking *Grhl3* showed reduced expression of *Tgm1* and barrier defects (Ting, Caddy et al. 2005), clearly showing the degree of functional conservation between members of this gene family.

Mammalian *Grhl1* plays a critical role in barrier formation and hair anchorage by regulating the expression of the desmosomal cadherin desmoglein 1 (*Dsg1*)(Wilanowski, Caddy et al. 2008). *Dsg1* is a protein that forms an important component of desmosomes (cell-cell adhesion complexes between suprabasal keratinocytes) and acts as a key regulator for the terminal differentiation of keratinocytes (Getsios, Simpson et al. 2009). *Grhl1* deficient mice showed reduced expressed of *Dsg1*, causing poor formation of properly composed suprabsal desmosomes, resulting in several desmosomal defects and subsequently, poor barrier function of the skin (Wilanowski, Caddy et al. 2008). In *Grhl3* mediated barrier formation and repair in mice, the RhoA activator *RhoGEF19* has been identified as an integral downstream target of *Grhl3*, playing an important role in cellular

polarity, actin polymerisation and wound healing (Caddy, Wilanowski et al. 2010). Therefore, both *Grhl1* and *Grhl3* TFs control barrier formation by regulating their respective downstream targets and it is critical to identify their targets to elucidate the molecular pathways underpinning barrier formation.

Grhl2 regulates a wide range of downstream targets, including *Cldn4*, *Cdh1*, *Ovol2* (Werth, Walentin et al. 2010, Aue, Hinze et al. 2015, Chung, Tan et al. 2016) for the maintenance of cell identity in kidneys, breast, and surface ectoderm. As a key tight junction protein, *Cldn4* is involved in establishment of oral periderm and maintenance of structural integrity during palatal fusion (Yoshida, Shimono et al. 2012). *Grhl3* like *Grhl2* is also involved in the maintenance of oral epithelia by binding to its key partners such as Gsk3β (Liu, Arron et al. 2007), *edn1* (Dworkin, Simkin et al. 2014) and PTEN (Darido, Georgy et al. 2011). Therefore, both *Grhl2* and *Grhl3* regulate craniofacial formation via the transcription of their downstream targets.

Grhl2 also plays a significant role in maintaining the integrity of non-neural ectoderm (NNE), absence of which causes poor integrity of NNE, thereby giving rise to NTDs in vertebrates. The suppression of *Zeb1* (Cieply, Riley et al. 2012) and active upregulation of epithelial genes - *E-cadherin* (Pyrgaki, Liu et al. 2011) and *Cldn4* (Werth, Walentin et al. 2010) and epithelial-mesenchymal (EMT) suppressors – *Esrp1, Sostdc1, Fermt1, Tmrprss2, and Lamc2* (Ray and Niswander 2016) by *Grhl2* is significant for the establishment of intact NNE, and potentially also the palatal epithelium.

In zebrafish, *grhl2b* plays a central role in the patterning and folding of MHB by regulating the expression of *engrailed 2a (eng2a)* and *spec1* (Dworkin, Darido et al. 2012). *eng2a* is integral for the molecular and central control of mesencephalon and metencephalon development, thus critical for both MHB maintenance and establishment (Joyner, Herrup et al. 1991, Wurst, Auerbach et al. 1994) and the *grhl2b-eng2a* transcriptional pathway in neural development is highly conserved in both flies and vertebrates (Attardi and Tjian 1993, Dieckgraefe and Weems 1999, Wilanowski, Tuckfield et al. 2002, Dworkin, Darido et al. 2012). *Spec1* on the other hand, regulates cellular morphogenesis, critical for MHB folding in zebrafish. Similarly, MHB morphogenesis and patterning mediated by *grhl3* is also dependent on transcriptional targets, *spec1* and *arhgef19* (Miles, Darido et al. 2017), suggesting similarities between the *grhl2b* and *grhl3* transcriptional networks in zebrafish neural development.

Determining the downstream targets, enhancer elements, upstream regulators and co-factors of *grhl* will help us undertsand the genetic mechanisms involved in epithelial birth defects (such as cleft palate and spina bifida). Besides the genetic factors, it has been found that epigenetic factors (environmental factors, such as smoking, alcohol, vitamin deficiency, etc) can exacerbate the incidence and severity of birth defects. Therefore, characterising environmental factors that can lead to birth defects, or more excitingly, rescue defects of genetic origin, provides a very promising therapeutic approach to gaining a more complete picture of factors that impact embryogenesis.

The following section will describe in detail the environmental factors that were selected for this study and their key roles in development and epithelial homeostasis.

Table 1.2 Some of the critical downstream target genes of *Grhl* in epithelial development.

Target gene	*Grhl* orthologue	Organism	Function	Reference
Dsg1	*Grhl1*	*Mus musculus*	Terminal differentiation of keratinocytes	Wilanowski, Caddy et al. 2008
Cldn4	*Grhl2*	*Mus musculus*	Maintenance of cell identity in gut endoderm, surface ectoderm and otic epithelium; establishment of oral periderm and palatal fusion	Yoshida, Shimono et al. 2012, Werth, Walentin et al. 2010
Cdh1	*Grhl2*	*Mus musculus*	Maintenance of cell identity in kidneys, breast and surface ectoderm; establishment of palate	Werth, Walentin et al. 2010, Pyrgaki, Liu et al. 2011
Ovol2	*Grhl2*	*Mus musculus*	Maintenance of cell identity in kidneys	Aue, Hinze et al. 2015
Gsk3	*Grhl3*	*Mus musculus*	Maintenance of oral epithelia	Liu, Arron et al. 2007
edn1	*grhl3*	*Danio rerio*	Maintenance of oral epithelia	Dworkin, Simkin et al. 2014
Pten	*Grhl3*	*Mus musculus*	Maintenance of oral epithelia	Darido, Georgy et al. 2011
eng2a	*grhl2*	*Danio rerio*	MHB patterning and folding	Dworkin, Darido et al. 2012
spec1	*grhl2b and grhl3*	*Danio rerio*	MHB patterning and folding	Dworkin, Darido et al. 2012, Miles, Darido et al. 2017
arghef19	*grhl3*	*Danio rerio*	MHB patterning and folding	Miles, Darido et al. 2017
Ddc	*grh*	*Drosophila melanogaster*	Cross-linking of protein/lipids in cuticle	Bray and Kafatos 1991
Tgm1	*Grhl3*	*Mus musculus*	Crosslinking of the structural components of the epidermis	Ting, Caddy et al. 2005
Tgm5	*Grhl3*	*Mus musculus*	Crosslinking of the structural components of the epidermis	Ting, Caddy et al. 2005

1.8 Environmental factors influencing birth defects

Any exposure that occurs to the fetus via the mother is typically considered 'environmental'. A strong correlation exists between the fetal development and the maternal health, diet and exposure to environmental chemicals. For instance, pregnant women lacking folic acid are more likely to have children with neural tube defects such as spina bifida and anencephaly (Rieder 1994, Pitkin 2007). Hence, folic acid supplementation is critical during pregnancy to prevent birth defects in the newborn, caused as a result of folate insufficiency. Some other commonly known environmental factors causing potential risk to the foetus include exposure to smoke (Shi, Wehby et al. 2008), caffeine (Suarez, Felkner et al. 2008, Schmidt, Romitti et al. 2009), alcohol (Ornoy and Ergaz 2010), iodine deficiency (Zimmermann 2012), magnesium deficiency (Komiya, Su et al. 2014) and carcinogens. Therefore, identifying environmental factors that may impede or promote foetal development is vital for the prevention of birth defects.

The underlying cause for the majority of birth defects is due to complex interactions between environmental and/or genetic factors. Fraser's reasearch in early 1950s, showed that maternal administration of cortisone induced cleft palate in pups. Additionally, the severity/incidence of cortisone induced cleft palate was further influenced by the genotype of the mice (Fraser and Fainstat 1951). This early experiment in the field of teratogenetics, clearly showed that using genetically sensitised animal models to determine the nature of influences that bioactive compound exposure can have on development is likely to better approximate the basis of congenital defects in humans.

An excellent animal model for studying these gene-environment interactions has been the *Grhl3* hypomorphic mutants (*curly tail* mice). As described earlier, *Grhl3*-deficient embryos displayed tail aberrations, accompanied by lumbosacral spina bifida and on occasion, exencephaly. When mitomycin C, a DNA inhibitor was administered on day 7 and 8 of pregnancy, an increased incidence of exencephaly was observed. Conversely, mitomycin C, when administered at day 9 of pregnancy, showed a drastic decrease in the number of tail and spinal defects, showing a 'remedial' effect (Seller and Perkins 1986). Likewise, administration of retinoic acid to *Grhl3 curly tail* mutants at day 8 showed an increased prevalence of NTDs and treatment at day 9 showed a decreased occurrence of NTDs (Seller, Embury et al. 1979, Seller and Perkins 1982). Similar results were obtained

when embryos were treated with hydroxyurea at day 8 and day 9 of pregnancy (Seller and Perkins 1983). Thus, administration of mitomycin C, retinoic acid and hydroxyurea on the *Grhl3*^{-/-}embryos seems to have both a teratogenic and a preventive effect depending on the time-point it was administered to the mother during pregnancy (Seller and Perkins 1986).

An elevated environmental temperature affects the closure of cranial folds resulting in an increased incidence of exencephaly. Interestingly, no effects on the frequency of posterior NTDs was observed in *curly tail* mice (Seller and Perkins-Cole 1987). Likewise, inositol deficiency was shown to increase the incidence of cranial NTDs in *curly tail* mouse embryos (Cockroft, Brook et al. 1992) however, no exacerbation in the progression of spinal neurulation was observed (Greene and Copp 1997). In fact, increasing inositol concentration had a protective effect against spina bifida in the *Grhl3* hypomorphs (Greene and Copp 1997). But in the *Grhl3* null mice, inositol had no role in preventing the incidence of NTDs, possibly due to the severity of the NTDs (Ting, Wilanowski et al. 2003)(Table 1.3).

Therefore, a greater understanding of how different environmental factors interact with *Grhl3*, or models of *Grhl3*-deficiency, could potentially help identify novel therapeutic options and risk factors for epithelial development.

Table 1.3 The effects of environmental factors on the neural tube development of curly tail mice (*Grhl3* hypomorphs) at varying developmental time points.

Environmental factor	Day of administration	Resultant effect	Reference
Mitomycin C	7, 8	↑exencephaly	Seller and Perkins 1986
	9	↓spinal and tail defects ; ✖ excencephaly	
Retinoic acid	8	↑ NTDs	Seller, Embury et al. 1979, Seller and Perkins 1982
	9	↓NTDs	
Hydroxylurea	8	↑ excencephaly	Seller and Perkins 1983
	9	↓ NTDs	
Elevated temperature	8, 9,10	↑excenphaly / No effect on posterior NTDs	Seller and Perkins-Cole 1987
Inositol	9.5,10.5	↓spina bifida	Greene and Copp 1997

1.8.1 Vitamins and minerals

- *Myo-inositol (vitamin B_8)*

Folic acid is a well-known supplement prescribed during pregnancy for the prevention of NTDs (Control 1991). However, folic acid does not prevent all NTDs, and hence inositol, also known as vitamin B_8 is often recommended to prevent spina bifida and anencephaly that are especially non-responsive to folic acid (Ray, Meier et al. 2002, Greene and Copp 2005).

Inositol deficiency in mouse is primarily responsible for cranial NTDs in mice (Cockroft, Brook et al. 1992). Prevention of NTDs was particularly seen in the *curly tail* mouse (*Grhl3* hypomorph) and folate deficiency induced mouse model when supplemented with inositol (Greene and Copp 1997, Greene and Copp 2005). However, the protective effect of inositol was not applicable to other mouse NTD models. For instance, *Grhl3* null mice showed no response when treated with inositol, possibly due to the severity of the NTDs associated with *Grhl3*$^{-/-}$ mice (Ting, Wilanowski et al. 2003).

Although inositol has several benefits, it is significant to understand the side effects inositol is likely to pose during pregnancy. In mice, there were no apparent deleterious effects observed (Cogram, Tesh et al. 2002), however, myoinositol supplementation was known to interact with valproic acid (an anti-epileptic drug with known teratogenic properties) and exacerbate the incidence of NTDs (Massa, Wlodarczyk et al. 2006). Thus, it is essential to understand the interactions of inositol with other drugs before administration during pregnancy.

Lastly, studies conducted so far show the beneficial effects of inositol in the prevention of NTDs, however, these studies may not have used sufficient sample size to generate statistically significant conclusions (Cavalli and Copp 2002, Cavalli, Tonni et al. 2011, Greene, Leung et al. 2016). Moreover, studies to date have showed the efficacy of inositol on women with recurrent NTDs-affected pregnancies and not on women without a history of NTDs. If future studies do confirm the effectiveness of inositol against NTDs, then this simple, inexpensive compound could be widely recommended as a supplement for pregnant mothers.

- *Nicotinamide (vitamin B$_3$)*

Nicotinamide, a form of vitamin B$_3$, is integral for the synthesis and oxidation of fatty acids and also in the metabolism of drugs and toxicants. Low dietary intake of vitamin B$_3$ coupled with a diet rich in saturated fats during the periconceptional period has shown an increased risk of congenital heart defects (CHD) especially outflow tract defects. (Smedts, Rakhshandehroo et al. 2008). Likewise, deficiency of vitamin B$_3$ in pregnant mothers caused spina bifida (Groenen, van Rooij et al. 2004). The underlying mechanism of niacin in neural tube closure is poorly understood. However, there are studies that attribute the incomplete neural tube closure to poor biosynthesis of cholesterol, often associated with deficiency of nicotinamide (Huang, Voyiaziakis et al. 1995, Tozawa, Ishibashi et al. 1999). Similarly, inadequate intake of nicotinamide, thiamine and pyroxidine during pregnancy resulted in an increased risk of an orofacial child (Krapels, van Rooij et al. 2004). Thus, nicotinamide supplementation during gestation is essential in preventing congenital anomalies in children.

- *Thiamine (vitamin B$_1$)*

Thiamine, also known as vitamin B$_1$, is crucial for glucose metabolism and plays a significant role in nerve, muscle, and heart function. Inadequate periconceptional consumption of thiamine along with niacin and pyridoxine resulted in an increased risk of children being born with orofacial clefts. The incidence of orofacial clefts in children significantly decreased when mothers were supplemented with thiamine and pyridoxine during pregnancy (Bienengräber, Fanghänel et al. 1997, Krapels, van Rooij et al. 2004).

Treatment for gestational diabetes resulted in an elevated incidence of infants born with a low birth weight, a risk factor for cardiovascular disease and diabetes mellitus. Thiamine supplementation during pregnancy enhances the glucose tolerance along with an increase in intra-uterine growth, thereby averting the incidence of infants born with low birth weight (Bakker, Maaten et al. 2000).

- *Cobalamin (vitamin B$_{12}$)*

Vitamin B$_{12}$, also known as cobalamin, is a water-soluble vitamin highly abundant in meat, fish, eggs, and dairy. It is essential for the synthesis of DNA, production of red blood cells and maintenance of the nervous system.

Vitamin B_{12} is well-known to interact closely with folate in the metabolic pathway of homocysteine, for the prevention of NTDs (Mills, Lee et al. 1995). Low levels or deficiency of maternal vitamin B_{12} (<250 ng/L) has been linked to increased levels of homocysteine (Hcy), a known teratogenic factor in maternal blood (Afman, Blom et al. 2003), causing increased risk of NTDs (Kirke, Molloy et al. 1993, Molloy, Kirke et al. 2009, Ceyhan, Beyan et al. 2010, Peker, Demir et al. 2016) and congenital heart defects (Verkleij-Hagoort, de Vries et al. 2006). Furthermore, vitamin B_{12} biomarkers such as methyl malonic acid (MMA)(Luo, Zhang et al. 2004) and Hcy were elevated in women with NTD affected pregnancies when compared to pregnant women with normal foetuses (Adams, Khoury et al. 1995, Ceyhan, Beyan et al. 2010). Thus, to prevent the risk of NTDs, pregnant women are often recommended to consume Vitamin B_{12} in order to maintain Vitamin B_{12} levels greater than 300 ng/L in their blood prior to pregnancy (Molloy, Kirke et al. 2009).

- *Iodine*

Iodine, a crucial element for the synthesis of thyroid hormones, is found in foods such as salt, seafood, eggs, and milk. Thyroid hormone plays an integral role in metabolism and is critical for early growth and development of most organs, especially the brain (Triggiani, Tafaro et al. 2009). Adequate levels of thyroid hormones are required for neuronal migration and myelination of the central nervous tissue, and insufficient amounts of iodine during pregnancy results in spontaneous abortions, stillbirth, and increased risk of congenital anomalies in children (Triggiani, Tafaro et al. 2009). Furthermore, iodine deficiency has also been linked to goitre, hypothyroidism, low childbirth weight, cretinism, and mental retardation (Cao, Jiang et al. 1994, Delange 2000, Pérez-lópez 2007, Triggiani, Tafaro et al. 2009). As the foetal thyroid does not secrete any hormone until the middle of the third trimester, hence mothers lacking iodine during the first trimester must be recommended iodine supplementation to prevent brain damage and hypothyroidism (De Escobar, Obregón et al. 2007).

1.8.2 Polyphenols

- *Resveratrol*

Resveratrol, a phytoalexin abundantly found in red grapes and blueberries, has been widely used for its anti-cancer (Elshaer, Chen et al. 2018), anti-viral (Abba, Hassim et al.

2015, Filardo, Di Pietro et al. 2020), neuroprotective (Albani, Polito et al. 2010), anti-aging (Baxter 2008), antioxidant (Baxter 2008) and anti-inflammatory properties (Das and Das 2007). Here I describe the role of resveratrol in prevention of embryonic deformities and epithelial cancers.

Diabetic pregnancy often results in embryonic abnormalities, referred to as diabetic embryopathy. The incidence of diabetic embryopathies was significantly reduced by the use of resveratrol, known to reduce the maternal blood sugar level (Do, Jung et al. 2012). Resveratrol administration in diabetic mice showed a significant reduction in the number of malformed embryos and rescued the developmental delays that were usually observed in these mice (Singh, Kumar et al. 2011). Resveratrol acts by normalizing hyperglycaemia-induced oxidative stress and by regularizing the expression patterns of retinoic acid receptors and neuronal markers, thereby preventing diabetic embryopathies (Singh, Kumar et al. 2011, Singh, Kumar et al. 2012).

Similarly, oxidative stress induced in chicken embryos when exposed to high glucose levels was stabilized by the administration of resveratrol (Tan, Zhang et al. 2015). Furthermore, resveratrol consumption in mice during pregnancy prevented TCDD (2,3,7,8-tetrachlorodibenzo-p-dioxin) and ethanol associated anti-teratogenic effects in both the mother and foetus when exposed to TCDD (Jang, Park et al. 2008) and ethanol (Kasdallah-Grissa, Mornagui et al. 2007) respectively. Correspondingly, in chickens, neural tube defects associated with valproic acid (VA) exposure during pregnancy were prevented by resveratrol administration (Hsieh, Chen et al. 2014).

Resveratrol has also been widely used in the chemotherapeutic treatment of non-melanoma skin cancers (Boyer, Jandova et al. 2012), hepatoma (Miura, Miura et al. 2004, Michels, Wätjen et al. 2006), fibrosarcoma (Mousa, Mousa et al. 2005), and leukaemia (Surh, Hurh et al. 1999, Gautam, Xu et al. 2000). Furthermore, resveratrol has been extensively studied for the treatment of numerous other cancers such as those of pancreas (Ding and Adrian 2002, Shankar, Nall et al. 2011), colon (Mahyar-Roemer, Katsen et al. 2001), lung (Atten, Godoy-Romero et al. 2005), oesophagus (Zhou, Yan et al. 2003), and prostate. In conclusion, resveratrol is an excellent polyphenol to prevent epithelial birth defects and cancers.

▪ *Curcumin*

Curcumin is a well-known anti-inflammatory phenolic compound present in the rhizomes of the turmeric spice plant. Several biological activities of curcumin including its antioxidant, anti-inflammatory, anti-carcinogenic, anti-tumour, anti-diabetic and anti-HIV properties have been extensively studied using both *in vitro* and *in vivo* approaches (Huang, Lysz et al. 1991, Oetari, Sudibyo et al. 1996, Srivivasan, Menon et al. 2003, Tu, Han et al. 2011). Thus, curcumin is widely used for the treatment of several disease conditions (Ammon and Wahl 1991).

Curcumin is also critical for strengthening epithelial integrity. The intestinal mucosal barrier acts as the first line of defence, preventing the passage of harmful molecules across the mucosa and into circulation. Studies in pigs and mice supplemented with curcumin in their diet, showed an overall improvement in the integrity, morphology, and immune status of the intestinal mucosal barrier, by blocking MAP3K and inhibiting NF-kB activation, thereby preventing barrier defects (Bereswill, Muñoz et al. 2010, Song, Wang et al. 2010, Xun, Shi et al. 2015). Similarly, hydrogen peroxide induced destruction of tight junction and barrier dysfunction was prevented when human intestinal epithelial cells were treated with curcumin (Wang, Wang et al. 2012). Intestinal ischemia-reperfusion (I/R), a life-threatening complication of digestive organ transplantation causes severe mucosal injury and impaired gut function. Curcumin treatment during I/R injuries in rats resulted in an increased ZO-1 protein expression and restoration of epithelial permeability and integrity of the mucosal barrier (Tian, Guo et al. 2016).

The effect of curcumin in strengthening the epithelial barrier is not only restricted to the intestinal mucosa. It has been reported that administration of curcumin protected the disruption of the female genital mucosal barrier during HIV and prevented viral replication of HIV-1 and HSV-2 (Ferreira, Nazli et al. 2015). Cell injury by oxidative stress is responsible for the destruction of renal epithelial cells and curcumin was identified to play a critical role against oxidative stress in the renal epithelia (Cohly, Taylor et al. 1998). Thus, curcumin is essential for maintaining epithelial homeostasis across multiple tissues.

Neural tube defects associated with maternal diabetes can be prevented by oral administration of curcumin during pregnancy (Wu, Wang et al. 2015). Hyperglycaemia

during pregnancy invokes multiple metabolic pathways resulting in increased production of reactive oxygen species and oxidative stress and eventually causing failed neural tube closure (Yang, Zhao et al. 2008, Li, Weng et al. 2011). Curcumin blocks the cellular stress and caspase activation, consequently preventing glucose induced NTDs (Wu, Wang et al. 2015). However, curcumin treatment at high dosages caused teratogenic effects in both zebrafish (Wu, Lin et al. 2007) and mouse embryos (Huang, Lan et al. 2013). Thus, the ideal dosage of curcumin must be determined through extensive dosage studies to make sure they cause no potential harm.

Curcumin displays a chemo preventive effect in cancers of colon, stomach (Singh, Hu et al. 1998), duodenum (Huang, Lou et al. 1994), oesophagus (O'Sullivan-Coyne, O'Sullivan et al. 2009) bowel (Mohandas and Desai 1999) and the mouth (Singh, Hu et al. 1998). Curcumin targets the key transcriptional factors, growth regulators, adhesion molecules, apoptotic genes and signalling molecules involved in carcinogenesis, thereby acting as an excellent chemotherapeutic agent (Aggarwal, Kumar et al. 2003).

- *Luteolin*

Luteolin (3,4,5,7-tetrahydroxy flavone), a flavonoid commonly present in many medicinal plants, fruits and vegetables is well-known for its antioxidant, anti-inflammatory and neuroprotective activities. Furthermore, luteolin acts as an excellent anti-cancer agent against wide range of epithelial cancers such as lung (Cai, Ye et al. 2011, Zhao, Yang et al. 2011), breast (Sun, Zhang et al. 2015), glioblastoma (Wang, Wang et al. 2017), prostrate (Wang, Li et al. 2014), colon (Pandurangan, Dharmalingam et al. 2013), gastric (Wu, Zhang et al. 2008) and pancreatic cancers (Li, Zhang et al. 2018). Luteolin stops the progression of cancers both *in vivo* and *in vitro* by suppressing the proliferation of tumour cells, activating cell cycle arrest and finally by initiating apoptosis (Horinaka, Yoshida et al. 2005). Additionally, luteolin inhibits EMT and promotes MET by upregulating epithelial biomarkers including *E-cadherin* and downregulating mesenchymal biomarkers such as *vimentin*, *snail,* and *N-cadherin* (Lin, Tsai et al. 2011), thereby preventing epithelial cancers.

1.9 Zebrafish as a model to understand epithelial development

1.9.1 Zebrafish (*Danio rerio*) as a model organism

Zebrafish, a tropical freshwater fish belonging to the Cyprinidae family, is predominantly found across the rivers of the Indian sub-continent. Zebrafish embryos share 70% genetic similarity to humans. They are transparent and their development is external, this ensures for easy visualization of the developmental processes that occur during embryogenesis (Veldman and Lin 2008). Development of zebrafish embryos is relatively fast when compared to other model organisms, with the major primary organ systems formed within 24 hours post-fertilization (24 hpf). The rapid development coupled with high fecundity rate enables one to observe the development of a number of embryos within a short span of time, making it an ideal model organism in the field of developmental biology.

Transient inhibition of gene function can be rapidly achieved through injecting Morpholino (MO) antisense oligonucleotides in single cell stage zebrafish embryos to understand the potential function of the gene of interest. Morpholinos are complementary ~25 bp long oligomers that bind to the mRNA sequence of the gene of interest and cause transient knockdown by inhibiting mRNA translation or splicing (Stainier, Raz et al. 2017). MO mediated knockdown is relatively simple and cost-effective, making this an attractive technique to understand gene function (Eisen and Smith 2008). Additionally, gene editing technologies such as CRISPR-Cas9 (clustered regularly interspaced short palindromic repeats), TALENs (transcription activator-like effector nucleases) or ZFNs (zinc- finger nucleases) have been prevalently employed for complete knockout of a gene (Wood, Lo et al. 2011, Joung and Sander 2013, Jiang and Doudna 2017, Ran 2013). All these positive attributes makes zebrafish an ideal model system for genetic studies (Veldman and Lin 2008).

Recently, zebrafish embryos have also been commonly used for high throughput toxicological and therapeutic screening to understand the relationship between chemicals and their effects on animal physiology (Veldman and Lin 2008). Zebrafish embryos act as a convenient model system to understand the various facets of developmental toxicology. Although, cell/organ cultures have been extensively used for this purpose, they may not be an ideal model system to understand the events in morphogenesis. Since zebrafish embryos are transparent, morphological assessment of various structures and organ systems can be easily visualized using both brightfield and fluorescence microscopy.

Large scale screening can be easily performed to understand the effect of small chemical molecules on the development of embryos. Lastly, genetic pathways underlying a 'phenotype' caused due to a test compound can be unravelled by evaluating exisiting databases describing the mutant phenotype and their associated genetic alteration (Augustine-Rauch, Zhang et al. 2010).

From the attributes listed above, it is clear that zebrafish are a versatile and an excellent model system. This model will continue to be largely used by researchers across the world especially in the arena of developmental genetics owing to the numerous advantages such as easy manipulation of embryos, large scale screening, easier maintenance and lower costs when compared to other model systems.

1.9.2 Zebrafish embryos to study epithelial biology

The ease of access and genetic tractability makes zebrafish a preferred outstanding model system to investigate epithelial development. Furthermore, optical transparency of the embryos allows for real time imaging of morphogenetic cell movements underlying epithelial establishment.

Zebrafish embryonic skin is bilayered, much like the mammalian epidermis. The two layers present in the embryonic epithelium are the enveloping layer (EVL) or the surface layer and epidermal basal layer (EBL) (Kimmel, Warga et al. 1990). EVL formed during the blastula stage is primarily involved in protection of the embryo, and often considered to be very similar to the mammalian periderm. EBL formed at the end of gastrulation after the formation of the three germ layers (ectoderm, mesoderm, and endoderm) is essential for offering protection along with exchange of gases.

Zebrafish embryonic epithelium is also analogous to the mammalian epithelium, in terms of the cell types present (Schwerte 2010, Chang and Hwang 2011). The cell structure and function of zebrafish epidermal cells is closely related to those in mammalian kidney, skin, and intestinal cells (Chang and Hwang 2011). Thus, understanding of zebrafish epithelia provides insights into the physiology and development of kidney and intestinal cells. Additionally, epithelial cells present in zebrafish epithelia express cell markers and genes (*grhl3, irf6, poky, chuk, ikk1, p63, lgl2, e-cadherin*) very similar to those expressed extensively in mammalian epithelium (Lee and Kimelman 2002, Sonawane, Martin-Maischein et al. 2009, Fukazawa, Santiago et al. 2010, Han, Mu et al. 2011). All these

attributes point to a high degree of conservation between the zebrafish and mammalian epithelium, thereby making zebrafish a perfect model system to understand conserved mechanisms of epithelial establishment.

1.9.3 *Grhl* orthologues in zebrafish

Unlike mouse and humans, the zebrafish has four orthologues namely, *grhl1*, *grhl2a, grhl2b* and *grhl3. grhl1* is dispensable for epidermal formation and function (Janicke, Renisch et al. 2010), however, it is known to play a pivotal role in the development of inner ear epithelia (Liu, Yang et al. 2015). *grhl2a* may be responsible for trunk and notochord patterning, as well as axial extension, while *grhl2b* plays an integral role in midbrain-hindbrain boundary (MHB) patterning and inner ear development (Han, Mu et al. 2011). Similar to *grhl2b*, *grhl3* is also responsible for MHB morphogenesis and is strongly and specifically expressed in all cells of the EVL during early EVL establishment and migration, at the maternal-zygotic transition phase (Miles, Darido et al. 2017). Furthermore, *grhl3* mis-expression leads to severe defects in subsequent epithelial development, including disrupted body axis formation, organism size, and cellular defects (particularly in the developing skin), highly consistent with aberrant EVL shape and morphology in early development (Miles, Darido et al. 2017). These exciting findings shed new light on the roles this family plays in epithelial development, and importantly, allows to define the molecular networks which underpin epithelial establishment.

1.10 *grhl3*$^{-/-}$ zebrafish

The *grhl3*$^{-/-}$ zebrafish line was generated by Dr. Lee Miles (former Post-Doctoral fellow, La Trobe University, Melbourne, Australia) using CRISPR-Cas9 mediated deletion (Miles, Darido et al. 2017). 3 *grhl3*$^{-/-}$ lines were generated and maintained: *grhl3*$^{-/-(+14bp)}$; *grhl3*$^{-/-(-31bp)}$ and *grhl3*$^{-/-(1-\Delta4)}$. Null embryos from all these lines were indistinguishable from each other, and these results are presented in chapter 3.

Initially, when housed at Monash University, where these lines were originally generated, the *grhl3*$^{-/-}$ embryos showed poor periderm integrity, culminating in periderm rupture and death by 11 hpf (Miles, Darido et al. 2017). A delay in development was also noted at 8 hpf (75% epiboly) resulting in premature contraction of the actin ring. Furthermore, ventral epithelial migration was significantly delayed, and the cell size was concomitantly decreased in the *grhl3*$^{-/-}$ embryos, clearly indicative of the dynamic cellular disruption

responsible for epithelial establishment (Miles, Darido et al. 2017). Following a 6-month period, *grhl3*$^{+/-}$ adults of all three fish lines were brought over and maintained at the La Trobe Animal Research and Teaching Facility (LARTF), Bundoora, VIC, Australia. Characterization of *grhl3*$^{-/-}$ embryos when monitored at LARTF showed the disappearance of the rupturing phenotype observed during somitogenesis, with subsequent rescue of lethality at this timepoint. *grhl3*$^{-/-}$ embryos displayed normal development until 19 hpf and exhibited a slight bend in the notochord from the onset of 19 hpf (Miles et al. 2017, unpublished). Lastly, null embryos survived well through early larval stages, displaying wide range of phenotypes such as fin fold defects, severe axial distension and shortening of body length (detailed in chapter 3).

The exact reason for the better survival and disappearance of the rupturing phenotype at LARTF is still unknown. Preliminary studies done at Monash University by Dr. Lee Miles showed disappearance of the rupturing phenotype in *grhl3*$^{-/-}$ embryos when incubated at 25°C as opposed to development at normal temperature (28.5°C). Therefore, I believe the better survival of *grhl3*$^{-/-}$ embryos might be due to the environmental factors such as temperature and variances in water quality between the Monash and La Trobe Aquatic Facility. This indicates that the development of *grhl3*$^{-/-}$ embryos is heavily influenced by environmental factors and could potentially act an excellent model system to understand the role of environmental factors in epithelial development, much like the *Grhl3*$^{-/-}$ mouse model (Ting, Wilanowski et al. 2003).

1.11 Rationale and aims of present study

1. To characterize the role of *grhl3* in epithelial development using CRISPR-generated *grhl3* zebrafish knockout lines.
2. To identify *grhl3*-dependent Gene Regulatory Networks (GRN) in epithelial development via in-silico analysis (PHYLO-PROM) and meta-analysis of published *grh* and *Grhl* RNA-SEQ datasets.
3. To determine the functional role of *grhl3*-target genes (*pvrl4,tbc1d2 tmem54a,* and *gldc*) in epithelial development by performing morpholino-mediated knockdown and generating zebrafish CRISPR knockout lines of candidate genes of *grhl3*. Additionally, performing rescue experiments with mRNA of differentially regulated genes of *grhl* in *grhl3*$^{-/-}$embryos. These genes (*pvrl4, tbc1d2 tmem54a,* and *gldc*)

were selected based on predictive in silico modelling, meta-analysis and identified implications in human diseases.

4. To understand the effects of polyphenols, vitamins, and minerals on the development of *grhl3*-deficient epithelia and to investigate potential gene-environment interactions (GEI) in epithelial development.

Chapter 2: Materials and methods

2.1 Materials

2.1.1 Solutions

Table 2.1 List of solutions used in this study. This table lists the names and composition of solutions referred to in the methods section and provides other details such as concentration, supplier, and catalogue number.

Solution	Components/Diluents and other specifications	Supplier & Catalogue no.
General lab solutions		
70% Ethanol	70% (v/v) Ethanol in Milli Q water	ChemSupply (Cat.# AL048)
4% PFA Paraformaldehyde	40 g PFA 80 ml of 10x PBS 720 ml dH_2O Add 1 N NaOH until the solution clears.	Sigma Aldrich (Cat.# 158127)
10x PBS Phosphate Buffered Saline	8% (w/v) NaCl 0.2% (w/v) KCl 1.44% (w/v) Na_2HPO_4 0.24% (w/v) KH_2PO_4	Sigma Aldrich (Cat.# S9625) Sigma Aldrich (Cat.# P3911) Sigma Aldrich (Cat.# S9763) Sigma Aldrich (Cat.# P0662)
1x PBST Phosphate Buffered Saline/Tween	100 ml 10x PBS 855 ml M.Q water 5 ml Tween 20	Sigma Aldrich (Cat.# P1379)
Zebrafish maintenance		
1x E3 medium	5 mM NaCl 0.17 mM KCl 0.33 mM $CaCl_2$ 0.33 mM $MgSO_4$	Sigma Aldrich (Cat.# S9625) Sigma Aldrich (Cat.# P3911) Sigma Aldrich (Cat.# 449709) Sigma Aldrich (Cat.# M7506)
10% AQUI-S® Aquatic anaesthetic	1 ml AQUI-S in 9 ml dH_2O	AQUI-S®
Genotyping		
50mM NaOH	0.2 g NaOH in 100 ml M.Q water	Sigma Aldrich (Cat.# SL178)
1M Tris-HCl (pH 8)	15.76 g in 100 ml M.Q water	Sigma Aldrich (Cat.# 10812846001)
Cloning		
LB media	20 gm LB media powder in 1 L M.Q water	Sigma Aldrich (Cat.#L3022)

Table 2.1 List of solutions used in this study (contd.)

Solution	Components/Diluents and other specifications	Supplier & Catalogue no.
In-situ hybridization		
20x SSC	175.3 g NaCl	Sigma Aldrich (Cat.# S9625)
Saline-Sodium Citrate	88.2 g Na_3-citrate	Sigma Aldrich (Cat.# S4641)
	800 ml dH_2O	
	Adjust the pH to 7.0 with 1 M HCl and add	
	dH_2O water to make up 1 litre.	
Proteinase K	20 mg Proteinase K	Sigma Aldrich (Cat.# P2308)
	1 ml M.Q water	
Prehybridization Buffer	250 ml 20x SSC	Sigma Aldrich (Cat.# F9037)
(HYB-)	500 ml Formamide	Sigma Aldrich (Cat.# P1379)
	1 ml Tween-20	
	250 ml distilled water	
Hybridisation Buffer (HYB+)	499.5 ml HYB- buffer	Sigma Aldrich (Cat.# R6625)
	5 mg/ml Torula RNA powder	Sigma Aldrich (Cat.#H3393)
	500 μl of 50 mg/ml heparin	
2x SSCT / 50% formamide	50 ml of 20 x SSC	
	250 ml of Formamide	Sigma Aldrich (Cat.# F9037)
	500 μl of Tween-20	Sigma Aldrich (Cat.# P1379)
	200 ml of dH_2O water	
Riboprobe solution	RNA probe (30-50 ng/µl)	
	HYB+ solution	
Blocking Reagent	5% Fetal Calf Serum	Sigma Aldrich (Cat.# F2442)
	2 mg/ml of Bovine Serum Albumin	Sigma Aldrich (Cat.# A7030)
	1% Dimethyl Sulfoxide (DMSO) in PBST	
Stain buffer	100 mM Tris pH 9.5	Sigma Aldrich (Cat.#T1503)
	50 mM $MgCl_2$	Sigma Aldrich (Cat.#M8266)
	100 mM NaCl	Sigma Aldrich (Cat.# S9625)
	0.1% Tween-20	Sigma Aldrich (Cat.# P1379)
	1 mM Levamisol	Sigma Aldrich (Cat.# BP212)
	Make up to required volume with distilled water.	
Actual stain substrate	0.33 mg/ml Nitro blue tetrazolium (NBT)	Roche (Cat.# 11681451001)
	0.17 mg/ml 5-bromo-4-chloro-3-indolyl phosphate (BCIP)	
	Diluted in stain buffer	

Table 2.1 List of solutions used in this study (contd.)

Solution	Components/Diluents and other specifications	Supplier & Catalogue no.
Histology and immunohistochemistry		
25% sucrose	25 g sucrose dissolved in 100 ml 1x PBS	Sigma Aldrich (Cat.# S7903)
35% sucrose	35 g sucrose dissolved in 100 ml 1x PBS	Sigma Aldrich (Cat.# S7903)
Blocking solution	2.5 ml 10x PBS	
	1.5 ml Normal Goat serum	Sigma Aldrich (Cat.# G9023)
	250 µl 0.2% Tween 20	Sigma Aldrich (Cat.# P1379)
	20.8 ml M.Q. water	
Staining		
0.1% Alcian Blue	0.1 g Alcian blue	Sigma Aldrich (Cat.# A5268)
	30 ml acetic acid	ChemSupply (Cat.# 695092)
	70 ml dH$_2$0	
	Solution filtered through Whatman filter paper	
Acid alcohol	70% ethanol	ChemSupply (Cat.# AL048)
	1% HCl	ChemSupply (Cat.# RP1104)
Bleaching solution	3% H$_2$0$_2$	Sigma Aldrich (Cat.# H1009)
	1% KOH solution	
Microinjection		
0.1 M KCl	0.75 g KCl in 100 ml M.Q water	Sigma Aldrich (Cat.# P3911)
0.5% Phenol red	0.25 gm phenol red in 50 ml 1x PBS	Sigma Aldrich (Cat.# 114529)

Table 2.2 Antibodies and stains used in immunohistochemistry.

Antibody/stain Name	Target species	Concentration	Provider & Catologue no.
Anti-Fibronectin	Human	1:200	Sigma Aldrich(Cat # F3648)
Anti-E-cadherin	Zebrafish	1:200	GenTex (Cat # GTX125890)
Donkey anti-rabbit 488	Rabbit	1:1000	Abcam (Cat # ab150073)
NucBlue™ Fixed Cell ReadyProbes™ Reagent (DAPI)	-	1:1000	Invitrogen (Cat # R37606)
Rhodamine Phalloidin	-	1:1000	ThermoFisher (Cat # R415)

2.1.2 Plasmids and constructs

pCS2+MCS

pCS2+GFP was a kind gift from A/Prof. Joan Heath; GFP was excised from pCS2+GFP by EcoRI/XbaI digestion. A 115-base pair fragment of the multiple cloning site (MCS) of pSL1180 (EcoRI/XbaI), was excised and ligated into the EcoRI/Xba1 sites of pCS2+ (Wettstein, Turner et al. 1997) resulting a vector with an increased number of restriction sites (including Xma1) for subsequent cloning steps. pCS2+ was used as it contains a 5' Xenopus β-globin UTR and 3' poly-A tail sequences which confer stability to newly synthesized mRNAs in-vivo (especially in Zebrafish and Xenopu*s*) by preventing degradation.

2.1.3 PCR oligonucleotides

The sequences of oligonucleotide sequences used throughout this study are listed in Table 2.3. Oligonucleotides were synthesized by Integrated DNA Technologies (Singapore).

Table 2.3 Oligonucleotides used in this study.

Zebrafish gene	Forward primer	Reverse primer
For genotyping		
grhl3 e4	CAGCTCTTCCCCTGAACTTG	ACATAAATGCGGACCTCAGG
grhl3 +14bp R	-	TGCCATGATTTCTGCTACAACA
grhl3 1-4del	GCCAACCTGCCAGATGGATTA	TAAATGCGGACCTCAGGTGT
tbc1d2 e3	GTTGTCACTGAACGAATGTGC	TAACTGAATGTGGCCCGAGT
klhdc8a e2	TTTCCAGTGCACGCGTCTAT	CTGTTCCTTCCCCATCCCAC
For RT-PCR		
cldn23a	CAACCAACAAGGCAACGACC	CAAGCCGAGAGCAGTTACGA
cldn23b	TTTCCCCACTCCCCAAATCG	CCAGATCGATTGACTCCCCG
ppl	CTGTGGCCAGTGCTGACA	TCCTGTACTCTCCTTCTTGAGC
prom2	AGGACCTTTGCTTGGTGGAT	GCATCAATCTTGGGTTTCGGC
Gm3579 (exd2)	CCACTGAGCCCATTCTAGCC	GACACACGAACTCTTTTTACCCA
oclna	GGTCTGCTGGCTGACTATCC	GACTGAATTACGGACGGGCA
oclnb	CTCTCAAGGCATCGGGGAAT	GGAGGATATTCATCTGTGTCAAGC
slc6a19a.1	TCAGCAGCTCAACATCAGCA	ATCTCTTGGGCAGCAGGTTC
slc6a19a.2	CATCGATTTACGCCGCCATC	CAGAAACGTCTGCATGTCGC
slc6a19b	CCTTGGCTTGTCCTCCATGT	GTCAAATAGGGCCAGCCAGT
aldh1a3	TTCCTGGATTTGGACCGACG	ATAGACTCGTGATGCAGCGG
sod3a	ACATTCTCCGAGTTCAGACGG	CCTCTTTGTATGTGAAGCGCC
sod3b	TGGCCCAAAGGAAAAGCTGA	GGATTCCAGTGACTGCCGAA
car6 (ca6)	GACCCTGTGGAACGACTACC	GCTTGCCTTGAACCGCTTTT
cldna	CGCTGTTGATTATTGGCGGG	CCCTTGGTTCCTCCAGATCG
cldnb	GGTGCCTCAGCTCTGTTGAT	AAGTTCTTTCCGGAGGGTGC
evlpa	CACTAAACCGCACTGACCCT	TTGGGCTGCAACTCTCTGTT
evlpb	AGACGTTCACTGAGTCGCTG	TTACCTTCTCACCGCGCTTT
ef1α	TTGGAAACGGATATGCTCCA	TCCTTACCTGAACGCCTGTCA

For synthesis of FL mRNA		
	Primer Sequence	
FL pvrl4 EcoRI-F	CAGCGAGAAAGTTGATCAACG	
FL pvrl4 XhoI-R	GTCTTAAAGCAGTCACGCAGG	
FL tbc1d2 EcoRI-F	TAGTGCCATCCGGACAAACAC	
FL tbc1d2 XhoI-R	TCGTACAGCTTTGGTAACATATC	
FL cldnb BamHI-F	GATCCAAGCATGGCATCAACCGG	
FL cldnb NheI-R	CCACAAAGTTCTTTCCGGAG	
FL ovol1a EcoRI-F	CCTACCGAGAGGAGACTGAAG	
FL ovol1a XhoI-R	CCTCTTTTTACATTTCCGTTGAC	

2.1.4 Morpholinos

Table 2.4 Morpholinos used in this study.

Gene	Stock conc.	Working conc.	Provider
pvrl4		100 µM, 150 µM, 200 µM, 300 µM, 500 µM, 600 µM	GeneTools
gldc		100 µM, 250 µM, 500 µM	GeneTools
tmem54a	1 mM	100 µM, 250 µM, 500 µM	GeneTools
tmem54b		100 µM, 250 µM, 500 µM	GeneTools
myoVb		200 µM	GeneTools

2.1.5 Vitamins, minerals, and polyphenols

Table 2.5 Environmental factors used in this study.

This table lists the environmental factor tested along with the concentration of the stock and working solutions.

Environmental factor	Stock conc.	Working conc.	Provider & Catalogue number
Vitamin/Mineral			
Myoinositol	0.5 M	6.75 mg/mL, 12.5 mg/mL, 25 mg/mL, 37.5 mg/mL, 50 mg/mL, 75 mg/mL.	Sigma Aldrich (I5125)
Nicotinamide	10 mM	1 µM, 2.5 µM, 5 µM, 10 µM, 20 µM.	Sigma Aldrich (N0636)
Thiamine	10 mM	1 µM, 2.5 µM, 5 µM, 10 µM, 20 µM.	Sigma Aldrich (T1270)
Cobalamin	10 mM	1 µM, 2.5 µM, 5 µM, 10 µM, 20 µM.	Sigma Aldrich (V6629)
Potassium Iodide	166 mg/mL	2.5 mg/mL, 5 mg/mL, 10 mg/mL	Sigma Aldrich (207969)
Polyphenol			
Resveratrol	1 mM	50 µM, 100 µM, 150 µM, 200 µM.	Sigma Aldrich (R5010)
Curcumin	10 mM	1 µM, 2 µM, 3 µM, 4 µM.	Sigma Aldrich (C1386)
Luteolin	10 mM	1 µM, 2.5 µM, 5 µM, 10 µM, 20 µM.	Sigma Aldrich (L9283)

2.1.6 Zebrafish

All zebrafish experiments were conducted in accordance with La Trobe University guidelines for the care and housing of zebrafish, under Animal Ethics Committee approval number AEC16-91 and OGTR NLRD approval number GMSC16-91. The CRISPR knockout zebrafish lines used in the study (*grhl3 and tbc1d2)* were designed and generated by Dr. Lee Miles, former Post-Doctoral fellow, La Trobe University, VIC, Australia.

The facility was maintained at 25ºC (± 3ºC) with a humidity of 50%. To mimic the day-night cycle, lights were automated to be turned on in the morning at 7:00 am and turned off at 9:00 pm, thereby following a light schedule of 14 h. The water conditions were kept at 26ºC (± 2°C) with a pH between 6.5-8.5 with minimal fluctuations to water hardness and conductivity. Fish were housed in stand-alone systems with self-cleaning drum filter to prevent the spread of infections between lines in the event of a disease outbreak.

2.2 Characterization of zebrafish lines

2.2.1 Fish husbandry and collection of embryos

Adult zebrafish were maintained in accordance with ethical and fish maintenance procedures at La Trobe University, Bundoora. Zebrafish of 3 months of age were used for breeding. To mimic the natural, shallow water breeding conditions of zebrafish, breeding tanks were placed within larger tanks. The male and females were used in a ratio of 1:2 and separated with the help a divider prior to the day of embryo collection. Adult breeders were maintained on a 14:10 light/dark cycle; when lights were switched on, females would lay eggs falling to the bottom of the tank though the perforations in the breeding tanks. The tank water was then strained through a nylon mesh strainer and the eggs were washed gently with embryo medium. The collected embryos were maintained in a Petri dish containing egg water at 28°C.

2.2.2 Quantitation of body length

grhl3$^{+/-}$ fish were set-up and embryos were collected as described in section 2.2.1. Dead and unfertilized embryos were discarded at 6 hpf. At 24 hpf, the number of live and dead embryos were recorded and following this time-point, the number of dead embryos were counted every day until 72 hpf for plotting the survival graph. At 48 hpf and 72 hpf,

embryos were dechorionated gently using a pair of forceps and imaged using the Nikon Camera DS-Ri2 connected to the Nikon SZM 18 Fluorescence microscope. Finally, the body length of phenotypically distinct embryos was quantitated using NIS-Elements® Imaging software and ImageJ to detect any variations in body length.

2.2.3 Time course analyses of zebrafish embryos

grhl3$^{+/-}$ and WT fish were set-up and embryos were collected as described in section 2.2.1. Unfertilized and dead embryos were removed at 6 hpf to ensure a healthy, viable environment for the development of live embryos. At 3 dpf, embryos obtained from *grhl3*$^{+/-}$ in-crosses were classified as either "phenotypic" or "non-phenotypic" embryos. The phenotypic population comprised primarily homozygous mutants and non-phenotypic embryos comprised both heterozygous and wild-type embryos. On day 5, the embryos were transferred to 1 L tanks and fed with microscopic multicellular aquatic invertebrates ("rotifers") that act as an excellent food-source for the growing zebrafish larvae. They were monitored until all the larvae die, to determine the maximum survival age of the mutants (Figure 2.1).
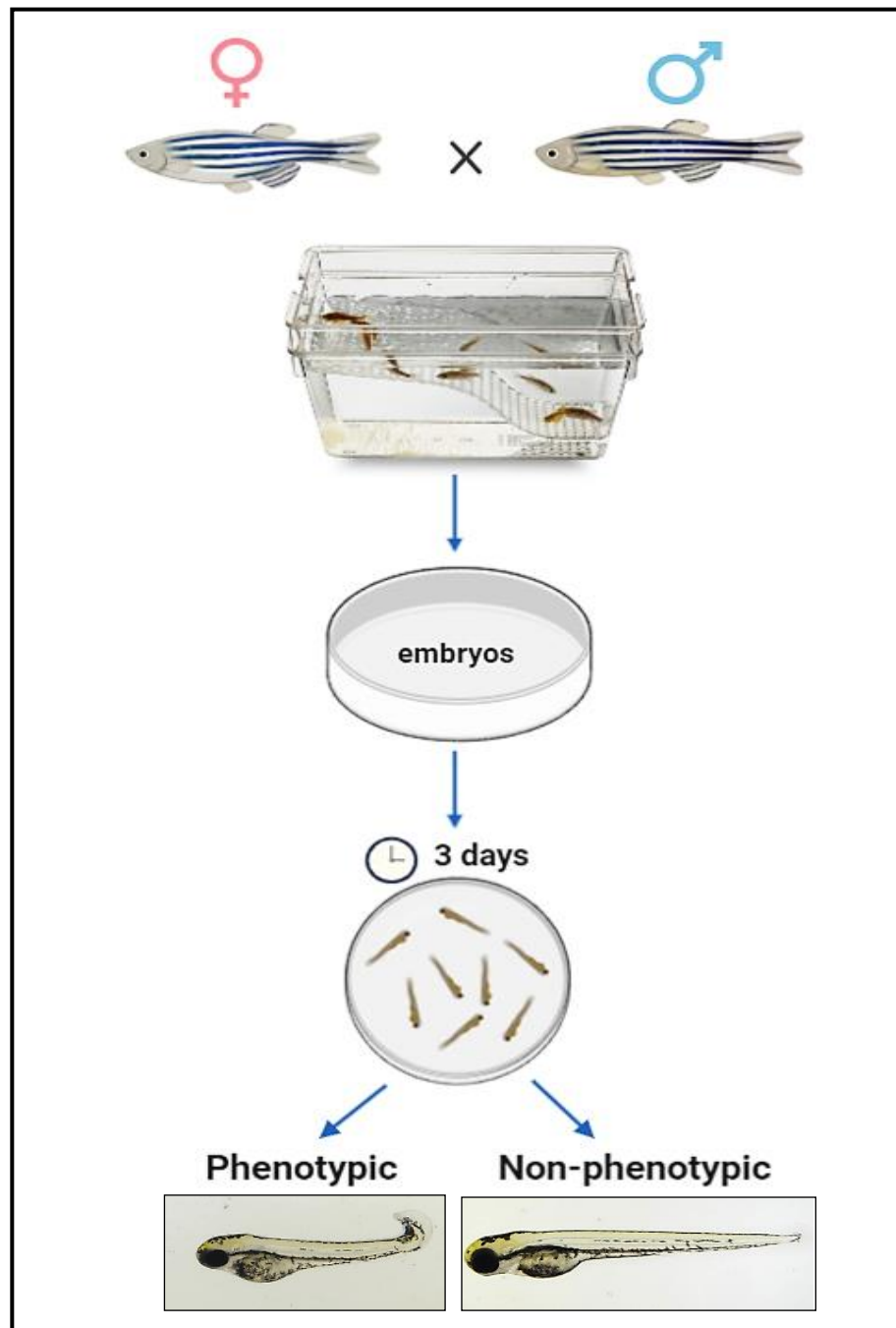
Figure 2.1 Schematic diagram showing the experimental set-up for the determination of maximum survival age of *grhl3* mutants.

(**A**) Males and females were used in a ratio of 1:2 and placed in a breeding tank separated with the help a divider. Following morning, divider was removed to allow mating of fish. Embryos deposited at the bottom of tank were collected and monitored. (**B**) At 3 dpf, embryos derived from inter-crossing *grhl3*^{+/-} fish were categorized into non-phenotypic siblings and phenotypic mutants and were monitored until death.

2.3 Bioinformatics techniques

2.3.1 Literature survey, collation of datasets and database creation

An extensive literature survey led to the identification of 41 *grh/Grhl* RNA-Seq and microarray datasets that had previously been generated from both *Drosophila* and mouse tissues, as well as several human cancer/short-hairpin RNA (shRNA) cell lines (Mathiyalagan, Miles et al. 2019). These datasets were collated and analysed for *Grhl*-dependent gene regulation based on the fold change difference.

The datasets from individual studies were converted to a common file format (.csv) (Figure 2.2 A) and imported into MySQL (**www.mysql.com**), a relational database management system that enables the identification of relationships between datasets (Figure 2.2 B). Inside the database, the data were combined into species-specific tables. Using information from Ensembl v.91, gene symbols from the original human data files were mapped to the human Ensembl gene_stable_ids; gene symbols from other species were mapped to human gene symbols and gene_stable_ids of their orthologous human genes (Figure 2.2 E). After mapping, all the human-mapped data were joined together into a single table, searchable by the original gene symbol in every species, as well as the gene symbol and gene_stable_id of the human orthologue, publication name, dataset name, type of *Grhl* regulator, and direction of *Grhl* regulation (positive or negative) and were designated as being derived from either "cell-line" or "tissue". For interactive visualization and exploring, the data were exported from the MySQL database, re-structured and uploaded into the Ordino tool (**https://ordino.caleydoapp.org**)(Figure 2.2 F). Database creation was done primarily by Ms. Agata Charzynska (Nencki Institute of Experimental Biology, Polish Academy of Sciences, Warsaw, Poland) and Dr. Michal Dabrowski (Nencki Institute of Experimental Biology, Polish Academy of Sciences, Warsaw, Poland), who are experts in the field of bioinformatics.
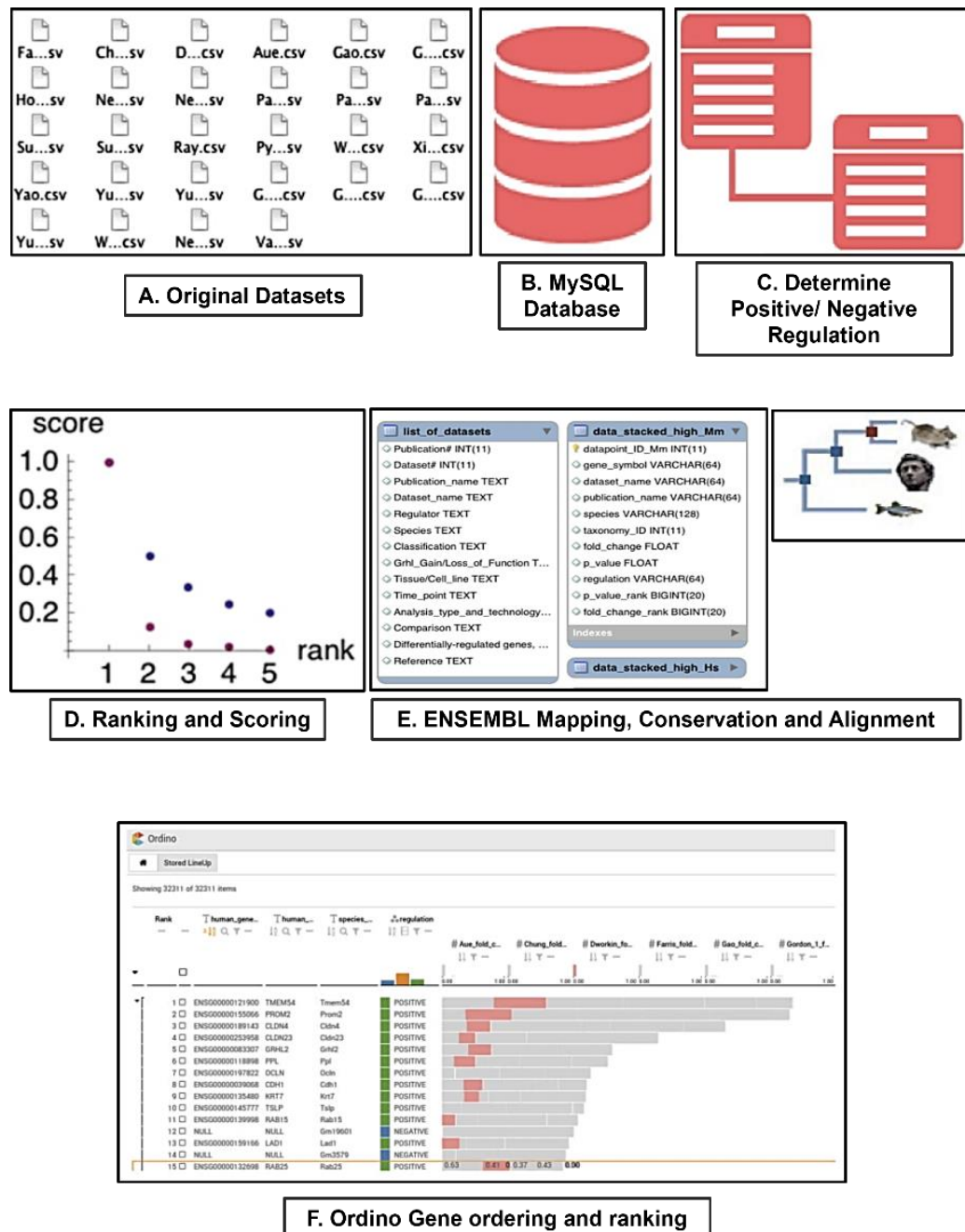
Figure 2.2 Meta-analysis pipeline methodology.

All published *grh/Grhl* Microarray/RNA-SEQ datasets were converted to a common file format (.csv) **(A)** and imported into MySQL **(B)**. Next, I determined whether genes within each dataset were positively or negatively regulated following functional modulation of *grh/Grhl* **(C)**, and genes across the datasets were ranked according to their regulation within each dataset. To achieve a common gene ranking, the fold change rank-based scores from individual datasets were aggregated into the sum of scores for each gene, separately for positively and negatively regulated genes **(D)**. Each gene symbol within all datasets was mapped to the appropriate gene using Ensembl. After mapping, a table of all the human-mapped data was generated, searchable by the original gene symbol in every species **(E)**. For interactive visualization and exploring, the data were exported from the MySQL database, re-structured and uploaded into Ordino **(F)**.

2.3.2 Scoring and gene ranking

To achieve a common gene ranking, Ms. Charzynska and Dr. Dabrowski aggregated the fold change rank-based scores from individual datasets to the sum of scores for each gene, separately for positively and negatively regulated genes. For datasets where p-values/false discovery rates (FDRs) were available, another set of scores, based on p-value/FDR ranks, and computed independently for positively and negatively regulated genes, are also available. For singular genes, and the direction of regulation, *p*-values/FDRs from multiple datasets were combined into a single p-value, using the standard Fisher's method. The ranks were then transformed into normalised scores that permitted aggregation of rank-based information from datasets comprising different numbers of genes. In order to do this, scoring function $f(r) = 1/r^k$ was used, where k was an arbitrary parameter, allowing us to determine the significance of a genes' rank across datasets. The constant of k = 3 was chosen, as it balanced the number of datasets that a given gene appeared in with instances in which this gene was highly ranked within an individual dataset (Figure 2.2 D). Therefore, the top ranked gene (Rank #1) within a given dataset would achieve a normalised score of 1 ($1/1^3$), whereas, if a gene did not appear within a particular dataset, it would be given a score of 0.

2.4 Molecular techniques

2.4.1 Real time PCR

2.4.1.1 RNA Extraction

RNA was extracted using Trizol (Invitrogen), according to the manufacturer's instructions. Briefly, total RNA was extracted on ice by adding minimum 300 µl Trizol/20 embryos and mixed well, ensuring embryo homogenisation by pipetting the lysate using 25- and 35-gauge syringe needles repeatedly. 1/10 volume of chloroform was added, the sample was mixed well and incubated on ice for 5 minutes. The sample was then centrifuged at 12,000 x g for 15 minutes at 4°C and the aqueous phase was transferred to a fresh Eppendorf tube. An equal volume of isopropanol was added to the aqueous phase and incubated for a minimum of 16 hours at -20°C. This was followed by centrifugation at 12,000 x g for 30 minutes at 4°C. The supernatant was removed, and RNA pellet was washed with 75% ethanol, briefly air dried and re-suspended in 20 µl sterile water.

2.4.1.2   Reverse Transcription and first strand cDNA synthesis

cDNA was synthesized by incubating ~1 µg RNA template with 5x iScript reaction mix, 1 µl iScript reverse transcriptase enzyme, 4 µl iScript Reaction Mix and finally the reaction was made up to 20 µl with MilliQ water. The reaction mix was incubated in a thermal cycler according to manufacturer's instructions (Bio-Rad, CA, USA; 25°C for 5 minutes, 46°C for 20 minutes, 95°C for 1 minute). The resultant cDNA was stored at - 20°C.

2.4.1.3   Real Time Polymerase Chain Reaction (RT-PCR)

1.5 mM working stock solution of primers was prepared for both the forward and reverse primers for each gene. A master mix was prepared using 0.4 µl of cDNA or RNase free water, 4.6 µl RNase free water and 5 µl Ssofast EvaGreen supermix (Bio-Rad, CA, USA). 8 µl of master mix solution was added to 2 µl of working primer stock to each well of a 96-well plate. Real time PCR was performed in triplicates for each gene. PCR was performed using the following conditions for 40 cycles, using a Bio-Rad CFX96 Real-System/C1000 Thermal Cycler: 95°C – 30 sec; 95°C - 5 sec; 60°C - 20 sec; and 95°C for 5 sec. Finally, the expression of all genes was normalised to the EF1α housekeeping gene to determine the relative levels of mRNA transcripts.

2.4.2 Genotyping zebrafish lines

2.4.2.1   Fin clipping

A tank filled with ~1 L system water was placed on the bench top. 1.5 ml 10% AQUI-S (aquatic anaesthetic) was added to the tank using a Pasteur pipette and mixed gently. Fish were anaesthetized by immersing in tank containing AQUI-S until the fish stopped moving (2-5 minutes). The anesthetized fish was then placed flat on the palm of the hand and a small portion of the fin was cut with a pair of sharp scissors or scalpel. Following this step, the fish was returned to a separate tank with fresh system water and the excised portion of the fin was placed at the bottom of a PCR tube. The tank was numbered along with the PCR tube containing the excised fin. This was done to identify the fish from where the DNA was extracted. Fish were housed in individual tanks until the genotypes were confirmed.

2.4.2.2   DNA Extraction

50 μl of 50 mM NaOH was added to the fin clips present in the PCR tubes. After this, they were incubated at 95°C for 10 minutes. This was then followed by neutralization with 5 μl (~1/10th the volume of NaOH) of Tris-HCl (pH 8.0). Finally, the mixture was vortexed, and was given a quick spin to ensure neutralization was complete. The extracted genomic DNA was stored at 4°C, until further use.

2.4.2.3   PCR

1 μl genomic DNA was combined with 10 μl GoTaq® Green Master Mix (Promega), 0.5 μl forward primer and 0.5 μl reverse primer in a final volume of 20 μl (made up with sterile water). The primers used for genotyping the *grhl3* and *tbc1d2* lines are listed in Table 2.3. PCR was performed using Bio-Rad C1000™ Thermal Cycler with an initial denaturation step of 95°C for 3 minutes, followed by 34 cycles of 95°C for 30 sec, 60°C/56°C for 30 sec and 72°C for 20 sec, before a final extension step of 72°C for 5 minutes.

2.4.2.4   Agarose Gel electrophoresis

To make a 3% gel, 3 g agarose was suspended in 100 ml distilled water and boiled until the agarose was completely dissolved. After 2 minutes of cooling, 1 μl SyBR Safe (Thermo Fisher) was added, mixed well and the gel was poured into a gel tray containing 20-well gel cassette combs. The gel was allowed to cool for 15-20 minutes, followed by the removal of gel combs to create wells. The samples were then loaded carefully into the wells and the gel was electrophoresed at 90 V for 1 hour. Gel was imaged using the Bio-Rad Molecular Imager® ChemiDoc™.

2.4.3 Generation of RNA probes via TOPO-Cloning

2.4.3.1   Amplification of the gene insert via PCR

500 ng DNA template, 10 μl 5x HF buffer (ThermoFisher Scientific), 1 μl 50 mM dNTPS (deoxynucleotide triphosphates) (ThermoFisher Scientific), 1.25 μl of the respective 10 μM forward and reverse primers for the gene of interest, 0.5 μl Phusion polymerase (1 unit/μl)(ThermoFisher Scientific) were taken in a PCR reaction tube and made up to 50 μl with M.Q. water. The PCR reaction was subjected an initial denaturation step of 94°C for 2 minutes and 30 seconds, followed by 35 cycles of 94°C for 30 seconds, 65°C for 1

minute, 72°C for 2-minute 30 sec, before a final extension of 72°C for 7 minutes using the Bio-Rad C1000™ Thermal Cycler.

2.4.3.2 Insertion of PCR-amplified DNA fragment into the pCRII-TOPO plasmid via TOPO-isomerase mediated cloning

4 µl of the PCR product generated in the previous section, 1 µl salt solution, and 1 µl TOPO® vector from the TOPO® TA Cloning® Kit (ThermoFisher Scientific) was added into a PCR tube and mixed gently. The reaction mix was incubated at room temperature for 30 minutes.

2.4.3.3 Bacterial transformation by heat shock

After performing the TOPO cloning reaction, the plasmid was transformed into DH5α *E. coli* cells. The DH5α *E. coli* cells were thawed on ice and 15-20 µl *E. coli* cells were added to 2 µl of the TOPO cloning reaction and mixed gently. Care was taken to make sure the reaction was performed on ice and with sterile tips kept at -20°C to prevent any form of contamination. The reaction was incubated for 30 minutes on ice, followed by heat shock of the cells for 30 seconds at 42°C without shaking. The reaction was immediately incubated on ice for 30 minutes. Following the incubation, 1 ml of Luria-Bertani (LB) medium was added to the transformation reaction. The tubes were capped tightly and incubated in an orbital shaker at 37°C for 1 hour at 200 rpm.

LB plates were prepared by dissolving 15 g/l LB agar in distilled water. The solution was autoclaved at 15 psi for 20 minutes and was allowed to cool to ~50°C. 50 µg/ml ampicillin was added to the solution and mixed well. The solution was then poured into Petri plates (~10-20 ml per plate) and allowed to set. 40 mg/ml X gaL was added to the plate and spread across evenly using a glass spreader. The plates were then allowed to dry and stored at 4°C. 50 µl from each transformation reaction was plated on to the LB plate and incubated at 37°C overnight. Only transformed cells would survive, while non-transformed bacteria would not survive, owing to ampicillin antibiotic selection.

2.4.3.4 Selection of successful recombinant plasmids

LacZ is crucial for the synthesis of β- galactosidase, an enzyme that helps break down the chromogenic substrate X gal to form the blue pigment 5,5'-dibromo-4,4'-dichloro-indigo. Upon successful recombination, lacZ sequence is disrupted following insertion of the

DNA fragment, whereby breakdown of X-gal fails to take place, resulting in the formation of white colonies. Several white colonies were seen on the LB plate suggesting successful transformation.

5-15 white colonies were selected from each plate to perform colony PCR to screen for successful integration of DNA fragment. Colony PCR was performed to identify the plasmids into which the DNA fragment had been successfully inserted. For setting up a colony PCR reaction mix, 10 µl GoTaq®, 8 µl M.Q water and 0.5 µl each of the forward and reverse primer for the gene of interest was added to a fresh PCR tube. A small portion of the white colony to be screened was scraped using a pipette tip and mixed well with the reaction mix. PCR reaction was then subjected to an initial denaturation of 95°C for 5 minutes, followed by 39 cycles of 95°C for 30 seconds, 50°C for 30 seconds, 72°C for 1 minute and a final extension of 72°C for 5 minutes.

A 1% gel was run as described in section 2.4.2.4 to visualize the colony PCR products and determine the relative size of recombinant plasmids. The successful recombinants containing correct insert were grown up for larger scale extraction in 5 ml Luria broth media supplemented with 50 mg/ml Ampicillin (Sigma; LB-Amp). These were incubated for 16-hours at 37°C with vigorous shaking (200-250 rpm).

2.4.3.5 Purification of the plasmid DNA (MINI prep)

Plasmids were purified using the PureYield™ Plasmid Miniprep System (Promega) according to manufacturer's instructions. The bacterial culture was centrifuged at 10,000 x g for 5 minutes. The supernatant was removed, and the bacterial pellet was re-suspended in 600 µl M.Q. water. The bacterial culture was transferred to a 1.5 ml Eppendorf tube, followed by addition of 100 µl cell lysis buffer to the bacterial culture. The tube was inverted 6 times and the solution turned opaque to clear blue, signifying complete lysis. 350 µl of cold neutralization solution was added and mixed thoroughly until a yellow precipitate formed, and the solution turned clear. This was followed by centrifugation at maximum speed for 3 minutes. The supernatant was carefully transferred to a PureYield™ Minicolumn placed on a PureYield™ Collection tube and centrifuged using a microcentrifuge at maximum speed for 15 seconds. The column was washed by adding 400 µl of column wash solution to the column and centrifuged for 30 seconds. The Minicolumn was finally transferred to a fresh 1.5 ml Eppendorf tube and 30 µl sterile water was added to the centre of the Minicolumn matrix. This was allowed to stand for 1

minute at room temperature, after which it was centrifuged at 13,000 x g for a minute for the elution of plasmid DNA. DNA was stored at -20°C.

2.4.3.6 DNA Sequencing

50 ng of the purified plasmid was combined with 1 μl of 3.2 pmol of appropriate forward primer in a PCR tube and incubated at 95°C for 10 minutes for drying. The tubes were capped and sent for sequencing. Sequencing was performed at the Garvan Institute of Medical Research, New South Wales, Australia.

The plasmids with the correct sequence were inoculated into and grown in Luria Broth. Plasmids were purified using the PureYield™ Plasmid Miniprep System as described in section 2.4.3.5.

2.4.3.7 Restriction Digestion

Restriction digestion was performed for linearizing the circular plasmid. The appropriate restriction enzyme for plasmid digestion was determined by vector map analysis. 10 μg plasmid DNA was combined with 5 μl 10x transcription buffer, and 2 μl restriction enzyme, in a final volume of 50 μl (with M.Q water). The reaction was incubated at 37°C for 2-2.5 hours. 1 μl of the reaction was run on a 1% gel, to see whether the plasmid has been linearized. A single band signified that the plasmid had been linearized. The plasmid was purified using the QIAquick® PCR Purification Kit (QIAGEN) according to manufacturer's instructions. The purified, linearized plasmid was eluted in 20 μl sterile water.

2.4.3.8 RNA Probe synthesis

Digoxigenin (DIG)-labelled riboprobes were synthesized using the DIG-RNA labelling kit (Roche) according to manufacturer's instructions. Briefly, 1 μg of linearized template DNA was incubated with 2 μl 10x transcription buffer, 2 μl DIG labelling mix, 1 μl RNAsin (Promega), 2 μl of T3, T7 or Sp6 polymerase (Promega) in a final volume of 20 μl (with water) at 37°C for 2.5 hours, before addition of 1 μl DNAse1 (Promega) and incubation for a further 20 minutes at 37°C. The reaction was terminated by addition of 2 μl 0.2 M EDTA (pH 8.0) and transcribed RNA was precipitated for a minimum of 30 minutes at -70°C with 4 μl 4M LiCl (Sigma) and 75 μl 100% ethanol. The solution was spun at 16,000 rpm for 45 minutes at 4°C. The supernatant was then removed, and the

pellet was washed in 70% ethanol at 4°C for 15 minutes at 16,000 rpm. The pellet was briefly air dried in the fume hood and the precipitated RNA was resuspended in 50 μl sterile water and 1 μl RNAsin.

2.4.4 In-situ hybridization

2.4.4.1 Embryo fixation and storage

Viable, phenotypically distinct embryos were collected and fixed in 4% PFA. After 24 h fixation at 4°C in 4% PFA/PBS, the embryos were washed 3 x 5 minutes in PBST to remove the fixative and dehydrated in a series of methanol solutions to strip cellular membranes. The embryos were incubated sequentially at RT in solutions of 25% Methanol/75% PBS/0.1% Tween 20 [PBST], 50% Methanol/50% PBST, 75% Methanol/25% PBST and finally 2 x 100% Methanol for 10 minutes per incubation, followed by storage for a minimum of 18 hours at -20°C in 100% Methanol before moving onto the next step.

2.4.4.2 Embryo rehydration and riboprobe hybridization

The prepared embryos were warmed to RT, then rehydrated using the same methanol series in reverse 75% Methanol/25% PBST, 50% Methanol/50% PBST, 25% Methanol/75% PBST, 2x PBST; 10 minutes per incubation at RT). Embryos were separated into Eppendorf tubes with each having 30 embryos per tube. The Eppendorf tubes were labelled appropriately with the probe names on the lids of tubes. The PBST was replaced with 500 μl HYB- solution (50% formamide, 1x SSC [final concentration], 0.1% Tween 20) and incubated for 15 minutes in a water bath at 70°C. The HYB- solution was removed and replaced with 500 μl HYB+ solution (HYB- solution supplemented with 5 mg/ml Torula RNA and 50 μg/ml heparin; Sigma), and the embryos were incubated for a further 6 hours at 70°C. Riboprobes synthesized above were diluted to 2 ng/μl in HYB+ solution and heated at 68°C for 10 minutes to remove any secondary structure that may be present. The HYB+ was carefully removed and replaced with 500 μl of riboprobe solution. This was then incubated for 18 hours at 70°C.

2.4.4.3 Riboprobe removal and DIG-labelled riboprobe detection

After hybridization, the riboprobe solutions were removed and stored in Eppendorf tubes at 20°C for re-use. The embryos were gently transferred into Corning Netwells™ (Product number: 3478). Following riboprobe removal, solutions were pre-warmed to

70°C before use and the washes were performed on a hot air oven set at 70°C. The embryos were washed for 30 minutes at 70°C with Pre-block Buffer A (50% formamide, 20x SSCT [300 mM NaCl, 30 mM Na$_3$-citrate, 0.1% Tween20, pH 7.0]), 60 minutes at 70°C in 20x SSCT (300 mM NaCl, 30 mM Na$_3$-citrate, 0.1% Tween20, pH 7.0) and 2 x 15 minutes at 65°C in 0.2x SSCT. The embryos were then washed gently with 1x PBST for 3 times (each wash lasting 5 minutes) at room temperature on a rocking platform. Following PBST washes, embryos were immersed in blocking solution (PBST/5% serum/0.2% BSA/1% Dimethyl Sulfoxide [DMSO; Sigma]) for 3-4 hours. The embryos were then incubated for 18 hours at 4°C in blocking solution with anti-DIG Fab-Alkaline Phosphate (AP) antibody fragments (1:5000; Roche).

2.4.4.4 AP colour development and riboprobe visualization

Following the 18-hour incubation, the primary antibody was removed, and the embryos were washed 4 x 30 minutes in 1x PBST at RT. The embryos were then washed 3 x 5 minutes in freshly made staining buffer (100 mM Tris pH 9.5, 50 mM MgCl$_2$, 100 mM NaCl, 0.1% Tween 20 [Sigma], 1 mM Levamisol [Sigma]). 100 ml of freshly-made AP (colour development) staining substrate (5 μl Nitro-Blue Tetrazolium Chloride [0.33 mg/ml; NBT; Sigma] and 5.1 μl 5-Bromo-4-Chloro-3'-Indoyphosphate p-Toluidine Salt [0.17mg/ml; BCIP; Sigma] per 1.5 ml staining buffer) was prepared at the end of the wash. Following the washes, embryos from each net well were transferred to each of the wells designated for the particular probe in a 6-well/12-well cell culture plates. Each well comprised 1 ml of freshly prepared AP Staining substrate. The embryos were developed in dark at RT without agitation for 1-3 hours (probe dependent). The colour reaction was stopped by washing 2 x 5 minutes with 1x PBST. Stained embryos were mounted in 80-100% glycerol and imaged with a Nikon SZM 18 Fluorescence microscope and Olympus DP10 digital camera.

2.4.5 Synthesis of mRNA for microinjection

2.4.5.1 Amplification of DNA templates

500 ng of DNA template, 10 µl 5x HF buffer, 1 µl 50 mM dNTPs, 1.25 µl of the respective 10 µM forward and reverse primers, 0.5 µl Phusion polymerase (1 unit/ µl) was taken in a PCR reaction tube and the remainder of the 50 µl PCR reaction mix was made up with M.Q water. Finally, PCR reaction was set up with an initial denaturation step of 94°C for 2 minutes and 30 seconds, followed by 35 cycles of 94°C for 30 seconds, 65°C for 1 minute, 72°C for 2-minute 30 sec, before a final extension of 72°C for 7 minutes using the Bio-Rad C1000™ Thermal Cycler.

2.4.5.2 Restriction digestion of vector and gene fragment

This step was performed to digest the gene fragment and vector prior to ligation. The appropriate restriction enzyme for vector digestion was determined by vector map analysis. For the synthesis of *pvrl4* and *tbc1d2* mRNA, pCS2+MCS vector was digested with BamHI and XhoI restriction enzymes. Similarly, the gene fragment was digested with BamHI and XhoI restriction enzymes. For the synthesis of *ovol1* mRNA, EcoRI and XhoI restriction enzymes were used to digest both the pCS2+ vector and the gene construct. All restriction enzymes were purchased from Promega, unless otherwise stated. 5-10 µg vector DNA was combined with 5 µl CutSmart buffer, and 2 µl of restriction enzymes, in a final volume of 50 µl (with water). The reaction was incubated at 37°C for 2-2.5 hours. The digested vector was run on a 1% gel as described in section 2.4.2.3.

2.4.5.3 Gel purification of vector

DNA from agarose gels was extracted using the Monarch® DNA Gel Extraction Kit (New England BioLabs). The vector DNA fragment to be purified was excised from the gel using a razor blade or scalpel. The gel slice was weighed, and 4 times the volume of Monarch gel dissolving buffer was added to the tube. The gel slice was incubated at 50°C and vortexed periodically for 5-10 minutes until the gel was completely dissolved. The column available with the kit was inserted into the collection tube. The sample was then loaded into the column and centrifuged at a maximum speed for 1 minute. The flow-through was discarded and the column was re-inserted into the collection tube. 200 µl of DNA wash buffer was added and centrifuged for 1 minute. This step was repeated twice. This was then followed by transfer of column into a sterile Eppendorf tube. 6-20 µl of

sterile water/DNA elution buffer was then added to the centre of matrix and allowed to stand for 1 minute at RT. Finally, it was spun for 1 minute to elute the DNA. Eluted vector DNA was stored at -20°C.

2.4.5.4 Ligation

A molar ratio of 3:1 (insert: vector) was used for the ligation of DNA fragments into the vector of choice. The formula, mass of vector (ng) x length of insert (kb)/length of vector (kb) = ng of insert for a 1:1 molar ratio was used, and this was multiplied by 3 to give a 3:1 molar ratio. 2 µl 10x T4 DNA Ligase Buffer (50mM Tris-HCl pH 7.5, 10mM MgCl$_2$, 10mM dithiothreitol, 1mM ATP, 25 ug/ml BSA) and 1 µl T4 DNA Ligase (New England Biolabs [NEB], Ipswich, MA, USA) were combined with the appropriate amounts of DNA vector and insert in a final volume of 20 µl (with sterile water). Ligations were incubated at 4°C overnight or at least 2 hours at room temperature. Ligated DNA was then stored at -20°C. Following ligation, steps described in sections 2.4.2.3 -2.4.3.6 were followed.

2.4.5.5 Restriction Digestion

Restriction digestion with NotI enzyme was performed for linearizing the circular plasmids of *pvrl4*, *ovol1a*, and *tbc1d2* genes. 10 µg plasmid DNA was combined with 5 µl 10x transcription buffer, and 2 µl restriction enzyme, in a final volume of 50 µl (with water). The reaction was incubated at 37°C for 2-2.5 hours. 1 µl of the reaction was run on 1% gel, to see whether the plasmid has been linearized. A clear band signifies that the plasmid has been linearized. The plasmid was purified using QIAquick® PCR Purification Kit (QIAGEN) according to manufacturer's instructions. The purified, linearized plasmid was eluted in 20-30 µl sterile water.

2.4.5.6 mRNA synthesis

mRNA was synthesized by incubating 1 µg of linearized template DNA with 2 µl 10x transcription buffer, 10 µl NTP/cap mix, 1 µl RNAsin (Promega), 2 µl of T3, T7 or Sp6 polymerase (Promega) in a final volume of 20 µl (with M.Q water) at 37°C for 2 hours, before addition of 1 µl DNAse1 (Promega) and incubation for a further 20 minutes at 37°C. The reaction was terminated by addition of 2 µl 0.2M EDTA (pH 8.0) and transcribed RNA was precipitated for a minimum of 30 minutes at -70°C with 4 µl 4 M LiCl (Sigma) and 75 µl 100% ethanol. The solution was spun at 16,000 rpm for 45

minutes at 4°C. Supernatant was then removed, and the pellet was washed in 70% ethanol at 4°C for 15 minutes at 16,000 rpm. The pellet was briefly air dried in fume hood and the precipitated RNA was resuspended in 50 µl sterile water and 1 µl RNAsin.

2.5 Methods for protein analysis

2.5.1 Immunohistochemistry

2.5.1.1   Specimen fixation

Embryos classified as *grhl3*^{-/-} mutants were raised to 5 dpf and 7 dpf alongside *grhl3* siblings (control). At the desired stages, larvae were anesthetized in 0.04% tricaine solution and fixed with 4% PFA overnight at 4°C. The embryos were then washed with 1x PBST three times, for a total of 15 minutes. This was then followed by immersion of the larvae in 25% sucrose (dissolved in 1x PBS) at room temperature until the embryos sink down to the bottom. 25% sucrose was then replaced with 35% sucrose (dissolved in 1x PBS). The embryos were kept immersed in 35% sucrose at room temperature until the embryos sink down to the bottom. The immersed embryos can be kept in 35% sucrose at 4°C for up to one week.

2.5.1.2   Embedding

The embryos were transferred to a cryomold filled with OCT (optimal cutting temperature) medium. Embryos were stirred gently to give a good wash with the OCT media, after which they were transferred to a new cryomold filled with OCT medium. Using a syringe needle, the embryos were submerged in the OCT medium and were aligned with their tails facing the centre of the mould and their heads facing the wall of the cryomold. The larvae were aligned straight and close to each other. The cryomold was then gently submerged into cold 2-Methyl Butane (Sigma Aldrich) for 5-10 minutes without disturbing the orientation of larvae, followed by immersion into liquid nitrogen. Cryoblocks were then stored at -80°C.

2.5.1.3   Cryosectioning

10 µM cryosections were cut using the cryostat (Leica CM1860) at a temperature of -20°C. Using a camel hairbrush, the folds on the cut section were removed and the section was transferred to a SuperFrost[TM] Plus slide kept at room temperature, by touching the

slide to the tissue. The slides were kept at RT for 1 hour for the sections to adhere well to the slide, after which they were stored at -80°C.

2.5.1.4 *Staining with primary and secondary antibodies*

Slides were removed from -80°C freezer and thawed to room temperature. Tissue sections were carefully circled with a PAP Hydrophobic pen. Slides were washed with 1x PBST three times and were then placed on a horizontal holder. 500 µl blocking solution was added to the slides and was incubated at 4°C for 4 hours. Blocking solution was then replaced with primary antibodies prepared in blocking solution and kept at 4°C overnight. The slides were washed with frequent changes of 1x PBST for 1 hour the following day. The slides were again incubated for 1 hour with blocking solution at room temperature. Blocking solution was then replaced with secondary antibody prepared in blocking solution. Rhodamine Phalloidin™ (Life Technologies, Eugene, OR, USA) and DAPI (4′,6-diamidino-2-phenylindole) were added to the antibody solution at this stage to stain the actin filaments and nuclei of the cells respectively. The slides were kept in dark for 1 hour at room temperature. Following the 1-hour incubation, slides were washed thoroughly with 1x PBST (4 x 10-minute washes). Finally, the slides were mounted with Antifade mounting media and cover slipped. Sides of the coverslip were sealed with nail polish and kept at 4°C in dark. The fluorescent slides were imaged using Zeiss Confocal LSM 780 PicoQuant FLIM microscope.

2.6 Staining techniques

2.6.1 Haematoxylin and eosin staining

Prior to staining, the slides were removed from the freezer and allowed to air dry at room temperature. Firstly, OCT was rinsed off from the slides by immersing the slides in water. The slides were then immersed in Haematoxylin staining solution for 3 minutes, which stained nuclei a dark purple. Next, slides were rinsed gently under tap water for 2 minutes or until the water ran clear. The slides were then immersed into Scott's tap water followed by a thorough rinse with tap water. The cytoplasm of the cells was stained with eosin for 2 minutes. The slides were finally washed with frequent exchanges of ethanol and xylene (3 times each) and cover slipped with DPX mounting medium. The slides were air-dried for an hour before imaging using the Olympus DP26 camera connected to an Olympus BX53 Fluorescence microscope.

2.6.2 Alcian blue staining

4 dpf *grhl3*$^{-/-}$ and *grhl3*$^{+/?}$ (control) embryos were anesthetized in 0.04% tricaine solution and fixed in 4% PFA overnight at 4°C. The specimens were rinsed with acid alcohol (70% ethanol:1% HCl) thrice for a total of 15 minutes. The embryos were then immersed in 0.1% Alcian blue solution overnight at room temperature. The embryos were washed thoroughly with acid alcohol for 4 times (1 hour/wash), followed by treatment with hydrogen peroxide solution (3% H_2O_2 in 1% KOH) for 1 hour at room temperature or until the eyes became transparent. Finally, the embryos were washed with 1x PBST twice and stored in 70% glycerol at 4°C.

2.6.3 Phalloidin staining

grhl3$^{-/-}$ and *grhl3*$^{+/?}$ embryos at 48 hpf were anesthetized in 0.04% tricaine solution and fixed in 4% PFA at RT for 30 minutes and then overnight at 4°C. Following overnight incubation, 4% PFA was removed, and embryos were washed with 1x PBS three times with each wash lasting 5 minutes. Embryos were then repeatedly washed with 1x PBST for 10 minutes and this step was repeated 5 times. Subsequently, embryos were incubated in phalloidin and DAPI in 1x PBST containing 1% NGS for 4 hours at RT. Embryos were then washed with 1x PBST for 5 x 30 minutes and post-fixed with 4% PFA for 30 minutes. Following post-fixation, embryos were rinsed in 1x PBST for 3 x 5 minutes. Finally, embryos were serially upgraded in 30%, 50% and 70% glycerol made in 1x PBS.

2.7 Animal manipulation protocols

2.7.1 Morpholino injections

2.7.1.1 Preparation of morpholino stock

Morpholino ordered from GeneTools was available in a sterile, lyophilized form. The amount of morpholino per vial was 300 nanomoles. In order to make a 1 mM stock, 300 µl sterile water was added to the lyophilized morpholino. The bottle was gently vortexed to ensure the morpholino was evenly suspended in solution. The stock solution was then aliquoted into 30 tubes with 10 µl in each Eppendorf tube and stored at -20°C for future use.

2.7.1.2   Preparation of morpholino sample for injection

The desired working concentration of morpholino was prepared by mixing the thawed morpholino stock with 1 μl phenol red, and sterile water was added to make up a 10 μl working mix. Phenol red dye was added for easy visualization of the morpholino injection into the embryo. The working solution was kept at room temperature prior to injection.

2.7.1.3   Preparation of injection plate

To make an injection plate into which the embryos are lined up for injection, 2-3 g agarose was combined with 100 ml embryo medium and was boiled until it was dissolved. This was then poured into a 60 cm^2 bacterial grade Petri dish. When the agarose was slightly cooled, a square mould containing 4 grooves was placed upside down on to the agarose. This created 4 long grooves once the gel solidified, and this is where the embryos were laid for injection. On the morning of injection, the plates were warmed to room temperature.

2.7.1.4   Zebrafish embryo harvest and maintenance

Fish were set-up the evening prior to the morning of injection. Embryos were collected the following morning after removing the divider separating the male and female fish. Eggs deposited at the bottom of the tank were collected by pouring the tank water through a fine-mesh strainer as described in section 2.2.1.

2.7.1.5   Injection of zebrafish embryos

The nitrogen pump was turned on, along with the microinjector. Microinjections were conducted using the pico-injector FemtoJet 4i (Eppendorf). The injection valve was connected to the microinjector, and the pressure was adjusted according to the volume of the liquid to be loaded into the needle. 2-3 μl of RNA morpholino was loaded into the needle. The needle was carefully placed into the injecting apparatus, making sure that it was tightly sealed without breaking either end of the needle. The needle tip was then gently broken with the help of forceps. Needle aperture and injection conditions were optimized so that the resultant bolus size was 2-2.5 nl (Dworkin, Simkin et al. 2014).

Single-cell stage embryos collected were aligned in the furrows of the injection plate with the help of a transfer pipette. The tip of the needle was pierced carefully through the

chorion to inject the RNA/morpholino into the yolk sac of embryos. Following injection, the embryos were placed in a Petri dish with ~30 ml egg water and maintained at 28.5°C in an incubator. Six hours post-injection, particulate matter, unfertilized and dead/contaminated embryos were removed from the plates of injected embryos. The injected embryos were monitored in a Petri plate until 72 hpf for any visible phenotypes using the Nikon SMZ 745T Dissecting microscope.

2.7.1.6 *Phenotype detection and imaging*

Embryos were assessed for phenotypic defects. Injected embryos with distinct phenotypes were dechorionated manually using two pairs of fine tweezers under a dissecting microscope, taking care not to disturb the embryo proper. The embryos were imaged using NIS software and Nikon DS-Ri2 camera connected to SZM 18 Fluorescence microscope.

The survival rates of the injected embryos were monitored until 72 hpf. At the end of 72 hpf, injected embryos derived from inter-crossing *grhl3*$^{+/-}$ fish were classified into non-phenotypic, class 1, class 2 and class 3 based on the severity of the phenotypes observed (these phenotypes will be described in greater detail in Chapter 3, Section 3.3). The number of embryos for each class was noted and imaged.

2.7.2 RNA injections

2.7.2.1 *Preparation of mRNA for micro-injection*

Full length mRNA for injection was synthesized as in section 2.4.5. Concentration of the RNA samples were quantified using NanoDrop™ 2000/2000c Spectrophotometer (ThermoFisher Scientific). The mRNAs were then run on a 1% agarose gel as in section 2.4.2.4 to ensure correct size and integrity. mRNA synthesized was stored in 5 μl aliquots to prevent frequent freeze thawing, thereby preventing degradation of the RNA. For injection, the desired concentration of RNA, 1.5 μl 0.1M KCl, 0.5 μl phenol red, and sterile M.Q water was added to make up a 5 μl reaction mix. The solution was mixed well and kept on ice.

Embryo collection, injection and imaging was performed as described for morpholino injection in section 2.7.1.

2.8 Chemical treatment

2.8.1 Chemical treatment, monitoring of embryos and imaging

Adult *grhl3*^{+/-} and WT fish were set-up and embryos were collected as described in section 2.2.1. For chemical treatment, 100 embryos derived from inter-crossing *grhl3*^{+/-} fish (alongside 100 WT embryos as controls) were taken per Petri dish and the experiment was performed in triplicates for each concentration (Figure 2.3). The embryos were continually monitored, and the death rate was recorded post treatment of the chemical. At 72 hpf, the embryos were classified as class 1, class 2 and class 3 based on their phenotypic severity and their numbers were recorded. This was done to understand the effect of the chemical on shifting the spectrum of phenotypes observed. Embryos with distinct phenotypes were imaged at 72 hpf.
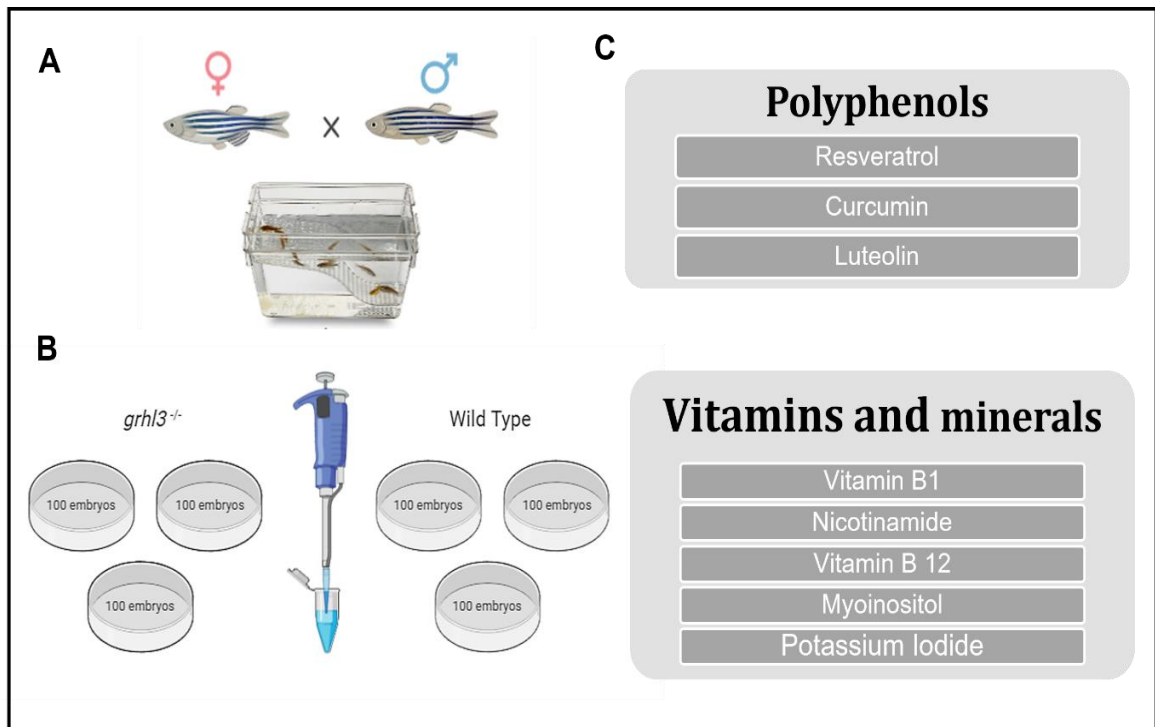
Figure 2.3 Schematic diagram showing the experimental set-up to test the effect of vitamins, minerals and polyphenols on embryos derived from inter-crossing *grhl3*^{+/-} adult zebrafish and WT embryos.

(**A**) Males and females were used in a ratio of 1:2 and placed in a breeding tank separated by a divider. The next morning, divider was removed to allow mating of fish. (**B**) Embryos deposited at the bottom of the tank were collected and split into 100 embryos per Petri dish. The experiment was performed in triplicates (for each dosage 3 Petri plates of 100 embryos were used). (**C**) Vitamins, minerals, and polyphenols used in the study are listed above.

2.8.2 Preparation of chemicals

- *Myoinositol*

Molecular weight of myoinositol is 180.16 g/mol. 0.5 M stock was prepared by dissolving 0.9 gm of myoinositol in 10 ml M.Q water. The stock was stored at -20°C in 1 ml aliquots.

Table 2.6 Working concentrations of myoinositol used in this study.

Working concentration (mg/ml)	Volume of embryo media (ml)	Volume of Stock (µl)
6.75	27.75	2.25
12.5	25.833	4.167
25	21.67	8.33
37.5	17.5	12.5
50	13.333	16.667
75	5	25
Control	30	

- *Nicotinamide*

Molecular weight of nicotinamide is 122.12 g/mol. 10 mM stock was prepared by dissolving 12.21 mg of nicotinamide in 10 ml M.Q water. The stock was stored at -20°C in 1 ml aliquots.

- *Thiamine chloride*

Molecular weight of thiamine chloride is 337.27 g/mol. 10 mM stock was prepared by dissolving 33.73 mg of thiamine chloride in 10 ml M.Q water. The stock was stored at -20°C in 1 ml aliquots.

- *Cobalamin*

Molecular weight of cobalamin is 1355.37 g/mol. 10 mM stock was prepared by dissolving 135.54 mg of cobalamin in 10 ml M.Q water. The stock was stored at -20°C in 1 ml aliquots.

Table 2.7 Working concentrations of nicotinamide /thiamine chloride /cobalamin used in this study.

Working concentration (µM)	Volume of embryo media	Volume of Stock (µl)	DMSO to be added (µl)
1	30 ml	3	30
2.5		7.5	30
5		15	30
10		30	30
20		60	30
Control			30

- *Potassium Iodide*

The molecular weight of Potassium Iodide is 166.01 gm/mol. 166 mg/ml stock was prepared by dissolving 1.66 gm in 10 ml M.Q water. Stock was stored as 1 ml aliquots at – 20°C.

Table 2.8 Working concentrations of potassium iodide used in this study.

Working concentration (mg/ml)	Volume of embryo media (ml)	Volume of Stock (µl)
2.5	24.623	376.5**µl**
5	24.247	753.01µl
10	23.494	1.51ml
Control	25.00	0

- *Resveratrol*

Molecular weight of Resveratrol is 228.25 g/mol. 100 mM stock was prepared by dissolving 114 mg of Resveratrol in 5 ml DMSO. The stock was stored at -20°C in 1 ml aliquots.

Table 2.9 Working concentrations of resveratrol used in this study.

Working concentration (µM)	Volume of embryo media	Volume of Stock (µl)	DMSO to be added (µl)
50	30 ml	15	45
100		30	30
150		45	15
200		60	0
Control		0	60

- *Curcumin*

Molecular weight of curcumin is 368.38 g/mol. 10 mM stock was prepared by dissolving 36.84 mg of curcumin in 10 ml DMSO. The stock was stored at -20°C in 1 ml aliquots.

Table 2.10 Working concentrations of curcumin used in this study.

Working concentration (µM)	Volume of embryo media	Volume of Stock (µl)	DMSO to be added (µl)
1	30 ml	3	27
2		6	24
3		9	21
4		12	18
Control		0	30

- *Luteolin*

Molecular weight of luteolin is 286.24 g/mol. 10 mM stock was prepared by dissolving 8.587 mg of luteolin in 3 ml of DMSO. The stock was stored at -20°C in 1 ml aliquots.

Table 2.11 Working concentrations of luteolin used in this study.

Working concentration (µM)	Volume of embryo media	Volume of Stock (µl)	DMSO to be added (µl)
1	30 ml	3	57
2.5		7.5	52.5
5		15	45
10		30	30
20		60	0

2.9 Image Acquisition

2.9.1 Imaging live and fixed embryos

Live whole embryos were mounted in 3% methylcellulose, while fixed embryos were mounted in 70% glycerol on a concave slide. The embryos were oriented using a small pipette tip prior to imaging. Once the embryos were positioned in desired orientation, they were visualised using SZM 18 Fluorescence microscope/Nikon SMZ 745T Dissecting Microscope and images were captured using the NIS software and Nikon DS-Ri2 camera.

2.9.2 Imaging histological sections

Histological sections were captured using the cellSens software and Olympus DP26 camera connected to Olympus BX53 Fluorescence microscope. Zeiss Confocal LSM 780 PicoQuant FLIM microscope was utilised for visualising immunohistochemical slides and ZEN BLUE Software was used for capturing and processing images.

2.9.3 Imaging zebrafish heads using confocal microscope

Fixed embryos stained with fluorescent antibodies/stains were mounted in 70% glycerol on a glass slide and positioned according to the site to be imaged. The embryo head was dissected using a scalpel blade along the line joining the head and the yolk sac. The cut portion of head was then oriented in such a way that the epidermis on the middle of the head faces up. Excess glycerol was removed, and cover slipped. To coverslip the

specimen, small portions of plasticine clay were used as spacers along the corners of the coverslip. The coverslip was then gently placed over the zebrafish head while observing under the microscope. The slides were visualized at 40x (water immersion) magnification using Zeiss Confocal LSM 780 PicoQuant FLIM microscope and captured using ZEN BLUE Software. Z-stack images were taken owing to the thickness of the specimen.

2.10 Statistical analysis

Statistical analyses for all experiments were performed using GraphPad Prism 8. Unpaired Student's T-test and Multiple T-test were used to compare the degree of significance between the control and experimental variable, where P values are as follows: * = $P \leq 0.05$, ** = $P \leq 0.01$, *** = $P \leq 0.005$, **** = $P \leq 0.001$.

Chapter 3: Role of grhl3 in epithelial development

3.1 Summary

Grhl3 is crucial for the establishment of epithelial barrier and homeostasis. In zebrafish, transient knockdown of *grhl3* resulted in epithelial deformities, including midbrain-hindbrain defects, convergent-extension (CE) defects (Miles, Darido et al. 2017) and craniofacial abnormalities (Dworkin, Simkin et al. 2014). This study further explored the role of *grhl3* in epithelial barrier formation, using a *grhl3* zebrafish knockout line generated via CRISPR/Cas9-mediated deletion. *grhl3* null embryos displayed three axial phenotypes that were classified as class 1, class 2 and class 3 based on the severity of axial defect observed. Additionally, embryonic lethality at 10 dpf, severe reduction in body length, orofacial defects and aberrant formation of intestinal epithelia were observed in *grhl3* mutants. These results suggest that *grhl3* is indeed a critical regulator of epithelial formation and exploring *grhl3* regulated epithelial development is crucial, as it provides insights into the aetiology of epithelial birth defects.

3.2 Introduction

The *Drosophila grainyhead* (*grh*) and vertebrate *Grainyhead-like* (*Grhl*) transcription factors are among the most critical genes for epithelial development, maintenance and homeostasis, and are remarkably well conserved from fungi to humans, as described in chapter 1. In zebrafish, morpholino mediated knockdown of *grhl3* contributes to epithelial defects such as aberrant folding and morphogenesis of midbrain-hindbrain boundary (before 24 hpf)(Miles, Darido et al. 2017), craniofacial hypoplasia (Dworkin, Simkin et al. 2014), shortening of body axis and curved tail at 96 hpf (Miles, Darido et al. 2017), suggesting the significance of *grhl3* in the epithelial homeostasis of zebrafish embryos.

MOs are known to cause non-specific phenotypes in zebrafish embryos (Heasman 2002), therefore, a *grhl3* CRISPR knockout was designed and established (by Dr. Lee Miles, Post-Doctoral Fellow, La Trobe University, Australia) to determine whether they reproduce the phenotypes as seen in *grhl3* morphants and also to further understand the role of *grhl3* in zebrafish tissue patterning, organ development and morphogenesis. Initial characterization of the *grhl3* null embryos displayed rupturing at the vegetal pole between ~80% epiboly and tail bud stage due to the weakening of the EVL/YSL interface (Miles, Darido et al. 2017). However, this phenotype disappeared, and the embryos survived past their embryonic stages when the fish lines were transferred to the aquatic facility at La

Trobe University, VIC, Australia from where they were generated and initially housed (Monash University)(detailed in Chapter 1 and 6). With the embryos surviving past gastrulation, it was easier to characterize the *grhl3* null embryos to understand the epithelial establishment at later stages of development. This chapter thus sought to understand the phenotypes observed in the *grhl3* null embryos and determine the consequences of *grhl3*-loss on growth and survival. As previously described, loss of *grhl3* contributes to craniofacial hypoplasia in zebrafish *grhl3* morphants, therefore, orofacial development in *grhl3* null embryos was investigated to determine similarities/differences in the craniofacial deformities detected between *grhl3* morphants and *grhl3* mutants.

Lastly, gut epithelial development was examined in *grhl3* null embryos as *grhl3* is highly expressed in endoderm-derived epithelia such as that of the gut (Kudryavtseva, Sugihara et al. 2003). Moreover, impaired differentiation of forestomach epithelium was observed in *Grhl3* mice (Yu, Lin et al. 2006). Therefore, I speculate that there may be defective barrier formation in the gut of *grhl3* null embryos and this hypothesis was tested by examining the histology of the gut epithelia of *grhl3*$^{-/-}$ embryos at 5 dpf (the timepoint when the intestine is established in zebrafish) and at 7 dpf (timepoint before the death of *grhl3* null embryos).

This chapter will therefore explore the functions of *grhl3* in axial patterning, survival, orofacial development, and establishment of intestinal epithelia.

3.3 Results

3.3.1 *grhl3*$^{-/-}$ embryos display severe axial defects and shortening of body length

Since the ATG-initiation codon is present in the exon 4 of *grhl3* gene, the zebrafish *grhl3* mutant was generated by targeting exon 4 at a site lying 3' to seven putative in-frame ATG-initiation codons via CRISPR/Cas 9 mediated deletion and homologous integration. Two *grhl3* mutant lines have been generated namely, *grhl3(+14bp)* and *grhl3(-31bp)* (Figure 3.1). The *grhl3*$^{-/-(+14bp)}$ mutant carries an insertion of stop cassette (to inhibit the synthesis of functional protein) at codon 143, resulting in a +14 bp gain within exon 4 of *grhl3* (Figure 3.1 and 3.2 C-D). *grhl3*$^{-/-(-31bp)}$ mutants contain a 31 bp deletion in exon 4, which results in a frameshift mutation to produce a truncated peptide of 224 amino acids lacking the conserved DNA binding domain (Figure 3.1 and 3.2 A-B). Lastly, a third line namely, *grhl3*$^{-/- (1-Δ4)}$ mutant was generated using two sets of guide RNAs, one targeting exon 1 and the other targeting exon 4. This led to the deletion of sequences between

exons 1 to 4, generating a non-functional *grhl3* protein of 118 amino acids (Figure 3.1 and 3.2 E-F).
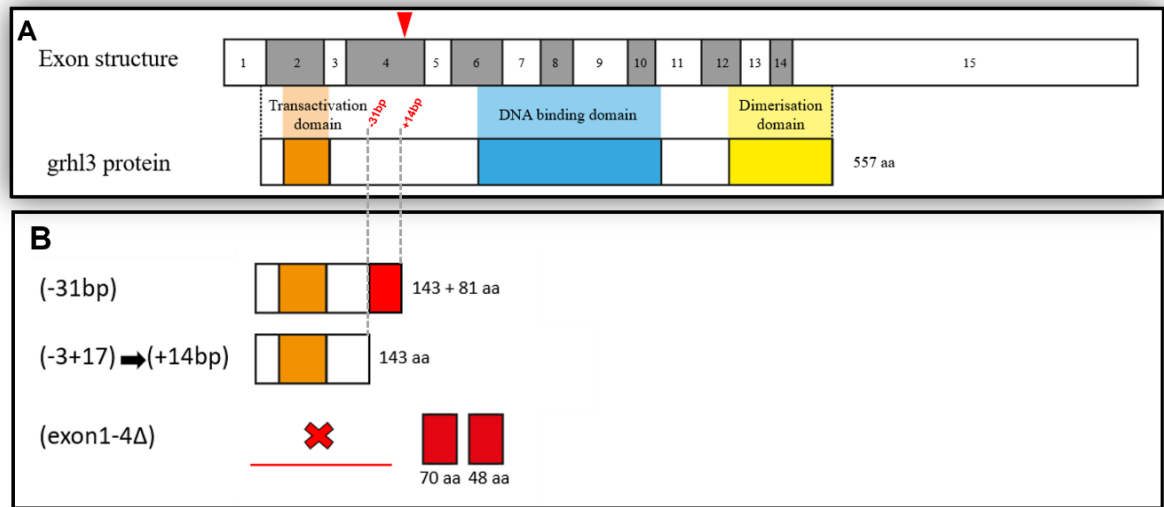
Figure 3.1 Structure of *grhl3* exons and protein

(A) Grey and white boxes indicate the exons. *grhl3* mutant was generated by targeting exon 4 at a site lying 3' to seven putative in-frame ATG-initiation codons (indicated by red arrow) via CRISPR/Cas 9 mediated deletion and homologous integration. A functional *Grhl* protein comprises 557 amino acids having a transactivation domain (orange), DNA binding domain (blue) and dimerization domain (yellow). **(B)** Structure of non-functional proteins of $grhl3^{-/-(+14bp)}$, $grhl3^{-/-(-31bp)}$ and $grhl3^{-/-(1-\Delta 4)}$ (Adapted from Miles 2017, and unpublished).

In order to determine the survival rate and phenotypes of $grhl3^{-/-(+14bp)}$, $grhl3^{-/-(-31bp)}$, and $grhl3^{-/-(1-\Delta 4)}$ embryos, $grhl3^{+/-(+14bp)}$, $grhl3^{+/-(-31bp)}$ and $grhl3^{+/-(1-\Delta 4)}$ fish were inter-crossed and embryos were collected. Survival rate of embryos derived from inter-crossing $grhl3^{+/-(1-\Delta 4)}$, $grhl3^{+/-(-31bp)}$ and $grhl3^{+/-(+14bp)}$ fish at 72 hpf were 88.3 ± 1.2%, 93.3 ± 2.2%, and 89.15 ± 2.4% respectively (Figure 3.3A). No significant differences were noted among the survival rate of embryos derived from the 3 $grhl3^{+/-}$ lines.

At 48 hpf, three phenotypes showing varying degrees of axial defects were seen in $grhl3^{-/-}$ embryos. Based on the severity of phenotypes they were classified as class 1, class 2, and class 3 embryos. Class 1 embryos exhibited minor fin fold defects, class 2 mutants displayed axial defects along with shortening of body length and class 3 $grhl3^{-/-}$ embryos exhibited the most severe phenotype displaying no axial extension beyond the yolk sac and showed severe axial defects (Figure 3.4A, 3.5A and 3.6A).
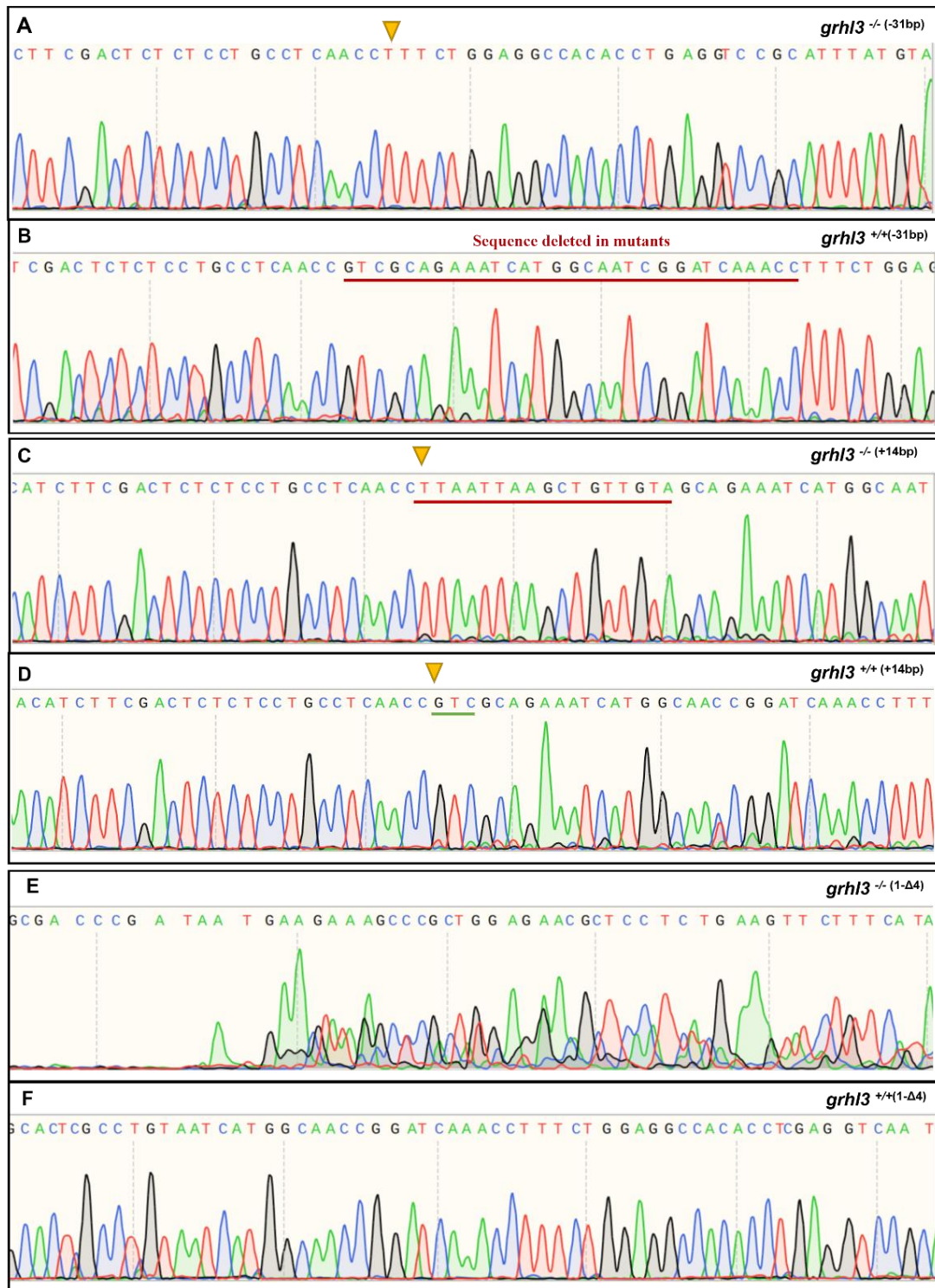
Figure 3.2 Sequencing chromatograms of *grhl3* mutant embryos.

(A-B) Sequencing of *grhl3*^{-/-(-31bp)} embryos showing the deletion of 31 bp. Yellow arrowhead (A) indicates the site of deletion and red underline (B) signifies the deleted sequence. (C-D) Sequencing of *grhl3*^{-/-(+14bp)} embryos showing the insertion of stop cassette. Green underline (D) indicates the position of the nucleotides that are deleted in *grhl3*^{-/-(+14bp)} embryos, yellow arrowhead denotes the CRISPR/Cas9 cut site and red underline (C) shows the insertion of 17 bp STOP cassette (E-F) Sequencing chromatograms of *grhl3*^{-/- (1-Δ4)} and *grhl3*^{+/+ (1-Δ4)} embryos.
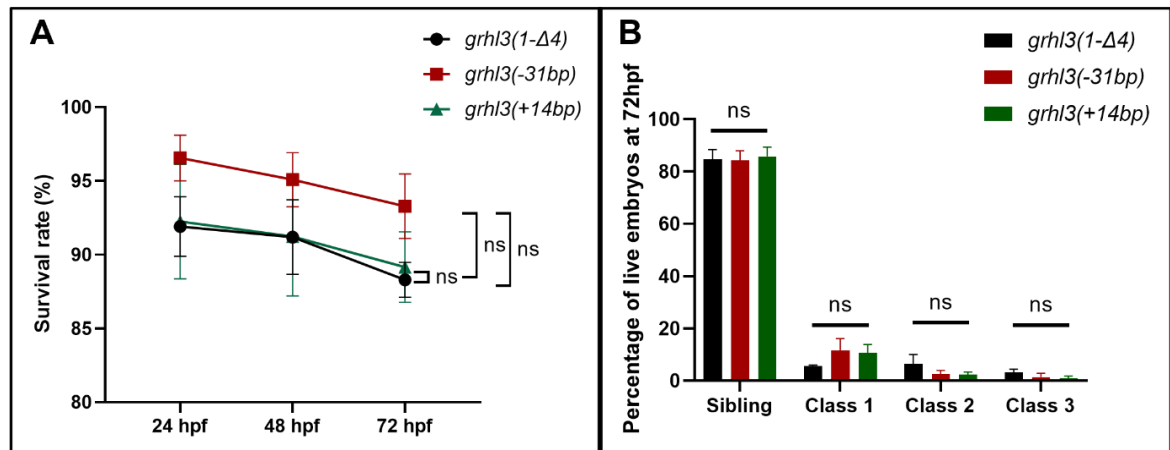
Figure 3.3 Analysis of *grhl3* lines based on survival rate and phenotypic incidence/severity of embryos.

(**A**) Comparison of survival rate of embryos derived from inter-crossing the *grhl3*$^{-/+(+14\ bp)}$, *grhl3*$^{-/+(-31\ bp)}$ and *grhl3*$^{-/+(1-\Delta4)}$ lines. (**B**) Comparison of the phenotypic incidence of class 1, class 2, and class 3 phenotypes in *grhl3*$^{-/-(+14bp)}$, *grhl3*$^{-/-(-31bp)}$ and *grhl3*$^{-/-(1-\Delta4)}$ embryos at 72 hpf. Data is represented as mean ± SEM; n=3. Statistical significance determined by Multiple t-tests with correction for multiple comparisons using the Holm-Sidak method; ns- non-significant.

The phenotypic incidence of *grhl3*$^{-/-(+14bp)}$ embryos were 10.69 ± 3.20% (class 1), 2.37 ± 0.97% (class 2), and 0.97 ± 0.85% (class 3) (Figure 3.4A) and percentage of class 1, class 2, and class 3 phenotypic *grhl3*$^{-/-(-31bp)}$ mutants were 11.63 ± 4.47%, 2.61 ± 1.34% and 1.44 ± 1.39% respectively (Figure 3.5A). 5.63 ± 0.38% (class 1), 6.38 ± 3.66 (class 2), and 3.20 ± 1.26% (class 3) *grhl3*$^{-/-(1-\Delta4)}$ mutants was present (Figure 3.6A). From the above results it is clear that class 1 *grhl3*$^{-/-}$ embryos were present at higher frequency (~6-10%) than class 2 (~2-6%) and class 3 (~1-3%) embryos. The varying degree of phenotypic incidence was observed uniformly across the *grhl3*$^{-/-}$ embryos derived from all three CRISPR-generated mutant lines. No significant differences were noted in terms of phenotypic incidence of *grhl3*$^{-/-}$ embryos derived from inter-crossing *grhl3*$^{-/+(+14\ bp)}$, *grhl3*$^{-/+(-31\ bp)}$ and *grhl3*$^{-/+(1-\Delta4)}$ lines. (Figure 3.3B).
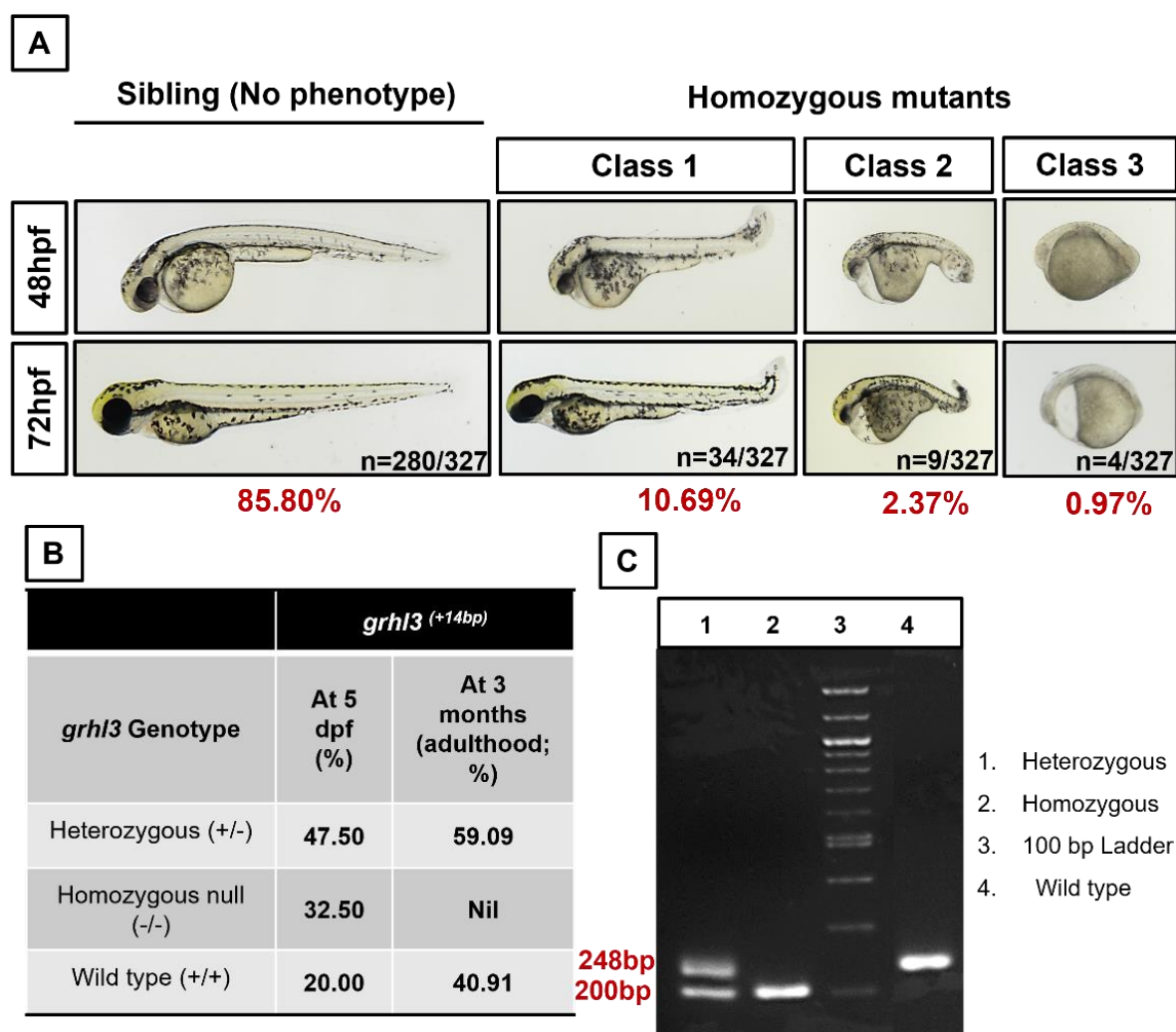
Figure 3.4 Characterization of *grhl3^{-/-(+14 bp)}* mutants.

grhl3^{+/-(+14 bp)} fish were inter-crossed and embryos derived from this mating were collected and monitored. **(A)** The three distinct appearances of *grhl3^{-/-(+14 bp)}* embryos at 48 hpf and 72 hpf have been classified as class 1, class 2 and class 3 based on the severity and incidence of their phenotypes. **(B)** Table shows the percentage of heterozygous, homozygous null and WT larvae/fish at 5 dpf and 3 months adulthood (derived from inter-crossing *grhl3^{+/-(+14 bp)}* fish). **(C)** 3% agarose gel displaying PCR products of DNA of embryos derived from inter-crossing *grhl3^{+/-(+14 bp)}* fish. PCR products comprising 2 bands in the gel (248 bp and 200 bp) indicate a heterozygous genotype; a single band at 200 bp corresponds to a homozygous-null genotype and a band at 248 bp corresponds to a wild-type genotype. Primers *grhl3* e4 Forward (F), *grhl3* e4 Reverse (R) and *grhl3(+14bp)* R were used for genotyping the embryos/fish.
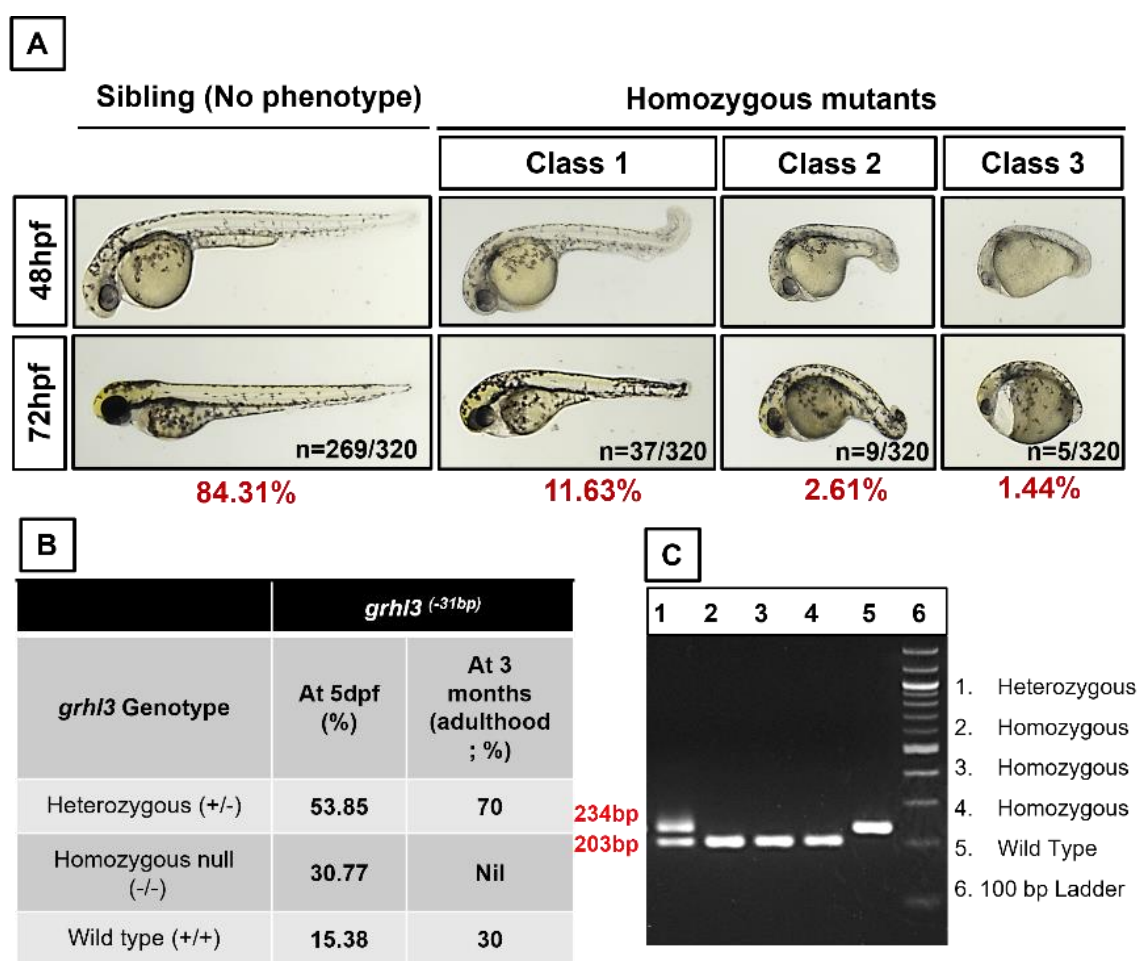
Figure 3.5 Characterization of *grhl3*^{-/-(-31 bp)} mutants.

grhl3$^{+/-(-31\ bp)}$ fish were inter-crossed and embryos derived from this mating were collected and monitored. **(A)** The three distinct appearances of *grhl3*$^{-/-(-31\ bp)}$ embryos at 48 hpf and 72 hpf have been classified as class 1, class 2 and class 3 based on the severity and incidence of their phenotypes. **(B)** Table shows the percentage of heterozygous, homozygous null and WT larvae/fish at 5 dpf and 3 months adulthood (derived from inter-crossing *grhl3*$^{+/-(-31\ bp)}$ fish). **(C)** 3% agarose gel displaying PCR products of DNA of embryos derived from inter-crossing *grhl3*$^{+/-(-31\ bp)}$ fish. PCR products comprising 2 bands in the gel (234 bp and 203 bp) is a heterozygous genotype; a single band at 203 bp is a homozygous null genotype and a band at 234 bp corresponds to a wild-type genotype. Primers *grhl3* e4 Forward (F), and *grhl3* e4 Reverse (R) were used for genotyping the embryos.

A

Sibling (No phenotype)   **Homozygous mutants**

| | **Class 1** | **Class 2** | **Class 3** |

48hpf

72hpf

n=210/248   n=14/248   n=16/248   n=8/248

84.79%   **5.63%**   **6.38%**   **3.20%**

B

grhl3 Genotype	grhl3 $^{(1-\Delta4)}$	
	At 5 dpf (%)	**At 3 months (adulthood; %)**
Heterozygous (+/-)	48.72	70.50
Homozygous null (-/-)	15.38	Nil
Wild type (+/+)	35.90	29.50

C

230bp
183bp

1. 100 bp Ladder
2. Homozygous
3. Homozygous
4. Homozygous
5. Heterozygous
6. Wild Type
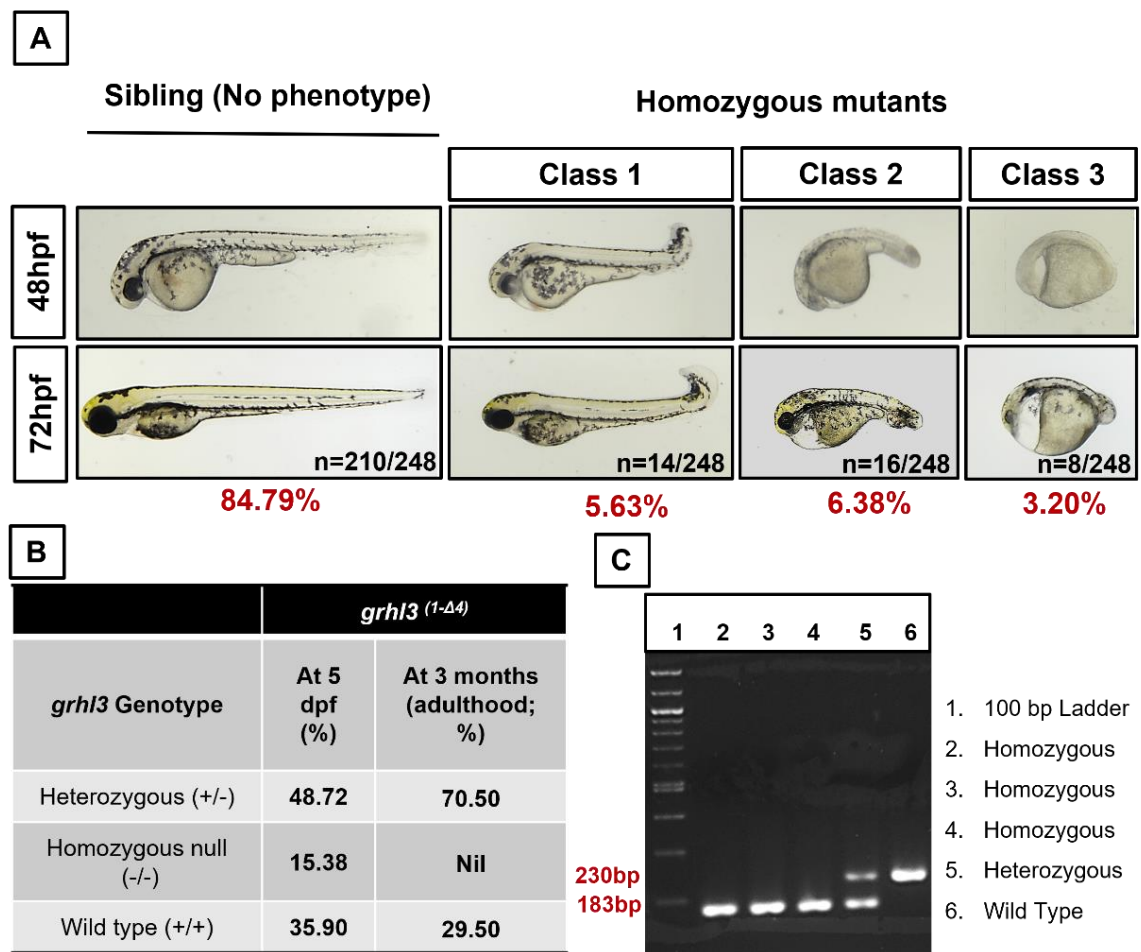
Figure 3.6 Characterization of grhl3$^{-/-(1-\Delta4)}$ mutants.

grhl3$^{+/-(1-\Delta4)}$ fish were inter-crossed and embryos derived from this mating were collected and monitored. (**A**) The three distinct appearances of *grhl3$^{-/-(1-\Delta4)}$* embryos at 48 hpf and 72 hpf have been classified as class 1, class 2 and class 3 based on the severity and incidence of their phenotypes. (**B**) Table shows the percentage of heterozygous, homozygous null and WT larvae/fish at 5 dpf and 3 months adulthood (derived from inter-crossing *grhl3$^{+/-(1-\Delta4)}$* fish). (**C**) 3% agarose gel displaying PCR products of DNA of embryos derived from inter-crossing *grhl3$^{+/-(1-\Delta4))}$* fish. PCR products comprising 2 bands in the gel (230 bp and 183 bp) is a heterozygous genotype; a single band at 183 bp is a homozygous null genotype and a band at 230 bp corresponds to a wild-type genotype. Primers *grhl3* e1-Δ4 Forward (F), *grhl3* e1-Δ4 Reverse (R) and *grhl3* e4 F were used for genotyping the embryos.

In order to determine whether the heterozygous, homozygous null and WT embryos derived from inter-crossing *grhl3*$^{+/-}$ fish follow mendelian ratio, genotyping was performed at 5 dpf (Figure 3.4C, 3.5C, and 3.6C). At 5 dpf, ~50% heterozygotes were present in a population of embryos derived from inter-crossing *grhl3*$^{+/-}$ fish (Figure 3.4B, 3.5B and 3.6B). Chi square test was performed to verify any deviations of the expected alleles in a population. There were no significant differences between the expected and observed numbers of mutants, heterozygotes, and WT, thus our data fits the expected Mendelian ratio i.e., 1:2:1) (Figure 3.7).

At 72 hpf, percentage of *grhl3*$^{-/-}$ embryos was expected to be 25%, however only ~15% phenotypic *grhl3*$^{-/-}$ embryos were seen. Genotyping of embryos derived from inter-crossing *grhl3*$^{+/- \ (+14bp)}$ fish at 5 dpf revealed ~30% embryos being homozygous nulls. Likewise, ~30% *grhl3* null embryos were present upon genotyping embryos derived from *grhl3*$^{+/- \ (-31bp)}$ fish. This suggests that ~50% of the null (*grhl3-/- (+14bp)* and *grhl3*$^{-/- \ (-31bp)}$) embryos were non-phenotypic. ~15% homozygous nulls were observed upon genotyping of embryos derived from inter-crossing *grhl3*$^{+/-(1-Δ4)}$ fish at 5 dpf. These results are strikingly similar to the percentage of phenotypic *grhl3* mutants at 3 dpf. Therefore, all the embryos with a *grhl3*$^{-/-(1-Δ4)}$ genotype display an axial phenotype, as opposed to *grhl3*$^{+/-(+14bp)}$ and *grhl3*$^{+/-(-31bp)}$ embryos. This suggests that the phenotypes of *grhl3*$^{-/-(1-Δ4)}$ embryos are much more severe than null embryos derived from *grhl3*$^{+/-(+14bp)}$ and *grhl3*$^{+/- (-31bp)}$ fish.

Lastly, in order to determine whether the *grhl3* mutants survive to adulthood, genotyping of *grhl3* fish was carried out at 3-months adulthood. Genotyping revealed the absence of homozygous mutants. Heterozygous population was present at a higher percentage (~70% *grhl3*$^{+/-(-31bp)}$ and *grhl3*$^{+/-(1-Δ4)}$; 60% *grhl3*$^{+/-(+14bp)}$) than the WT (~30% *grhl3*$^{+/+(-31bp)}$ and *grhl3*$^{+/+(1-Δ4)}$; 60% *grhl3*$^{+/+(+14bp)}$) (Figure 3.4B, 3.5B and 3.5B). Therefore, we can conclude that *grhl3*$^{-/-}$ mutants do not survive to adulthood.
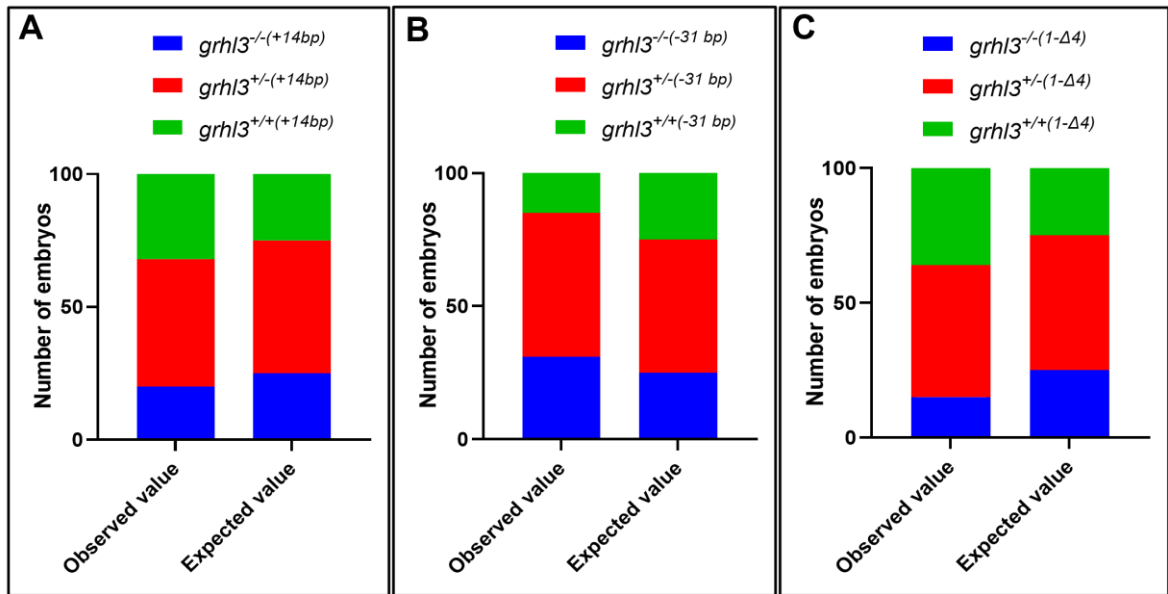
Figure 3.7 Chi square test to verify whether the genotypes present in embryos derived from inter-cross of *grhl3*⁺ᐟ⁻ parents follows Mendelian ratios.

Embryos derived from inter-crossing (**A**) *grhl3*⁺ᐟ⁻⁽⁺¹⁴ ᵇᵖ⁾ (**B**) *grhl3*⁺ᐟ⁻⁽⁻³¹ ᵇᵖ⁾(**C**) *grhl3*⁺ᐟ⁻⁽¹⁻ᐞ⁴⁾ fish were genotyped at 5 dpf. Chi Square test was performed with the expected and observed number of homozygous nulls, heterozygotes, and wild type in a clutch to verify whether the results obtained fits the Mendelian ratio.

In order to determine the consequences of *grhl3* deletion on the growth of zebrafish embryos, the body length of class 1, class 2, and class 3 *grhl3*⁻ᐟ⁻ mutant embryos and non-phenotypic siblings were quantitated (n=10). This was performed for embryos derived from all the three *grhl3*⁺ᐟ⁻ lines. The mean body length of class 1, class 2, and class 3 *grhl3*⁻ᐟ⁻⁽⁺¹⁴ᵇᵖ⁾ embryos were 2.5 ± 0.15 mm, 1.6 ± 0.2 mm, and 1.2 ± 0.1 mm respectively (Figure 3.8A) and that of class 1, class 2, and class 3 *grhl3*⁻ᐟ⁻⁽⁻³¹ᵇᵖ⁾ embryos were 2.6 ± 0.3 mm, 1.6 ± 0.2 mm, and 1.15 ± 0.1 mm respectively (Figure 3.8B). 2.3 ± 0.15 mm (class 1), 1.5 ± 0.1 mm (class 2) and 1.2 ± 0.1 mm (class 3) was the body length of *grhl3*⁻ᐟ⁻⁽¹⁻ᐞ⁴⁾ embryos (Figure 3.8C). The body length of *grhl3*⁺ᐟ?⁺ ⁽⁺¹⁴ᵇᵖ⁾, *grhl3*⁺ᐟ?⁽⁻³¹ᵇᵖ⁾ and *grhl3*⁺ᐟ?⁽¹⁻ᐞ⁴⁾ siblings (control) were 3.5 ± 0.1 mm, 3.5 ± 0.1 mm, and 3.4 ± 0.1 mm respectively. A significant reduction in the body length of class 1 (~2.5 mm), class 2 (~1.6 mm) and class 3 (~1.2 mm) *grhl3*⁻ᐟ⁻ embryos was observed relative to controls (~3.5mm) (Figure 3.8). Thus, *grhl3*⁻ᐟ⁻ embryos display severe growth restriction in the absence of *grhl3* gene.
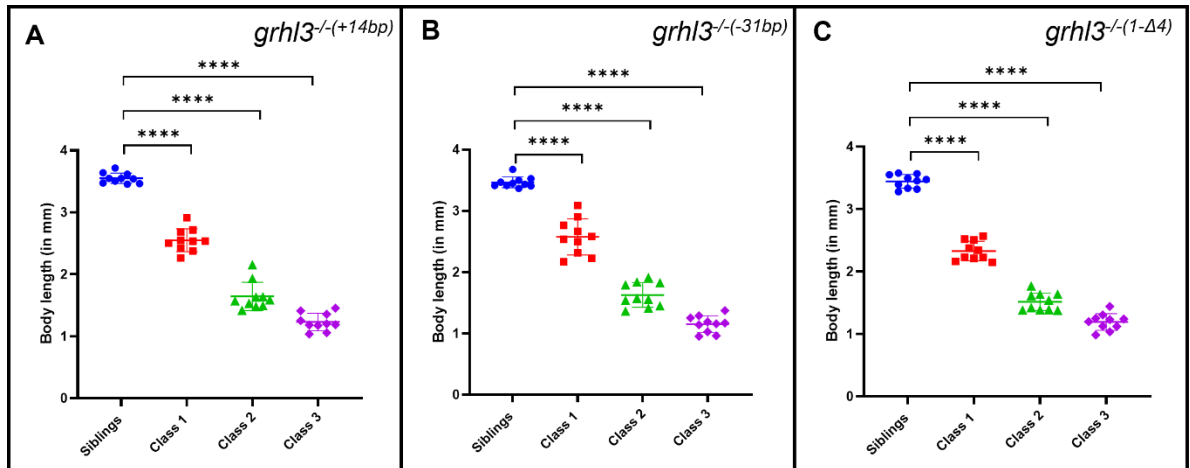
Figure 3.8 Quantitation of body length of *grhl3⁻/⁻* embryos.

Quantitation of body length of non-phenotypic siblings, class 1, class 2, and class 3 *grhl3⁻/⁻* embryos derived from inter-crossing **(A)** *grhl3⁺/⁻⁽⁺¹⁴ ᵇᵖ⁾*, **(B)** *grhl3⁺/⁻⁽⁻³¹ ᵇᵖ⁾* and **(C)** *grhl3⁺/⁻⁽¹⁻Δ⁴⁾* fish. Data is represented as mean ± SEM; n=10. Statistical significance determined by Student's t-tests ****$P < 0.001$.

3.3.2 *grhl3⁻/⁻* embryos do not survive beyond 10 dpf

Since the *grhl3* mutants do not survive to adulthood, therefore, I investigated the age at which they die. To determine the consequences of *grhl3* on viability, *grhl3* mutant, heterozygous and WT embryos were monitored for survival. *grhl3⁻/⁻⁽⁻³¹ᵇᵖ⁾* embryos showed a sharp decline in their numbers at 7 dpf; the survival rate falling from 84.5% at 6 dpf to 11.26% at 7 dpf (Figure 3.9B). Finally, all the embryos die by 10 dpf. Likewise, *grhl3⁻/⁻⁽⁺¹⁴ᵇᵖ⁾* embryos showed an increased mortality at 7 dpf (from 73.27% at 6 dpf to 4.95% at 7 dpf), however all the embryos underwent death at 9 dpf as opposed to 10 dpf (Figure 3.9A). In *grhl3⁻/⁻⁽¹⁻Δ⁴⁾* embryos, a sharp decrease in survival rate was noted at the beginning (73.21%) and at 8 dpf (14.28%). Like the *grhl3⁻/⁻⁽⁺¹⁴ᵇᵖ⁾* these embryos do not survive past 9 dpf (Figure 3.9C). No differences in survival rate were observed between the *grhl3⁺/⁻⁽¹⁻Δ⁴⁾*/*grhl3⁺/⁻⁽⁺¹⁴ᵇᵖ⁾* in contrast to WT embryos. However, reduction in survival rate was observed in *grhl3⁺/⁻⁽⁻³¹ᵇᵖ⁾* (73.55%) embryos when compared to WT embryos (90.90%) at 10 dpf. These results demonstrate that *grhl3* is required for embryo survival in zebrafish. I suspect that the reduced viability of *grhl3⁻/⁻* embryos might be attributed to the craniofacial deformities and defective formation of intestinal epithelia described in subsequent sections (3.3.3 - 3.3.6).
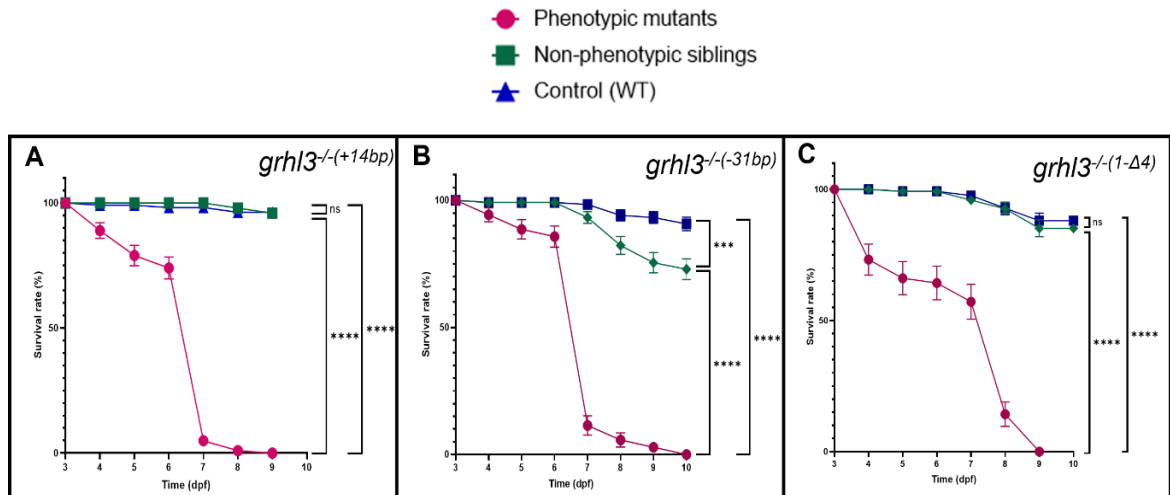
Figure 3.9 Determination of the maximum survival age *grhl3*⁻/⁻ mutants.

At 72 hpf, embryos were classified into phenotypic mutants (pink) and non-phenotypic siblings (green). For control, WT (blue) embryos were used. The survival rate of **(A)** *grhl3*⁻/⁻(+14 bp), **(B)** *grhl3*⁻/⁻(-31 bp) and **(C)** *grhl3*⁻/⁻(1-Δ4) embryos were recorded and monitored until all the mutants undergo death. Comparison of survival curves by Log-rank (Mantel-Cox) test ***P < 0.005; ****P < 0.001; ns - non-significant.

3.3.3 Loss of *grhl3* causes defects in jaw formation

In order to determine the consequences of germline *grhl3* deletion on craniofacial development, Alcian blue staining was performed on *grhl3*⁻/⁻(+14bp) and *grhl3* sibling embryos at 4 dpf to visualise the craniofacial cartilage. *grhl3*⁻/⁻(+14bp) embryos displayed absence of ceratobranchials, reduction in the distance between lower and upper jaw, and diminished distance between ceratohyal and Meckel's cartilage (MC)(Figure 3.10A-H). The distance between lower and upper jaw in *grhl3*⁻/⁻(+14bp) embryos and *grhl3*⁺/⁻(+14bp) siblings was 26.1 ± 7.6 µm and 82.9 ± 7.1 µm respectively (Figure 3.10I) and the distance between ceratohyal and MC in *grhl3*⁻/⁻(+14bp) embryos and *grhl3*⁻/⁺(+14bp) siblings was 83.6 ± 9.6 µm and 158.3 ± 12.4 µm respectively (Figure 3.10J). The distance between lower and upper jaw and the distance between ceratohyal and MC was significantly reduced in *grhl3*⁻/⁻(+14bp) mutants in comparison to siblings. Lastly, jaw defects observed in class 2 and class 3 *grhl3*⁻/⁻(+14bp) embryos displayed defective development of jaw structures and were much more severe than the craniofacial defects observed in class 1.

Similar jaw phenotypes were seen in *grhl3*⁻/⁻(-31bp) (Figure 3.11) and *grhl3*⁻/⁻(1-Δ4) embryos (Figure 3.12). The distance between lower and upper jaw in *grhl3*⁻/⁻(-31bp) embryos and control (*grhl3*⁺/? (-31bp)) was 24.3 ± 3.2 µm and 91.6 ± 8.2 µm respectively and the distance between ceratohyal and MC in *grhl3*⁻/⁻(-31bp) embryos and control was 86.3 ± 9.25 µm and

136.5 ± 5.4 µm respectively (Figure 3.11I-J). In *grhl3$^{-/-(1-\Delta4)}$* embryos and control, (*grhl3$^{+/?(1-\Delta4)}$* siblings) the distance between upper and lower jaw was 25.1 ± 8.25 µm and 77.2 ± 3.3 µm and the distance between ceratohyal and MC 68.35 ± 3.72 µm and 144.2 ± 11.3 µm respectively (Figure 3.12I-J). In addition, class 2 *grhl3$^{-/-(1-\Delta4)}$* embryos displayed overlapping of both the Meckel's' cartilage and ceratohyal with barely any distance between the two structures (Figure 3.12F). Class 3 *grhl3$^{-/-(1-\Delta4)}$* embryos were completely absent at 4 dpf and hence the severity of jaw defects could not be explored in *grhl3$^{-/-(1-\Delta4)}$* embryos.

Figure 3.10 Craniofacial development in *grhl3^-/-(+14 bp)* embryos at 4 dpf.

(**A-H**) Class 1, class 2, class 3 *grhl3^-/-(+14bp)* embryos and siblings (4 dpf) stained with Alcian blue, showing the (**A-D**) lateral and (**E-H**) ventral views of the craniofacial cartilage (palatoquadrate [**pq**], ceratohyal [**ch**] Meckel's cartilage [**mc**], ethmoid plate [**ep**], hyosymplectic [**hs**]).The distance between (**I**) upper and lower jaw (indicated by vertical double-headed red arrow) and (**J**) the distance between Meckel's cartilage and ceratohyal (indicated by horizontal double-headed red arrow) were measured and analysed in *grhl3^-/-(+14bp)* embryos and siblings using ImageJ software. Data is represented as mean ± SEM; n=5. Statistical significance determined by Student's t-test ****$P < 0.001$.

Figure 3.11 Craniofacial development in *grhl3*^{-/-(-31 bp)} embryos at 4 dpf.

(**A-H**) Class 1, class 2, class 3 *grhl3*^{-/-(-31 bp)} embryos and siblings (4 dpf) stained with Alcian blue, showing the (**A-D**) lateral and (**E-H**) ventral views of the craniofacial cartilage (palatoquadrate [**pq**], ceratohyal [**ch**] Meckel's cartilage [**mc**], ethmoid plate [**ep**], hyosymplectic [**hs**]). The distance between (**I**) upper and lower jaw (indicated by vertical double-headed red arrow) and (**J**) the distance between Meckel's cartilage and ceratohyal (indicated by horizontal double-headed red arrow) were measured and analysed in *grhl3*^{-/-(-31 bp)} embryos and siblings using ImageJ software. Data is represented as mean ± SEM; n=5. Statistical significance determined by Student's t-test ****P < 0.001.
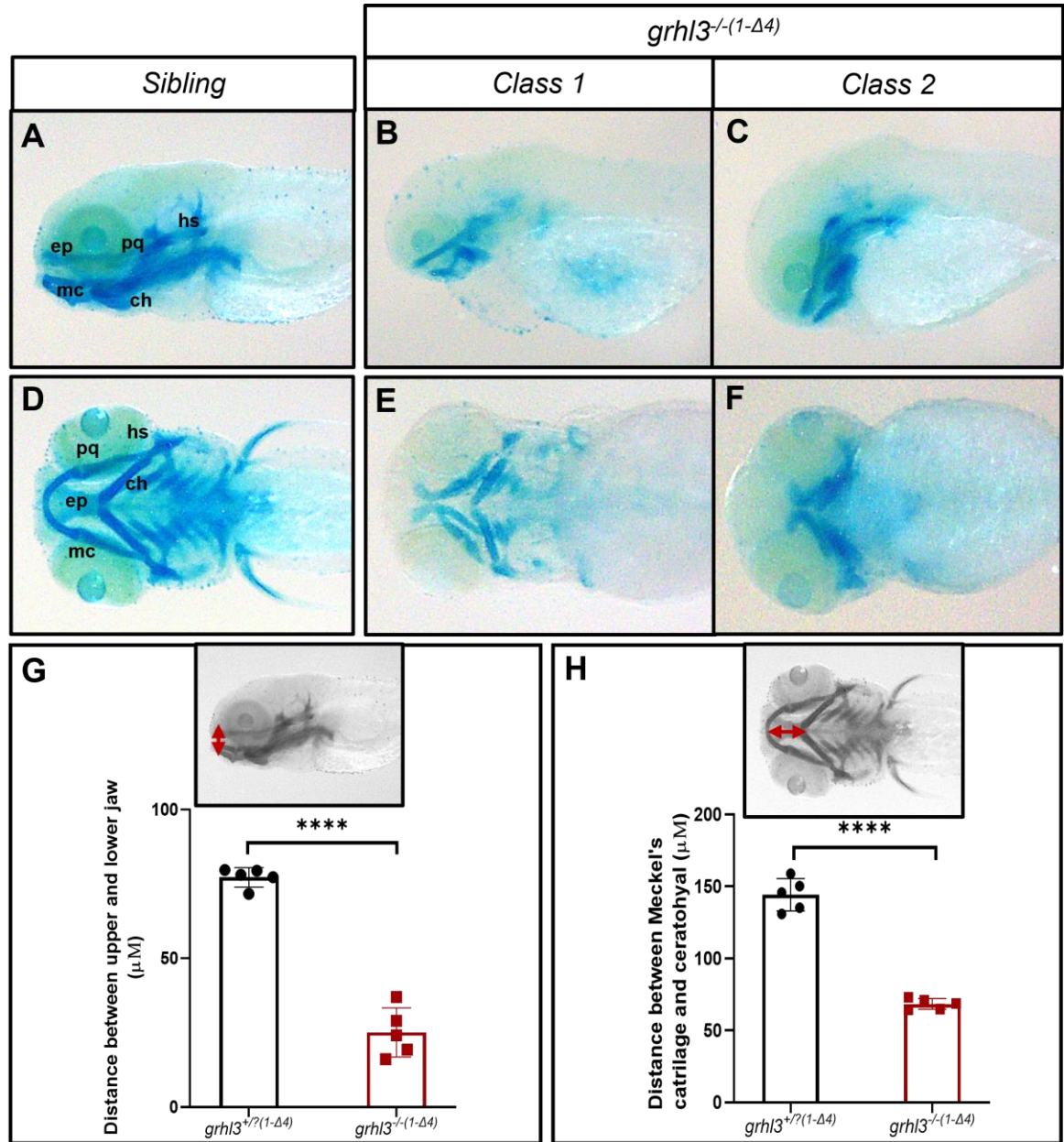
Figure 3.12 Craniofacial development in *grhl3⁻/⁻(1-Δ4)* embryos at 4 dpf.

(**A-H**) Class 1, class 2, class 3 *grhl3⁻/⁻(1-Δ4)* embryos and siblings (4 dpf) stained with Alcian blue, showing the (**A-D**) lateral and (**E-H**) ventral views of the craniofacial cartilage (palatoquadrate [**pq**], ceratohyal [**ch**] Meckel's cartilage [**mc**], ethmoid plate [**ep**], hyosymplectic [**hs**]). The distance between (**I**) upper and lower jaw (indicated by vertical double-headed red arrow) and (**J**) the distance between Meckel's cartilage and ceratohyal (indicated by horizontal double-headed red arrow) were measured and analysed in *grhl3⁻/⁻(1-Δ4)* embryos and siblings using ImageJ software. Data is represented as mean ± SEM; n=5. Statistical significance determined by Student's t-test ****P < 0.001.

To further explore the role of *grhl3* in jaw development, H&E staining was performed on cryosections taken along the rostral region of class 1 *grhl3*^{-/-} larvae and *grhl3* siblings (7 dpf). The formation of the ceratohyal was normal in *grhl3* mutants, however the space surrounding the ceratohyal appeared to be smaller in size in comparison to controls. The mean area of the orofacial cavity was 5802.4 $\pm$ 1586.85 µm^2 in *grhl3*^{-/-} embryos and 12720.7 $\pm$ 1221.8 µm^2 in siblings. Statistical analyses revealed a significant reduction in the mean area of orofacial cavity ($p=0.000455$; $n=5$) of *grhl3*^{-/-} embryos at 7 dpf relative to controls. (Figure 3.13). The reduction in the size of orofacial cavity might be because of the reduced space between upper and lower jaw. These results demonstrate that *grhl3* plays a critical role in the development of the oral cavity, and the formation of lower and upper jaw, consistent with other studies demonstrating orofacial defects in *grhl3* morphants (Dworkin, Simkin et al. 2014).

The survival rates, axial defects and craniofacial defects seen in *grhl3*[-/-(+14bp)], *grhl3*[-/-(1-Δ4)] and *grhl3*[-/-(-31bp)] embryos were virtually identical, with no substantive differences observed in embryos of any of these three lines. Therefore, these data validated each CRISPR-knockout to have resulted in the same phenotypes, due to disruption of *grhl3*-signalling. Hence, all subsequent experiments were performed using embryos derived from any of these three *grhl3* lines.
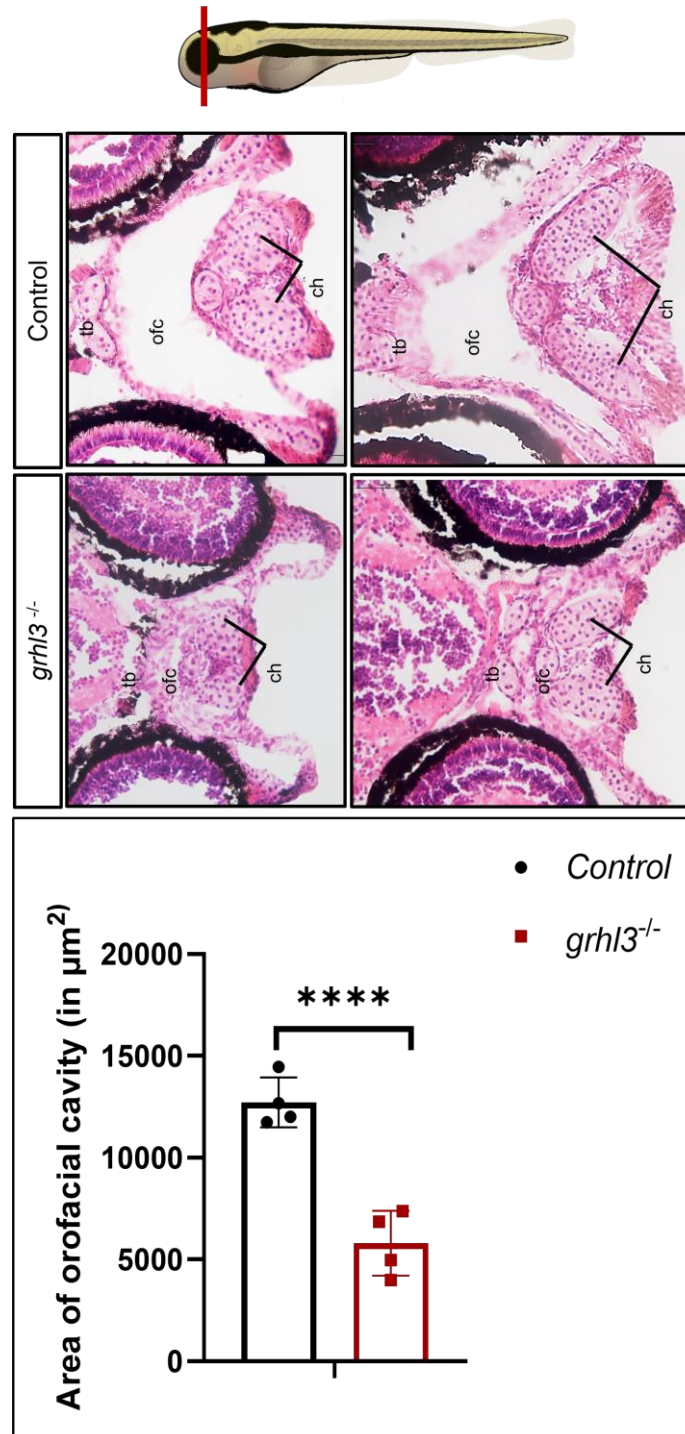
Figure 3.13 Size of the orofacial cavity in *grhl3-/-* mutants.

(A) H&E staining of transverse-sections across the rostral region of 7 dpf class 1 *grhl3-/-* mutant (bottom) and control (top) embryos (ceratohyal [**ch**] trabecular bar [**tb**], orofacial cavity [**ofc**]). **(B)** Area of orofacial cavity was quantitated in *grhl3-/-* (red) and control (black) embryos using ImageJ software. Data is represented as mean ± SEM; n=3. Statistical significance determined by Student's t-test ****P < 0.001.

3.3.4 The size of swim bladder is reduced in *grhl3^{-/-}* embryos at 5 dpf

The zebrafish swim bladder is an epithelialized gas-filled sac that is required for balance. In order to investigate if *grhl3* had a role in inflation of the swim bladder, transverse cryosections along the gut region of 5-day old class 1 *grhl3^{-/-}* embryos were stained with haematoxylin and eosin. The size of the swim bladder in mutants appeared much smaller in comparison to controls. When quantitated, the average area of swim bladder in mutants (n=5) was 12022 ± 4072.8 μm^2 while in siblings it was 26336.17 ± 10749.61 μm^2 (Figure 3.14). Thus, a severe reduction in the size of swim bladder (p=0.024) was observed in mutants relative to control. This might be attributed to poor inflation of the swim bladder in *grhl3* mutants, suggesting the importance of *grhl3* in the regulation of swim bladder inflation.
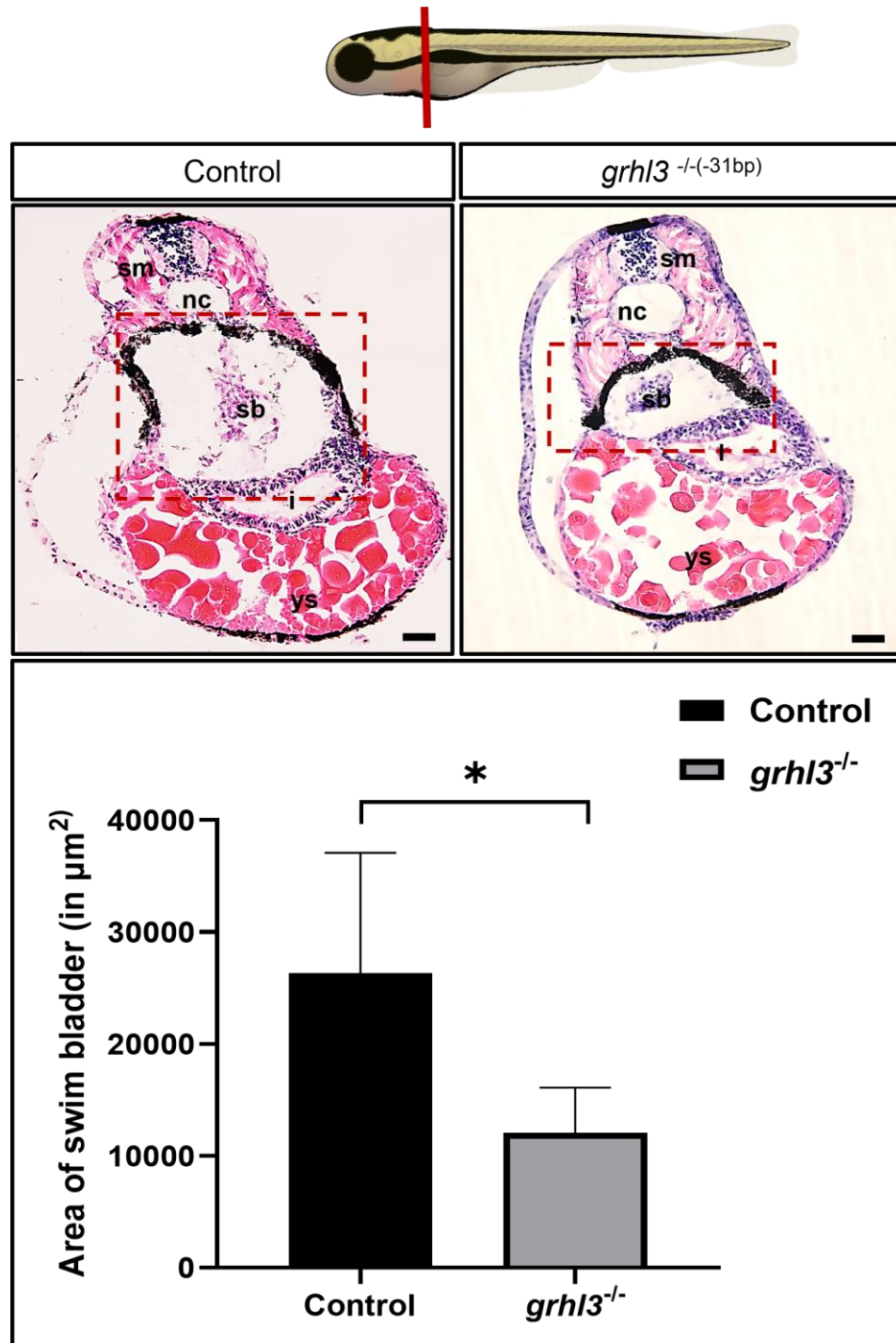
Figure 3.14 Area of swim bladder in *grhl3⁻/⁻* mutants.

(A) H&E staining of transverse-sections across the gut region of class 1 *grhl3⁻/⁻* (right) and control (left) embryos at 5 dpf (swim bladder [**sb**]; intestine [**i**]; yolk sac [**ys**]; notochord [**nc**]; somatic muscle [**sm**]) **(B)** Area of the swim bladder was quantitated in class 1 *grhl3⁻/⁻* (grey) and control (black) embryos using ImageJ software. Data is represented as mean ± SEM; n=3. Statistical significance determined by Student's t-test *P < 0.05.

3.3.5 Gut epithelia appeared normal in *grhl3⁻ᐟ⁻*mutants at 5 dpf and showed no variation in the expression of epithelial markers fibronectin and e-cadherin

In order to investigate if *grhl3* has a role in the establishment of gut epithelia, transverse cryosections were taken along the pharynx, oesophagus, oesophageal-intestinal junction (OI) and intestine of 5-day old class 1 *grhl3⁻ᐟ⁻* embryos and siblings (control). The sections were then stained with haematoxylin and eosin. No aberrant morphology was observed in the epithelia of pharynx, oesophagus, OI junction and intestine (Figure 3.15).

In order to further determine whether the gut epithelium was formed correctly, I investigated the expression of epithelial-identity markers fibronectin and e-cadherin. *grhl3⁻ᐟ⁻* embryos at 5 dpf showed no differences in the expression of fibronectin and e-cadherin proteins in the transverse sections of oesophagus and caudal intestine respectively (Figure 3.16). These results indicate that *grhl3* does not have a role in the formation of intestinal epithelia at 5 dpf.
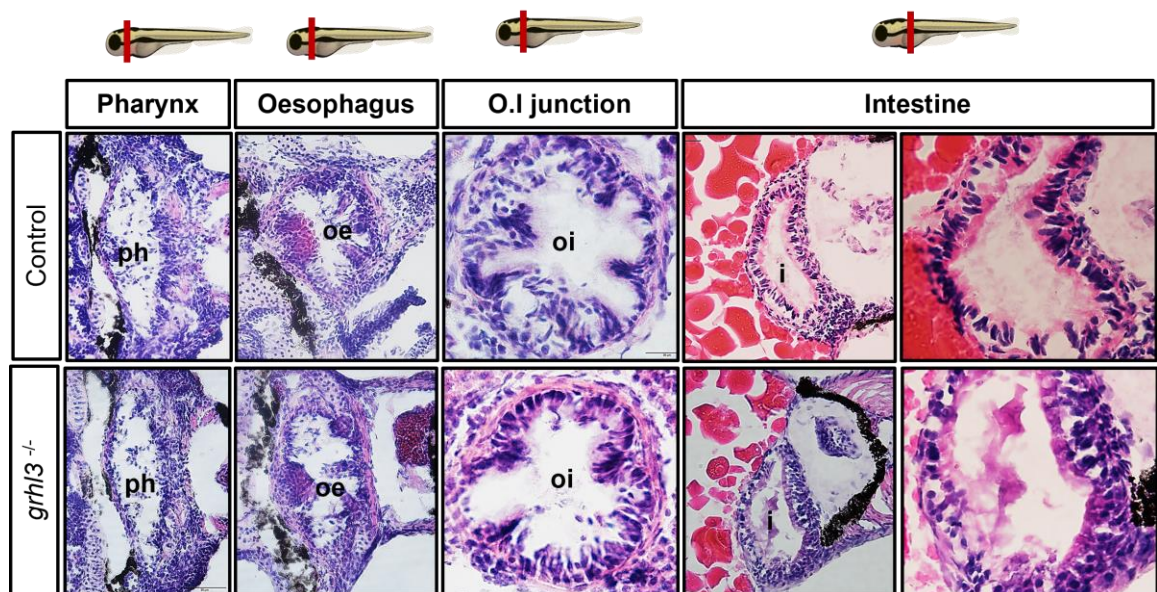
Figure 3.15 Gut epithelial morphology in *grhl3⁻ᐟ⁻* mutants at 5 dpf.

H&E staining of transverse-sections across the pharynx (**ph**), oesophagus (**oe**), oesophageal-intestinal (**oi**) junction and intestine (**i**) of 5-day-old class 1 *grhl3⁻ᐟ⁻* (bottom) and control (top) embryos.
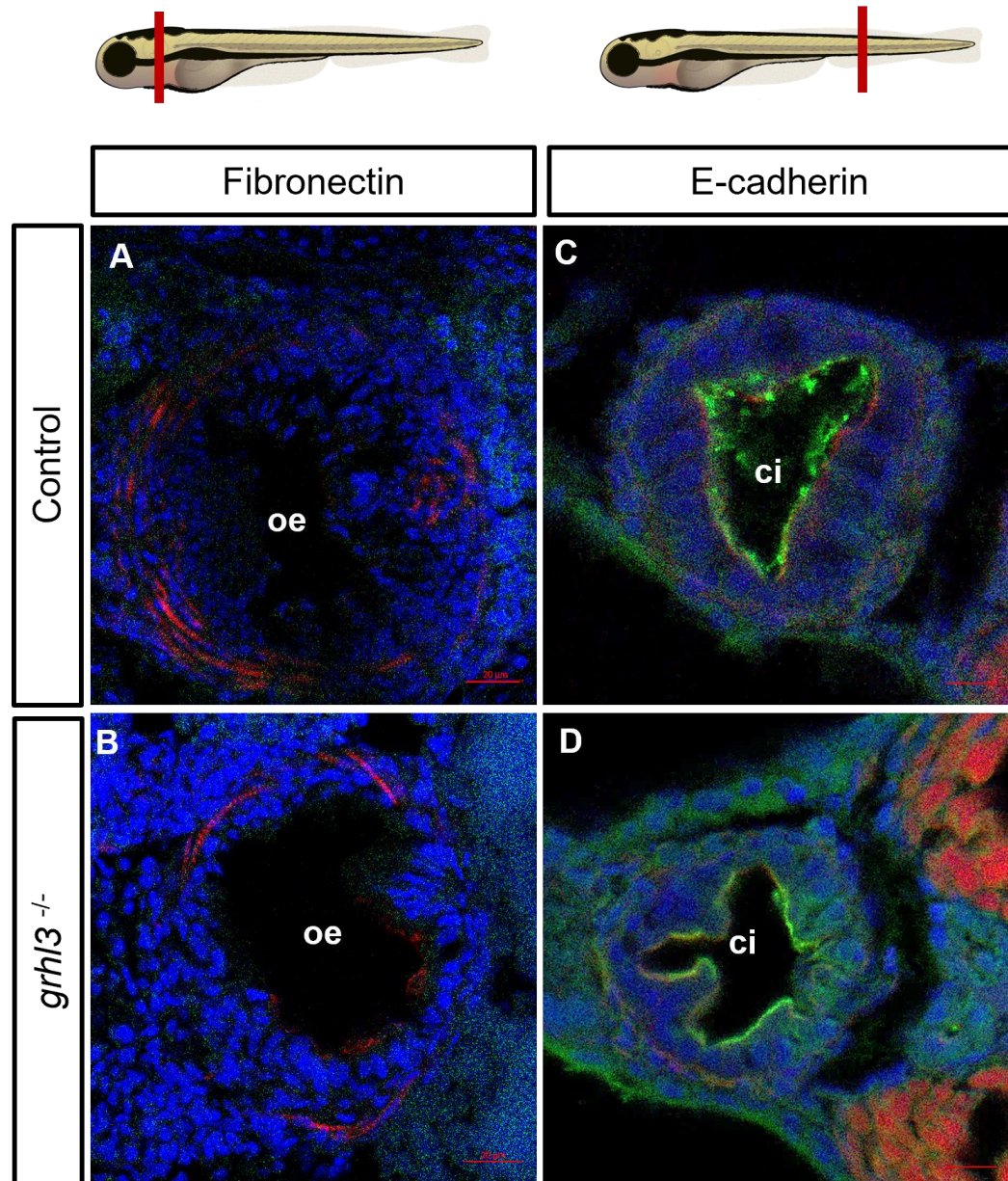
Figure 3.16 Expression of e-cadherin and fibronectin in the oesophagus and caudal intestine of *grhl3⁻/⁻* embryos.

(**A-B**) Immunofluorescent staining of fibronectin (green), DAPI (nuclei, blue) and rhodamine phalloidin (actin filaments, red) in the oesophagus (**oe**) of class 1 *grhl3⁻/⁻* and control embryos at 5 dpf. (**C-D**) Immunofluorescent staining of e-cadherin (green), DAPI (nuclei, blue) and rhodamine phalloidin (actin filaments, red) in the caudal intestine (**ci**) of class 1 *grhl3⁻/⁻* and control embryos at 5 dpf. Scale bars represent 20 µm and 10 µm respectively.

3.3.6 Loss of *grhl3* contributes to severe intestinal defects at 7 dpf

Since no gut epithelial defects were detected at 5 dpf, I investigated the gut epithelial morphology in class 1 *grhl3*^{-/-} larvae at a later time-point (7 dpf). Majority of the larvae die at 7 dpf ; therefore, I investigated the probable cause for their death by examining the morphology of gut epithelia at this time-point. No aberrant epithelial morphology was identified in the oesophageal intestinal junction of *grhl3*^{-/-} embryos at 7 dpf (Figure 3.17). However, *grhl3*^{-/-} mutants displayed haemorrhage in the lumen of rostral and caudal intestine. Additionally, the basement and apical membranes were poorly established and failed to form a distinct boundary both on the external and internal surfaces of the rostral intestinal epithelium. Lastly, rostral intestinal epithelial cells lining the intestine were disorganized and the cell shape was altered relative to controls (Figure 3.17). These results indicate the crucial role played by *grhl3* in the organization and morphogenesis of intestinal epithelial cells and in the establishment of intestinal epithelia at 7 dpf.
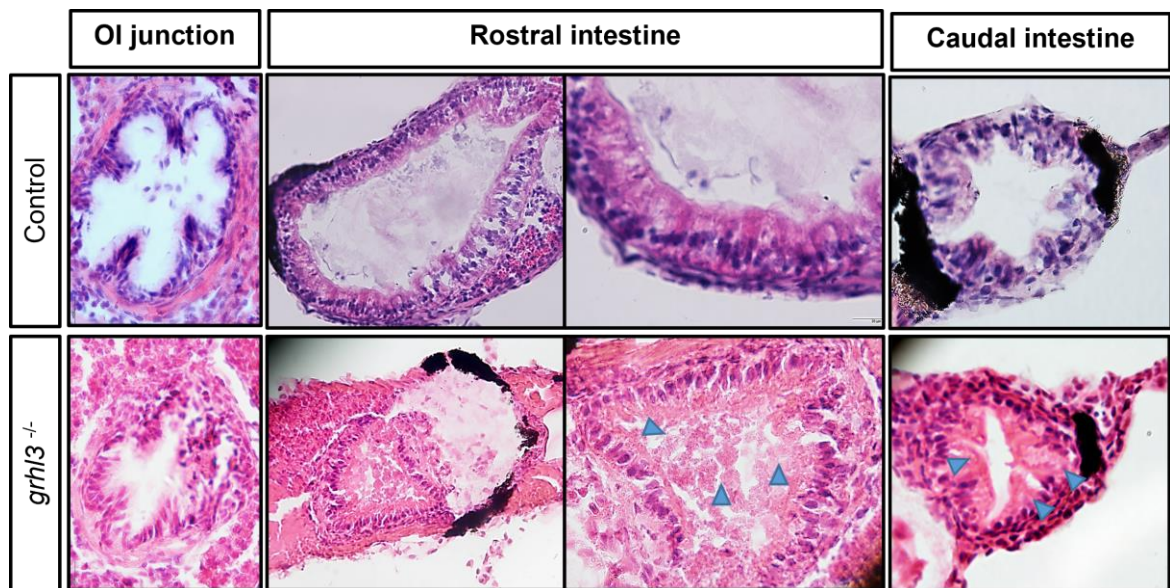
Figure 3.17 Gut epithelial morphology in *grhl3*^{-/-} mutants at 7 dpf.

H&E staining of transverse-sections across the oesophageal-intestinal junction and rostral and caudal intestine of 7 dpf class 1 *grhl3*^{-/-} (bottom) and control (top) embryos.

3.4 Discussion

I present here the novel phenotypes displayed by *grhl3* CRISPR knockout zebrafish embryos. Phenotypic analysis of *grhl3*-/- embryos revealed the presence of axial defects and reduced axial length very similar to the *grhl3* morphants (Dworkin, Simkin et al. 2014). However, *grhl3* null embryos displayed three axial defects with varying degrees of severity as opposed to the *grhl3* morphants, which showed only a single convergence-extension (CE) defect. Although it is possible that the mechanisms behind each of the three defects are the same, the precise reason for the occurrence of three axial phenotypes in *grhl3*-/- embryos is currently unknown. However, these findings are completely consistent with phenotypes observed in both the *curly-tail* and *Grhl3*-/- mouse lines (Ting, Wilanowski et al. 2003). Although homozygous-mutant embryos of both lines are genetically identical, embryos of both strains present with phenotypically distinct presentations of NTD severity, as outlined in Chapter 1. These data point to undiscovered epigenetic influences in the regulation of *Grhl3/grhl3* dependent signalling, and excitingly, these appear to be conserved between zebrafish and higher vertebrates.

The axial phenotype observed in *grhl3* morphants and mutants was analogous to the posterior spinal cord defects seen in murine hypomorphic *Grhl3* (*curly tail*) mutants (Gustavsson, Greene et al. 2007). Although the mechanisms of neurulation vary between zebrafish and mammals, it is proposed that the common NTD-like phenotypes seen in fish and mouse might be attributed to the convergence-extension movements of the pre-tubular plate, common to both species or more presumably these phenotypes might be caused via unique mechanisms that are yet to be discovered.

The axial defects in *grhl3* larvae hinders their swimming movements thereby making it difficult to obtain food post 5 dpf. Furthermore, upon assessing the size of the swim bladder of *grhl3*-/- embryos, it was found to be significantly reduced, suggesting that inflation of swim bladder fails to take place in the absence of *grhl3* gene. Swim bladder, a gas-filled sac, (Fänge 1966) homologous to the tetrapod lungs, is used to regulate buoyancy and help remain fish at their current water depth, thereby minimising the energy expended in swimming (Finney, Robertson et al. 2006). Failure of swim bladder inflation in *grhl3* mutants contributes to poor buoyancy and the larvae may have issues regulating their depth in water. Poor swim bladder inflation might be attributed to the axial defects that prevent the *grhl3*-/- larvae from swimming towards the surface to

swallow the surface air (Lindsey, Smith et al. 2010, Marrs, Clendenon et al. 2010). Furthermore, malformed craniofacial skeleton in *grhl3* mutants i.e., the shortening of distance between lower and upper jaw; absence of ceratobranchials and basihyal, reduction in the size of orofacial cavity and the diminished distance between MC and ceratohyal; might not allow larvae to swallow air effectively (Marrs, Clendenon et al. 2010), contributing to reduction in the size of swim bladder. Thus, poor swimming motions due to axial defects coupled with failure of swim bladder inflation and craniofacial defects becomes challenging for the larvae to obtain food (i.e., free, floating rotifers), possibly resulting in lethality of *grhl3*^{-/-} larvae.

The jaw defects detected in *grhl3* mutants were closely similar to hypoplasia observed in *grhl3* morphants (Dworkin, Simkin et al. 2014). Therefore, I speculate the craniofacial defect observed in *grhl3* mutants is likely to be caused due to changes in pharyngeal microenvironment as seen in *grhl3* morphants. *grhl3*, expressed in the medial endoderm and endodermal pouches of pharynx, drives the differentiation of NCC (Dworkin, Simkin et al. 2014). Maintenance of the NCC population within the pharyngeal arches is critical for the formation of craniofacial cartilage and this critical process is brought about largely by endothelin (*edn1*)(Dworkin, Simkin et al. 2014) signalling regulated by *grhl3*. Therefore, loss of *grhl3* leads to disruption of signalling from pharynx due to aberrant formation of pharyngeal epithelium. This contributes to apoptosis of NCCs in *grhl3* morphants, resulting in severe craniofacial hypoplasia (Dworkin, Simkin et al. 2014). The next step to confirm the role of *grhl3* in craniofacial formation would be is to evaluate the expression of NCC markers (such as *edn1*, *dlx3* and *hand2*) and perform apoptotic analysis (TUNEL) to determine the underlying cause of craniofacial defects in *grhl3*^{-/-} embryos.

In mice, *Grhl3* was found to be expressed in the endoderm derived epithelia, such as that of the gut (Kudryavtseva, Sugihara et al. 2003) and the loss of *Grhl3* contributed to defects in forestomach epithelium (Yu, Lin et al. 2006). Similarly, *grhl3*-deficiency in zebrafish embryos at 7 dpf resulted in intestinal epithelial defects such as haemorrhage and poor membrane formation in the rostral intestine. The accumulation of blood in the intestinal lumen can be linked to weakened intestinal epithelia due to loss of *grhl3*. However, at 5 dpf, *grhl3*-deficient embryos showed normal epithelial formation and differentiation in the gut. Furthermore, e-cadherin, an epithelial marker, and a direct target of *Grhl3* (Alotaibi, Basilicata et al. 2015), showed no differences in expression in

the caudal intestine of mutants and control demonstrating that loss of *grhl3* does not affect the development of intestinal epithelia at 5 dpf.

Absence of intestinal defect at 5 dpf might be because embryos draw nourishment from the yolk sac until 5 dpf, after which they begin to feed exogenously. Differentiation of intestinal cells and barrier formation is reliant on the presence of microflora obtained from the environment from 5 dpf (Bates, Mittge et al. 2006). As the larvae display difficulty in swimming and jaw defects, there is poor colonization of microflora exogenously from the environment contributing to arrest in cell differentiation (Bates, Mittge et al. 2006) and poor uptake of proteins and essential nutrients (Farber, Pack et al. 2001, Wallace, Akhter et al. 2005). Lack of nutrients can affect the development of organs especially liver, intestine, muscle and gonads (Watts, Powell et al. 2012). This may be why we see discrepancies in results upon examination of the intestinal epithelium of *grhl3*$^{-/-}$ embryos at 5 dpf and 7 dpf.

3.5 Conclusion and future directions

Taken together, this study showed that the axial phenotypes and craniofacial hypoplasia seen in *grhl3* null embryos was analogous to the defects observed in *grhl3* morphants, thereby confirming the role of *grhl3* in axial patterning and formation of craniofacial cartilage. Furthermore, the intestinal epithelial defects observed at 7-day old *grhl3* mutants, highlights the novel role played by *grhl3* in formation of intestinal epithelia. Future studies must investigate the expression of patterning markers (*shh, pax6, ptc, twhh*), intestinal formation genes (*hes, hox* family of genes) and neural crest markers (*dlx2, edn1, hand2, dlx3, sox9b, snai1b*) in *grhl3*$^{-/-}$ and WT embryos via in-situ hybridization to understand the gene expression differences in *grhl3*$^{-/-}$ embryos relative to WT embryos. This will shed light on the possible mechanism involved in the aetiology of axial defects, intestinal epithelial defects, and craniofacial abnormalities in *grhl3*$^{-/-}$ embryos.

3.6 Supplementary data

Supplementary table 3.1 Exon 4 sequence of *grhl3*^{-/-(+14bp)}, *grhl3*^{-/-(-31bp)} and *grhl3*^{-/-(1-Δ4)} mutant embryos.

The sequence in red signifies the stop cassette insertion.

grhl3 exon 4 sequence	CAGCTCTTCCCCTGAACTTGCCCCGCTGGAGAACGCTCACATCATGAAGTTC CTTTCAGAAAACATGTCCTTCAACCCCTCAAAGCCTAGCACTGACAGCTACA CAACAGACAACTATGATAAGCAAGTCAACCTGAACAACATCTTCGACTCTC TCCTGCCTCAACCGTCGCAGAAATCATGGCAATCGGATCAAACCTTTCTGGA GGCCACACCTGAGGTCCGCATTTATGT
grhl3 (+14bp) exon 4 sequence	CAGCTCTTCCCCTGAACTTGCCCCGCTGGAGAACGCTCACATCATGAAGTTC CTTTCAGAAAACATGTCCTTCAACCCCTCAAAGCCTAGCACTGACAGCTACA CAACAGACAACTATGATAAGCAAGTCAACCTGAACAACATCTTCGACTCTC TCCTGCCTCAACCttaattaagctgttgtaGCAGAAATCATGGCAATCGGATCAAACCT TTCTGGAGGCCACACCTGAGGTCCGCATTTATGT
grhl3 (-31 bp) exon 4 sequence	CAGCTCTTCCCCTGAACTTGCCCCGCTGGAGAACGCTCACATCATGAAGTTC CTTTCAGAAAACATGTCCTTCAACCCCTCAAAGCCTAGCACTGACAGCTACA CAACAGACAACTATGATAAGCAAGTCAACCTGAACAACATCTTCGACTCTC TCCTGCCTCAAccttTCTGGAGGCCACACCTGAGGTCCGCATTTATGT
grhl3(1-Δ4) exon 4 sequence	**Deletion of exon 4**

Chapter 4: Role of the grhl3 Gene Regulatory Network (GRN) in epithelial development

4.1 Summary

As transcription factors, the *Grhl*-genes bind to the promoters of several target genes and activate (or repress) a cascade of transcriptional networks to drive epithelial development and homeostasis. To identify the genes that are potentially regulated by *Grhl,* three major approaches were used. Firstly, in-silico analysis was performed whereby promoters of all mammalian genes were aligned to search for the presence of the conserved *grhl* binding site (AACCGGTT). Secondly, meta-analysis of all 41 currently published *grh* and *Grhl* RNA-SEQ and microarray datasets was performed in order to identify the transcriptional networks controlled by *grh*/*Grhl* genes across disparate biological contexts. Thirdly, I cross-referenced our results with published ChIP and ChIP-SEQ datasets to determine which of the critical effector genes are likely to be direct targets, based on promoter or enhancer occupancy of *grh*/*Grhl* genes. Finally, to interrogate the predictive strength of our approach, I experimentally validated the expression of the top 10 candidate *grhl* target genes in epithelial development in a zebrafish model lacking *grhl3* and found that orthologues of seven of these (*cldn23, ppl, prom2, ocln, slc6a19, aldh1a3*, and *sod3*) were significantly downregulated at 48 hours post-fertilisation. Thus, my study provides an excellent resource for the identification of putative *grh*/*Grhl* effector target genes.

Much of the work outlined in this chapter was published (Mathiyalagan, Genes, 2019), and has been adapted and re-formatted for inclusion in this thesis.

4.2 Introduction

Epithelia are highly dynamic tissues, actively regulating embryonic growth and expansion, as well as providing essential biochemical and mechanical signal-transduction cues. Understanding the nature of the genetic networks that regulate normal epithelial development is therefore the cornerstone of understanding birth defects due to epithelial aberrations. These include not only significant congenital abnormalities, (neural tube defects, cleft lip/palate, intestinal dysfunction), but importantly, also underpin numerous epithelial disorders in later life (such as psoriasis, eczema, ectodermal dysplasia and critically, cancers). Therefore, identifying the genes that drive epithelial formation and maintenance is a necessary first step to develop therapies that may ultimately ameliorate both the severity and incidence of congenital and adult-onset epithelial pathologies.

grh/*Grhl* transcription factor, one of the key regulators of epithelial homeostasis drives epithelial formation by binding to a promoter or enhancer element and regulating subsequent transactivation or repression of target effector genes, alongside recruitment of transcriptional co-factors. The *grh*/*Grhl* binding site is exceptionally well-conserved through evolution, broadly taking the form AA<u>C</u>CG<u>G</u>TT (with the first "C" and second "G" largely invariant, as shown in experimentally validated assays) (Wilanowski, Caddy et al. 2008). Although several upstream regulatory factors, such as branchless/FGF8, IRF6 (Botti, Spallone et al. 2011, Kousa, Zhu et al. 2019) and Erk; (Hemphala, Uv et al. 2003, Mace, Pearson et al. 2005), and interacting co-factors such as LMO4 (Yu, Lin et al. 2006, Hislop, Caddy et al. 2008) have been described, the delineation of *grh*/*Grhl*-dependent transcriptional networks has largely focussed on the identification and characterisation of direct downstream target genes. To this end, in order to identify and predict direct downstream *grh/Grhl*-targets, in-silico analysis was performed by Prof. Tony Papenfuss, A/Prof. Tomasz Wilanowski and Prof. Stephen Jane (unpublished), in which the promoters of all placental mammal genes were aligned and screened for the presence of a conserved *grh*/*Grhl* binding site. This approach identified a catalogue of genes, (a database which was termed "PHYLO-PROM") and this database formed an excellent database resource from which to select and experimentally validate putative candidates that may be direct *Grhl*-target genes. Bona fide target genes which have been experimentally characterised form this database include e.g., *Tgm1*/5 (Cangkrama, Darido et al. 2016), *ARHGEF19* (Caddy, Wilanowski et al. 2010), *Dsg1* (Wilanowski, Caddy et al. 2008), *eng2a* (Dworkin, Darido et al. 2012), *spec1* (Dworkin, Darido et al. 2012), *edn1* (Dworkin, Simkin et al. 2014) and PTEN (Darido, Georgy et al. 2011).

The predicted target genes from PHYLO-PROM were then compared with the RNA SEQ dataset derived from 1st pharyngeal arch of *Grhl2*-/- mouse to determine any commonly identified putative targets of *Grhl* between PHYLO-PROM and the mouse RNA-SEQ dataset. A literature study of these potential target genes was carried out to determine whether they have been validated in literature as *Grhl* target, to confirm the reliability of this approach.

It is still unclear how the *grh/Grhl*-dependent transcriptome regulates numerous disparate functional processes across different biological contexts. What is clear though, is that the functional interaction between *grainyhead*-signalling and target gene regulation is highly dependent on tissue, developmental/disease stage and organism, and the incredible

heterogeneity of these regulations suggest that delineation of *grh*/*Grhl* transcriptional network will shed significant light on understanding both embryonic development and disease.

Currently, 41 Microarray/RNA-SEQ datasets probing *Grhl* function have been reported in the literature, from both *Drosophila* and mouse tissues, as well as several human cancer/short-hairpin RNA (shRNA) cell lines (Table 4.1). In order to delineate the *grh*/*Grhl* transcriptional network, I have interrogated these datasets to bring greater clarity to the *Grainyhead*-dependent transcriptome and to begin to understand the critical effector genes that operate broadly across disparate contexts, as well as identifying those that have more restricted roles in specific processes, particularly epithelial development.

Using our recently described *grhl3*$^{-/-}$ zebrafish that present with epithelial defects (Miles, Darido et al. 2017), I performed Q-RT-PCR to determine the expression of zebrafish orthologues of the ten most-differentially regulated epithelial genes, thereby functionally testing the predictive strength of our meta-analysis approach in a novel animal model.

Lastly, during my PhD, my supervisor was contacted by A/Prof. Mahendra Sonawane and his team at Tata Institute of Fundamental Research (TIFR), Mumbai, India, who had independently determined that *grhl3* interacts with *myoVb* (an actin based molecular motor) during the maintenance of epithelial integrity. To this end, I was able to perform some experiments to validate the *grhl3-myovb* interaction using *myoVb* morpholinos in our *grhl3*$^{+/-}$ fish.

Therefore, this chapter collates multiple "big-data" approaches and provides an experimental pipeline for determining and testing novel *grh/Grhl*-dependent functional interactions across various disease contexts.

Table 4.1 Published datasets used for meta-analysis.

Microarray and RNA-SEQ datasets including tissue of origin were classified as being derived from either "primary epithelia", "cell line – cancer", "cell line – non-cancer", "other mammalian" or "other non-mammalian" for subsequent analyses.

Gene	Species	Dataset	Tissue / Cell line	Classification/Origin	Reference
grh	*Drosophila melanogaster*	1	2-3 hour whole embryos	*Other - non-mammalian*	Nevil et al., *Genetics* , 2017
		2	11-12 hour whole embryos	*Other - non-mammalian*	Nevil et al., *Genetics* , 2017
		3	15-16 hour whole embryos	*Other - non-mammalian*	Nevil et al., *Genetics* , 2017
		4	13-16 hour whole embryos	*Other - non-mammalian*	Yao et al., *Development* , 2017
		5	13-16 hour whole embryos	*Other - non-mammalian*	Yao et al., *Development* , 2017
		6	Stage 16-17 whole embryos	*Other - non-mammalian*	Yao et al., *Development* , 2017
Grhl	*Neurospora crassa*	7	48 hour aerial hyphae and conidia	*Other - non-mammalian*	Pare et al., *PLoS ONE* , 2012
Grhl2	*Mus musculus*	8	E9.5 Non-neural ectoderm	*Primary Epithelia*	Ray et al., *Development* ,2016
		9	E16.5 Lung epithelium	*Primary Epithelia*	Kersbergen et al., *Dev. Biol* ., 2018
		10	E16.5 Lung epithelium	*Primary Epithelia*	Kersbergen et al., *Dev. Biol* ., 2018
		11	E9.5 Cranial tissue	*Other - mammalian*	Pyrgaki et al., *Dev. Biol* ., 2011
		12	Extraembryonic trophectoderm-derived tissues at E7.5	*Other - mammalian*	Walentin et al., *Development* , 2015
		13	E9.5 Placenta	*Other - mammalian*	Walentin et al., *Development* , 2015
		14	E9.5 First pharyngeal arch (PA1)	*Other - mammalian*	Carpinelli et al., *submitted* , 2019
		15	Immortalised Mouse Lung Epithelial Cells (**MLE15**)	*Cell line - Non-Cancer*	Varma et al*., J. Biol. Chem* ., 2012
		16	NIH3T3 fibroblast cells	*Cell line - Non-Cancer*	Werner et al., *J. Biol. Chem* ., 2013
		17	IMCD-3 (inner medullary collecting duct) cell line	*Cell line - Non-Cancer*	Aue et al., *J AmSoc Nephrol* , 2015
Grhl2	*Canis familiaris*	18	Madin-Darby Canine Kidney (**MDCK**) cells	*Cell line - Non-Cancer*	Pifer et al., *Mol. Biol. Cell* , 2016
		19	Madin-Darby Canine Kidney (**MDCK**) cells	*Cell line - Non-Cancer*	Pifer et al., *Mol. Biol. Cell* , 2016
Grhl2	*Homo Sapiens*	20	"Early Passage" Primary Normal Human Epidermal Keratinocytes (**NHEK**)	*Primary Epithelia*	Chen et al., *Cell Death Dis* ., 2012
		21	"Late passage" **NHEK**	*Primary Epithelia*	Chen et al., *Cell Death Dis* ., 2012
		22	Undifferentiated primary human bronchial epithelial cells	*Primary Epithelia*	Gao et al., *PNAS,* 2014
		23	**4T1** breast tumour cells	*Cell line - Cancer*	Xiang et al., *PLOS ONE,* 2012
		24	**HMLE-Twist-ER cells**	*Cell line - Cancer*	Cieply et al., *Cancer Res.* , 2012
		25	**MSP** (mesenchymal sub-population) cells obtained from HMLE cells	*Cell line - Cancer*	Farris et al., *Mol Cancer Res* . 2016
		26	**OVCA429** (ovarian cystadenocarcinoma; intermediate epithelial [IE] phenotype)	*Cell line - Cancer*	Chung et al., *Scientific Reports* , 2016
		27	**LNCaP** (human prostate carcinoma cells)	*Cell line - Cancer*	Paltoglou et al., *Cancer Res* . 2017
Grhl3	*Mus musculus*	28	Embryonic day 18.5 (E18.5) embryo backskin	*Primary Epithelia*	Yu et al., *Dev. Biol* ., 2006
		29	E14.5 Bladder	*Primary Epithelia*	Yu et al., *EMBO J* , 2009
		30	E16.5 Bladder	*Primary Epithelia*	Yu et al., *EMBO J* , 2009
		31	E18.5 Bladder	*Primary Epithelia*	Yu et al., *EMBO J* , 2009
		32	E14.5 Skin	*Primary Epithelia*	Gordon et al., *J Clin. Invest* ., 2014
		33	E16.5 Skin	*Primary Epithelia*	Gordon et al., *J Clin. Invest* ., 2014
		34	E18.5 Skin	*Primary Epithelia*	Gordon et al., *J Clin. Invest* ., 2014
		35	Adult Skin	*Primary Epithelia*	Gordon et al., *J Clin. Invest* ., 2014
		36	Adult Skin	*Primary Epithelia*	Gordon et al., *J Clin. Invest* ., 2014
		37	Adult Skin	*Primary Epithelia*	Gordon et al., *J Clin. Invest* ., 2014
Grhl3	*Homo sapiens*	38	**NHEK** (Neonatal Human Epidermal Keratinocytes) cells	**Primary Epithelia**	Hopkin et al., *PLoS Genet* . 2012
		39	**NHEKs** and adult psoriasis skin	**Primary Epithelia**	Gordon et al., *J Clin. Invest* ., 2014
Grhl3-Isoform 1	*Homo Sapiens*	40	Human Embryonic Kidney neuroepithelial cell line (**HEK-293**)	**Cell line - Non-Cancer**	Haendeler et al., *Arter. Thromb. Vasc. Biol* ., 2013
Grhl3-Isoform 3	*Homo Sapiens*	41	**HEK-293**	**Cell line - Non-Cancer**	Haendeler et al., *Arter. Thromb . Vasc. Biol* ., 2013

4.3 Results

4.3.1 Predicted target genes of Grhl identified via in-silico analysis (PHYLO-PROM)

As TFs, *grh/Grhl* proteins bind to the promoters of target genes, where they homo- and heterodimerise to regulate transcription, through recruitment of transcriptional coactivators. In order to determine the potential targets genes of *Grhl*, the promoters of all mammalian genes were aligned and searched for the *Grhl* conserved site (AA**C**CG**G**TT). A database comprising of 305 candidate target genes of *Grhl* (termed PHYLO-PROM) was established via this method.

This predictive dataset was then compared with a list of 368 genes that were determined to be differentially regulated in the 1st pharyngeal arch of 5 x *Grhl2*^{-/-} mice and 5 x wild-type control littermates via RNA-SEQ (Carpinelli, DMM, 2020) (Figure. 4.1). This was done to identify genes that were both a predicted target (PHYLO-PROM), and a differentially regulated gene (1st arch RNA-SEQ data dataset) of *Grhl*. 21 genes were found to be differentially expressed following *Grhl* deregulation and were also identified as putative *Grhl* targets, of which 4/21 of these genes have been previously validated as *Grhl* targets (*Cldn4*, *Cdh1*, *Ppl* and *Arhgef19*).

This study was done as a prelude to the meta-analysis approach which encompassed all the published RNA-Seq datasets of *Grhl* across numerous disparate biological contexts, to identify genes differentially expressed following *Grhl* loss.

4.3.2 Meta-analysis reveals the most consistently differentially regulated genes following *grh/grhl* misexpression

In order to analyse the *grh/Grhl* transcriptome across multiple disparate biological contexts, we standardised all published *grh/Grhl* Microarray/RNA-SEQ datasets into a common format that allowed for direct comparison of differing methodologies and results, together with the corresponding published fold-changes and p-values. Differences in methodologies and data reporting in published studies created a need to integrate lists of regulated genes that were of different lengths, selected using different (study-specific) criteria. As studies varyingly examined the effects of either loss- or gain of function of *grh/Grhl*, we divided the data based on whether a gene was positively or negatively regulated under normal homeostatic conditions. That is, if a gene was found to be downregulated in an experimental paradigm following loss of *grh/Grhl*, we deemed it to

be positively regulated. Next, the positively and the negatively regulated genes were separately ranked on the basis of the reported fold-change within each dataset.

Our analysis allowed us to determine the genes that are both most frequently, and also most substantially, differentially regulated following gain/loss of *grh/Grhl* function. From these comparisons, we determined which genes exhibited the greatest degree of regulation following disruption of *grh/Grhl* signalling. We determined this by 1) frequency of altered expression (the number of datasets a given gene appeared in as "regulated"); and 2) degree of regulation, measured by the score based on the rank given to a gene in a particular dataset with respect to other differentially regulated genes. These analyses allowed us to reveal the genes that appeared within at least one dataset and determine the top differentially regulated genes following *grh/Grhl* de-regulation or misexpression, across all biological contexts thus far tested and described in the literature.

From these analyses, we compiled a list of the top 50 most-highly differentially regulated genes (following *grh/Grhl* modulation) across various tissues and cell lines and at different developmental time points (Table 4.2). As *grh/Grhl* genes bind to the promoter of target genes in order to drive transcription, I determined whether any of these genes had previously been identified as being bound to by *grh/Grhl* factors in ChIP or ChIP-SEQ datasets. In total, 15 of the top 50 genes in our list (30%; *tmem54, prom2, cldn4, ppl, cdh1, rab15, lad1, rab25, Epcam, Tacstd2, st14, Esrp1, Prss22, spint1* and *prss8*) were known to be bound to by *grh/Grhl* factors, indicating the strong predictive power of our approach. Additionally, seven genes in our list - *cldn4, rab15, rab25, epcam, cdh1, tslp,* and *spint1* - had been previously characterised as direct *Grhl*-target genes through biological validation experiments, further highlighting the predictive strength of our approach.

A.

PHYLO-PROM | RNA-Seq
(Predicted Direct Target genes)(FDR<0.015)

305 | 21 | 368

21 predicted target genes are differentially regulated in the 1st pharyngeal arch of *Grhl2-/-* mice

B.

Predicted direct *Grhl2*-target genes in RNA-Seq dataset		
Ovol1	OVO homolog-like 1 (Drosophila)	-3.760
Arhgef19	Rho guanine nucleotide exchange factor (GEF) 19	-3.753
Cldn4	Claudin 4	-3.326
Pvrl4	poliovirus receptor-related 4	-3.126
Grhl2	Grainyhead-like 2	-3.027
Ppl	Periplakin	-2.817
Cdh1	cadherin 1/E-Cadherin	-2.471
Tbc1d2	TBC1 domain family, member 2	-1.138
Tfap2c	transcription factor AP-2, gamma	-0.996
Sh3bgrl2	SH3 domain binding glutamic acid-rich protein like 2	-0.473
Nhs	Nance-Horan syndrome	-0.336
Rbm18	RNA binding motif protein 18	-0.210
Rcc2	regulator of chromosome condensation 2	-0.186
Nr2f2	nuclear receptor subfamily 2, group F, member 2	0.308
Mxra8	matrix-remodelling associated 8	0.349
Vat1	vesicle amine transport protein 1 homolog (	0.364
Kctd12b	potassium channel tetramerisation domain containing 12b	0.384
Npr3	natriuretic peptide receptor 3	0.652
Cbln1	cerebellin 1 precursor protein	1.019
Nog	Noggin	1.318
Klhdc8a	kelch domain containing 8A	3.000
Red = Previously validated direct Grhl-targets		

Disease Models and Mechanisms, 2020

Figure 4.1 Putative targets of *Grhl* as identified from PHYLO-PROM and RNA Seq dataset derived from *Grhl2-/-* mouse pharyngeal arch.

Promoters of all mammalian genes were aligned and searched for the highly conserved *Grhl* binding site (AA<u>CC</u>G<u>G</u>TT). A database (PHYLO-PROM) of 305 predicted candidate target genes was generated. **(A)** PHYLO-PROM genes were compared to a list of 368 genes differentially regulated in RNA-Seq dataset of the *Grhl2-/-* mouse pharyngeal arch. **(B)** A final list of 21 predicted target genes that were differentially regulated was generated.

Table 4.2 The top 50 most differentially regulated genes in all biological contexts following modulation of *grh/Grhl function*.

The overall top 50 differentially regulated (both positively and negatively) genes of *grh*/*Grhl* as identified by analysis of all published Microarray and RNA-SEQ datasets. 15 out of the 50 predicted target genes had previously been validated in literature through either large-scale ChIP-SEQ genome mining experiments, or through experimental validation (highlighted in red).

Rank	Gene	Regulation	Normalised Score	Known relationships with Grhl Transcription Factors	
				Locus bound by GRHL (ChIP and ChIP-SEQ)	*Experimental validation*
1	Tmem54	POSITIVE	0.184	*Aue, et al. 2015,Walentin et al. 2015*	
2	Prom2	POSITIVE	0.182	*Aue, et al. 2015,Walentin et al. 2015*	
3	Cldn4	POSITIVE	0.148	*Chung, et al. 2016, Werth et al., 2010, Varma et al., 2012*	*Senga, et al. 2012, Varma et al. 2012, Tanimizu and Mitaka 2013, Aue et al. 2015*
4	Cldn23	POSITIVE	0.113		
5	Grhl2	POSITIVE	0.089		
6	Ppl	POSITIVE	0.0868	*Aue, Hinze et al. 2015*	
7	Ocln	POSITIVE	0.0777		
8	Cdh1	POSITIVE	0.0754	*Aue, et al. 2015, Chung, et al. 2016, Werth et al. 2010, Varma et al. 2012*	*Werth, et al. 2010, Pyrgaki, et al. 2011, Xiang, et al. 2012, Gao, et al. 2013, Tanimizu and Mitaka 2013, Chung, et al. 2016, Nishino, Takano et al. 2017, Pan, et al. 2017*
9	Krt7	POSITIVE	0.0752		
10	Tslp	POSITIVE	0.0741		
11	Rab15	POSITIVE	0.0708	*Walentin et al. 2015*	
12	Gm19601	NEGATIVE	0.069		
13	Lad1	POSITIVE	0.0661	*Walentin et al. 2015*	
14	Gm3579	NEGATIVE	0.065		
15	Rab25	POSITIVE	0.0631	*Aue, et al. 2015*	*Senga, et al. 2012*
16	Epcam	POSITIVE	0.0618	*Chung, et al. 2016*	*Xiang, et al. 2012*
17	Snx31	POSITIVE	0.0607		
18	Slc6a19	NEGATIVE	0.0579		
19	Zasp66	NEGATIVE	0.0578		
20	Ap1m2	POSITIVE	0.0576		
21	Sfn	POSITIVE	0.0565		
22	IL36RN	POSITIVE	0.0562		
23	2310001H18Rik	POSITIVE	0.0562		
24	Il17re	POSITIVE	0.0558		
25	Macc1	POSITIVE	0.0558		
26	Evpl	POSITIVE	0.055		
27	Gm20305	NEGATIVE	0.0547		
28	Aldh1a3	POSITIVE	0.0538		
29	Tacstd2	POSITIVE	0.0531	*Chung, et al. 2016*	
30	Sprr1a	POSITIVE	0.0528		
31	St14	POSITIVE	0.0525	*Chung, et al. 2016*	
32	Rbbp8	POSITIVE	0.0521		
33	Tmprss11b	POSITIVE	0.0519		
34	Cldn7	POSITIVE	0.0515		
35	CG10345	NEGATIVE	0.0501		
36	Sod3	NEGATIVE	0.05		
37	CG12480	NEGATIVE	0.0499		
38	Esrp1	POSITIVE	0.0499	*Chung, et al. 2016*	*Xiang, et al. 2012*
39	Prss22	POSITIVE	0.0497	*Aue, et al. 2015*	
40	Cyp2b19	NEGATIVE	0.0497		
41	Car6	NEGATIVE	0.0497		
42	Car2	POSITIVE	0.0495		
43	Fmo2	NEGATIVE	0.0493		
44	Elovl1	NEGATIVE	0.0492		
45	Elovl7	NEGATIVE	0.0492		
46	Defb3	POSITIVE	0.0488		
47	Spint1	POSITIVE	0.0481	*Chung, et al. 2016, Walentin et al. 2015*	*Walentin, et al. 2015, Matsushita, et al. 2018*
48	Prss8	POSITIVE	0.0481	*Chung, et al. 2016*	
49	Cldn6	POSITIVE	0.0481		
50	Gsta2	NEGATIVE	0.0479		

4.3.3 Biological pathways regulated by *grhl* genes in epithelia, as identified by Gene Ontology (GO) analysis

In order to determine the overall biological processes regulated by the *grh/Grhl* pathway, we performed GO (Gene Ontology) pathway analysis, using gProfiler's GOStat (Gene Group Functional Profiling) with the default background set of all human genes. Mindful of obvious limitations such as tissue origin, disease state and temporal/developmental time point, we nonetheless analysed all the disparate datasets to determine an "overall" snapshot of *grhl*-target gene biology (Table 4.3). We found that this analysis largely confirmed previous known roles of the *Grhl* family. The major biological functions ascribed to genes regulated by the *Grhl* family were "cell-cell adhesion" "tissue [epithelia/epidermis] development", "animal organ/skin development", "water homeostasis" and "epithelial cell morphogenesis", consistent with known *grh/Grhl*-dependent functions in epithelial morphogenesis and maintenance as well as preventing trans-epidermal water loss and maintaining epithelial integrity through suppressing the epithelial-mesenchymal transition (EMT). Somewhat surprisingly, the GO term "protein cross-linking" was also highlighted in our *grh/Grhl* transcriptome analysis. *grh/Grhl* factors are thought to be constitutively bound to the promoters/enhancers of target genes, achieving transcriptional specificity through recruitment of partner protein co-activators as development proceeds (Nevil, Bondra et al. 2017). These co-factors may include members of the Polycomb and Trithorax groups in Drosophila (Tuckfield, Clouston et al. 2002, Nevil, Bondra et al. 2017) and the vertebrate transcription factor LMO4 (Hislop, Caddy et al. 2008) in mice, although as very few such co-factors are known, enrichment of this GO term may suggest a novel, hitherto unsuspected *grh/Grhl* role in assembly, formation, or maintenance of the core transcriptional apparatus.

Table 4.3 Gene Ontology (GO) analysis of the most differentially regulated cellular processes in all biological contexts, following modulation of *grh/Grhl* function.

Functional Gene Ontology (GO) annotations are over-represented among the 200 genes positively regulated by *grh/Grhl* with highest evidence of regulation across all species (highest fold change score aggregated over all the datasets).

source	term name Gene Ontology (Biological process)	term ID	n. of term genes	n. of query genes	n. of common genes	corrected p-value
BP	biological adhesion	GO:0022610	1351	80	18	1.69e-02
BP	cell adhesion	GO:0007155	1343	80	18	1.56e-02
BP	cell-cell adhesion	GO:0098609	776	79	14	6.29e-03
BP	cell-cell adhesion via plasma-membrane adhesion molecules	GO:0098742	245	79	10	1.43e-04
BP	calcium-independent cell-cell adhesion via plasma membrane cell ...	GO:0016338	23	79	6	9.48e-07
BP	developmental process	GO:0032502	6212	78	45	3.91e-03
BP	anatomical structure development	GO:0048856	5793	78	44	1.43e-03
BP	tissue development	GO:0009888	1926	66	27	6.12e-08
BP	epithelium development	GO:0060429	1218	77	26	8.22e-10
BP	epidermis development	GO:0008544	459	77	19	2.62e-11
BP	multicellular organismal process	GO:0032501	7414	74	48	4.19e-03
BP	multicellular organism development	GO:0007275	5321	78	41	3.72e-03
BP	system development	GO:0048731	4760	78	40	5.09e-04
BP	animal organ development	GO:0048513	3428	77	35	2.65e-05
BP	skin development	GO:0043588	412	77	21	1.18e-14
BP	water homeostasis	GO:0030104	69	77	5	2.14e-02
BP	epithelial cell differentiation	GO:0030855	759	77	19	1.83e-07
BP	epithelial cell differentiation involved in embryonic placenta development	GO:0060671	3	25	2	1.39e-02
BP	epidermal cell differentiation	GO:0009913	353	77	16	1.13e-09
BP	keratinocyte differentiation	GO:0030216	299	77	16	8.72e-11
BP	keratinization	GO:0031424	224	77	15	2.25e-11
BP	cornification	GO:0070268	111	73	11	8.16e-10
BP	multicellular organismal water homeostasis	GO:0050891	64	77	5	1.48e-02
BP	regulation of water loss via skin	GO:0033561	22	77	5	5.79e-05
BP	establishment of skin barrier	GO:0061436	20	77	5	3.43e-05
BP	epithelial cell morphogenesis	GO:0003382	32	25	3	2.65e-02
BP	embryonic placenta morphogenesis	GO:0060669	25	31	3	2.17e-02
BP	labyrinthine layer morphogenesis	GO:0060713	21	31	3	1.26e-02
BP	branching involved in labyrinthine layer morphogenesis	GO:0060670	12	31	3	2.11e-03
BP	epithelial cell morphogenesis involved in placental branching	GO:0060672	3	25	2	1.39e-02
BP	peptide cross-linking	GO:0018149	59	64	5	3.86e-03

4.3.4 *Grhl*-dependent target genes are well-conserved between mouse and human, less so between mouse and Drosophila, and human and Drosophila

In order to determine how well-conserved *grh/Grhl*-dependent transcriptional pathways were between mouse, *Drosophila* and human, I generated separate lists for each organism using only species-specific large-scale microarray/RNA-SEQ datasets. This analysis comprised 20 datasets from mouse, 6 datasets from *Drosophila*, and 12 datasets from human (Table 4.4). Using the top 50-ranked mouse genes as our root list for comparison, I determined which of these genes were ranked in the top 10% differentially regulated genes in both *Drosophila* (in the top 1,300 of ~13,000 genes in the *Drosophila* genome) and human (top 2,500 out of ~25,000 total human genes), reasoning that genes which fell below this ranking threshold were less likely to be biologically-relevant in the context of *grh/Grhl* transcription (Table 4.4). Our analyses showed that 32 of the top 50 mouse genes had an identifiable *Drosophila* orthologue, with 4/32 orthologues of these mouse genes – *Grhl2 (grh), Car6 (CAH7), Car2 (CAH1)* and *unc93a (GC4928)* – also being differentially-regulated in *Drosophila*. Unsurprisingly, the degree of conservation was

greater in human, with 47/50 human orthologues identified, and 17/47 of these mouse targets appearing in the top 10% differentially regulated human genes. Moreover, 13 of these orthologues – PROM2, CLDN4, PPL, GRHL2, CDH1, LAD1, RAB25, TMPRSS13, AP1M2, KLK6, SFN, CLDN1 and RPTN - appeared within the top 500 (top ~2%) most-differentially regulated genes in humans, suggesting that these genes may substantially underpin *Grhl*-dependent transcriptional networks in mammalian species.

Similarly, the top 50-ranked genes from human datasets were compared with top 10% differentially regulated genes of *grh/Grhl* in both mouse and *Drosophila* (Table 4.5). It was revealed that 33/50 human genes had a corresponding *Drosophila* orthologue with 4/33 genes – PTGES *(cg33178),* NOX5 *(Nox),* SERPINE1 *(Spn42Db)*, and ITGA2 *(if)* identified in human datasets showing significant regulation in *Drosophila*. Upon comparison with mouse datasets, it was found that 46/50 genes had a corresponding mouse orthologue with 19/47 of these genes occurring in the top 10% differentially regulated mouse genes (top 2,500 out of 25,000 total mouse genes). 7 of these orthologues namely, *Tmprss13, Elf5, Epcam, Krt7, Cldn4, Cdh2, Aldh3b2* appeared in the top 2% of differentially regulated genes in mouse datasets implying that these genes are critical regulators of *Grhl* in mammalian species. These data are particularly striking, given the large differences in source material used to generate each of the datasets, comprising different organisms, disease states, developmental timepoints and manipulating different *grh/Grhl* orthologues.

Table 4.4 Conservation of differentially regulated genes between mouse, *Drosophila* and human across all biological contexts following modulation of *grh/Grhl* function.

Top 50 most differentially regulated genes of *Grhl* in mouse RNA Seq datasets compared across the list of differentially regulated genes obtained from *Drosophila* and human datasets.

Rank	*Mus musculus* gene symbol	Regulation	Average normalised score	Significant differential regulation in *Drosophila*				Significant differential regulation in in *Homo sapiens*			
				Orthologue	Rank	Regulation	Average normalised score	Orthologue	Rank	Regulation	Average normalised score
1	Prom2	Positive	0.163	prominin-like				PROM2	361	Positive	0.0116
2	Tmem54	Positive	0.154	*No known orthologue*				TMEM54	1062	Positive	0.0178
3	Cldn4	Positive	0.116	*No known orthologue*				CLDN4	28	Positive	0.0264
4	Cldn23	Positive	0.106	*No known orthologue*				CLDN23			
5	Ppl	Positive	0.0812	shot				PPL	110	Positive	0.0187
6	Grhl2	Positive	0.0752	grh	577	Positive	0.0323	GRHL2	159	Positive	0.0165
7	Rab15	Positive	0.0663	RabX4				RAB15			
8	Ocln	Positive	0.0655	Su(Tpl)				OCLN	1141	Positive	0.00717
9	Gm19601	Negative	0.0645	*No known orthologue*				POLR2K*			
10	Tslp	Positive	0.064	*No known orthologue*				TSLP	1957	Positive	0.00534
11	Gm3579	Negative	0.0608	*No known orthologue*				*No known orthologue*			
12	Cdh1	Positive	0.0592	CadN2				CDH1	138	Positive	0.0177
13	Snx31	Positive	0.0568	CG5734				SNX31			
14	Slc6a19	Negative	0.0542	CG43066				SLC6A19			
15	2310001H18Rik	Positive	0.0526	*No known orthologue*				*No known orthologue*			
16	Il17re	Positive	0.0522	*No known orthologue*				IL17RE			
17	Evpl	Positive	0.0514	shot				EVPL	2179	Positive	0.00501
18	Gm20305	Negative	0.0512	*No known orthologue*				*No known orthologue*			
19	Lad1	Positive	0.0508	Nuak1				LAD1	412	Positive	0.0102
20	Aldh1a3	Positive	0.0503	CG31075				ALDH1A3	1528	Positive	0.00614
21	Sprr1a	Positive	0.0494	CG17377				SPR1A			
22	Rbbp8	Positive	0.0487	*No known orthologue*				RBBP8NL			
23	Tmprss11b	Positive	0.0485	CG11836				TMPRSS2			
24	Sod3	Negative	0.0468	CG5948				SOD3			
25	Cyp2b19	Negative	0.0465	Cyp18a1				CYP2B6			
26	Car6	Negative	0.0464	CAH7	582	Positive	0.0323	CA6			
27	Car2	Positive	0.0463	CAH1	590	Positive	0.0323	CA2			
28	Fmo2	Negative	0.0461	Fmo-2				FMO2			
29	Defb3	Positive	0.0456	*No known orthologue*				HBETAD3			
30	Rab25	Positive	0.0453	Rab11				RAB25	241	Positive	0.0137
31	Prss8	Positive	0.045	CG16749				PRSS8			
32	Cldn6	Positive	0.045	*No known orthologue*				CLDN6			
33	Gsta2	Negative	0.0448	GstS1				GSTA1/2/3/5			
34	Aox4	Negative	0.0446	ry				AOX1			
35	Tmprss13	Positive	0.0441	Sb				TMPRSS13	5	Positive	0.0346
36	Smpdl3b	Positive	0.0437	CG32052				SMPDL3B			
37	Ap1m2	Positive	0.0434	AP-1mu				AP1M2	464	Positive	0.0105
38	Pax8	Negative	0.0433	sv				PAX8			
39	Klk6	Positive	0.0433	CG12951				KLK6	176	Positive	0.0157
40	Il33	Positive	0.0425	*No known orthologue*				IL33			
41	Fabp5	Positive	0.0424	fabp				FABP5			
42	Sfn	Positive	0.0419	14-3-3zeta				SFN	418	Positive	0.0109
43	Cldn1	Positive	0.0417	*No known orthologue*				CLDN1	442	Negative	0.0108
44	Slpi	Positive	0.041	CG5639				SLPI			
45	Unc93a	Negative	0.0409	CG4928	1219	Negative	0.041	UNC93A			
46	Krt6b	Positive	0.0408	LamC				KRT6B			
47	Macc1	Positive	0.0399	*No known orthologue*				MACC1			
48	Rptn	Positive	0.0393	*No known orthologue*				RPTN	79	Positive	0.0203
49	Gsta1	Negative	0.039	*No known orthologue*				GSTA1			
50	9930013L23Rik	Positive	0.0387	*No known orthologue*				CEMIP			

Table 4.5 Conservation of differentially regulated genes between human, *Drosophila* and mouse across all biological contexts following modulation of *grh/Grhl* function.

Top 50 most differentially regulated genes of *Grhl* in human RNA Seq datasets were compared across the list of differentially regulated genes obtained from *Drosophila* and mouse datasets.

Rank	*Homo sapiens* gene symbol	Regulation	Average normalised score	Significant differential regulation in *Drosophila*				Significant differential regulation in *Mus musculus*			
				Orthologue	Rank	Regulation	Average normalised score	Orthologue	Rank	Regulation	Average normalised score
1	IL36RN	Positive	0.0526	No known orthologue				Il1f5	5458	Negative	0.00393
2	ALOX15	Positive	0.0421	No known orthologue				Alox15			
3	CCDC88A	Negative	0.0379	Girdin				Ccdc88a			
4	ELF5	Positive	0.0369	aop				Elf5	157	Positive	0.0285
5	TMPRSS13	Positive	0.0346	Sb				Tmprss13	38	Positive	0.0441
6	RDH12	Positive	0.0345	CG2065	1389	Positive	0.016	Rdh12	824	Negative	0.0145
7	HIST1H2BJ	Positive	0.0323	His2B:CG33884				Hist1hb2bj			
8	DLX4	Negative	0.0323	Dll	2143	Negative	0.0126	Dlx4			
9	FAT4	Negative	0.0323	ft	2216	Positive	0.012	Fat4			
10	EPCAM	Positive	0.0323	No known orthologue				Epcam	126	Positive	0.0322
11	HOPX	Positive	0.0323	No known orthologue				Hopx	738	Negative	0.0151
12	SERPINA3	Negative	0.0323	Spn28Dc				Serpina3	756	Negative	0.0198
13	AHSG	Negative	0.0323	No known orthologue				Ahsg			
14	KRT7	Positive	0.0323	LamC				Krt7	66	Positive	0.0381
15	SELE	Negative	0.0323	Hasp				Sele	2481	Positive	0.00717
16	PCDHGA5	Positive	0.0323	Cad96Cb				Pcdhga5			
17	LOC652614	Negative	0.0323	No known orthologue				Aim1			
18	IRX4	Positive	0.0323	ara				Irx4	2358	Positive	0.00746
19	LOC645769	Positive	0.0322	No known orthologue				No known orthologue			
20	ALOXE3	Positive	0.0315	No known orthologue				Aloxe3	1610	Positive	0.00977
21	HRNR	Positive	0.0312	No known orthologue				Hrnr			
22	ALDH3B2	Positive	0.031	Aldh-III				Aldh3b2	130	Positive	0.0314
23	ITGB6	Positive	0.0307	mys				Itgb6	1013	Positive	0.0128
24	ITGA2	Positive	0.029	if	256	Negative	0.0323	Itga2	3518	Positive	0.00552
25	EPHB3	Positive	0.0289	Eph				Ephb3	1105	Positive	0.0123
26	ANKRD22	Positive	0.028	CG9766				Ankrd22			
27	AIM1	Positive	0.0267	aurA				Aim1			
28	CLDN4	Positive	0.0264	No known orthologue				Cldn4	3	Positive	0.116
29	CD24	Positive	0.026	No known orthologue				Cd24a	5015	Positive	0.00423
30	ANKRD20A11P	Negative	0.0256	No known orthologue				No known orthologue			
31	SOD1	Negative	0.0256	Sod1				Sod1			
32	SERPINE1	Negative	0.0256	Spn42Db	83	Negative	0.0585	Serpine1			
33	BPIL2	Positive	0.0256	No known orthologue				Bpil2			
34	FAM26E	Negative	0.0256	No known orthologue				Fam26e			
35	NOX5	Positive	0.0256	Nox	1130	Negative	0.0263	No known orthologue			
36	ALB	Negative	0.0256	No known orthologue				Alb			
37	PTGES	Negative	0.0256	CG33178	1003	Negative	0.0263	Ptges	1120	Positive	0.0121
38	MEX3B	Positive	0.0256	CG11360	1522	Negative	0.0263	Mex3b			
39	TRIL	Positive	0.0256	haf				Tril	3094	Positive	0.00607
40	LOC100130494	Negative	0.0255	No known orthologue				No known orthologue			
41	HIST1H3B	Negative	0.0249	His3:CG31613				Hist1h3b			
42	KRT19	Positive	0.0246	LamC				Krt19	530	Positive	0.0177
43	CHAC1	Positive	0.0243	CG10365				Chac1			
44	PDE1C	Negative	0.0239	Pde1c				Pde1c			
45	CDH2	Negative	0.0239	CadN2				Cdh2	424	Negative	0.0192
46	MET	Negative	0.0236	CCHa1-R				Met	2500	Negative	0.00712
47	TYMS	Negative	0.0232	Ts				Tyms	4435	Positive	0.00465
48	GALNT3	Positive	0.0227	Pgant9				Galnt3	581	Positive	0.0172
49	RN7SK	Negative	0.0226	No known orthologue				Rn7sk			
50	A2ML1	Positive	0.0225	Tep4				A2ml1			

4.3.5 Differentially regulated genes of *Grhl3/Grhl2/grh* across all biological contexts

In order to determine the similarity in transcriptional pathways regulated by *Grhl3, Grhl2* and *grh,* I generated individual lists for each orthologue, using large-scale microarray/RNA-SEQ datasets specific for each *Grhl* orthologue. This analysis encompassed 6 *grh* datasets from 2 publications, 20 *Grhl2* datasets from 16 publications and 14 *Grhl3* datasets from 6 publications. The top 50 differentially regulated *grh* genes were then compared with top 5,000 differentially regulated genes of *Grhl2* and *Grhl3* (Table 4.6). 6/50 *grh* differentially regulated genes were identified to be regulated by *Grhl2 – CG5326, CG6472, Spn47C, Hsp26, CG17843, kibra* and 6/50 *grh* genes were differentially regulated by *Grhl3 - CG6472, Spn47C, CG17843, CG10924, how,* and *kibra*.

Similarly, the top 50-ranked genes from *Grhl2* datasets were compared with top 5,000 genes differentially regulated in *Grhl3* and *grh* RNA seq datasets (Table 4.7). 15/50 *Grhl2* regulated genes were found to be regulated in *Grhl3* datasets– *Tmem54, Prom2, Cldn4, Rab15, Krt7, Cdh1, IL36RN, Sfn, St14, Kcnk1, Prss22, Prss8, Sptlc3, MaI*, and *Tex19.1* while only 3 genes were regulated in *grh* RNA Seq datasets – *Fermt1, dsp* and *DLX4*.

Lastly, comparison was made between the top 50-ranked *Grhl3* regulated genes and top 5,000 genes from the *Grhl2* and *grh* RNA-Seq datasets (Table 4.8). 11/50 *Grhl3* differentially regulated genes were identified to be regulated by G*rhl2 – Cldn23, Tslp, Ppl, Ocln, Aldh1a3, Klk6, Evpl, Gldc, Pglyrp1, Cldn4, Il33* and 6/50 genes were commonly found between the top 50 *Grhl3*-regulated genes and top 5,000 *grh* regulated genes, namely, *Ppl, Car6, Unc39a, Evpl, Gm10639,* and *Pla2g3*. ~12% of *grh*-regulated genes were commonly present in *Grhl2/Grhl3* RNA Seq datasets while 22-30% genes were commonly regulated between *Grhl2* and *Grhl3* datasets, signifying the similarity in gene regulatory network regulated by various *grh*/*Grhl* orthologues to drive epithelial homeostasis.

Table 4.6 The top 50 most differentially regulated genes of *grh*.

Most differentially regulated genes of *grh* were compared across the list of differentially regulated genes of *Grhl2* and *Grhl3* to identify genes that are commonly regulated among the 3 orthologues.

Rank	Gene	Regulation	Average normalised score	Differential regulation by *Grhl3*			Differential regulation by *Grhl2*		
				Rank	Regulation	Average normalised score	Rank	Regulation	Average normalised score
1	Zasp66	Negative	0.0581						
2	CG10345	Negative	0.0503						
3	CG12480	Negative	0.0501						
4	CG5326	Negative	0.0495	826	Positive	0.0112			
5	CG16733	Positive	0.0471						
6	bcd	Positive	0.0461						
7	CG15282	Positive	0.0448						
8	ps	Negative	0.0434						
9	gfzf	Positive	0.0429						
10	rtet	Positive	0.0417						
11	CG6472	Negative	0.0363	725	Positive	0.012	509	Positive	0.0142
12	Cpr47Eb	Positive	0.0359						
13	Pcd	Positive	0.0358						
14	CG13731	Negative	0.0357						
15	CG5278	Negative	0.0356						
16	Lcp4	Positive	0.0344						
17	drosomycin-5	Negative	0.0344						
18	CG14105	Positive	0.0341						
19	Spn47C	Positive	0.0337	2185	Positive	0.00606	1743	Negative	0.00732
20	Cpr78Cc	Negative	0.0335						
22	CG17919	Positive	0.0329						
23	betaTub56D	Positive	0.0327				6011	Negative	0.00308
24	tej	Positive	0.0325						
25	Gadd45	Positive	0.0325						
26	Hsp26	Positive	0.0318	356	Positive	0.0168			
27	CG17843	Positive	0.0315	1335	Positive	0.00845	2765	Negative	0.00578
28	CG33978	Positive	0.0312						
29	CG9689	Positive	0.031						
30	A3-3	Negative	0.031						
31	CG13705	Negative	0.0309						
32	CG9542	Positive	0.0309						
33	CG14567	Positive	0.0308						
34	GV1	Negative	0.0306						
35	CG10924	Positive	0.03						
36	CG10924	Positive	0.03				425	Positive	0.0155
37	ImpL1	Positive	0.0298						
38	chinmo	Negative	0.0297						
39	CG13046	Negative	0.0297						
40	how	Negative	0.0291				1265	Negative	0.00875
41	drd	Negative	0.0291						
42	kibra	Negative	0.0289	3070	Positive	0.00498	2327	Positive	0.00632
43	kibra	Negative	0.0289				1299	Positive	0.00866
44	CG13675	Negative	0.0287						
45	mael	Positive	0.0284						
46	CG10625	Negative	0.0282						
47	CG9691	Positive	0.028						
48	CG3588	Positive	0.0276						
49	if	Positive	0.0276						
50	CG34007	Positive	0.0276						

Table 4.7 The top 50 most differentially regulated genes of *Grhl2* in all biological contexts.

Most differentially regulated genes of *Grhl2* were compared across the list of differentially regulated genes of *grh* and *Grhl3* to identify genes that are commonly regulated among the 3 orthologues.

Rank	Gene	Regulation	Average normalised score	Differential regulation by *Grhl3*			Differential regulation by *Grh*		
				Rank	Regulation	Average normalised score	Rank	Regulation	Average normalised score
1	Tmem54	Positive	0.184	170	Negative	0.0226			
2	Prom2	Positive	0.182	1962	Negative	0.00657			
3	Cldn4	Positive	0.112	54	Positive	0.0363			
4	Grhl2	Positive	0.0889						
5	Rab15	Positive	0.0707	1885	Negative	0.0068			
6	Krt7	Positive	0.0706	2679	Negative	0.00542			
7	Gm19601	Negative	0.0689						
8	Rab25	Positive	0.063						
9	Lad1	Positive	0.0626	5056	Positive	0.00347			
10	Epcam	Positive	0.0617						
11	Cdh1	Positive	0.0607	380	Negative	0.0166			
12	Ap1m2	Positive	0.0575						
13	IL36RN	Positive	0.0561	4115	Negative	0.0042			
14	Il17re	Positive	0.0557						
15	Macc1	Positive	0.0557						
16	Gm20305	Negative	0.0547						
17	Tacstd2	Positive	0.053	5080	Negative	0.00345			
18	Rbbp8nl	Positive	0.052						
19	Sfn	Positive	0.0519	3713	Positive	0.00448			
20	Cldn7	Positive	0.0515						
21	Esrp1	Positive	0.0498						
22	Spint1	Positive	0.048						
23	St14	Positive	0.0475	3184	Positive	0.00489			
24	Kcnk1	Positive	0.0474	2332	Negative	0.0058			
25	Tnk1	Positive	0.0468						
26	Pax8	Negative	0.0462						
27	ALOX15	Positive	0.045						
28	Prss22	Positive	0.0432	2021	Positive	0.00644			
29	Prss8	Positive	0.0426	1003	Negative	0.01			
30	CCDC88A	Negative	0.0405						
31	Arhgef19	Positive	0.0403						
32	Mapk13	Positive	0.0385						
33	Dsp	Positive	0.0383				676	Negative	0.0136
34	Sptlc3	Positive	0.0383	673	Negative	0.0126			
35	Mal	Positive	0.0381	831	Negative	0.0112			
36	9530027K23Rik	Positive	0.0381						
37	Tmprss4	Positive	0.037						
38	Ldoc1	Positive	0.0369						
39	Tex19.1	Positive	0.0368	1762	Negative	0.00717			
40	Fermt1	Positive	0.0364				1433	Positive	0.011
41	Mpzl2	Positive	0.0362						
42	Fgf15	Negative	0.0362						
43	Hbb-y	Positive	0.0362						
44	Rhox4d	Positive	0.036						
45	Bcl2a1b	Positive	0.0357						
46	Bcl2a1b	Positive	0.0357						
47	Atp8b1	Positive	0.0349						
48	Loxl2	Negative	0.0345						
49	HIST1H2BJ	Positive	0.0344						
50	DLX4	Negative	0.0344				714	Negative	0.0134

Table 4.8 The top 50 most differentially regulated genes of *Grhl3* in all biological contexts.

Most differentially regulated genes of *Grhl3* were compared across the list of differentially regulated genes of *grh* and *Grhl2* to identify genes that are commonly regulated among the 3 orthologues.

Rank	Gene	Regulation	Average normalised score	Differential regulation by *Grhl2*			Differential regulation by *Grh*		
				Rank	Regulation	Average normalised score	Rank	Regulation	Average normalised score
1	Cldn23	Positive	0.0906	191	Positive	0.0224			
2	Tslp	Positive	0.0683	2832	Positive	0.0057			
3	Gm3579	Negative	0.065						
4	Ocln	Positive	0.0633	487	Positive	0.0144			
5	Ppl	Positive	0.0584	99	Positive	0.0283	680	Negative	0.0136
6	Slc6a19	Negative	0.0579						
7	2310001H18Rik	Positive	0.0561						
8	Aldh1a3	Positive	0.0537	2138	Positive	0.00656			
9	Tmprss11bnl	Positive	0.0518						
10	Sod3	Negative	0.05						
11	Cyp2b19	Negative	0.0496						
12	Car6	Negative	0.0496				1241	Positive	0.0118
13	Fmo2	Negative	0.0493						
14	Defb3	Positive	0.0487						
15	Gsta2	Negative	0.0478						
16	Aox4	Negative	0.0476						
17	Klk6	Positive	0.0462	883	Positive	0.0107			
18	Cldn1	Positive	0.0446						
19	Slpi	Positive	0.0437						
20	Unc93a	Negative	0.0437				104	Negative	0.0254
21	Krt6b	Positive	0.0436						
22	Sprr1a	Positive	0.0435						
23	Rptn	Positive	0.042						
24	Gsta1	Negative	0.0416						
25	Evpl	Positive	0.0415	559	Positive	0.0134	677	Negative	0.0136
26	9930013L23Rik	Positive	0.0413						
27	Fabp7	Positive	0.041						
28	Adh6a	Negative	0.0407						
29	Wfdc12	Positive	0.0397						
30	Fxyd4	Positive	0.0397						
31	Krt78	Negative	0.0395						
32	Gldc	Negative	0.0393	3155	Negative	0.00532			
33	Gdpd1	Negative	0.0391						
34	Hyal4	Negative	0.0386						
35	Lce3f	Positive	0.0386						
36	Gm9992	Negative	0.0385						
37	Pglyrp1	Negative	0.0382	1806	Positive	0.00717	326	Negative	0.0205
38	Gm10639	Negative	0.0378						
39	Gdpd3	Negative	0.0377						
40	Cldnb8	Positive	0.0377						
41	Slc46a2	Negative	0.0369						
42	Lce3a	Positive	0.0367						
43	Cldn4	Positive	0.0363	4	Positive	0.112			
44	Il33	Positive	0.0363	1175	Positive	0.00911			
45	Abpa	Negative	0.0362						
46	Cobl	Negative	0.0359						
47	Pla2g3	Negative	0.0354				421	Negative	0.0167
48	Celsr1	Positive	0.0352						
49	Lce3c	Positive	0.0349						
50	Krt84	Positive	0.0347						

4.3.6 Refining meta-analyses to encompass only large-scale datasets generated from epithelial tissue or cancer cell lines reveals *grh/Grhl* transcriptome specificity

As the *grh/Grhl* family are key regulators of epithelial establishment, development, maintenance, and homeostasis, we refined our meta-analyses to only include datasets generated from primary epithelial tissues (Table 4.1). These data encompassed 18 datasets from 7 separate publications, and restricted our data to *Grhl*-dependent transcriptomes derived from epithelia from mouse embryonic skin (Yu, Lin et al. 2006), bladder (Yu, Mannik et al. 2009), non-neural ectoderm (Ray and Niswander 2016) and lung epithelium (Kersbergen, Best et al. 2018), human neonatal epidermal keratinocytes (Hopkin, Gordon et al. 2012), and undifferentiated primary human bronchial epithelial cells (Gao, Vockley et al. 2013), as well as adult mouse and human psoriatic skin (Gordon, Zeller et al. 2014), and allowed us to identify the top differentially regulated genes in epithelial development, the top 50 of which are shown in Table 4.9. This list includes numerous well characterised genes known to be expressed in epithelia and are involved in the maintenance of epithelial integrity and structural stability, such as *Claudins 1/4/23*, *Periplakin*, *Envoplakin*, *Occludin* and *Prominin 2* (Table 4.9). Interestingly, the top 50 genes include five "predicted" genes – *Gm19601*, *Gm3579*, *231000H18Rik*, *Gm20305* [possible pseudogene] and *Gm10639* – that are yet to be ascribed a function.

Similarly, list of top 30 differentially regulated genes following *Grhl* loss in each of the following categories (a) mammalian tissue (Supplementary table 4.2), (b) non-mammalian tissues (Supplementary table 4.3) and (c) non-cancerous cells (Supplementary table 4.1) were generated. Next, I determined which of the top 50 "epithelial" *grh/Grhl*-regulated genes may also be de-regulated in *Grhl*-influenced cancerous cells (Table 4.10). I generated a dataset of differentially regulated genes in those RNA-SEQ/Microarray datasets that were designated as derived from "cancer cell-lines" (Table 4.10). These experiments typically included control cancer cells compared to those in which *Grhl* activity was modulated through short-hairpin (shRNA) knockdown, and included 4T1 breast tumour cells (Xiang, Deng et al. 2012), human mammary epithelial (HMLE-Twist-ER) cells (Cieply, Riley et al. 2012), MSP (mesenchymal sub-population) cells obtained from HMLE cells (Farris, Pifer et al. 2016), OVCA429 (ovarian cystadenocarcinoma; intermediate epithelial [IE] phenotype) cells (Chung, Tan et al. 2016) and LNCaP (human prostate carcinoma) cells (Paltoglou, Das et al. 2017). Surprisingly, only two genes appeared in both the "epithelial targets" and

"cancer targets" tables – *Tmem54* and *Claudin-4*, a previously experimentally-validated *Grhl*-target. I did note several instances of different family members expressed across both sets (e.g. *Sod3, Krt6b/78, Tmprss4/11bnl* and *Cldn1/23/b8* in epithelia, and *Sod1/2, Krt7/19, Tmprss13* and *Cldn7* in cancer), suggesting that loss of *Grhl*-mediated transcription may lead to similar biological consequences, albeit mediated via different (possibly secondary, or indirect) target pathways. However, these results indicate that the *Grhl*-dependent transcriptome is largely context and tissue-type dependent, with little evidence of conserved mechanisms operating in epithelial homeostasis and epithelial cancer.

Table 4.9 The top 50 most differentially regulated genes in primary epithelia following modulation of *grh/Grhl* function.

Orthologues of the genes highlighted in red were screened and validated in subsequent Q-RT-PCR experiments in *grhl3⁻ᐟ⁻* zebrafish.

Rank	Gene	Regulation	Average normalised Score
1	*Cldn23*	Positive	0.0954
2	*Ppl*	Positive	0.0693
3	*Prom2*	Positive	0.0689
4	*Gm19601*	Negative	0.0689
5	*Tslp*	Positive	0.0684
6	*Gm3579*	Negative	0.065
7	*Ocln*	Positive	0.0633
8	*Slc6a19*	Negative	0.0579
9	*2310001H18Rik*	Positive	0.0562
10	*Gm20305*	Negative	0.0547
11	*Aldh1a3*	Positive	0.0538
12	*Tmprss11bnl*	Positive	0.0519
13	*Snx31*	Positive	0.0517
14	*Sod3*	Negative	0.05
15	*Cyp2b19*	Negative	0.0496
16	*Car6*	Negative	0.0496
17	*Cldn4*	Positive	0.0494
18	*Fmo2*	Negative	0.0493
19	*Defb3*	Positive	0.0488
20	*Gsta2*	Negative	0.0479
21	*Aox4*	Negative	0.0476
22	*Evpl*	Positive	0.047
23	*Klk6*	Positive	0.0462
24	*Il33*	Positive	0.0455
25	*Cldn1*	Positive	0.0446
26	*Slpi*	Positive	0.106
27	*Unc93a*	Negative	0.106
28	*Krt6b*	Positive	0.105
29	*Sprr1a*	Positive	0.105
30	*Rptn*	Positive	0.102
31	*Gsta1*	Negative	0.101
32	*Cemip*	Positive	0.0999
33	*Fabp7*	Positive	0.0991
34	*Adh6a*	Negative	0.0985
35	*Wfdc12*	Positive	0.0961
36	*Fxyd4*	Positive	0.096
37	*Krt78*	Negative	0.0956
38	*Tmem54*	Positive	0.0953
39	*Gldc*	Negative	0.0951
40	*Gdpd1*	Negative	0.0945
41	*Slurp1*	Positive	0.0939
42	*Hyal4*	Negative	0.0934
43	*Lce3f*	Positive	0.0933
44	*Unc93a2*	Negative	0.0932
45	*Sptlc3*	Positive	0.0926
46	*Pglyrp1*	Negative	0.0924
47	*Gm10639*	Negative	0.0915
48	*Gdpd3*	Negative	0.0912
49	*Cldnb8*	Positive	0.0912
50	*Tmprss4*	Positive	0.0894

Table 4.10 The top 50 most differentially regulated genes in cancer cell lines following modulation of *grh/Grhl* function.

Rank	Gene	Regulation	Average normalised score
1	ALOX15	Positive	0.045
2	CCDC88A	Negative	0.0405
3	FAT4	Negative	0.0345
4	EPCAM	Positive	0.0345
5	IL36RN	Positive	0.0345
6	AHSG	Negative	0.0345
7	Krt7	Positive	0.0345
8	Sele	Negative	0.0345
9	AIM1	Positive	0.0285
10	CD24	Positive	0.0277
11	ALOXE3	Positive	0.0274
12	SOD1	Negative	0.0274
13	ITGB6	Positive	0.0274
14	SERPINE1	Negative	0.0274
15	NOX5	Positive	0.0274
16	ALB	Negative	0.0274
17	Epcam	Positive	0.0274
18	Ptges	Negative	0.0274
19	KRT19	Positive	0.0263
20	TYMS	Negative	0.0248
21	ALOX12P2	Positive	0.0239
22	Cat	Negative	0.0239
23	FGF2	Negative	0.0239
24	CRISP3	Positive	0.0239
25	SYN3	Negative	0.0239
26	Cldn4	Positive	0.0239
27	Otop1	Negative	0.0239
28	SLC1A6	Positive	0.0217
29	NQO1	Negative	0.0217
30	TMPRSS13	Positive	0.0217
31	ATOH8	Negative	0.0217
32	Cldn7	Positive	0.0217
33	Xdh	Negative	0.0217
34	NCF2 (p67-PHOX)	Positive	0.0202
35	GLUD1	Negative	0.0202
36	ITGA2	Positive	0.0202
37	SMARCA1	Negative	0.0202
38	ALDH3B2	Positive	0.0202
39	BRSK1	Negative	0.0202
40	Lamc2	Positive	0.0202
41	Olfr1372-ps1	Negative	0.0202
42	SOD2	Positive	0.019
43	ITGB8	Positive	0.019
44	CDH2	Negative	0.019
45	A2ML1	Positive	0.019
46	TMEM45A	Negative	0.019
47	Tmem54	Positive	0.019
48	Dnahc6	Negative	0.019
49	CDH1	Positive	0.0189
50	GALNT3	Positive	0.0188

4.3.7 Expression of differentially regulated epithelial genes in a novel vertebrate model

In order to determine the predictive power of our meta-analysis approach, to identify novel *grhl*-dependent putative target genes (both direct and indirect), I analysed the expression of our top-ranked genes that were differentially regulated in epithelia, by performing Q-RT-PCR on cDNA from *grhl3*$^{-/-}$ mutant zebrafish. This model was utilised to test our meta-analyses, as none of the large-scale datasets were generated from zebrafish tissue, hence, this model would speak to the genetic conservation of *grhl*-dependent pathways across vertebrates.

From the genes that were differentially regulated in epithelia (Table 4.9), I identified the top 10 genes that had an identifiable zebrafish orthologue, or orthologues. The roles of these ten mammalian genes – *Cldn23, Ppl, Prom2, Ocln, Slc6a19, Aldh1a3, Sod3, Car6, Cldn4* and *Evpl* – were sub-functionalised into a total of 17 zebrafish orthologues, based on sequence conservation homology (Table 4.11). Next, I performed Q-RT-PCR on fifty 48 hours post-fertilisation (hpf) WT and *grhl3*$^{-/-}$ embryos (experiment performed in triplicates) to determine the relative expression of each of these fish orthologues. Of the 17 zebrafish orthologues analysed, I found that 10 - *cldn23a, cldn23b, ppl, prom2, oclna, slc6a19a.1, slc6a19b, aldh1a3, sod3a* and *evplb* - showed statistically significant differences in expression between WT and *grhl3*$^{-/-}$ fish (primarily down-regulation) (Figure 4.12). I utilised whole embryos for my analyses, not just epithelial tissue, and analyses was performed only at a single developmental timepoint. Nonetheless, even within these experimental constraints, the fact that 10/17 zebrafish orthologues were significantly differentially regulated highlights the remarkable conservation of *grhl*-dependent pathways across the evolutionary spectrum and demonstrates the strong predictive power of our approach for identifying novel, biologically relevant transcriptional networks downstream of g*rh/Grhl* function.

Table 4.11 Zebrafish orthologues of differentially regulated mammalian genes.

The top 10 differentially regulated genes following *Grhl*-dependent modulation in primary epithelia that had identifiable zebrafish orthologues, showing the function of each gene in mammals. Zebrafish orthologues of these ten mammalian genes comprise a total of 18 separate genes.

| Rank	Gene	Gene name	Zebrafish orthologue(s)	Function
1	**Cldn23**	Claudin 23	*cldn23a, cldn23b*	Integral membrane proteins and components of tight junctions
2	**Ppl**	Periplakin	*ppl*	Components of desmosomes and of the epidermal cornified envelope in keratinocytes
3	**Prom2**	Prominin 2	*prom2*	Membrane glycoproteins
4	**Ocln**	Occludin	*oclna, oclnb*	Integral membrane proteins and components of tight junction strands
5	**Slc6a19**	Solute Carrier 6 Family Member 19	*slc6a19a.1, scl6a19a.2, slc6a19b*	Mediates resorption of neutral amino acids across the apical membrane of renal and intestinal epithelia
6	**Aldh1a3**	Aldehyde Dehydrogenase 1 Family Member A3	*aldh1a3*	Catalyzes the formation of retinoic acid
7	**SOD3**	Superoxide Dismutase 3	*sod3a, sod3b*	Protection of brain, lungs and other tissues from oxidative stress
8	**Car6**	Carbonic Anhydrase 6	*car6*	Reversible hydratation of carbon dioxide
9	**Cldn4**	Claudin 4	*cldna, cldnb*	Integral membrane protein
10	**Evpl**	Envoplakin	*evpla, evplb*	Component of the cornified envelope of keratinocytes
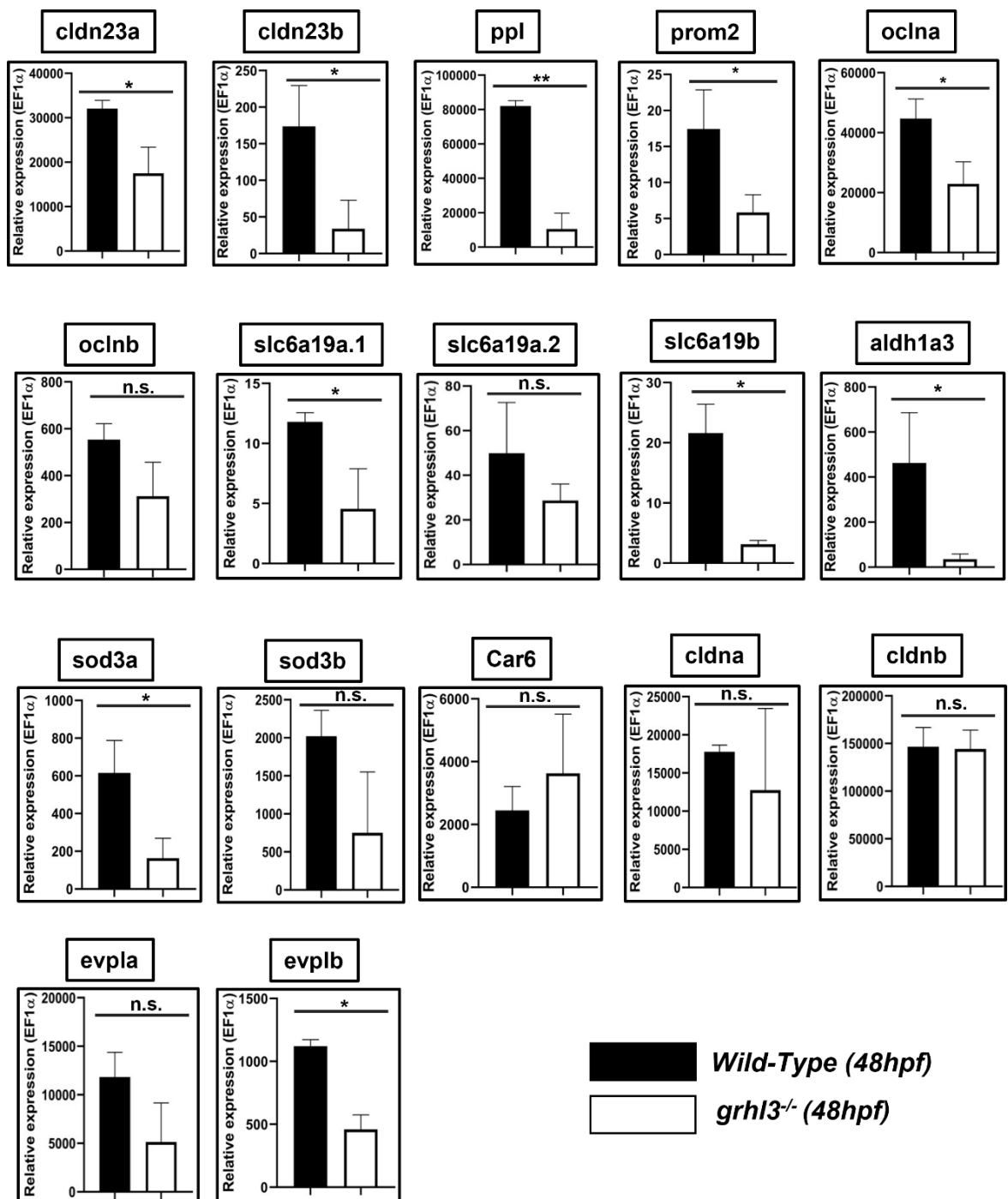
Figure 4.2 Q-RT-PCR analysis of zebrafish orthologue expression in 48 hpf WT and *grhl3*^{-/-} embryos.

Gene expression was normalised to expression of housekeeping gene EF1a. Of the 18 fish orthologues selected, 10 showed differential expression in WT (black bars) vs *grhl3*^{-/-} (white bars) embryos. $*p<0.05$, $**p<0.01$, n.s., non-significant

4.3.8 Validation of *myoVb* as *grhl3* target via experimentation

Myosin vb (*myoVb*), an actin-based molecular motor was identified to be a novel upstream regulator of *grhl3* in epithelial homeostasis by A/Prof. Mahendra Sonawane and his research group at the Tata Institute of Fundamental Research (TIFR), Mumbai, India. In collaboration with their team, I performed *myoVb* knockdown experiments in our novel *grhl3* deficient model to understand the *grhl3-myovb* interaction in epithelial homeostasis.

myoVb is one among several genes involved in the maintenance of epithelial homeostasis of zebrafish embryos (Sonawane and Nuesslein-Volhard, unpublished). In zebrafish embryos lacking *myoVb,* perturbation in epithelial homeostasis contributes to rounding up of peridermal cells (commonly referred to as the blistering phenotype) at 48 hpf. However, most MO:*myovb* embryos recover and no longer exhibit this phenotype beyond 72 hpf (Sonal, Sidhaye et al. 2014). The disappearance of the rounding cell phenotype in *myoVb* morphants is hypothesized to be due to retention and re-integration of peridermal cells into epithelium brought about by *grhl3* (Phatak, Kulkarni et al. 2021). Furthermore, transcriptome analysis of *myovb* mutant embryos using RNA seq revealed *grhl3* to be one of the many epithelial genes to be upregulated (Phatak, Kulkarni et al. 2021). An increased expression of *grhl3* was also identified in epidermal regions bearing rounded up cells in MO injected embryos (Phatak, Kulkarni et al. 2021). Thus, in order to determine the interaction between *grhl3* and *myoVb*, embryos derived from inter-crossing *grhl3* fish were subjected to MO mediated knockdown of *myoVb* at 200 µM (minimum concentration at which the blistering phenotype is observed, without showing toxicity related effects).

Upon close observation Dr. Lee Miles (former Post-Doctoral Fellow, La Trobe University) found that knockdown of *myovb* in *grhl3* siblings contributed to rounding up of epidermal cells, predominantly along the head region between 36 – 48 hpf. However, in *grhl3* mutant embryos, loss of *myovb* showed no rounding up of epidermal cells at 48 hpf or at any other timepoints (Figure 4.3A). Thus, concomitant loss of *grhl3* and *myovb* prevents rounding of cells in MO:*myovb* injected *grhl3$^{-/-}$* embryos.

In order to determine the survival of MO:*myovb* injected *grhl3$^{-/-}$* embryos, Dr. Lee Miles monitored the injected embryos until 72 hpf. The MO:*myovb* injected *grhl3$^{-/-}$* embryos (n= 51) and control *grhl3$^{-/-}$* embryos (n= 51) showed a survival of 74.4 ± 16.4% and 74.75 ± 13.5% respectively at 72 hpf. Survival of MO:*myovb* injected *grhl3* siblings (n= 144)

and control *grhl3* siblings (n= 218) at 72 hpf were 64.7 ± 24.75% and 96.9 ± 10.2% respectively (Figure 4.3B)(Phatak, Kulkarni et al. 2021). Statistical analysis revealed no significant differences between control and MO:*myovb* injected *grhl3* mutant and sibling embryos, signifying the absence of toxicity induced death in MO:*myovb grhl3*^{-/-} embryos.
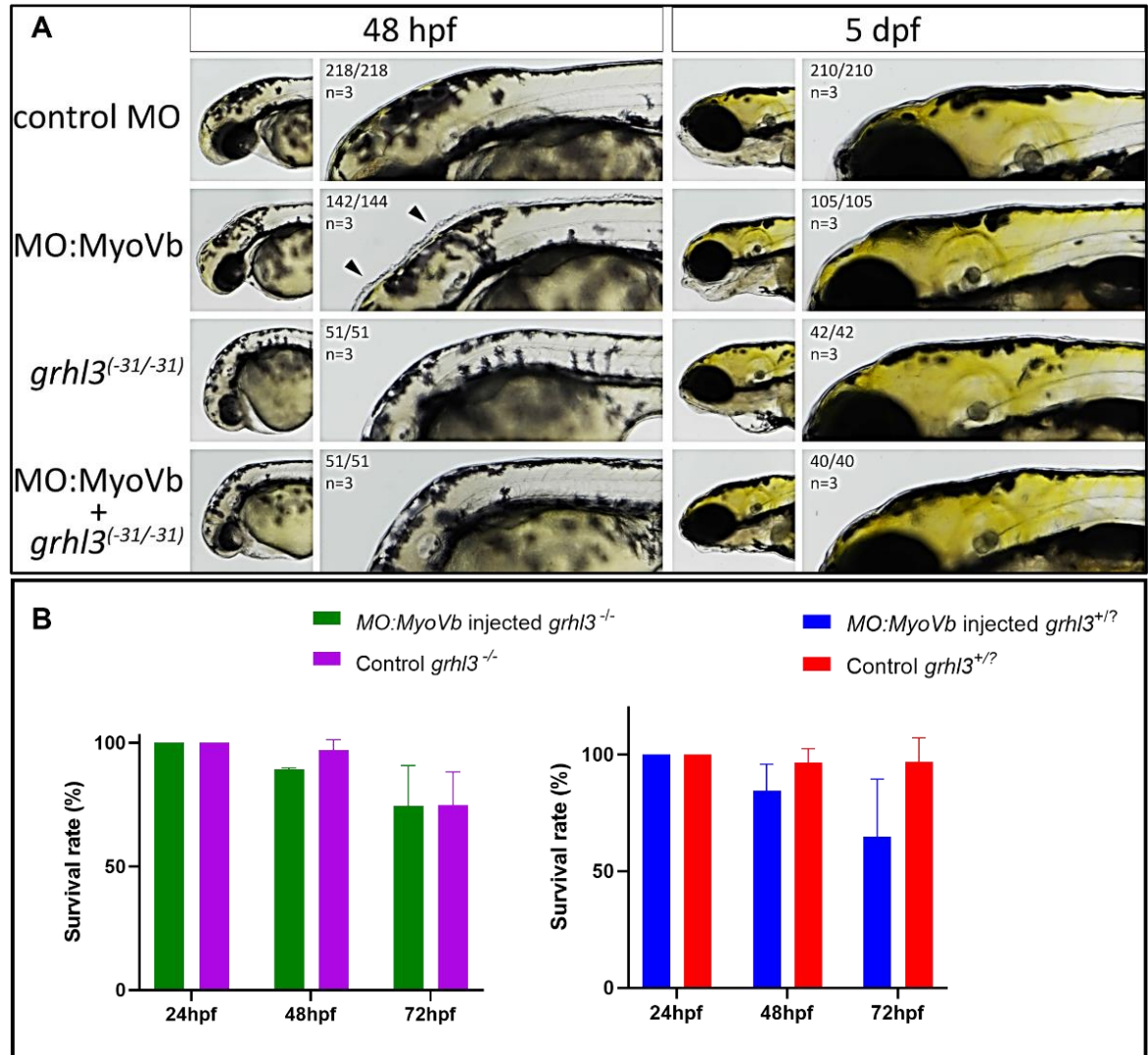
Figure 4.3 MO-mediated knockdown of *myoVb* in *grhl3*^{-/-} embryos.

(A) Phenotypes observed in *grhl3*^{-/-} embryos due to loss of *myoVb* at 48 hpf and 5 dpf. Arrowheads indicate the rounding cell phenotype. **(B)** Survival rate of MO:*myoVb* injected g*rhl3* mutants and siblings vs. control *grhl3* mutant and siblings at 24 hpf, 48 hpf and 72 hpf. Data is represented as mean ± SEM. Statistical significance was determined by Student's t-test.

(Figure generated by me, from Dr. Lee Miles's preliminary data)

Lastly, in order to understand the organization of peridermal cells along the head region of MO:*myovb* injected *grhl3* mutants and siblings, I performed phalloidin staining on PFA fixed embryos at 48 hpf. Confocal imaging of the head region of MO:*myovb grhl3*$^{-/-}$ embryos displayed abnormally large peridermal cells (Figure 4.4D). In addition, multiple sites of extrusion i.e., regions were peridermal cells shed from epithelium, were detected in both MO:*myovb grhl3*$^{-/-}$ embryos (Figure 4.4D) and MO:*myovb grhl3*$^{+/-}$ siblings (Figure 4.4C). The extrusion sites are indicated by the formation of cell rosettes (structures where the cells are arranged in a cluster that resembles a flower and are usually formed following cell extrusion). Therefore, loss of *grhl3* and *myovb* contributes to extrusion of peridermal cells.
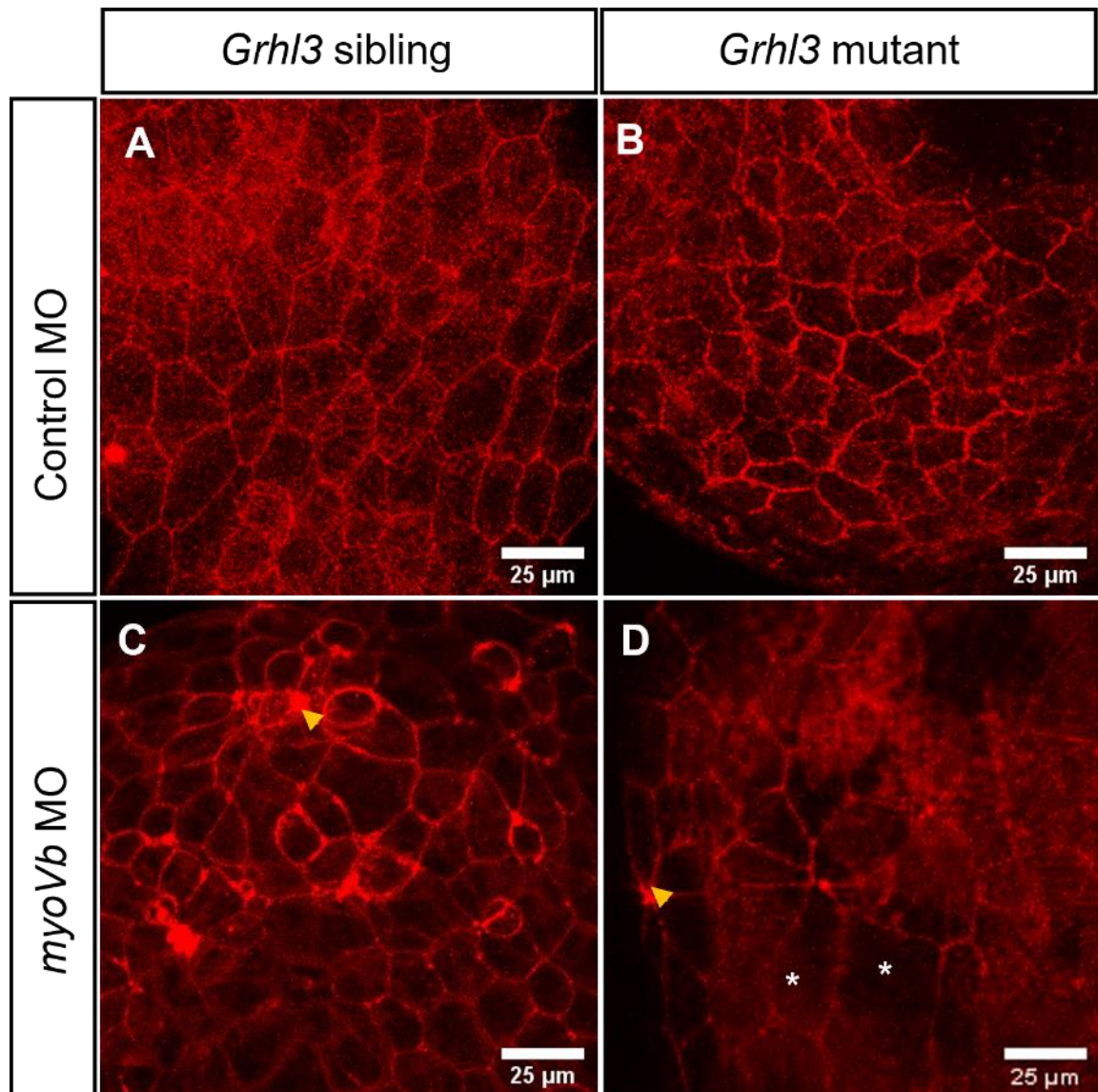
Figure 4.4 Morphology of peridermal cells along the head region of MO:*myoVb* injected *grhl3* mutants and siblings.

MO:*myoVb* injected *grhl3* mutants and siblings were subjected to phalloidin staining (red) at 48 hpf. The head was dissected and mounted on a slide for confocal imaging. Morphology of peridermal cells along the head region of **(A-B)** *control* MO injected *grhl3* mutants and siblings and **(C-D)** MO:*myoVb* injected *grhl3* mutants and siblings is shown. Asterisks indicate large cells; arrowhead shows rosettes that indicate extrusion sites. Scale bar: 25 µm.

4.4 Discussion

In this study, we interrogated large-scale transcriptomic data to uncover novel genetic mechanisms that operate downstream of activation or repression by *grh/Grhl* genes. Firstly, in-silico analysis performed, revealed a list of 21 genes commonly present in the *Grhl2⁻/⁻* mouse pharyngeal RNA seq dataset and the PHYLO-PROM database. Of these 21 genes, 4 (*Cldn4*, *Cdh1*, *Ppl* and *Arhgef19)* of them have been previously validated as *grhl* targets, signifying the robust predictive power of this approach in identifying targets of *Grhl*.

The second approach to identifying differentially regulated genes of *grhl* involved collation of all currently published large-scale RNA-SEQ and microarray datasets from multiple disparate animal models, developmental timepoints, tissues and also cancer cell lines to delineate conserved *grh/Grhl*-dependent genetic networks. Using a novel ranking-based algorithm approach to draw synergies between disparate methodologies, I identified the top-differentially regulated genes following gain or loss of *grh/Grhl* function in all datasets, as well as refining my analyses to the top-differentially regulated genes in primary epithelia and in cancer. I also examined the conservation of mechanisms in mouse, *Drosophila* and human; uncovered the transcriptional networks regulated by *Grhl* orthologues (*grh*, *Grhl2* and *Grhl3)* and lastly, the predictive strength of the meta-analysis approach was tested to determine which of the top-ranked genes were differentially regulated in a novel vertebrate grhl-loss-of-function model, the zebrafish. Taken together, this study brings cohesion and clarity to the existing "big-data" approaches to tackle *grh/Grhl*-dependent transcription and opens up new avenues (and identifies novel putative targets) to further experimentally delineate *grh/Grhl*-dependent transcriptional genetic regulatory networks.

Across the 41 disparate Microarray/RNA-SEQ datasets of the top 50 genes we identified, 15 had previous connections to Grhl transcription factors, either through ChIP/ChIP-SEQ experiments to identify regions of genome occupancy by Grhl proteins, or through targeted biological experiments to empirically determine novel functional relationships. The genes to which Grhl-factors bind, and drive/repress transcription can be considered true "direct" target genes. A number of our top 50 genes fall into this category, namely *Cldn4, Cdh1 (E-Cadherin), Rab25, Epcam, Esrp1* and *Spint1,* with a further nine genes - *Tmem54, Prom2, Ppl, Lad1, Tacstd2, St14, Prss22,* and *Prss8* showing instances of

promoter-binding by *Grhl*-factors in ChIP-analyses, but currently lacking empirical experimental validation to determine true biological interactions. As such, these nine genes would appear to be the prime candidates for future studies into identifying novel *Grhl*-target genes through established analyses such as *in vitro* luciferase activation assays, genetic complementarity in animal models (e.g. through generating *Grhl*/Gene-of-interest doubly heterozygous mice) or models to rescue *Grhl* loss-of function phenotypes, as we have shown previously by rescuing aberrant developmental phenotypes in *grhl2b* or *grhl3*-deficient zebrafish embryos with *eng2a* (Dworkin, Darido et al. 2012) and *edn1* (Dworkin, Simkin et al. 2014) mRNA microinjection, respectively.

The *Grhl*-family are well-known in both embryogenesis and cancer. Multiple studies have highlighted substantial developmental abnormalities in animal models lacking *Grhl* factors. These include numerous skin formation, maintenance and healing defects (Ting, Caddy et al. 2005, Caddy, Wilanowski et al. 2010, Boglev, Wilanowski et al. 2011, Petrof, Nanda et al. 2014, Goldie, Cottle et al. 2018), impaired neural tube closure (Ting, Wilanowski et al. 2003), facial and palatal clefting (Pyrgaki, Liu et al. 2011, Peyrard-Janvid, Leslie et al. 2014), regulation of skull bone apposition (Goldie, Arhatari et al. 2016) and impaired formation of the lower jaw (Dworkin, Simkin et al. 2014). These latter (craniofacial) defects are interesting owing to the fact that they are secondary consequences of disrupted epithelial formation – either the overlying cranial skin not allowing cranial bones to grow and expand (Goldie, Arhatari et al. 2016) or through decreased endodermal *edn1*-signalling from the endodermal epithelium to cranial neural crest cells (Dworkin, Simkin et al. 2014). These studies parallel recent findings in human craniofacial disorders, namely Van der Woude Syndrome (VWS), a congenital syndrome characterised by palatal clefting. Disruption of the thin epithelial layer covering the developing palatal shelves – the periderm – leads to clefting in both mice and humans due to adhesions forming between the palatal shelves and tongue *in utero* (Peyrard-Janvid, Leslie et al. 2014). Critically, VWS is also known to be caused by mutations in a critical *Grhl*-co-factor, IRF6 (Ingraham, Kinoshita et al. 2006) in both mice and humans. These studies show that understanding the Grhl-dependent transcriptome is likely to uncover further novel biological pathways in the aetiology of craniofacial (and other epithelial) disorders caused by a primary epithelial defect.

In the context of cancer, *Grhl*-factors perform tumour-suppression roles in the epithelia of both skin (Darido, Georgy et al. 2011) and oesophagus (Georgy, Cangkrama et al. 2015),

as well as maintaining epithelial identity through suppression of the epithelial-mesenchymal transition (EMT) in cancers of epithelial origin (Cieply, Riley et al. 2012). Strikingly, and somewhat surprisingly, our study found virtually no correlation between the top 50 differentially regulated genes in normal epithelia as compared to cancerous cells, with only two genes – Tmem54 and Claudin 4 – appearing in both lists. This suggests perhaps that in general terms, the normal *grh/Grhl*-dependent transcriptional pathways that operate in epithelial development, homeostasis and maintenance are not the most highly de-regulated in epithelial cancers. A number of caveats exist in this interpretation, naturally, chief among them being a lack of direct comparison between normal and cancerous epithelia derived from the same source. Additionally, the published microarray/RNA-SEQ datasets defining the role of *Grhl* in cancers follow the experimental paradigm of inhibiting or over-expressing *Grhl*-factors in already tumorigenic cell lines, which is a separate biological question to the analysis of the transcriptome of cancers that arise directly due to aberrant *Grhl*-function. Transcriptomic analyses of tumours arising in *Grhl3*-deficient mice relative to non-cancerous adjoining tissue, such as skin and oesophagus (Darido, Georgy et al. 2011, Georgy, Cangkrama et al. 2015), would add important data points to our current meta-analyses.

Lastly, in order to investigate the *myoVb-grhl3* transcriptional network, MO mediated knockdown of *myoVb* was performed in *grhl3*⁻/⁻ embryos. Loss of *myoVb* in *grhl3* null embryos revealed absence of rounding up of cells along the head region at 48 hpf. However, rosettes were formed in MO:*myoVb grhl3*⁻/⁻embryos, signifying extrusion (shedding) of peridermal cells. Usually, loss of *myoVb* contributes to epidermal regions bearing rounded up cells and it has been found that these cells eventually get re-integrated into the epithelium at 72 hpf (Phatak, Kulkarni et al. 2021). The regions bearing rounded up cells show high *grhl3* expression, which aids in the retention and reintegration of these rounded cells into epithelium. Thus, due to the absence of *grhl3* and loss of *myoVb,* re-integration of rounded up cells into epithelium is prevented, thereby resulting in extrusion of peridermal cells. Therefore, we can conclude that both *myovb* and *grhl3* genetically interact to mediate epithelial homeostasis.

4.5 Conclusions and future directions

Overall, this study demonstrates that meta-analysis of previously published RNA-Seq datasets is able to identify novel targets of *grhl* transcription. The depth and robustness of

this approach is clearly demonstrated by the fact that many of the genes identified via this method have been previously validated in the literature. Moreover, the experimental validation of altered expression of our identified target genes using a vertebrate model that was not included in any of the published datasets highlights the power of this type of analysis to predict conserved gene targets across different model organisms. Our experimental paradigm naturally has certain caveats and limitations, that any analysis must keep in mind, such as the degree and direction of target regulation in fish compared to mammals, analysis of gene expression over separate developmental and perhaps adult timepoints, and specific analyses through in-situ hybridization (ISH)/ immunohistochemistry (IHC) of mRNA/protein distribution specifically in epithelial tissues, e.g., developing EVL and skin. Moreover, grh (and presumably also Grhl) proteins are known be post-translationally modified through processes such as phosphorylation (Hemphala, Uv et al. 2003, Kim and McGinnis 2011), which further confounds the precise nature of grh/Grhl-dependent regulation (or co-regulation) of transcriptional targets. Nonetheless our experimental approach in fish successfully identified 10 gene orthologues that are significantly differentially regulated, as predicted by the meta-analysis database construction algorithms we have developed and utilised here. Lastly, our analyses did not determine which of these genes may be true direct targets based on promoter occupancy of the target gene promoter by *grh/Grhl*, although such direct binding and activation/repression approaches would be the next logical extension of our meta-analyses. This comprehensive study highlighting the differentially regulated *grhl* genes acts as an excellent resource for researchers working in the field of *grhl*-signalling to identify novel molecular pathways that underpin epithelial development and disease.

4.6 Supplementary data

Differentially regulated genes of *grhl* in non-cancer cell lines, mammalian tissues and non-mammalian tissues following *grhl3* loss.

Supplementary table 4.1 The top 50 most differentially regulated genes in non-cancer cell lines following modulation of *grh/Grhl* function.

The topmost differentially regulated genes compared with the list of *grhl* differentially regulated genes generated for cancer lines.

Rank	Gene	Regulation	Average normalised score	Differential regulation by cancer cell lines		
				Rank	Regulation	Average normalised score
1	MPZL2	Negative	0.0419	70	Positive	0.0153
2	PCDHGA5	Positive	0.0345			
3	LOC652614	Negative	0.0345			
4	IRX4	Positive	0.0345			
5	Prss22	Positive	0.0345	346	Positive	0.00876
6	Serpina3h	Negative	0.0345			
7	Fabp5	Positive	0.0345	702	Positive	0.00631
8	Bex1	Negative	0.0345	140	Negative	0.0127
9	Bex1	Negative	0.0345	1269	Negative	0.00472
10	IGF2	Positive	0.0345			
11	LOC645769	Positive	0.0344			
12	Cldn4	Positive	0.0282	26	Positive	0.0239
13	MEX3B	Positive	0.0274			
14	TRIL	Positive	0.0274			
15	Tmem54	Positive	0.0274	47	Positive	0.019
16	Vim	Negative	0.0274	52	Negative	0.018
17	Fgb	Positive	0.0274			
18	Hddc2	Negative	0.0274	2515	Negative	0.00348
19	DIO2	Positive	0.0274			
20	DOCK8	Negative	0.0274			
21	LOC100130494	Negative	0.0272			
22	Grhl2	Positive	0.0265	57	Positive	0.0176
23	SPON2	Positive	0.0239			
24	2310007B03Rik	Positive	0.0239			
25	Zeb1	Negative	0.0239			
26	Hapln1	Positive	0.0239			
27	Scgb3a1	Negative	0.0239			
28	TMEM176B	Positive	0.0239			
29	IL17RE	Negative	0.0239			
30	MLLT1	Positive	0.0232			
31	NAALADL2	Negative	0.022			
32	RBAK	Positive	0.0217			
33	SIGLEC11	Negative	0.0217			
34	TBX2	Positive	0.0217			
35	KIAA1614	Negative	0.0217			
36	Rab25	Positive	0.0217	97	Positive	0.0147
37	Col6a1	Negative	0.0217			
38	Klf12	Positive	0.0217			
39	Enpp2	Negative	0.0217			
40	TIMP3	Positive	0.0217			
41	ODZ4	Negative	0.0217			
42	SEC16A	Positive	0.0209			
43	CXorf36	Positive	0.0202			
44	OR6C6	Positive	0.0202			
45	9930023K05Rik	Positive	0.0202			
46	Gper	Negative	0.0202			
47	Cldn8	Positive	0.0202	53	Positive	0.018
48	CACNA1G	Positive	0.0202			
49	DKK2	Negative	0.0202			
50	ELAVL1	Positive	0.0195			

Supplementary table 4.2 The top 30 most differentially regulated genes in mammalian tissues following modulation of *grh/Grhl* function.

Rank	Gene	Human orthologue	Regulation	Normalized score
1	Tmem54	*TMEM54*	Positive	0.0981
2	Prom2	*PROM2*	Positive	0.0928
3	Rab15	*RAB15*	Positive	0.0562
4	Grhl2	*GRHL2*	Positive	0.0485
5	Cldn4	*CLDN4*	Positive	0.0468
6	Pax8	*PAX8*	Negative	0.0463
7	Lad1	*LAD1*	Positive	0.0453
8	Spint1	*SPINT1*	Positive	0.0412
9	Cdh1	*CDH1*	Positive	0.0371
10	Ldoc1	*LDOC1*	Positive	0.0369
11	Tex19.1	*TEX19*	Positive	0.0368
12	Fgf15	*FGF19*	Negative	0.0362
13	Rhox4d	*No known orthologue*	Positive	0.036
14	Pgm2	*PGM1*	Negative	0.0345
15	Utf1	*UTF1*	Positive	0.0345
16	Tmprss13	*TMPRSS13*	Positive	0.0345
17	1600012P17Rik	*No known orthologue*	Positive	0.0329
18	Esrp1	*ESRP1*	Positive	0.0326
19	Ap1m2	*AP1M2*	Positive	0.0317
20	Tcfap2a	*No known orthologue*	Positive	0.0316
21	Tnk1	*TNK1*	Positive	0.0316
22	Kcnk1	*KCNK1*	Positive	0.0315
23	Sfn	*SFN*	Positive	0.0312
24	Hrc	*HRC*	Positive	0.0302
25	Plac1	*PLAC1*	Positive	0.0301
26	Irx2	*IRX2*	Positive	0.0297
27	9530027K23Rik	*No known orthologue*	Positive	0.0297
28	Pappa	*PAPPA*	Negative	0.0291
29	Cldn6	*CLDN6*	Positive	0.0291
30	Epcam	*EPCAM*	Positive	0.0288

Supplementary table 4.3 The top 30 most differentially regulated genes in non-mammalian tissues following modulation of *grh/Grhl* function.

Rank	Gene	Human orthologue	Regulation	Normalized score
1	Zasp66	*No known orthologue*	Negative	0.0579
2	CG10345	*No known orthologue*	Negative	0.0502
3	CG12480	*No known orthologue*	Negative	0.05
4	CG5326	ELOVL1	Negative	0.0493
5	CG5326	ELOVL7	Negative	0.0493
6	CG16733	*No known orthologue*	Positive	0.0472
7	bcd	*No known orthologue*	Positive	0.0459
8	CG15282	*No known orthologue*	Positive	0.0448
9	ps	NOVA2	Negative	0.0432
10	ps	NOVA1	Negative	0.0432
11	gfzf	*No known orthologue*	Positive	0.0429
12	rtet	MFSD10	Positive	0.0412
13	CG6472	LIPC	Negative	0.0364
14	CG6472	LPL	Negative	0.0364
15	CG6472	LIPG	Negative	0.0364
16	Cpr47Eb	*No known orthologue*	Positive	0.0357
17	Pcd	PCBD2	Positive	0.0356
18	Pcd	PCBD1	Positive	0.0356
19	CG13731	*No known orthologue*	Negative	0.0355
20	CG5278	*No known orthologue*	Negative	0.0355
21	Lcp4	*No known orthologue*	Positive	0.0345
22	drosomycin-5	*No known orthologue*	Negative	0.0345
23	CG14105	TTC36	Positive	0.0341
24	Spn47C	SERPINE3	Positive	0.0337
25	Spn47C	SERPINE2	Positive	0.0337
26	Spn47C	SERPINE1	Positive	0.0337
27	Spn47C	SERPINI1	Positive	0.0337
28	Spn47C	SERPINI2	Positive	0.0337
29	Cpr78Cc	*No orthologue*	Negative	0.0333
30	CG17919	*No orthologue*	Positive	0.0329

Chapter 5: Functional role of grhl3-target genes in epithelial development

5.1 Summary

In order to determine putative novel, direct *grhl* target genes, in-silico analysis (PHYLO-PROM) and meta-analysis of 41 *grh/Grhl* RNA seq datasets was performed as described in chapter 4. Six genes (*pvrl4, tbc1d2, ovol1, gldc* and *tmem54*) that showed differential gene expression following *grhl* loss, and that were also predicted targets in PHYLO-PROM, were selected for experimentation in zebrafish embryos on the basis of their function in epithelial development and implications in human diseases. To investigate the role of the predicted *grhl* target genes, both rescue experiments and gene knockdown/knockout experiments were carried out in zebrafish embryos. Firstly, microinjection of full-length mRNA of *pvrl4*, *tbc1d2*, and *ovol1* was performed in *grhl3*-/- embryos to see whether they could rescue the epithelial defects seen in these embryos. A rescue in phenotypic severity was observed when *grhl3*-/- embryos were injected with *pvrl4* mRNA. This indicates not only the significance of the gene in epithelial establishment, but also positions it functionally downstream of *grhl3*. Secondly, a knockout of *tbc1d2* was performed by CRISPR/Cas9 mediated genome editing, and morpholino mediated knockdown of *pvrl4, gldc* and *tmem54* genes was done in WT embryos to understand their role in epithelial barrier formation and orofacial development. From our observations, I have identified a new role for *tmem54a* for the first time in orofacial development and axial patterning of zebrafish embryos. Finally, in order to determine the degree of axial defects and craniofacial abnormalities in the absence of both *grhl3* and potential target gene, MO-knockdown of *pvrl4, tmem54* and *gldc* was performed in *grhl3*-/- embryos. However, unexpectedly, no worsening of the phenotypes was detected in *grhl3*-/- embryos suggesting, that *grhl3* does not co-operate with *pvrl4, tmem54* or *gldc* in craniofacial patterning and axial establishment. In conclusion, this study provides insights into the roles of differentially regulated genes of *grhl3,* and their possible interaction with *grhl3* in epithelial establishment using zebrafish embryos.

5.2 Introduction

Elucidating the functional role of genes that are differentially regulated following *grhl* de-regulation in epithelial formation is integral to identify interactions between *grhl3* and the putative target gene. This will ultimately help determine the transcriptional networks regulated by *grhl3* in various epithelial and developmental processes. Since disruption of these molecular pathways contributes to epithelial birth defects, such as spina bifida, Van der Woude syndrome and exencephaly, identifying the underlying genetic mechanisms helps us understand the aetiology of such birth defects.

In this chapter, I sought to understand the epithelial function of genes differentially expressed following *grhl3* loss. Furthermore, I was keen to determine the functional similarities between *grhl3* and their putative targets. Putative *grhl* candidates for experimental validation in zebrafish was identified via in-silico analysis, whereby promoters of all mammalian genes were aligned to search for the presence of the conserved *grhl* binding site (AA**C**CG**G**TT). This was then compared with the list of genes differentially regulated in the RNA seq dataset derived from the 1st pharyngeal arch of *Grhl2*$^{-/-}$ mice (detailed in chapter 4). In all, 21 genes were commonly identified between the two datasets, of which three genes were selected for rescue experiments: *pvrl4, ovol1,* and *tbc1d2*. PVRL4 encodes for Nectin-4, a critical cell-adhesion molecule found to be implicated in the formation of cadherin-based adherans junctions (Brancati, Fortugno et al. 2010), and is also integral for the establishment of a protective and functional epithelial barrier. *Ovol* family of TFs act as crucial regulators of embryogenesis (Dai, Schonbaum et al. 1998, Mackay, Hu et al. 2006). In addition, *Ovol* TFs determine epithelial lineage and regulate differentiation during embryonic development (Mackay, Hu et al. 2006, Teng, Nair et al. 2007, Sun, Li et al. 2019)

While *Ovol1*and *Pvrl4* act as regulators of epithelial barrier formation and differentiation, *TBC1D2* acts as a signal effector that contributes to cadherin degradation, leading to reduced cell-cell adhesion. Having understood the role of these genes in epithelial and developmental processes, I investigated if they interact with *grhl3* in regulating epithelial differentiation. To investigate this, firstly mRNA of these genes was synthesised and microinjected into *grhl3* null embryos. A rescue in the severity of *grhl3* phenotypes would indicate that the gene might be a potential downstream target of *grhl3*.

Secondly, since the discrete function of *tbc1d2* was yet to be clearly delineated, a CRISPR/Cas9 *tbc1d2* knockout zebrafish line was established to investigate the role of *tbc1d2* in axial patterning and craniofacial establishment (Figure 5.1). Finally, 2 genes (*gldc* and *tmem54*) that were differentially regulated following *Grhl* misexpression in primary epithelia (as identified from meta-analysis), were selected along with *pvrl4* for morpholino-mediated knockdown experiments in *grhl3* null and WT embryos.

pvrl4 showed a partial rescue when injected in *grhl3*$^{-/-}$ embryos, hence, in order to explore its role in epithelial establishment, knockdown-based experiments were performed. *GLDC* on the other hand, plays a critical role in the synthesis of glycine dehydrogenase which aids in the breakdown of glycine. *GLDC* mutation in humans contributes to glycine encephalopathy and mice deficient in *Gldc* display a myriad of developmental defects such exencephaly, open neural tube, hydrocephaly, and growth retardation (Pai, Leung et al. 2015, Autuori, Pai et al. 2017). Having numerous implications in both human and mouse models, I was keen to investigate its role in zebrafish and determine phenotypic conservation in epithelial development between mouse and fish due to loss of *Gldc*.

Findings from chapter 4 revealed *Tmem54a*, a gene that encodes transmembrane protein, was differentially expressed following *Grhl* deregulation in primary epithelia. Furthermore, *Tmem54* was also found to be bound by *Grhl* TFs via ChIP-Seq analysis (Aue, Hinze et al. 2015, Walentin, Hinze et al. 2015), signifying that it might be a true target of *Grhl*. However, very little is known about the functions of either mammalian *Tmem54*, or the zebrafish orthologue *tmem54a*. Thus, in order to investigate the role played by this gene in epithelial development and craniofacial formation along with *pvrl4* and *gldc*, transient knockdown of these genes was performed in zebrafish embryos. Together, this study investigated the role of *pvrl4, tbc1d2, ovol1, gldc*, and *tmem54* and their interactions with *grhl3* in epithelial development. This is key to understand the *grhl3*-dependent transcriptional pathways underlying epithelial establishment.
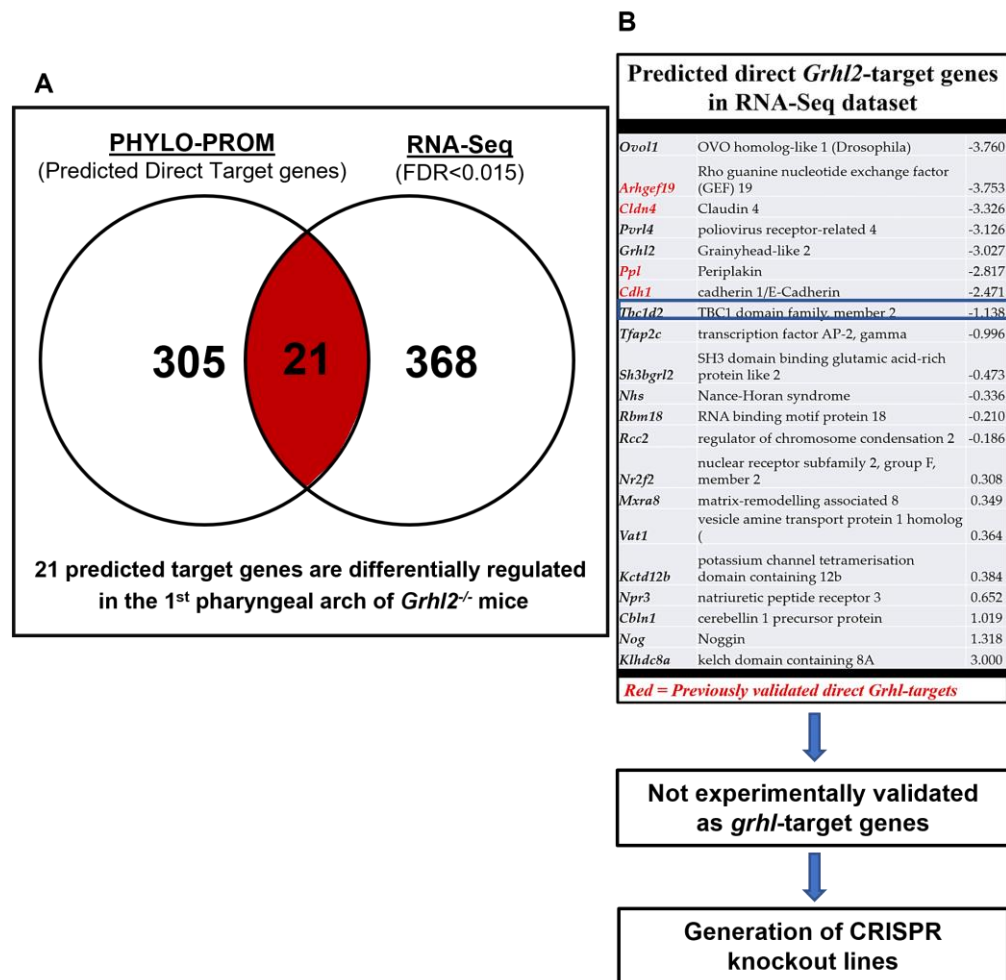
Figure 5.1 Selection of differentially regulated genes of *Grhl* for generation of CRISPR knockout lines

(A) Promoters of all mammalian genes were aligned and searched for the presence of the *Grhl*-binding site generating a list of 305 genes (PHYLO-PROM). This list was compared with the 368 genes determined to be differentially regulated in the RNA-seq dataset derived from the 1st pharyngeal arch of *Grhl2-/-* mice. **(B)** 21 genes identified from in-silico analysis were found to be differentially regulated in the RNA seq dataset derived from pharyngeal arch of *Grhl2-/-* mice. Genes with poorly defined functions (such as, *tbc1d2*) were selected for the generation of CRISPR knockout lines.

5.3 Results

5.3.1   Microinjection of *pvrl4* mRNA partially rescues the severity of phenotypes seen in *grhl3$^{-/-}$* embryos

In order to determine whether *pvrl4* rescues the severity of *grhl3$^{-/-}$* phenotypes, *pvrl4* mRNA was injected in single cell stage embryos derived from inter-crossing *grhl3$^{+/-}$* fish at concentrations of 25 ng/µl, 50 ng/µl and 75 ng/µl. As a control, embryos derived from inter-crossing *grhl3$^{+/-}$* fish were injected with EGFP at the same concentration as that of the mRNA; data was collected from a minimum of 3 individual experiments (n=3).

Key findings on survival rate of embryos: WT embryos were injected with *pvrl4* mRNA to determine any toxicity associated with the mRNA prior to experimentation on embryos derived from inter-crossing *grhl3$^{+/-}$* fish. Survival rate of WT embryos at 25 ng/µl (not shown), 50 ng/µl (Figure 5.2B) and 75 ng/µl (Figure 5.3B) of *pvrl4* mRNA was 97.3 ± 4.5%, 96.4 ± 3.4% and 71.4 ± 1.2% at 72 hpf respectively. Control embryos showed a survival percentage of 98.2 ± 3.9% at 25 ng/µl (not shown), 97.74 ± 1.2% at 50 ng/µl (Figure 5.2B) and 90.9 ± 2.7% at 75 ng/µl (Figure 5.3B). No significant variation in survival rate was observed at 25 ng/µl and 50 ng/µl however, increased lethality was seen at 75 ng/µl (p<0.01) relative to control. Therefore, mRNA injection at high concentrations contributes to lethality of embryos.

Survival rate of embryos derived from inter-crossing *grhl3$^{+/-}$* fish injected with *pvrl4* mRNA at 25 ng/µl was 92.6 ± 5.4% and that of control embryos was 94.4 ± 4.6% at 72 hpf (Figure 5.4B). Statistical analysis revealed no significant difference in terms of survival of *pvrl4* mRNA (25 ng/µl) injected embryos relative to control (EGFP). Injection of *pvrl4* mRNA at a concentration of 50 ng/µl in embryos derived from inter-crossing *grhl3$^{+/-}$* fish showed a survival rate of 87.9 ± 1.0% while that of control showed a survival of 75.6 ± 0.9% (Figure 5.5B). A significant increase (p=0.018) in the survival rate of injected embryos was seen at 50 ng/µl in comparison to controls.

Key findings on phenotypic incidence and severity in embryos: ~99% WT embryos injected with *pvrl4* mRNA and EGFP showed normal development with no aberrant phenotypes (Figure 5.2A). Phenotypic incidence of sibling, class 1, class 2, and class 3 phenotypes in *pvrl4* mRNA injected embryos derived from inter-crossing *grhl3$^{+/-}$* fish (25 ng/µl) were 87.4 ± 1.94%, 5.9 ± 4.8%, 4.5 ± 0.7% and 2.21 ± 2.2% respectively (Figure

5.4C). No significant differences were noted between the *pvrl4* injected *grhl3^{-/-}* embryos (25 ng/µl) and control in terms phenotypic severity. *pvrl4* injection at 50 ng/µl resulted in 82.88 ± 0.45% sibling, 8.59 ± 0.83% class 1, 5.95 ± 2.58% class 2, and 2.6 ± 0.25% class 3 phenotypes while control injection showed 63.3 ± 6.1% sibling, 8.5 ± 0.6% class 1, 18.4 ± 1.2% class 2, and 9.8 ± 4.3% class 3 phenotypes (Figure 5.5C). No significant differences were observed in the percentage of class 1 and class 3 phenotypic *grhl3^{-/-}* embryos. However, a significant increase in the sibling population (p=0.0003) and a decline in class 2 mutants was observed (p=0.005) relative to controls suggesting a partial phenotypic rescue in the severity of the *grhl3^{-/-}* embryos when injected with 50 ng/µl *pvrl4*.

Summary: Survival rate of WT embryos showed no significant difference upon injection of *pvrl4* mRNA at 25 ng/µl and 50 ng/µl in comparison to control. However, increased lethality was observed in WT embryos injected with *pvrl4* mRNA at 75 ng/µl relative to controls. This might be due to toxicity associated with mRNA at high concentrations. A decrease in the percentage of class 2 *grhl3^{-/-}* mutants and an increase in the percentage of sibling population in *pvrl4* mRNA injected embryos derived from inter-crossing *grhl3^{+/-}* fish indicates a "phenotypic shift" away from the most severe phenotypic penetration of axial defects in *grhl3^{-/-}* embryos.

5.3.2   Microinjection of *tbc1d2* mRNA showed no phenotypic shift in *grhl3^{-/-}* embryos

tbc1d2 mRNA was injected into single cell stage WT embryos and embryos derived from inter-crossing *grhl3^{+/-}* fish at concentrations of 25 ng/µl, 50 ng/µl and 75 ng/µl. The data was generated from outcomes of 3 individual experiments (n=3).

Key findings on survival rate of embryos: WT embryos injected with *tbc1d2* mRNA at 25 ng/µl (not shown) and 50 ng/µl (Figure 5.2B) showed survival percentages of 97.4 ± 6.4% and 90.7 ± 6.4% at 72 hpf, respectively. No significant differences were observed in WT embryos injected with 25 ng/µl and 50 ng/µl *tbc1d2* mRNA, relative to controls. Injection at 75 ng/µl in WT embryos revealed 83.0 ± 0.8% survival while control embryos showed a survival rate of 90.96 ± 2.7% at 72 hpf (Figure 5.3B). A significant increase (~6-10%; p=0.015) in lethality of WT embryos at 75 ng/µl was observed. This might be due to toxicity induced upon injection of *tbc1d2* mRNA.

tbc1d2 mRNA injected into embryos derived from inter-crossing $grhl3^{+/-}$ fish at concentrations of 25 ng/µl and 50 ng/µl showed survival rates of 94.65 ± 3.3% (Figure 5.4B) and 91.5 ± 2.3% (Figure 5.6B) respectively. Like WT embryos, no significant differences were observed in *tbc1d2* injected embryos derived from inter-crossing $grhl3^{+/-}$ fish, relative to control (~90%).

Key findings on phenotypic incidence and severity in embryos: Injection at 25 ng/µl in embryos derived from inter-crossing $grhl3^{+/-}$ fish resulted in 74.45 ± 9.8% sibling, 13.5 ± 11.5% class 1, 5.7 ± 1.4% class 2, and 6.3 ± 3.1% class 3 $grhl3^{-/-}$ phenotypes (Figure 5.4C). The phenotypic incidence of sibling, class 1, class 2, class 3 mutants of *tbc1d2* mRNA (50 ng/µl) injected embryos were 75.7 ± 5.4%, 13.5 ± 2.8%, 5.7 ± 0.1% and 5.2 ± 2.7% respectively (Figure 5.6C). Statistical analysis revealed no significant differences in phenotypic severity of $grhl3^{-/-}$ embryos following injection at 25 ng/µl and 50 ng/µl relative to control (EGFP).

Summary: No significant differences in terms of survival rate and phenotypic severity were detected in *tbc1d2* mRNA injected embryos derived from inter-crossing $grhl3^{+/-}$ fish and WT embryos at 25 ng/µl and 50 ng/µl. However, lethality was observed in WT embryos injected with *tbc1d2* mRNA (75 ng/µl) possibly due to toxicity of *tbc1d2* over expression. Hence, *tbc1d2* mRNA was not injected in embryos derived from inter-crossing $grhl3^{+/-}$ fish at concentrations ≥ 75 ng/µl.

Similarly, microinjection with *ovol1* mRNA at 25 ng/µl and 50 ng/µl (Supplementary figure 5.1, 5.2 and 5.3) yielded no rescue in the severity of $grhl3^{-/-}$ embryos. Therefore, in future, concentrations >50 ng/µl of *ovol1* mRNA must be injected to determine whether any rescue of $grhl3^{-/-}$ phenotypes takes place.
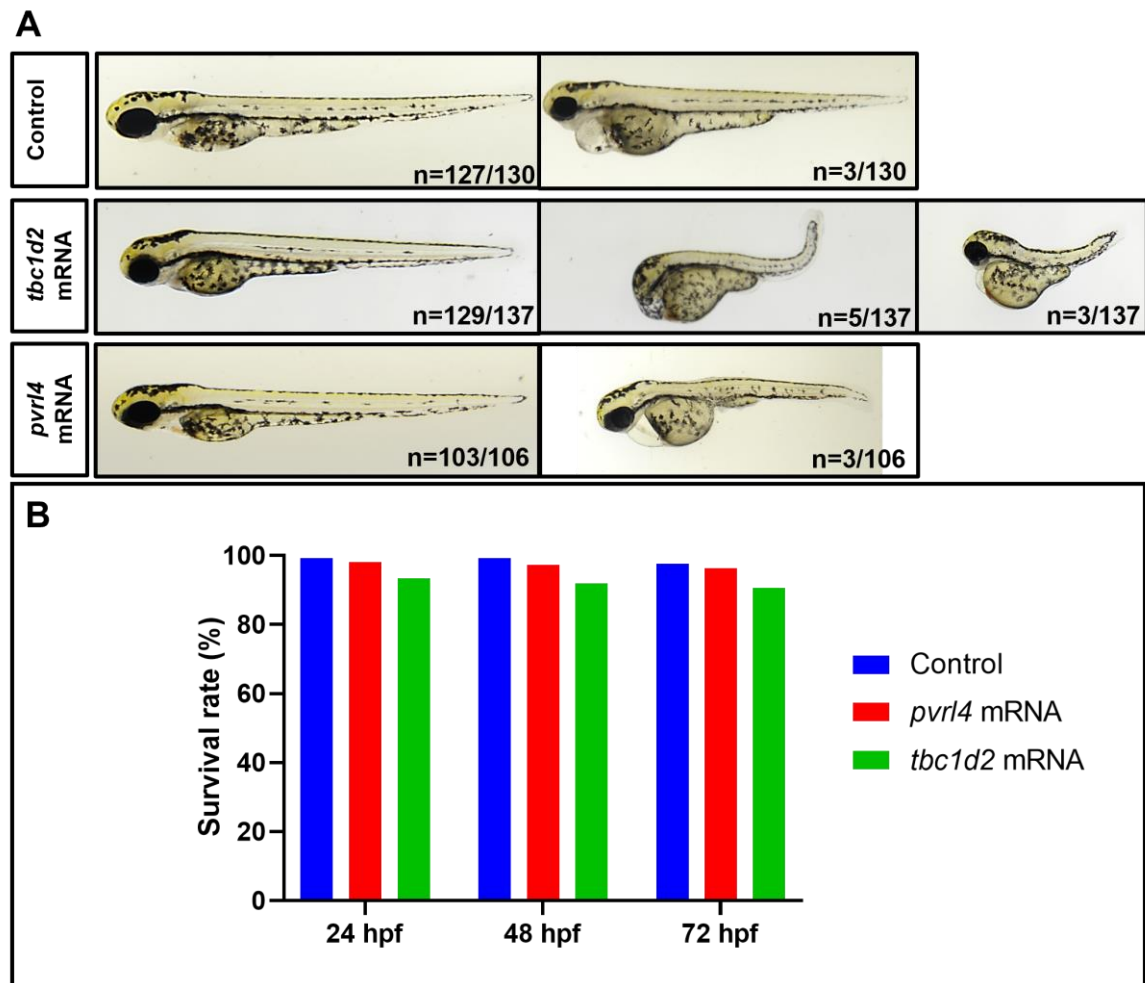
Figure 5.2 Microinjection of *tbc1d2* mRNA (50 ng/µl) and *pvrl4* mRNA (50 ng/µl) showed no toxicity in WT embryos.

tbc1d2 mRNA and *pvrl4* mRNA was injected in single cell stage WT embryos at 50 ng/µl. Control embryos were injected with EGFP (50 ng/µl) at 0 hpf. (**A**) Phenotypes of *tbc1d2* and *pvrl4* injected embryos were imaged at 72 hpf. (**B**) Survival rate of injected WT embryos was quantitated and analysed. Data is represented as mean ± SEM. Statistical significance determined by Multiple t-tests with correction for multiple comparisons using the Holm-Sidak method.
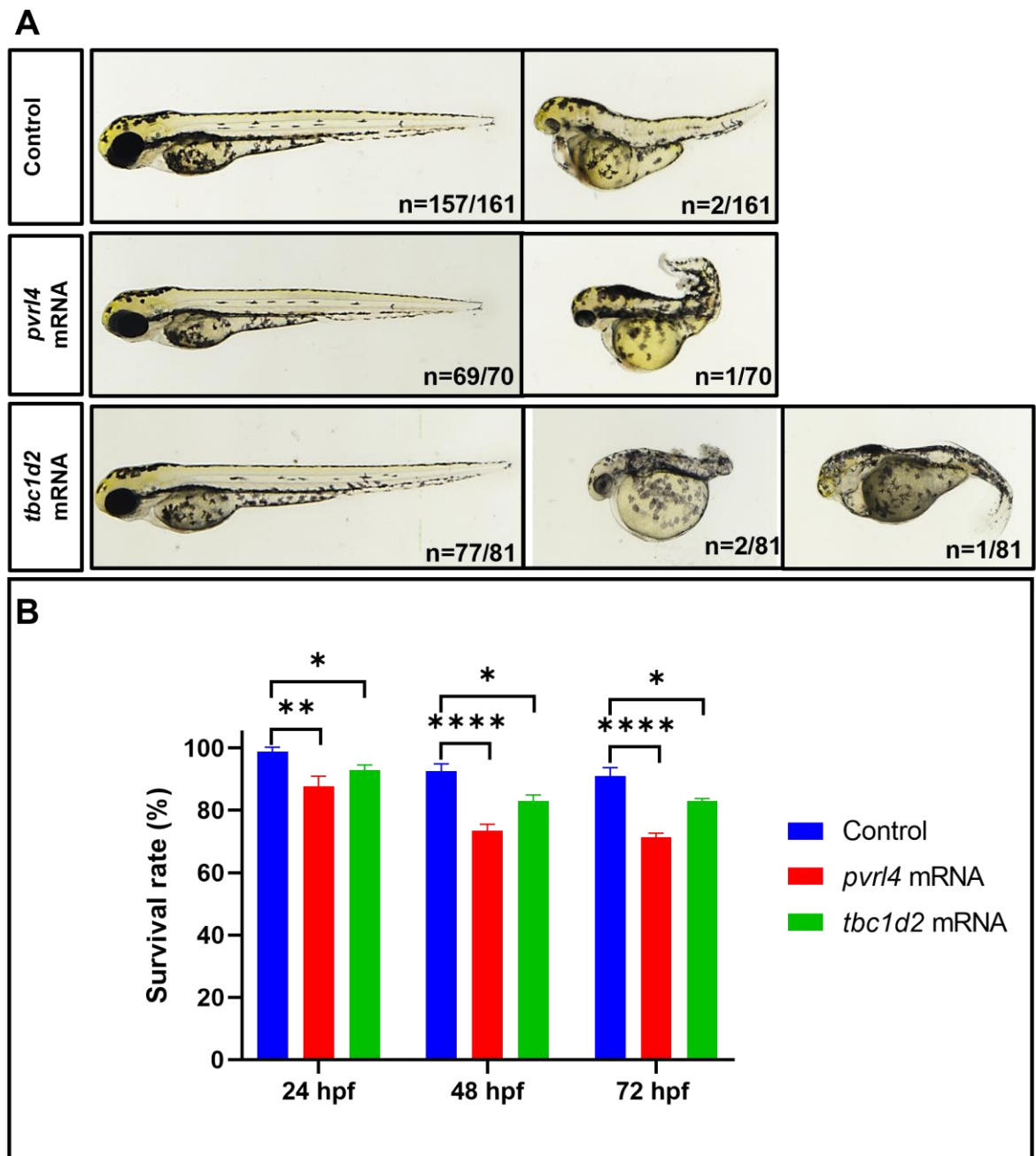
Figure 5.3 Microinjection of *tbc1d2* mRNA (75 ng/µl) and *pvrl4* mRNA (75 ng/µl) showed toxicity in WT embryos.

tbc1d2 mRNA and *pvrl4* mRNA was injected into single cell stage WT embryos at 75 ng/µl. Control embryos were injected with EGFP (75 ng/µl). (**A**) Phenotypes of *tbc1d2* and *pvrl4* injected WT embryos were observed until 72 hpf and imaged at 72 hpf. (**B**) Survival graph for injected embryos was plotted and analysed. Data is represented as mean ± SEM. Statistical significance was determined by Multiple t-tests with correction for multiple comparisons using the Holm-Sidak method *P < 0.05; ****P < 0.001.

Figure 5.4 Microinjection of *tbc1d2* mRNA (25 ng/µl) and *pvrl4* mRNA (25 ng/µl) showed no phenotypic rescue in *grhl3⁻/⁻* embryos.

tbc1d2 mRNA and *pvrl4* mRNA was injected into single cell stage embryos derived from inter-crossing *grhl3⁺/⁻* fish at 25 ng/µl. Control embryos were injected with EGFP (25 ng/µl) at 0 hpf. (**A**) Phenotypes of *tbc1d2* and *pvrl4* injected *grhl3⁻/⁻* embryos were observed until 72 hpf, and embryos were imaged at 72 hpf. (**B**) Survival rate and (**C**) phenotypic incidence of sibling, class 1, class 2, and class 3 phenotypes in *tbc1d2* and *pvrl4* mRNA injected embryos derived from inter-crossing *grhl3⁺/⁻* fish was quantitated and analysed. Data is represented as mean ± SEM. Statistical significance determined by Multiple t-tests with correction for multiple comparisons using the Holm-Sidak method; ns – non-significant.
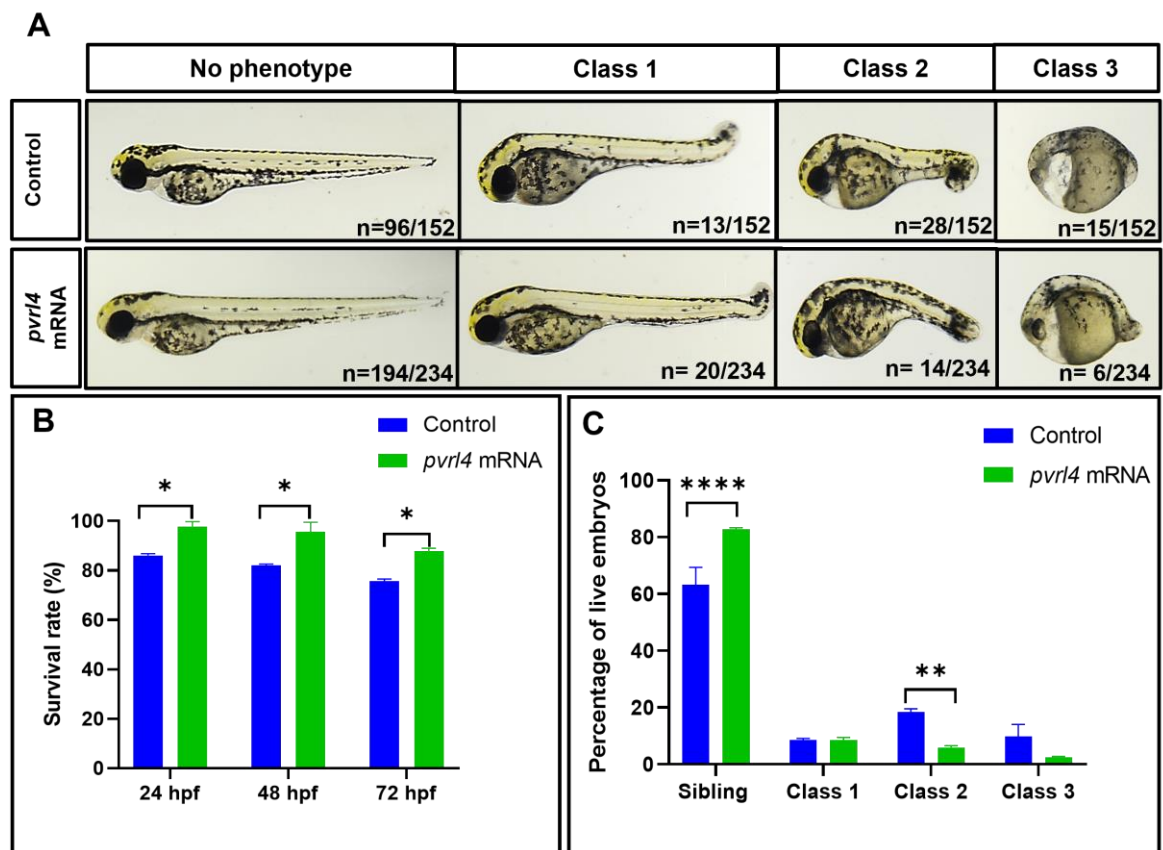
Figure 5.5 Microinjection of *pvrl4* mRNA (50 ng/µl) showed phenotypic shift in the severity of *grhl3*⁻/⁻ embryos.

pvrl4 mRNA was injected into single cell stage embryos derived from inter-crossing *grhl3*⁺/⁻ fish at 50 ng/µl. Control embryos were injected with EGFP (50 ng/µl) at 0 hpf. **(A)** Phenotypes of *pvrl4* mRNA injected *grhl3*⁻/⁻ embryos were imaged at 72 hpf. **(B)** Survival rate and **(C)** phenotypic incidence of sibling, class 1, class 2, and class 3 phenotypes in *pvrl4* mRNA injected embryos derived from inter-crossing *grhl3*⁺/⁻ fish was quantitated and analysed. Data is represented as mean ± SEM. Statistical significance determined by Multiple t-tests with correction for multiple comparisons using the Holm-Sidak method *$P < 0.05$; **$P < 0.01$; ****$P < 0.001$.
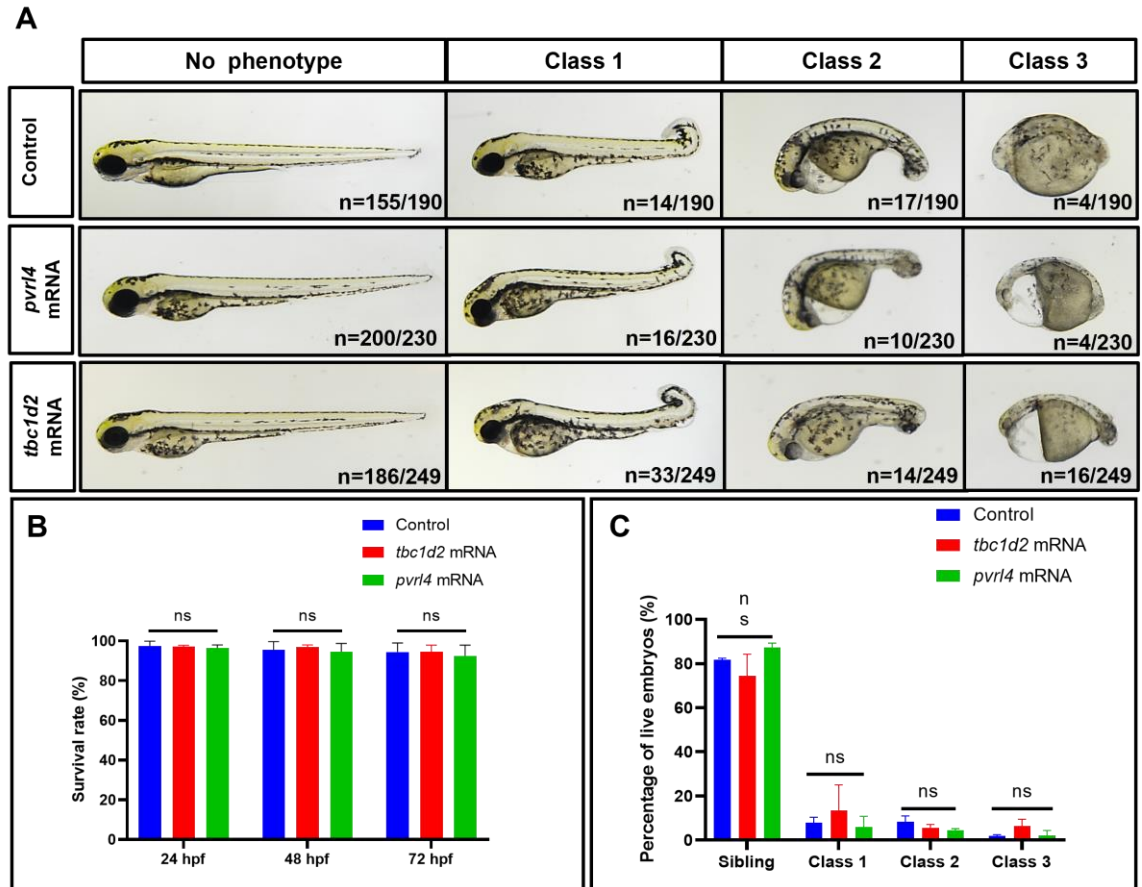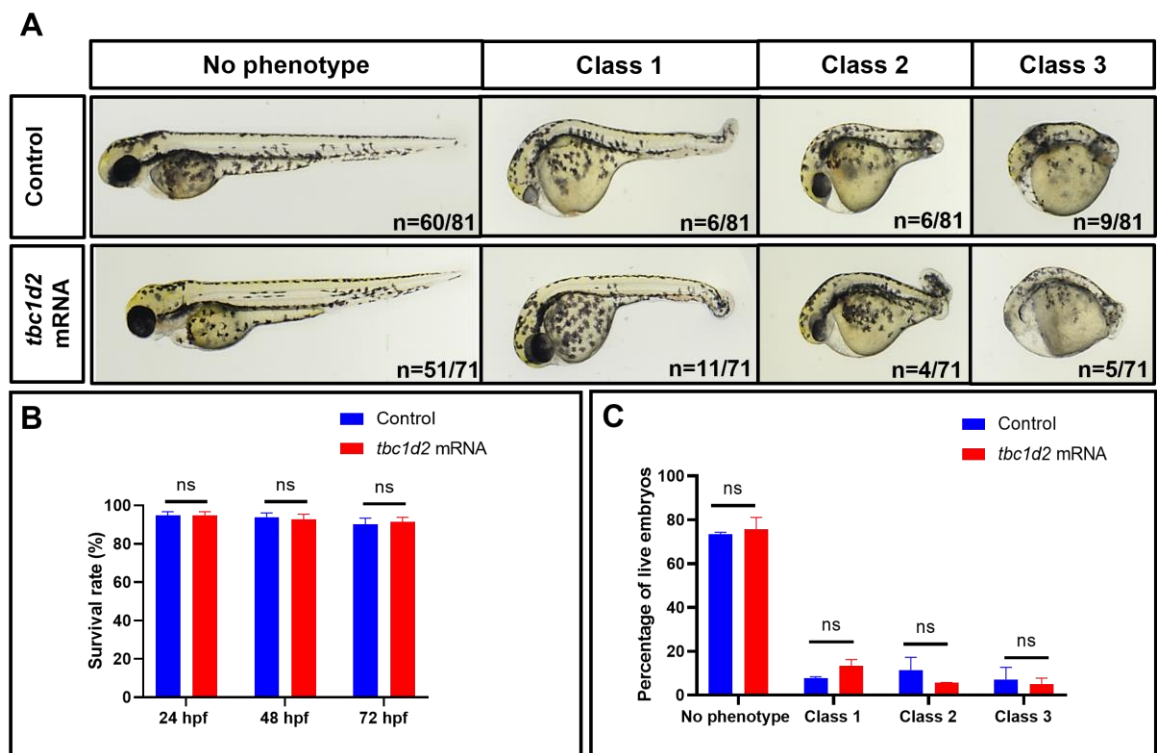
Figure 5.6 Microinjection of *tbc1d2* mRNA (50 ng/µl) resulted in no observable phenotypic shift in the severity of *grhl3⁻ᐟ⁻* embryos.

tbc1d2 mRNA was injected into single cell stage embryos derived from inter-crossing *grhl3⁺ᐟ⁻* fish at 50 ng/µl. Control embryos were injected with EGFP (50 ng/µl) at 0 hpf. (**A**) Phenotypes of *tbc1d2* mRNA injected *grhl3⁻ᐟ⁻* embryos were observed until 72 hpf and imaged at 72 hpf. (**B**) Survival rate and (**C**) phenotypic incidence of sibling, class 1, class 2, and class 3 phenotypes in *tbc1d2* mRNA injected embryos derived from inter-crossing *grhl3⁺ᐟ⁻* fish was quantitated and analysed. Data is represented as mean ± SEM. Statistical significance determined by Multiple t-tests with correction for multiple comparisons using the Holm-Sidak method; ns – non-significant.

5.3.3 Knockout of *tbc1d2,* a differentially regulated putative target gene of *grhl3*, showed normal epithelial development

Since the function of *tbc1d2* is largely unknown, and this gene has also not been experimentally validated as a *Grhl* target gene, a *tbc1d2*$^{-/-}$ mutant line was generated using CRISPR/Cas9 mediated mutagenesis. A *tbc1d2* mutant was generated by targeting exon 3 at a site lying 3' to the in-frame ATG-initiation codon. Two separate lines, namely *tbc1d2(+47bp)* and *tbc1d2(-21bp),* were generated by Dr. Lee Miles (Supplementary table 5.1). The *tbc1d2(+47bp)* line carries a stop cassette insertion at codon 194. *tbc1d2 (-21bp)* carries a deletion of 21 bp at codon 183. Embryos from both these knockout lines were characterized to understand the role of *tbc1d2* in epithelial establishment.

In order to determine whether the genotypes of embryos derived from inter-crossing *tbc1d2*$^{+/-}$ fish follow Mendelian ratio, larvae were genotyped at 5 dpf. Genotyping at 5 dpf of embryos collected from inter-crossing *tbc1d2*$^{+/-(+47)}$ fish revealed 48.6 ± 5.4% heterozygous, 21.6 ± 3.1% homozygous null and 29.7 ± 2.3% wild-type embryos (Figure 5.7A). Likewise, upon genotyping embryos collected from inter-crossing *tbc1d2*$^{+/-(-21)}$ fish, 47.4 ± 4.8% heterozygotes, 19.2 ± 2.7% homozygous nulls and 33.4 ± 2.1% wild types were detected. Chi square analysis of the genotyping results revealed no significant variation between observed and expected number of heterozygotes, homozygous nulls, and WT at 5 dpf (Figure 5.7D-E). Thus, our data fits the expected Mendelian ratios.

In order to determine the viability of homozygous nulls, adults derived from inter-crossing *tbc1d2*$^{+/-}$ fish were genotyped at 6 months adulthood. Genotyping of fish derived from inter-crossing *tbc1d2*$^{+/-(+47)}$ revealed 42.5 ± 5.0% heterozygotes, 20.3 ± 3.6% homozygous nulls and 37.2 ± 2.4% WT. Similarly, genotyping of adult fish derived from inter-crossing *tbc1d2*$^{+/-(-21)}$ fish revealed 47.4 ± 4.8% heterozygotes, 19.2 ± 2.7% homozygous nulls and 33.4 ± 2.1% wild types (Figure 5.7A-C). This indicates that *tbc1d2* homozygous null larvae survive to adulthood.

In order to characterize the *tbc1d2*$^{-/-(+47)}$ and *tbc1d2*$^{-/-(-21)}$ embryos*, tbc1d2*$^{-/-(+47)}$ and *tbc1d2*$^{-/-(-21)}$ lines were inter-crossed and null embryos were collected. At 3 dpf, *tbc1d2*$^{-/-}$ embryos from both lines were screened for the presence of phenotypic abnormalities by light microscopy. *tbc1d2*$^{-/-}$ embryos displayed normal development with no phenotypic abnormalities (Figure 5.8). Furthermore, the survival rate in both *tbc1d2*$^{-/-(+47)}$ and *tbc1d2*$^{-}$

$^{/-(-21)}$ embryos was ~99%, with minimal death, similar to control (WT; ~100%) (Figure 5.8B). Thus, no significant differences were observed in survival between control embryos and *tbc1d2*$^{-/-}$ embryos of either line.

Lastly, in order to analyse the craniofacial development in *tbc1d2*$^{-/-(+47)}$ and *tbc1d2*$^{-/-(-21)}$ embryos, Alcian blue staining was performed on 4-day old *tbc1d2*$^{-/-(+47)}$ and *tbc1d2*$^{-/-(-21)}$ embryos fixed in 4% PFA. Both *tbc1d2*$^{-/-(+47)}$ (Figure 5.9A-B) and *tbc1d2*$^{-/-(-21)}$ (Figure 5.9C-D) embryos showed normal jaw formation with no observable defects. Therefore, it can be concluded that *tbc1d2*$^{-/-}$ embryos display no obvious morphological defects and craniofacial abnormalities.

A

tbc1d2 Genotype	*tbc1d2 (+47bp)*		*tbc1d2 (-21bp)*	
	At 5dpf (%)	At 6 months (adulthood; %)	At 5dpf (%)	At 6 months (adulthood; %)
Heterozygous (+/-)	48.6 ± 5.4	42.5 ± 5.0	47.4 ± 4.8	49.5 ± 2.8
Homozygous null (-/-)	21.6 ± 3.1	20.3 ± 3.6	19.2 ± 2.7	20.0 ± 1.1
Wild type (+/+)	29.7 ± 2.3	37.2 ± 2.4	33.4 ± 2.1	30.5 ± 4.9
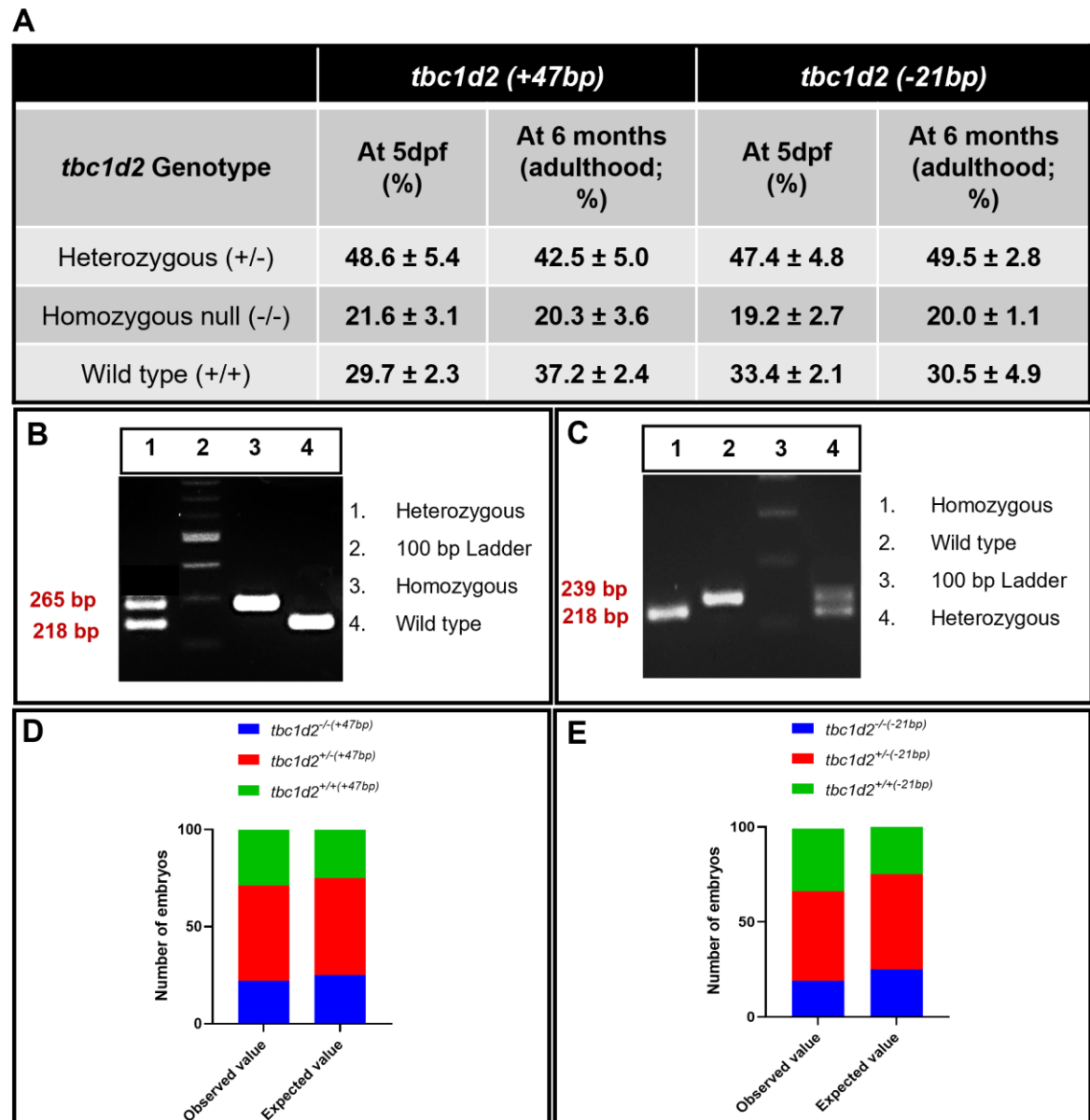
Figure 5.7 Genotyping of *tbc1d2$^{-/-}$* embryos.

(**A**) Table showing the percentage of heterozygous, homozygous null and WT larvae/fish at 5 dpf and 6 months adulthood (derived from inter-crossing heterozygous fish from the same *tbc1d2* line i.e., either *tbc1d2$^{+/-(+47\ bp)}$* or *tbc1d2$^{+/-(-21\ bp)}$* fish). (**B**) 3% agarose gel displaying PCR products of DNA of embryos/fish derived from inter-crossing *tbc1d2$^{+/-(+47\ bp)}$* fish. PCR products comprising 2 bands in the gel (265 bp and 218 bp) indicate a heterozygous genotype; a single band at 265 bp is a homozygous null genotype and a band at 218 bp is a wild-type genotype. (**C**) 3% agarose gel displaying PCR products of DNA of embryos/fish derived from inter-crossing *tbc1d2$^{+/-(-21\ bp)}$* fish. PCR products comprising 2 bands on the gel (239 bp and 218 bp) indicate a heterozygous genotype; a single band at 218 bp is a homozygous null genotype and a band at 239 bp is a wild-type genotype. Primers *tbc1d2 e3* Forward (F) and *tbc1d2 e4* Reverse (R) were used for genotyping the embryos/fish. (**D-E**) Chi square analysis was performed to verify the expected and observed number of homozygous, heterozygous, and wild-type embryos derived from inter-crossing *tbc1d2$^{+/-(+47\ bp)}$*/*tbc1d2$^{+/-(-21\ bp)}$* fish at 5 dpf.

Figure 5.8 Phenotypic characterization and survival rates of *tbc1d2*$^{-/-(+47\ bp)}$ and *tbc1d2*$^{-/-(-21\ bp)}$ embryos.
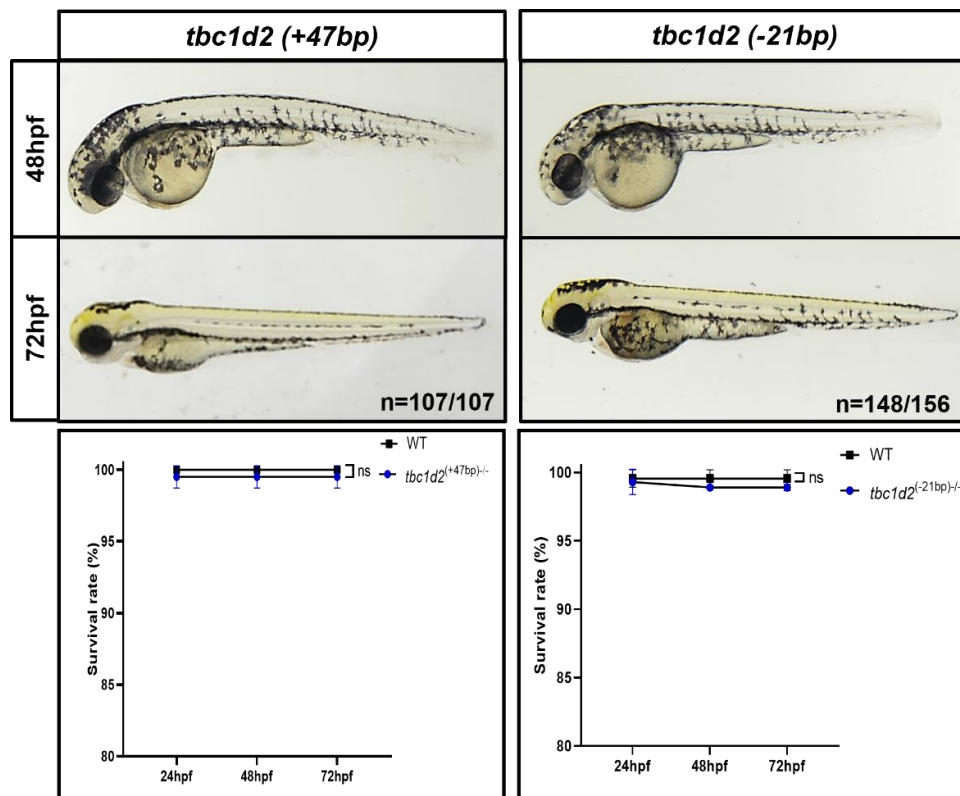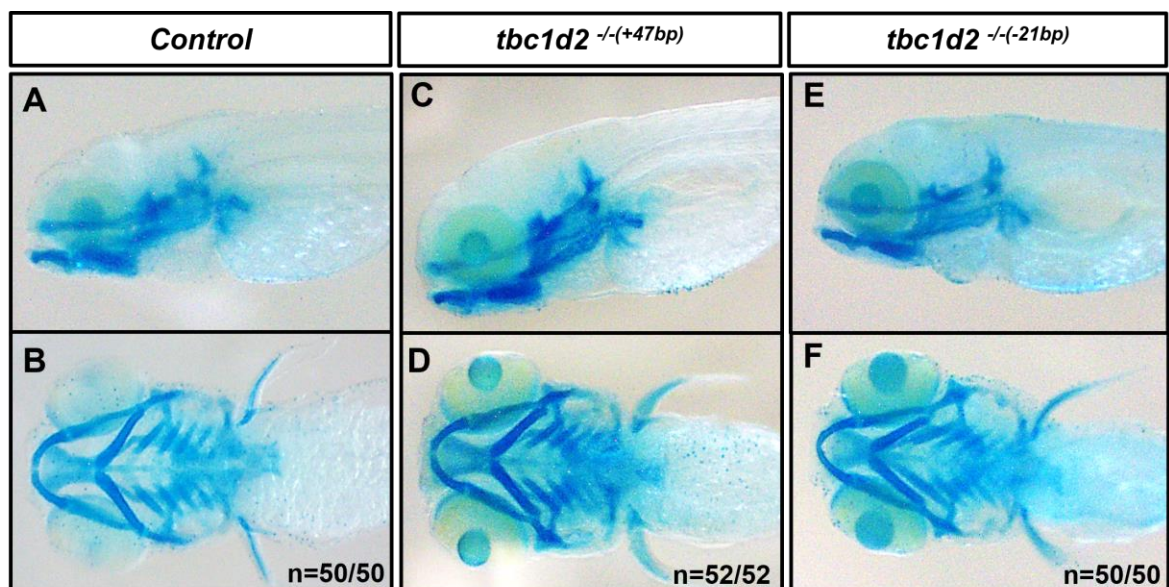

Figure 5.9 Craniofacial development in *tbc1d2*$^{-/-}$ embryos at 4 dpf.
The ventral (top) and lateral (bottom) views of the craniofacial cartilage of Alcian blue stained (**A-B**) WT (control), (**C-D**) *tbc1d2*$^{-/-(+47\ bp)}$ and (**E-F**) *tbc1d2*$^{-/-(-21\ bp)}$ embryos.

5.3.4   Mild craniofacial defects caused due to loss of *pvrl4*.

As microinjection of *pvrl4* mRNA led to a partial rescue of the severe axial phenotypes in *grhl3*$^{-/-}$ embryos, this suggested a key role for *pvrl4* in epithelial development. Therefore, MO-mediated inhibition of *pvrl4* in WT embryos was carried out in order to determine the consequences of *pvrl4*-loss on epithelial development.

MO:*pvrl4* was injected at varying concentrations 100 µM, 150 µM, 200 µM, 300 µM, 500 µM, and 600 µM in WT embryos at 0 hpf (results described below). Following this, concentrations 100 µM, 250 µM and 500 µM were widely used for MO injections as high concentrations beyond 500 µM led to toxicity and concentrations <100 µM were too low to cause a discernible phenotype. The ng injected per embryo did not exceed beyond 7 ng/embryo (Table 5.1). Control embryos were injected with *control* MO at 0 hpf. Mean and SD values to plot the graphs were obtained from outcomes of 2 individual experiments (n=2).

Key findings on survival rate of embryos: In order to determine the correlation between dosage of *pvrl4* MO injected and the survival rate, WT embryos were injected with varying concentrations of MO:*pvrl4* (100 µM, 150 µM, 200 µM, 300 µM, 500 µM, and 600 µM). Survival rate of WT embryos injected with MO:*pvrl4* at concentrations ranging from 100 µM-600 µM ranged between 88-98% at 72 hpf (Figure 5.10B), showing no significant differences relative to controls. MO:*pvrl4* was then injected in embryos derived from inter-crossing *grhl3*$^{+/-}$ fish to determine whether or not the morpholino contributes to lethality of *grhl3* null embryos. Upon injection with MO:*pvrl4*, embryos derived from inter-crossing *grhl3*$^{+/-}$ fish showed survival rates of 78.6 ± 1.3% (100 µM), 86.02 ± 0.4% (250 µM) and 75.5 ± 2.9% (500 µM) (Figure 5.11B). Statistical analysis revealed no significant differences between control and injected embryos. Therefore, MO:*pvrl4* is safe and does not pose lethality of injected embryos derived from inter-crossing *grhl3*$^{+/-}$ fish at concentrations <500 µM.

Key findings on phenotypic incidence of embryos: In order to determine the correlation between dosage of *pvrl4* MO injected and the incidence of non-craniofacial phenotypes, I injected WT embryos at dosages of 100 µM-600 µM. I found that injection of MO dosages up to a concentration of 300 µM did not lead to any observable phenotypes. Injection of MO:*pvrl4* at a concentration of 500 µM led to pericardial edema and axial

development impairment in 55/269 embryos (20.45%). Similarly, injection at 600 µM led to pericardial edema and axial development impairment in 44/269 embryos (16.35%)(Figure 5.10A). As both pericardial oedema and axial impairment are characteristic of toxicity, these data indicate that the MO:*pvrl4* was toxic at concentrations of 500 µM and above.

In order to determine the severity of *grhl3$^{-/-}$* embryos injected with MO:*pvrl4*, embryos with aberrant phenotypes were observed and their numbers were recorded. Embryos derived from inter-crossing *grhl3$^{+/-}$* fish injected with 100 µM MO:*pvrl4* showed 90.4 ± 5.3%, 6.2 ± 4.2%, 2.3 ± 1.2% and 0.95 ± 0.95% of non-phenotypic sibling, class 1, class 2, and class 3 phenotypes respectively. In embryos derived from *grhl3$^{+/-}$* fish, MO:*pvrl4* injection at 250 µM and 500 µM resulted in 2 additional phenotypes (pericardial edema (PE); pericardial oedema along with axial defect (PE + curvature in body axis) (Figure 5.11A). Embryos derived from inter-crossing *grhl3$^{+/-}$* fish injected with MO:*pvrl4* at 250 µM showed 6.5 ± 3.4% with class 1 phenotype, 3.9 ± 1.5% with class 2 phenotype, 0.57 ± 0.8% with class 3 phenotype, 3.6 ± 1.9% with pericardial edema (PE) and 13.1 ± 5.9% with PE + curvature in body axis. In embryos injected with 500 µM MO:*pvrl4*, 53.6 ± 11.3% non-phenotypic siblings, 3.29 ± 0.3% class 1, 4.2 ± 1.5% class 2, 0.44 ± 0.6% class 3, 17.2 ± 7.9% PE, and 21.3 ± 0.8% PE + curvature of body axis phenotypes were observed (Figure 5.11C).

A significant decrease (p<0.001) in the population of non-phenotypic siblings was seen in MO:*pvrl4* injected embryos at 100 µM and 250 µM. The PE phenotype in embryos injected with 500 µM MO:*pvrl4* showed an increase relative to controls (p=0.004).

Table 5.1 List of morpholinos and the amount of MO injected per embryo.

Working concentration		Injection/embryo (in ng)
in µM	*in ng/µL*	*2 nL working solution injected per embryo*
MO pvrl4		
100	550	1.1
150	825	1.65
200	1100	2.2
250	1375	2.75
300	1650	3.3
500	2750	5.5
600	3300	6.6
MO gldc		
100	504.25	1.0085
250	1260.625	2.52125
500	2521.25	5.0425
MO tmem54a		
100	464	0.928
250	1160	2.32
500	2320	4.64
MO tmem54b		
100	620	1.24
250	1550	3.1
500	3100	6.2
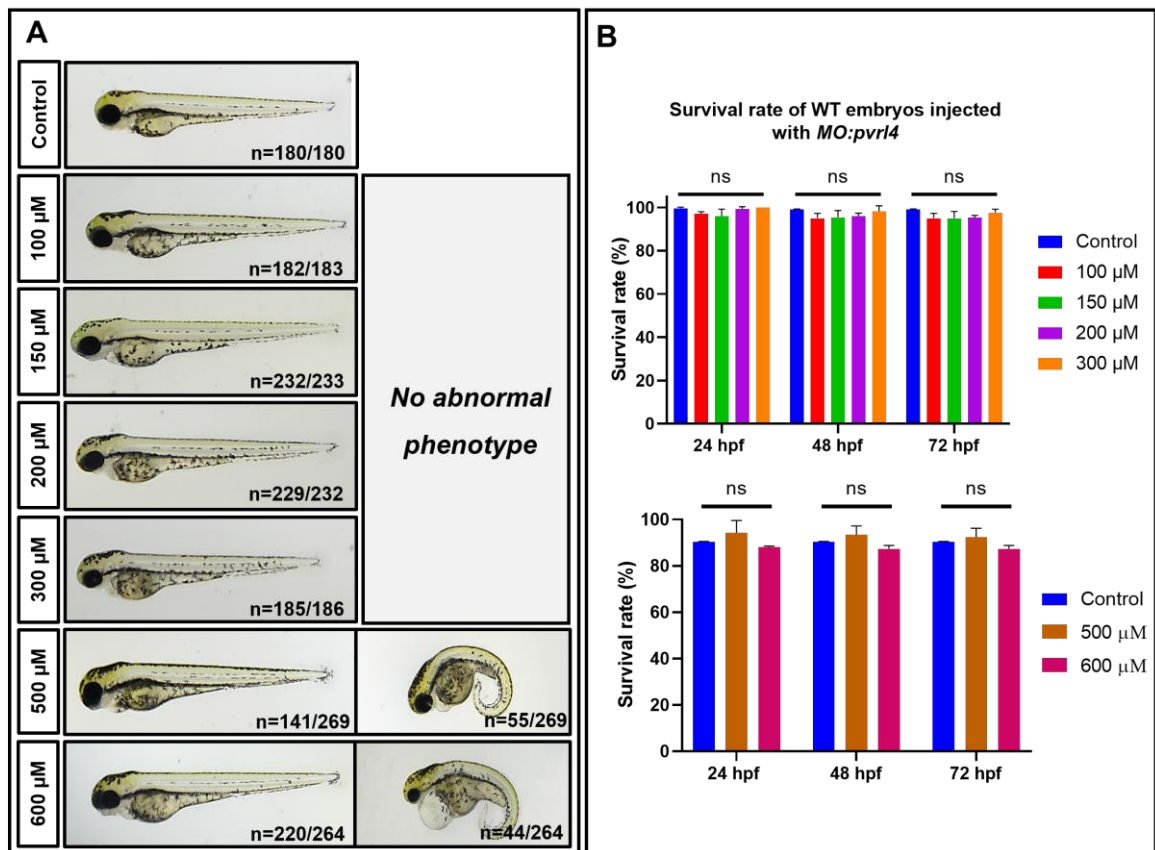
Figure 5.10 Impact of MO mediated knockdown of *pvrl4* in WT embryos.

WT embryos were injected with MO:*pvrl4* at 100 μM, 150 μM, 200 μM, 300 μM, 500 μM and 600 μM at 0 hpf. Control embryos were injected with MO:control at 0 hpf. (**A**) Phenotypes of MO:*pvrl4* injected embryos were observed until 72 hpf and imaged at 72 hpf. (**B**) Survival graph for injected embryos was plotted and analysed. Data is represented as mean ± SEM. Statistical significance determined by Multiple t-tests with correction for multiple comparisons using the Holm-Sidak method; ns - non-significant.
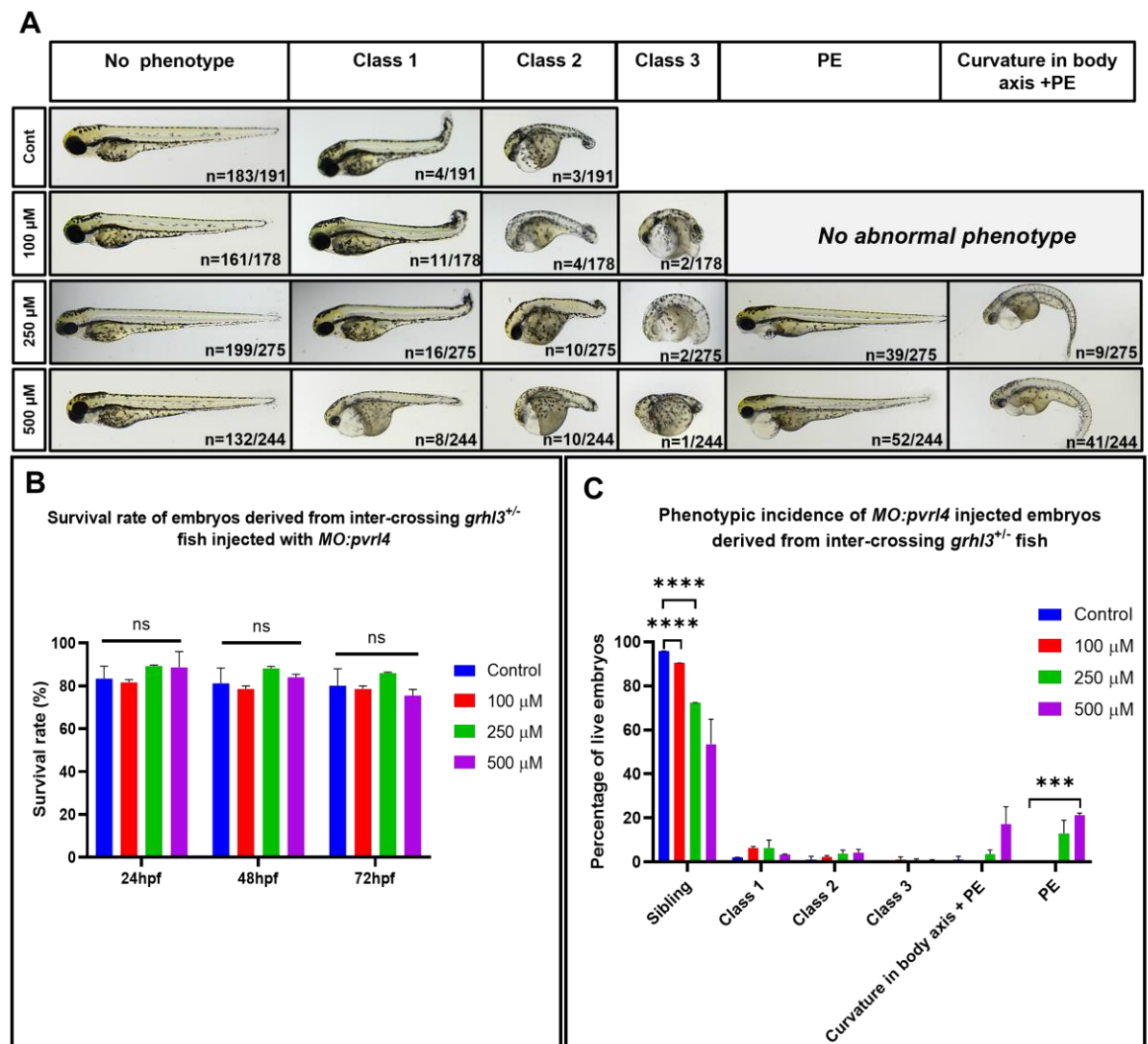
Figure 5.11 Impact of MO mediated knockdown of *pvrl4* in *grhl3*^{-/-} embryos.

Embryos derived from inter-crossing *grhl3*^{+/-} fish were injected with MO:*pvrl4* (100 μM, 250 μM, and 500 μM) at 0 hpf. Control embryos were injected with MO:control at 0 hpf. (**A**) Phenotypes of MO*:pvrl4* injected embryos were observed until 72 hpf and imaged at 72 hpf. (**B**) Survival rate and (**C**) phenotypic incidence of sibling, class 1, class 2, class 3, and pericardial oedema (PE) phenotypes in MO:*pvrl4* injected embryos derived from inter-crossing *grhl3*^{+/-} fish was quantitated and analysed. Data is represented as mean ± SEM. Statistical significance determined by Multiple t-tests with correction for multiple comparisons using the Holm-Sidak method, ns-non-significant, ***P < 0.005; ****P < 0.001.

Key findings on craniofacial development of embryos: MO:*pvrl4* (500 µM) injected WT embryos at 4 dpf were fixed in 4% PFA O/N. This was then followed by Alcian blue staining to examine the craniofacial cartilage. 20/25 embryos showed normal jaw formation in injected WT embryos while 5/25 embryos displayed an extension of the angle between ceratohyal arch (as indicated by the green arrow in Figure 5.12), and only 2 out of 5 pairs of ceratobranchials were formed (as indicated by the red arrow in Figure 5.12). It was found that injected embryos showing pericardial oedema predominantly displayed poor formation of ceratohyal and ceratobranchials, while the other cartilage elements showed normal development.

grhl3^{-/-} embryos injected with (500 µM) and stained with Alcian blue displayed no worsening of the existing jaw defect relative to control. *grhl3*[+/?] embryos showing pericardial edema due to MO:*pvrl4* injection exhibited loss of ceratobranchials and displayed poor formation of the ceratohyal. The phenotype displayed was very similar to the jaw defect seen in control *grhl3*^{-/-} embryos (Figure 5.13).
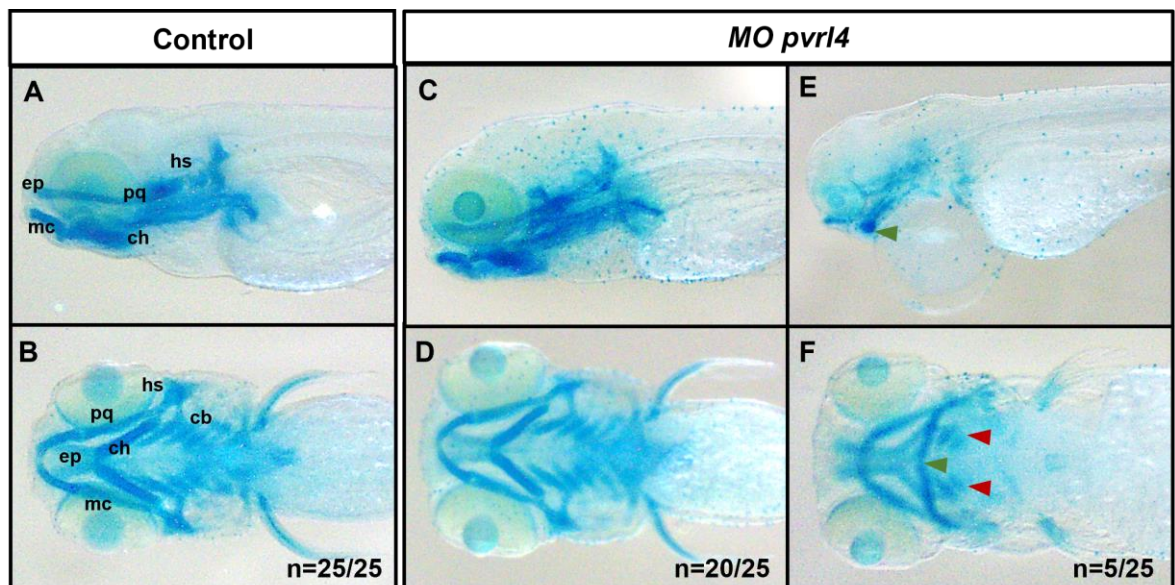
Figure 5.12 Craniofacial formation in MO:*pvrl4* injected WT embryos at 4 dpf.

(**A, C, E**) Lateral and (**B, D, F**) ventral views of Alcian blue stained cartilage of MO:*pvrl4* injected WT embryos relative to controls (MO:control injected embryos*)*. Green and red arrowheads indicate the defective formation of ceratohyal and loss of ceratobranchials respectively. (Palatoquadrate [**pq**], ceratohyal [**ch**] Meckel's cartilage [**mc**], ethmoid plate [**ep**], hyosymplectic [**hs**], ceratobranchials [**cb**]).
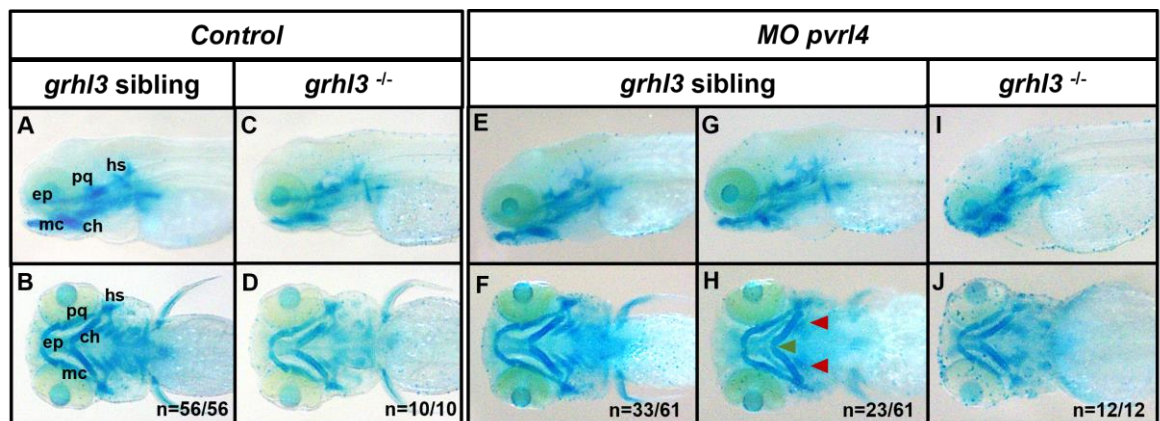
Figure 5.13 Craniofacial formation in MO:*pvrl4* injected *grhl3⁻/⁻* embryos at 4 dpf.

(**A, C, E, J, I**) Lateral and (**B, D, F, H, J**) ventral views of Alcian blue stained cartilage of MO:*pvrl4* injected *grhl3* siblings and *grhl3⁻/⁻* embryos relative to controls (MO:control injected embryos*)*. Green and red arrowheads indicate the defective formation of ceratohyal and loss of ceratobranchials respectively. (Palatoquadrate [**pq**], ceratohyal [**ch**] Meckel's cartilage [**mc**], ethmoid plate [**ep**], hyosymplectic [**hs**], ceratobranchials [**cb**]).

Summary: The dosage (100 µM-600 µM) administered in WT embryos did not lead to significant lethality of embryos. Likewise,100 µM, 250 µM and 500 µM MO:*pvrl4* had no significant impact on the survival of embryos derived from inter-crossing *grhl3⁺/⁻* adults

At 500 µM and 600 µM, a proportion (~16-20%) of injected WT embryos displayed PE along with axial defect. In embryos derived from *grhl3⁺/⁻* fish, PE + the curvature of body axis phenotype was seen in embryos at 250 µM and 500 µM. Presence of axial defects at concentration of 250 µM clearly indicate that *grhl3⁻/⁻* embryos are highly susceptible to the MO injection relative to WT embryos that showed no phenotypes when injected at 250 µM.

MO:*pvrl4* (500 µM) injected WT embryos showing PE displayed poor formation of the ceratohyal. Similarly, *grhl3⁺/ʔ* embryos with PE displayed poor establishment of ceratohyal and absence of ceratobranchials comparable to the jaw defect observed in *grhl3⁻/⁻* embryos. Thus, *pvrl4* is crucial for axial patterning and craniofacial formation in zebrafish embryos.

5.3.5   Loss of *tmem54a* contributes to minor fin fold defects and severe craniofacial abnormalities

Morpholino mediated knockdown of both *tmem54a* and *tmem54b* was performed to understand their role in epithelial establishment. Control embryos were injected with control MO at 0 hpf. Mean and SD values to plot the graphs were obtained from outcomes of 2 individual experiments (n=2).

Key findings on survival rate of embryos: The survival rate of MO:control injected WT embryos was $95.4 \pm 1.6\%$ and the survival rate of MO:*tmem54a* injected embryos at 100 µM, 250 µM and 500 µM was $94.75 \pm 3.3\%$, $86.1 \pm 12.8\%$ and $73.1 \pm 18.5\%$ respectively at 72 hpf (Figure 5.14B). Although reduction in survival rate of embryos injected with 500 µM MO:*tmem54a* was observed, statistical analysis revealed no significant differences between control and MO:*tmem54a* injected embryos.

Embryos derived from inter-crossing *grhl3*$^{+/-}$ fish injected with MO:*tmem54a* at 100 µM, 250 µM and 500 µM showed survival rates of $82.7 \pm 0.8\%$, $78.5 \pm 4.4\%$ and $75.6 \pm 1.4\%$ respectively and that of *MO*:control was 85.2 ± 0.7 % at 72 hpf (Figure 5.15B). A significant reduction (p=0.03) in the survival of 500 µM MO:*tmem54a* injected embryos derived from inter-crossing *grhl3*$^{+/-}$fish was observed relative to MO:control. Thus, MO:*tmem54a* injection at concentration 500 µM might be toxic to injected *grhl3*$^{-/-}$ embryos, contributing to lethality.

Key findings on phenotypic incidence of embryos: MO:*tmem54a* injection in WT embryos at 100 µM displayed 86.95% with normal development, 9.4% with mild curvature of body axis and 3.6% with severe axial defects. 19.2% displayed normal development, 56.45% showed mild curvature of body axis and 24.35% exhibited axial defects when injected with 250 µM MO:*tmem54a*. At 500 µM, 18.8% showed normal development, 45.3% displayed mild curvature of body axis and 35.9% exhibited axial defects (Figure 5.14A).

Embryos derived from inter-crossing *grhl3*$^{+/-}$ fish injected with MO:*tmem54a* displayed class 1, class 2, class 3 phenotypes, and a proportion of *grhl3* siblings showed mild curvature of body axis and axial defects. The percentage of non-phenotypic siblings, class 1, class 2, and class 3 mutants were $24.4 \pm 13.75\%$, $1.4 \pm 0.15\%$, $2.4 \pm 2.3\%$ and 0% at 100 µM respectively and $26.1 \pm 10.2\%$ (siblings), $2.5 \pm 0.9\%$ (class 1), $1.85 \pm 2.6\%$ (class

2) and 0% (class 3) at 250 µM respectively. Curvature of body axis phenotype was seen in $68.45 \pm 6.9\%$ embryos at 100 µM and $59.0 \pm 1.6\%$ at 250 µM and severe axial bending phenotype was displayed in $3.3 \pm 4.7\%$ and $10.5 \pm 13.5\%$ embryos at 100 µM and 250 µM MO:*tmem54a* respectively. Absence of class 1 and class 2 phenotypes were observed at 500 µM MO:*tmem54a* injection. However, $0.5 \pm 0.75\%$ class 3 phenotype, $48.8 \pm 2.9\%$ curvature of body axis phenotype and $41.3 \pm 3.3\%$ axial defects were present. In control embryos, $94.9 \pm 1.3\%$ non-phenotypic siblings, $1.4 \pm 1.0\%$ class 1, $3.4 \pm 1.8\%$ class 2, and $0.33 \pm 0.5\%$ class 3 mutants were present (Figure 5.15A).

grhl3 siblings injected with 100 µM, 250 µM and 500 µM MO:*tmem54a* showed curvature of body axis phenotype and a significant increase in the incidence of this phenotype was seen relative to control. Likewise, a significant increase in the incidence of axial defect was observed when injected with MO:*tmem54a* at 500 µM. Since ~90% of the *grhl3* siblings injected with 500 µM MO:*tmem54a* showed axial phenotypes, there was a significant decrease in the non-phenotypic sibling population relative to control (Figure 5.15C). Overall, loss of *tmem54a* contributes to axial defects in embryos derived from inter-crossing *grhl3*$^{+/-}$ fish and WT embryos.

Key findings on craniofacial development of embryos: Alcian blue staining was performed on MO:*tmem54a* (250 µM) injected WT embryos fixed in 4% PFA at 4 dpf. Upon close observation, it was found that the MO:*tmem54a* injected embryos displayed severe jaw defects, showing absence of critical orofacial structures such as ceratobranchials, Meckel's cartilage and palatoquadrate. Injected embryos with severe axial defect exhibited more severe orofacial defects, showing loss of all essential jaw structures (Figure 5.14C-H)(Mork and Crump 2015).

Alcian blue staining of MO:*tmem54a* injected embryos derived from *grhl3*$^{+/-}$ fish revealed similar craniofacial defects to those seen in injected WT embryos. *grhl3*$^{+/?}$ siblings displayed two jaw phenotypes much like WT embryos, with 6/24 embryos showing the absence of essential jaw structures while 18/24 embryos displaying loss of all jaw structures. (Figure 5.16). Therefore, loss of *tmem54a* contributes to severe orofacial deformities in zebrafish.
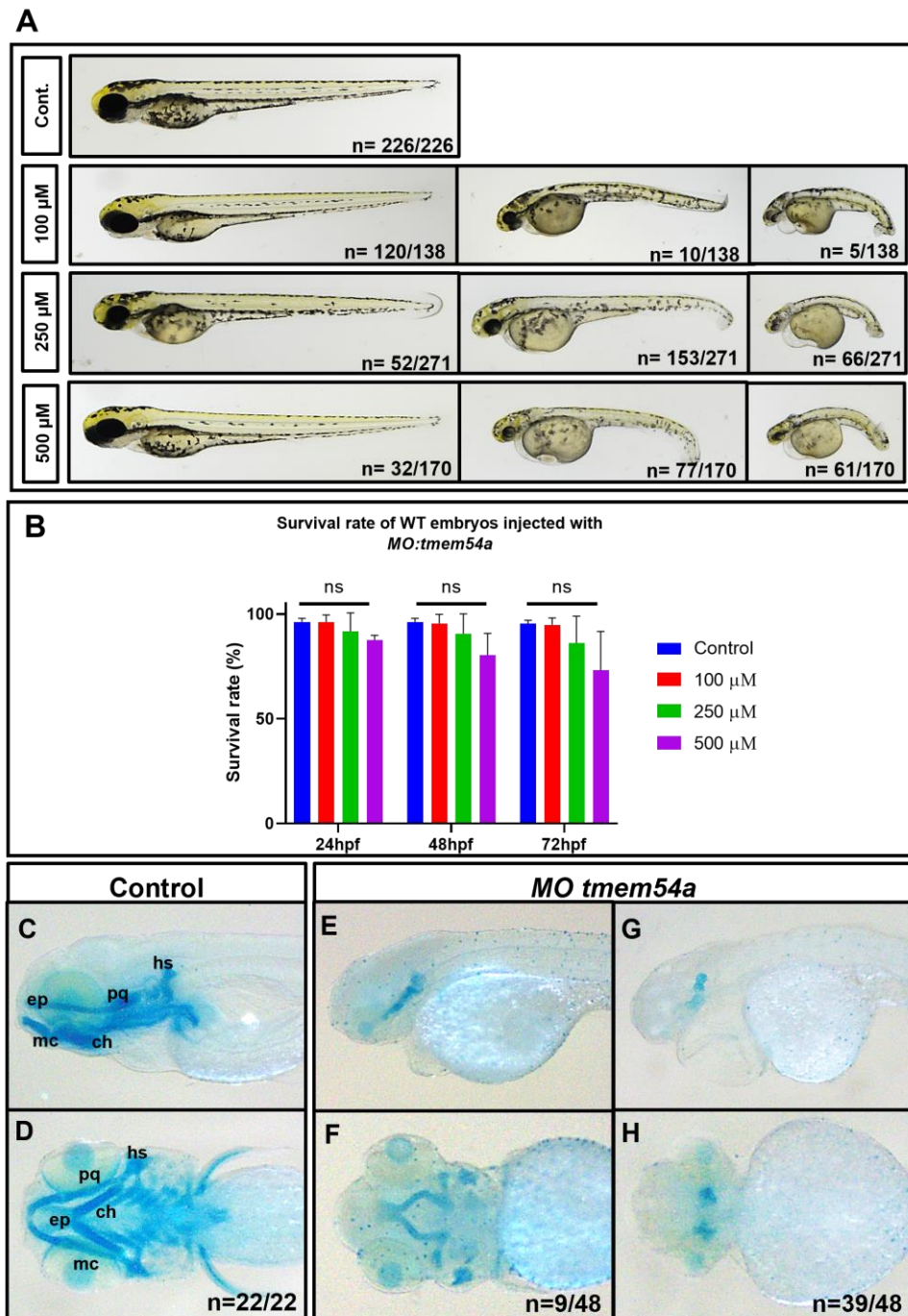
Figure 5.14 Impact of MO mediated knockdown of *tmem54a* in WT embryos.

WT embryos were injected with MO:*tmem54a* (100 μM, 250 μM, and 500 μM) at 0 hpf. Control embryos were injected with MO:control at 0 hpf. (**A**) Phenotypes of MO:*tmem54a* injected WT embryos were observed until 72 hpf and imaged at 72 hpf. (**B**) Survival graph for injected embryos was plotted and analysed. Data is represented as mean ± SEM. Statistical significance determined by Multiple t-tests with correction for multiple comparisons using the Holm-Sidak method; ns – non-significant. (**C, E, G**) Lateral and (**D, F, H**) ventral views of Alcian blue stained cartilage of MO:*tmem54a* injected WT embryos relative to control. (Palatoquadrate [**pq**], ceratohyal [**ch**] Meckel's cartilage [**mc**], ethmoid plate [**ep**], hyosymplectic [**hs**].
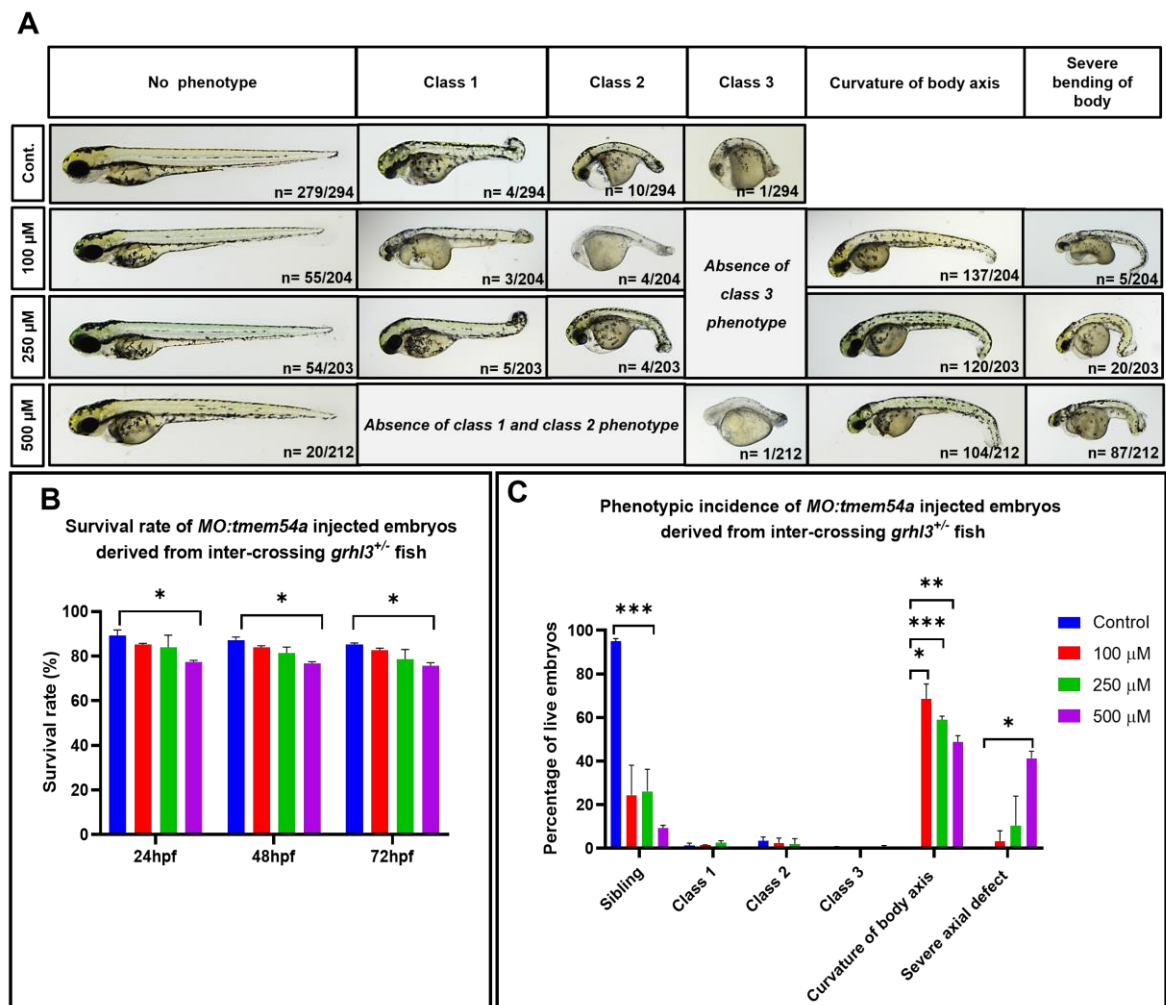
Figure 5.15 Impact of MO mediated knockdown of *tmem54a* in *grhl3^{-/-}* embryos.

Embryos derived from inter-crossing *grhl3^{+/-}* fish were injected with MO:*tmem54a* (100 μM, 250 μM, and 500 μM) at 0 hpf. Control embryos were injected with MO:control at 0 hpf. (**A**) Phenotypes of MO:*tmem54a* injected embryos were observed until 72 hpf and imaged at 72 hpf. (**B**) Survival rate and (**C**) phenotypic incidence of sibling, class 1, class 2, class 3, curvature of body axis and severe axial bending phenotypes in MO:*tmem54a* injected embryos derived from inter-crossing *grhl3^{+/-}* fish was quantitated and analysed. Data is represented as mean ± SEM. Statistical significance determined by Multiple t-tests with correction for multiple comparisons using the Holm-Sidak method *P < 0.05; **P < 0.01; ***P < 0.005.
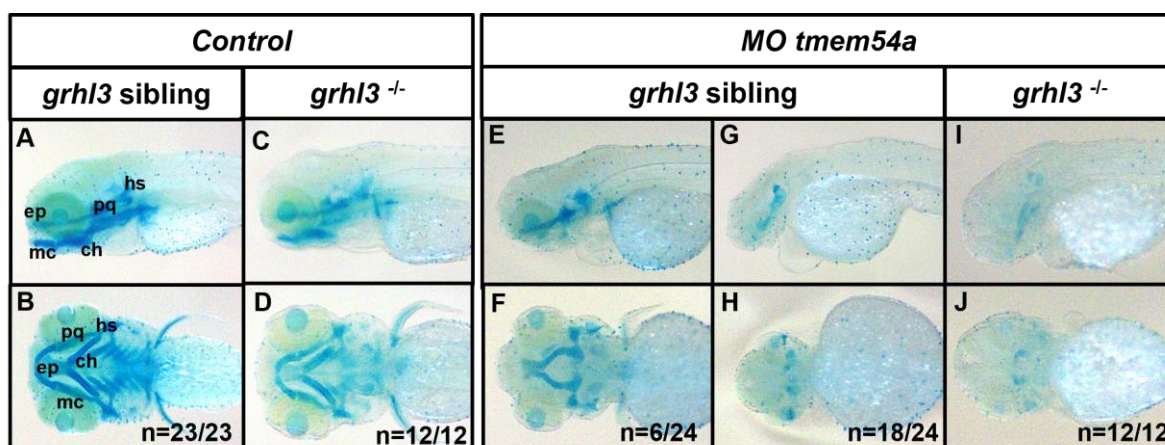
Figure 5.16 Craniofacial formation in MO:*tmem54a* injected *grhl3^-/-* embryos at 4 dpf.

(**A, C, E, G, I**) Lateral and (**B, D, F, H, J**) ventral views of Alcian blue stained cartilage of MO*:tmem54a* injected *grhl3* siblings and *grhl3^-/-* embryos relative to controls (MO:control injected embryos*)*. (Palatoquadrate [**pq**], ceratohyal [**ch**] Meckel's cartilage [**mc**], ethmoid plate [**ep**], hyosymplectic [**hs**].

Summary: Statistical analysis of the survival rate of MO:*tmem54a* injected WT embryos revealed no significant differences between injected embryos and control. Similarly, no significant variation was observed in embryos derived from inter-crossing *grhl3^+/-* fish injected with 100 µM and 250 µM MO:*tmem54a* relative to control. However, a significant lethality of embryos derived from inter-crossing *grhl3^+/-* fish was observed at 500 µM because of the toxicity induced by MO:*tmem54a* at this concentration.

WT embryos upon injection of MO:*tmem54a* displayed two phenotypes: (a) mild curvature of body axis and (b) severe axial defect. Both these phenotypes were observed in embryos derived from inter-crossing *grhl3^+/-* fish in addition to class 1, class 2, and class 3 phenotypes of *grhl3^-/-* embryos. Furthermore, a significant increase in curvature of body axis phenotype in *grhl3* siblings was detected in MO:*tmem54a* injected embryos at 100 µM, 250 µM and 500 µM concentrations. Thus, loss of *tmem54a* is associated with defects in the establishment of body axis.

Cartilage staining of MO:*tmem54a* injected WT and *grhl3^+/?* siblings revealed the presence of two jaw phenotypes based on their phenotypic severity (a) absence of essential jaw structures in embryos showing curvature of body axis and (b) loss of all jaw structures in embryos displaying severe axial defect. MO*:tmem54a* injection in *grhl3^-/-* embryos exhibited complete absence of craniofacial formation. From these studies, it can

be concluded that *tmem54a* is critical for the establishment of body axis and craniofacial development in zebrafish embryos.

5.3.6 Neural crest cells (NCCs) successfully migrate to the pharyngeal arches in *pvrl4* morphants and *tmem54a* morphants

In order to determine whether the craniofacial abnormalities seen in *pvrl4* morphants and *tmem54a* morphants arose due to impaired migration of NCCs to the pharyngeal arches, I analysed the expression of transcription factor AP2 (Tfap2), a factor integral for the development of epidermis and migratory cells of the NCCs (Knight, Nair et al. 2003, Hoffman, Javier et al. 2007).

To analyse the expression of *tfap2a*, *tmem54a* morphants and *pvrl4* morphants were collected at 24 hpf and expression was determined by in-situ hybridization. No differences in *tfap2a* expression was detected in *pvrl4* and *tmem54a* morphants relative to controls, suggesting that there was no substantial impairment to NCC migration into the pharyngeal arches.
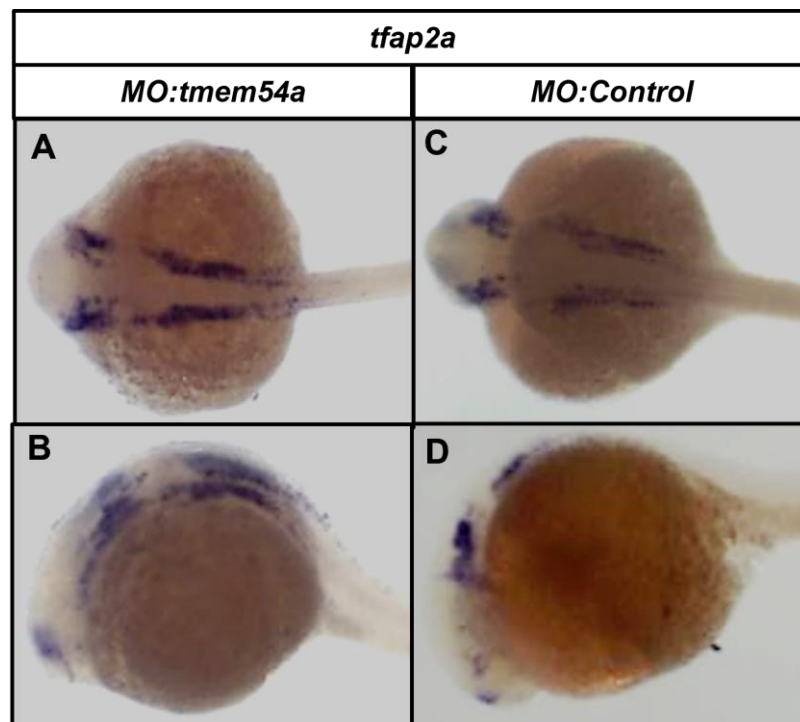
Figure 5.17 Neural crest migration in *tmem54a* morphants.

Expression of *tfap2a* in **(A-B)** *tmem54a* morphants at 24 hpf relative to **(C-D)** controls.
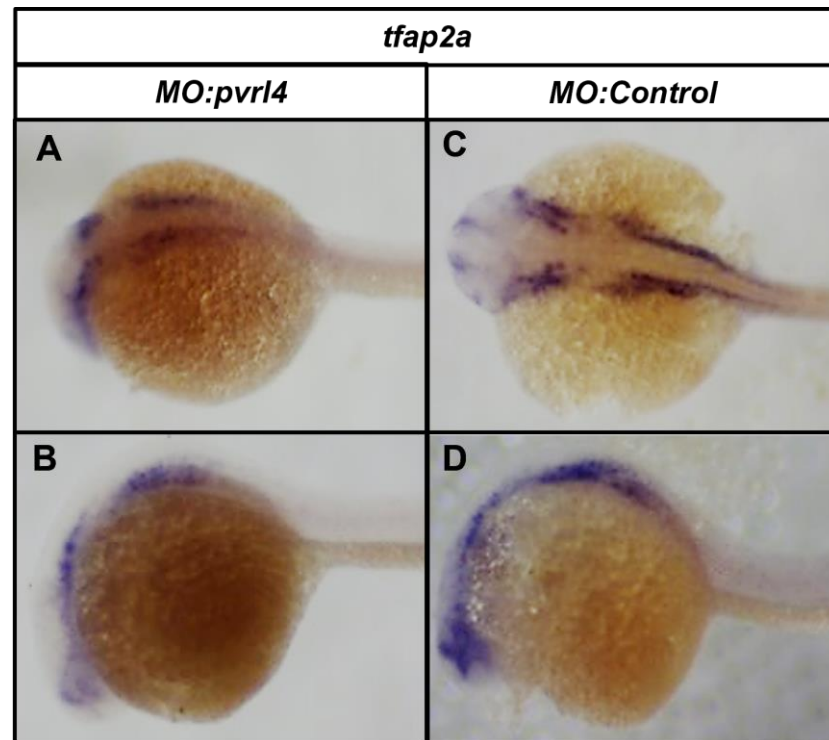
Figure 5.18 Neural crest migration in *pvrl4* morphants.

Expression of *tfap2a* in **(A-B)** *pvrl4* morphants at 24 hpf relative to **(C-D)** controls.

5.3.7 Loss of *tmem54b* shows normal epithelial barrier formation and orofacial development

Key findings on survival rate of embryos: The survival rate of MO:control injected WT embryos was 82.6 ± 1.0% and that of MO*:tmem54b* injected embryos at 100 µM, 250 µM and 500 µM were 75.3 ± 4.8%, 89.6 ± 9.8% and 73.4 ± 22.8% respectively at 72 hpf (Figure 5.19B). Statistical analysis revealed no significant differences between control and MO*:tmem54b* injected embryos.

Embryos derived from inter-crossing *grhl3*$^{+/-}$ fish injected with MO*:tmem54b* at 100 µM, 250 µM and 500 µM showed survival of 90.8 ± 5.2%, 81.4 ± 4.7% and 75.9 ± 1.6% respectively and that of MO:control was 89.7 ± 6.2% at 72 hpf (Figure 5.20B). No significant differences were noted between injected and control embryos. Therefore, MO*:tmem54b* administered at dosages 100 µM, 250 µM and 500 µM is relatively safe and does not contribute to toxicity associated deaths.

Key findings on phenotypic incidence of embryos: No aberrant phenotypes were observed in WT embryos injected with MO*:tmem54b* at concentrations 100 µM and 250 µM. However, pericardial oedema along with mild curvature in body axis was seen in

51/203 embryos injected with MO:*tmem54b* at 500 µM (Figure 5.19A). Likewise, 23 out of 210 embryos derived from inter-crossing *grhl3*$^{+/-}$ fish injected with 500 µM displayed pericardial edema (PE) coupled with slight curvature of body axis (Figure 5.20A). The percentage of siblings in MO:*tmem54b* injected embryos was 85.2 ± 3.9% at 100 µM, 93.8 ± 5.1% at 250 µM, 87.1 ± 8.4% at 500 µM and 87.1 ± 6.1% in control. The percentage of mutants were 6.8 ± 1.8% (class 1), 6.1 ± 0.75% (class 2) and 1.5 ± 2.1% (class 3) at 100 µM; 0.7 ± 0.9% (class 1), 1.8 ± 1.35% (class 2), and 3.6 ± 2.7% (class 3) at 250 µM; and 0.4 ± 0.5% (class 1), 1.4 ± 2.0% (class 2), and 2.8 ± 1.9% (class 3) at 500 µM. In control embryos, 4.0 ± 3.2% class 1, 3.9 ± 5.5% class 2, and 5.0 ± 2.7% class 3 mutants were present (Figure 5.20C). Slight differences in the percentage of phenotypic mutants were seen between control and MO:*tmem54b* injected embryos, however the differences were not statistically significant.

Key findings on craniofacial development: MO:*tmem54b* injected WT embryos were fixed in 4% PFA at 4 dpf, followed by Alcian blue staining to determine the consequences of *tmem54b* loss on the formation of craniofacial cartilage. No jaw defects were observed, and normal jaw formation was established in injected MO:*tmem54b* WT embryos (Figure 5.19C-F). Alcian blue staining of embryos derived from inter-crossing *grhl3*$^{+/-}$ fish injected with MO:*tmem54b* exhibited no jaw abnormalities in the *grhl3* siblings and worsening of the existing jaw defect in *grhl3*$^{-/-}$ embryos was not seen (Figure 5.21). This suggests that *tmem54b* does not play a substantial role in the formation craniofacial cartilage.

Summary: No significant differences in terms of survival were observed in MO:*tmem54b* injected WT embryos and embryos derived from *grhl3*$^{+/-}$ fish relative to control. Loss of *tmem54b* contributes to minor curvature of body axis and pericardial edema in small percentage of embryos injected with 500 µM MO:*tmem54b,* likely due to MO-mediated toxicity.

The phenotypic incidence of class 1, class 2 and class 3 mutants showed no significant variation between MO:*tmem54b* injected *grhl3*$^{-/-}$ embryos and that of control. Furthermore, no worsening of *grhl3*$^{-/-}$ phenotypes was observed. Lastly, *tmem54b* morphants showed normal craniofacial development. These findings suggest that *tmem54b,* unlike *tmem54a* might not play a critical role in axial patterning and craniofacial formation.
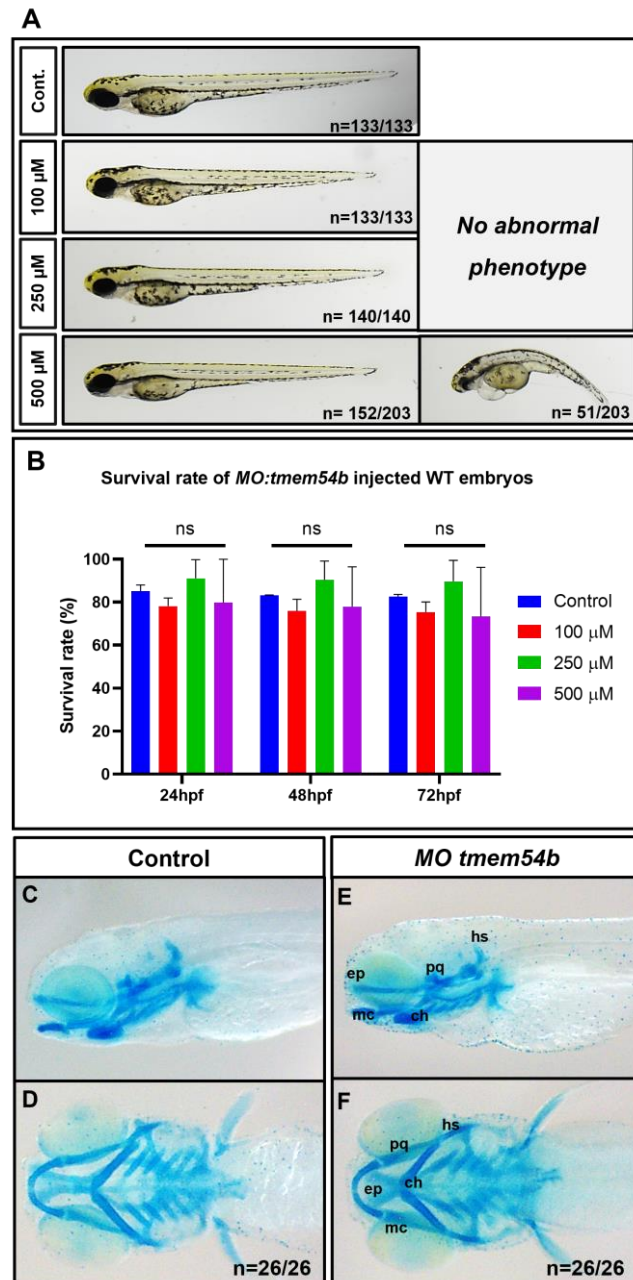
Figure 5.19 Impact of MO mediated knockdown of *tmem54b* in WT embryos.

WT embryos were injected with MO:*tmem54b* (100 μM, 250 μM, and 500 μM) at 0 hpf. Control embryos were injected with MO:control at 0 hpf. (**A**) Phenotypes of MO:*tmem54b* injected WT embryos were observed until 72 hpf and imaged at 72 hpf. (**B**) Survival graph for injected embryos was plotted and analysed. Data is represented as mean ± SEM. Statistical significance determined by Multiple t-tests with correction for multiple comparisons using the Holm-Sidak method, ns – non-significant. (**C, E**) Lateral and (**D, F**) ventral views of Alcian blue stained cartilage of MO:*tmem54b* injected WT embryos relative to controls. (Palatoquadrate [**pq**], ceratohyal [**ch**] Meckel's cartilage [**mc**], ethmoid plate [**ep**], hyosymplectic [**hs**].

Figure 5.20 Impact of MO mediated knockdown of *tmem54b* in *grhl3$^{-/-}$* embryos.

Embryos derived from inter-crossing *grhl3$^{+/-}$* fish were injected with MO:*tmem54b* (100 μM, 250 μM, and 500 μM) at 0 hpf. Control embryos were injected with MO:control at 0 hpf. (**A**) Phenotypes of MO:*tmem54b* injected embryos were observed until 72 hpf and imaged at 72 hpf. (**B**) Survival rate and (**C**) phenotypic incidence of sibling, class 1, class 2, and class 3 phenotypes in MO:*tmem54b* injected embryos (derived from inter-crossing *grhl3$^{+/-}$* fish) was quantitated and analysed. Data is represented as mean ± SEM. Statistical significance determined by Multiple t-tests with correction for multiple comparisons using the Holm-Sidak method; ns – non-significant.

Control		tmem54b	
grhl3 sibling	*grhl3* -/-	*grhl3* sibling	*grhl3* -/-

Figure 5.21 Craniofacial formation in MO:*tmem54b* injected *grhl3*-/- embryos at 4 dpf.

(**A, C, E, G**) Lateral and (**B, D, F, H**) ventral views of Alcian blue stained cartilage of MO:*tmem54b* injected *grhl3* siblings and *grhl3*-/- embryos relative to controls (MO:control injected embryos*). (Palatoquadrate [**pq**], ceratohyal [**ch**] Meckel's cartilage [**mc**], ethmoid plate [**ep**], hyosymplectic [**hs**].

5.3.8 Transient knockdown of *gldc* shows normal epithelial establishment

MO:*gldc* was injected at concentrations 100 µM, 250 µM and 500 µM in WT embryos and embryos derived from inter-crossing *grhl3*+/- fish. For control, embryos were injected with control MO at 0 hpf. Mean and SD values to plot the graphs were obtained from outcomes of 2 individual experiments (n=2).

Key findings on survival rate of embryos: The survival rate of MO:control injected WT embryos was 84.9 ± 2.2% and the survival rate of MO:*gldc* injected embryos at 100 µM, 250 µM and 500 µM was 90.7 ± 6.6%, 92.7 ± 2.6% and 88.7 ± 12.3% respectively at 72 hpf (Figure 5.22B). No significant differences were noted between control and MO:*gldc* injected WT embryos.

Embryos derived from inter-crossing *grhl3*+/- fish injected with MO:*gldc* at 100 µM, 250 µM and 500 µM showed survival of 83.2 ± 0.2%, 79.0 ± 4.8% and 77.0 ± 9.5% respectively and the survival of control embryos was 79.5 ± 2.9% at 72 hpf (Figure 5.23B). Statistical analysis revealed no significant differences between MO:*gldc* injected and control embryos. Therefore, the concentrations administered in both WT embryos and embryos derived from *grhl3*+/- fish were relatively safe and does not contribute to toxicity induced deaths.

Key findings on phenotypic incidence of embryos: Injection of MO*:gldc* in WT embryos displayed no aberrant phenotypes (Figure 5.22A). Likewise, embryos derived from *grhl3*$^{+/-}$ fish, showed no abnormal phenotypes other than the already existing *grhl3*$^{-/-}$ phenotypes (Figure 5.23A). The percentage of siblings in 100 µM, 250 µM and 500 µM MO*:gldc* injected embryos was 91.9 ± 5.5%, 97.1 ± 0.2% and 95.00 ± 0.8% respectively and that of control was 94.3 ± 2.1%. The percentage of *grhl3* mutants was 2.1 ± 0.1% (class 1), 2.2 ± 1.1% (class 2) and 3.8 ± 4.4% (class 3) at 100 µM; 0.3 ± 0.5% (class 1), 1.1± 0.6% (class 2) and 1.4 ± 0.1% (class 3) at 250 µM and 0.7 ± 0.8% (class 1), 1.8 ± 0.6% (class 2) and 2.5 ± 0.4% (class 3) at 500 µM. In control embryos, 2.1 ± 2.9% class 1, 2.1 ± 0.02% class 2, and 1.5 ± 0.7% class 3 mutants were present (Figure 5.23C). No significant differences in phenotypic incidence was seen between control and MO*:gldc* injected *grhl3* mutants.

Key findings on craniofacial development of embryos: WT embryos injected with MO*:gldc* were fixed in 4% PFA at 4 dpf. This was then followed by Alcian blue staining to examine the craniofacial cartilage in *gldc* morphants. No jaw defects were observed, and normal jaw formation was established in injected WT embryos (Figure 5.22C-F). Alcian blue staining of MO*:gldc* injected *grhl3*$^{-/-}$ embryos showed no worsening of the existing jaw defect. Additionally, MO*:gldc* injected *grhl3* siblings displayed no craniofacial abnormalities due to the loss of *gldc* (Figure 5.24). This implies that *gldc* might not play a significant role in craniofacial formation.

Summary: No significant differences in terms of survival were observed in MO*:gldc* injected WT embryos and MO*:gldc* injected embryos derived from *grhl3*$^{+/-}$ fish, relative to controls. Furthermore, loss of *gldc* did not contribute to any abnormal phenotypes and craniofacial defects in the injected embryos. The phenotypic incidence of class 1, class 2 and class 3 mutants showed no significant variation between MO*:gldc* injected *grhl3*$^{-/-}$ embryos and that of control. Thus, *gldc* does not play an integral role in epithelial patterning and development.
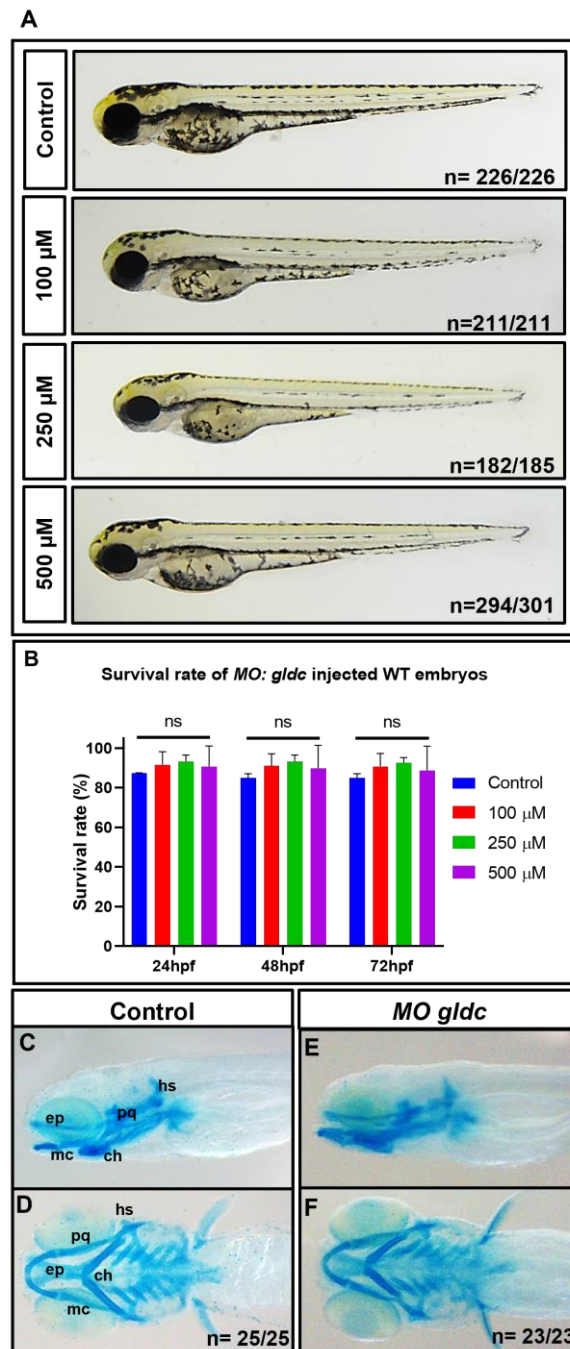
Figure 5.22 Impact of MO mediated knockdown of *gldc* in WT embryos.

WT embryos were injected with MO*:gldc* (100 μM, 250 μM, and 500 μM) at 0 hpf. Control embryos were injected with MO:control. (**A**) Phenotypes of MO*:gldc* injected WT embryos were imaged at 72 hpf. (**B**) Survival graph for injected embryos was plotted and analysed. Data is represented as mean ± SEM. Statistical significance determined by Multiple t-tests with correction for multiple comparisons using the Holm-Sidak method, ns – non-significant. (**C, E**) Lateral and (**D, F**) ventral views of Alcian blue stained cartilage of *gldc* morphants relative to controls. (Palatoquadrate [**pq**], ceratohyal [**ch**] Meckel's cartilage [**mc**], ethmoid plate [**ep**], hyosymplectic [**hs**].
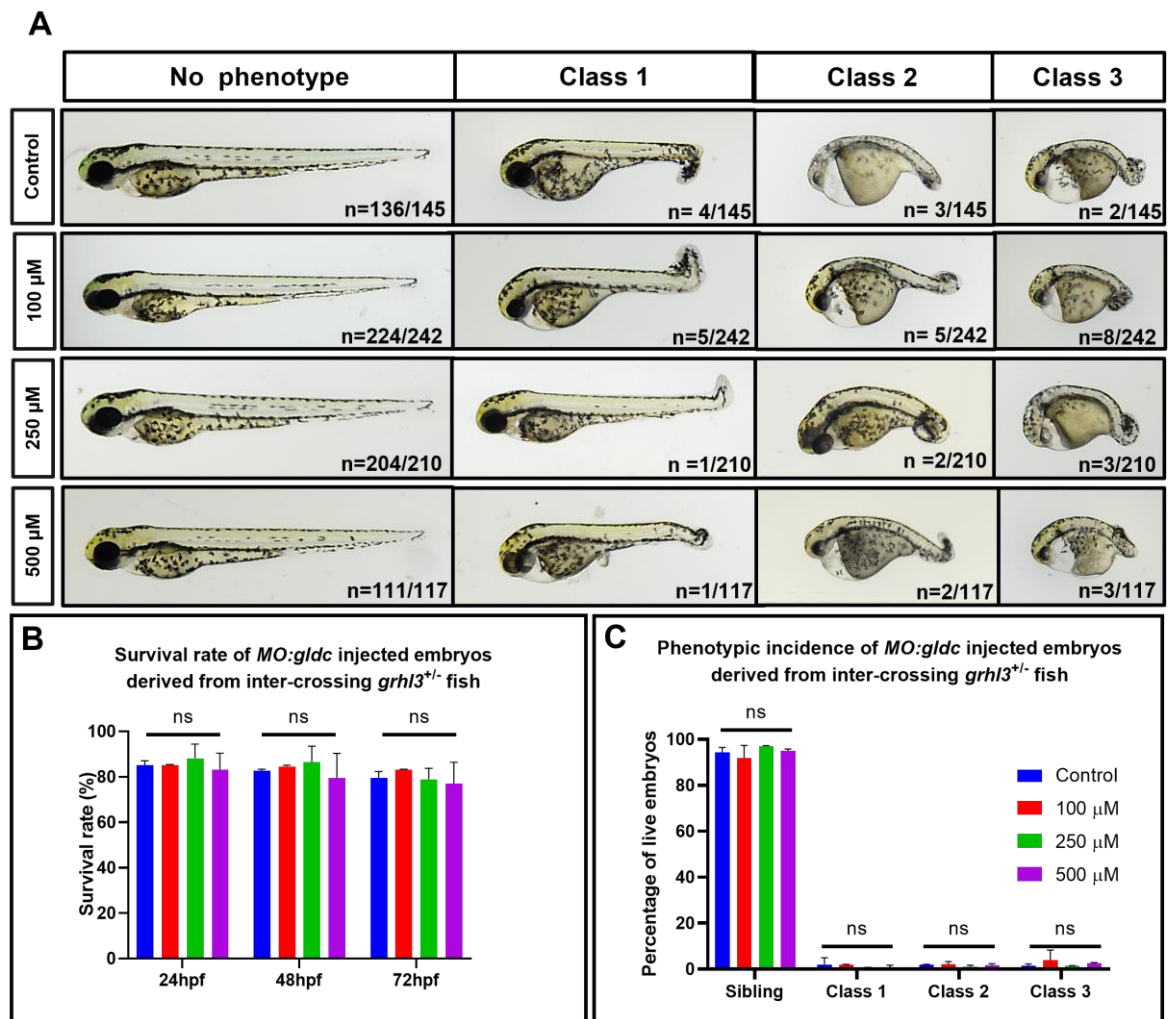
Figure 5.23 Impact of MO mediated knockdown of *gldc* in *grhl3*$^{-/-}$ embryos.

Embryos derived from inter-crossing *grhl3*$^{+/-}$ fish were injected with MO*:gldc* (100 μM, 250 μM, and 500 μM) at 0 hpf. Control embryos were injected with MO:control. (**A**) Phenotypes of MO*:gldc* injected embryos were observed until 72 hpf and imaged at 72 hpf. (**B**) Survival rate and (**C**) phenotypic incidence of sibling, class 1, class 2, and class 3 phenotypes in MO*:gldc* injected embryos (derived from inter-crossing *grhl3*$^{+/-}$ fish) was quantitated and analysed. Data is represented as mean ± SEM. Statistical significance determined by Multiple t-tests with correction for multiple comparisons using the Holm-Sidak method, ns – non-significant.
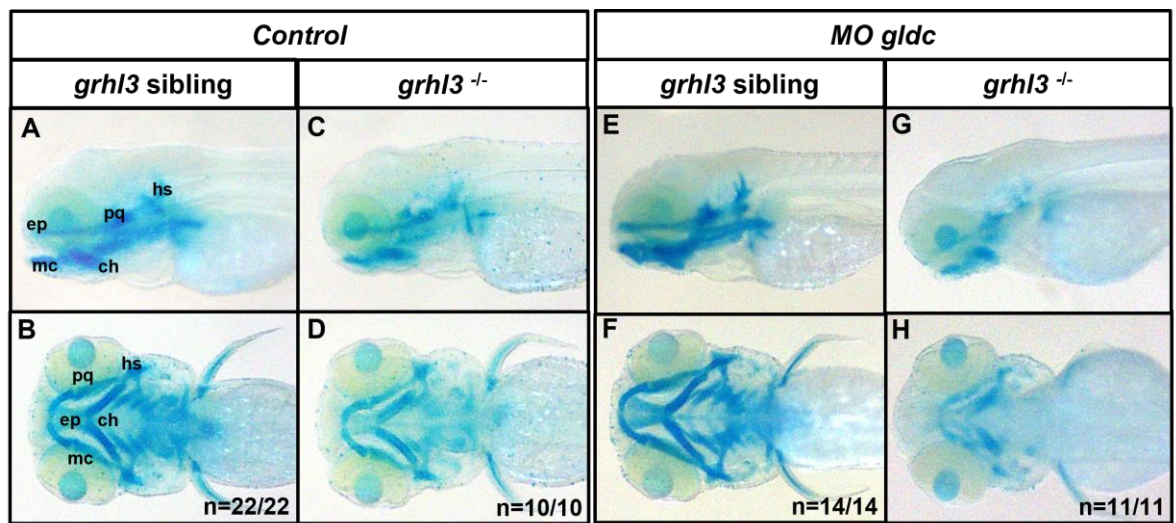
Figure 5.24 Craniofacial formation in MO:*gldc* injected *grhl3$^{-/-}$* embryos at 4 dpf.

(**A, C, E, G**) Lateral and (**B, D, F, H**) ventral views of Alcian blue stained cartilage of MO:*gldc* injected *grhl3* siblings and *grhl3$^{-/-}$* embryos relative to controls (MO:control injected embryos*)*. (Palatoquadrate [**pq**], ceratohyal [**ch**] Meckel's cartilage [**mc**], ethmoid plate [**ep**], hyosymplectic [**hs**].

Table 5.2 Summary of the results obtained in chapter 5.

Experiments to determine the role of differentially regulated genes of *grhl*	Gene	Gene selected via	Impact on axial development	Impact on craniofacial development
CRISPR knockout	*tbc1d2*	In-silico analysis	No abnormal phenotypes observed upon characterization	No craniofacial defect
Rescue experiments with FL mRNA of putative targets of *grhl*	*tbc1d2*	In-silico analysis	No rescue in the severity of *grhl3$^{-/-}$* embryos	
	pvrl4	In-silico analysis	Injection at 50 ng/µl showed partial rescue in the severity of phenotypes	
	ovol1a	In-silico analysis	No rescue in the severity of *grhl3$^{-/-}$* embryos	
Morpholino mediated knockdown (in WT embryos)	*pvrl4*	In-silico analysis	Severe axial defect in embryos injected with 500 µM *MO:pvrl4*	Malformation in ceratohyal of lower jaw.
	gldc	Meta-analysis	Normal phenotype	No craniofacial defect
	tmem54a	Meta-analysis	Varying degrees of axial defects	Severe craniofacial defect showing loss of essential jaw structures
	tmem54b	Meta-analysis	Mild curvature of body axis in embryos injected with 500 µM *MO:tmem54b*	No craniofacial defect

5.4 Discussion

5.4.1 *tbc1d2* CRISPR mutants display no gross epithelial defects or craniofacial abnormalities

tbc1d2 has been identified to be a key regulator in cadherin degradation, thereby contributing to reduced cell-adhesion (Frasa, Maximiano et al. 2010). In order to further understand the role of *tbc1d2* in epithelial homeostasis and craniofacial formation in zebrafish, CRISPR mediated *tbc1d2* knockout lines were established and characterised. No gross epithelial defects and axial defects were seen. Likewise, jaw structures upon examination showed normal development. These findings suggest that loss of *tbc1d2* has no substantial roles in the formation of craniofacial cartilage and axial patterning in zebrafish embryos. Another possibility could be because the CRISPR knockouts show incomplete penetrance or genetic compensation (Zvelebil, Oliemuller et al. 2013, El-Brolosy and Stainier 2017, Sztal, McKaige et al. 2018). Genetic compensation is a phenomenon whereby the pathogenic mutation does not show the expected adverse phenotype. This might be due to compensatory actions of *tbc1d2* related genes such as *rac1* (Frasa, Maximiano et al. 2010) and *vps34* (Jaber, Mohd-Naim et al. 2016), thereby recompensing for gene deletion and resulting in a broadly normal phenotype (Zvelebil, Oliemuller et al. 2013).

5.4.2 Significance of *pvrl4* and *tbc1d2* mRNA in rescuing the severe phenotypes of *grhl3*-/- embryos

Since *grhl3*-/- embryos display early embryonic defects (Miles, Darido et al. 2017), they are ideal for mRNA injection of potential *grhl* targets such as *pvrl4* and *tbc1d2* to determine whether these mRNAs can rescue the *grhl3*-dependent phenotypes. A limitation of microinjection experiments is occasional non-specific toxicity imposed by mRNA/morpholino (Au - Rosen, Au - Sweeney et al. 2009) which was why WT embryos were injected first, allowing me to determine the optimal mRNA/MO dosages that did not lead to toxicity-mediated phenotypes. These dosages were subsequently used for injection into *grhl3*-/- embryos.

Microinjection of *pvrl4* mRNA (50 ng/µl) showed partial rescue in the phenotypic severity of *grhl3* mutant embryos with an increase in the sibling population and decrease in the class 2 phenotypic mutants at 72 hpf. Since *pvrl4* is critical for cell adhesion

(Brancati, Fortugno et al. 2010), it perhaps compensates for the loss of *grhl3* during early developmental stages to lessen the adversity of *grhl3*$^{-/-}$ epithelial phenotypes. Conversely, no rescue in the phenotypic severity of *tbc1d2* injected *grhl3*$^{-/-}$ embryos might be because *tbc1d2* does not play a role in epithelial development, or alternately, it might not be a critical target of *grhl3* in epithelial formation. In future, to understand the transcriptional regulation between *grhl3* and *pvrl4/tbc1d2*, ChIP- (chromatin immunoprecipitation) assays must be performed to determine whether *grhl3* binds to the promoter of each of these targets. Determining how proteins, particularly transcription factors, interact with DNA to regulate gene expression is critical for understanding the biological processes involved in epithelial homeostasis.

5.4.3 Importance of *pvrl4*, *gldc* and *tmem54* in epithelial and orofacial development

This study explored the function of putative target genes of *grhl* including *tmem54, pvrl4,* and *gldc* via MO mediated knockdown. Two orthologues of *tmem54* have been identified in zebrafish - *tmem54a* and *tmem54b*. Of these two orthologues, loss of *tmem54b* showed no orofacial abnormalities, however, mild convergent-extension axis phenotype was noticed when the *tmem54b* MO was injected at 500 µM. Conversely, loss of *tmem54a* led to curvature of body axis in addition to severe jaw deformities. *tmem54a* morphants showed absence of Meckel's cartilage, ceratobranchials and palatoquadrate. A similar degree of severe jaw deformity and axial defects were observed in *hdac1* (histone deacetylase) morphants (Pillai, Coverdale et al. 2004), suggesting a close functional association between these two genes. Moreover, it has been found from the STRING (Search tool for the Retrieval of Interacting Genes/Proteins) interaction database (a biological database of known and predicted protein-protein interactions) that *hdac1* protein interacts with *tmem54,* however the mechanism underlying their interaction is unknown. *Hdac1* is critical for the embryonic development of *Drosophila* (Mannervik and Levine 1999, Mottus, Sobel et al. 2000), *Xenopus* (Almouzni, Khochbin et al. 1994), mice, murine (Milstone, Lawson et al. 2017) and bovine models (McGraw, Robert et al. 2003). In zebrafish, *hdac1* is required for the development of eye, CNS and for maintenance of neural crest populations (Pillai, Coverdale et al. 2004). Furthermore, *hdac1* has been found to play a critical role in the differentiation of neural crest cells to form craniofacial cartilage (Ignatius, Unal Eroglu et al. 2013). Based upon the degree of severity of jaw phenotypes observed in *hdac1* and *tmem54a* morphants, I speculate that

both *tmem54a* and *hdac1* might interact with each other to drive the neural crest cell differentiation to form the craniofacial cartilage. In *tmem54a* morphants, NCCs have been successfully found to migrate to the pharyngeal arches, however in future it is critical to investigate the expression of other NCC markers such as *dlx2* (integral for pharyngeal homing) in *tmem54a* morphants to determine whether the orofacial defects caused were due to NCC defects.

Hdac1 also acts as a negative regulator of the canonical *Wnt* signalling cascade during early dorsal-ventral patterning (Nambiar and Henion 2004) and acts as a positive regulator of the non-canonical *Wnt* pathway (Nambiar, Ignatius et al. 2007) that is critical for anterior posterior elongation in zebrafish. Thus, shortened body axis and curved tail phenotype is observed in *hdac1* morphants (Pillai, Coverdale et al. 2004), analogous to the axial phenotypes observed in *tmem54a* morphants. I believe *tmem54a* might interact with *Hdac1* to regulate the non-canonical *Wnt* pathway for the establishment of anterior-posterior axis. Unravelling the genetic interaction between *hdac1*, *grhl3* and *tmem54* is critical to understand the genomic pathways regulated in epithelial formation.

Transient knockdown of *pvrl4* (at 500 µM), a gene involved in cell adhesion, caused severe axial defects along with pericardial edema in ~20% of embryos while the rest of the embryos appeared normal. Pericardial edema and axial defect seen in the injected embryos could be attributed to the toxicity induced by high concentration of the MO:*pvrl4*. Furthermore, jaw analysis of the MO:*pvrl4* injected embryos revealed aberrant formation of the ceratohyal whereby the angle between ceratohyal was much greater than what was typically observed in control. A similar jaw phenotype and axial defect was observed in *sox9b* morphants (Xiong, Peterson et al. 2008) suggesting a functional interaction between *pvrl4* and *sox9b*.

Sox9 is a transcription factor involved in the development of neural crest, placodes, cartilage, and bone (Cheung and Briscoe 2003). In zebrafish, two orthologues of mammalian *Sox9* have been identified namely, *sox9a* and *sox9b*. Of which, *sox9b* has been shown to be an early marker of cranial and trunk neural crest markers (Li, Zhao et al. 2002). Having observed the close resemblances in axial and jaw phenotypes of *pvrl4* and *sox9b* morphants I speculate that *pvrl4* much like *sox9b* might play an integral role in the differentiation of the neural crest cells either directly or indirectly to form the

craniofacial cartilage. Determining the expression of *sox9b* and other NCC markers in *pvrl4* morphants in future might shed light on the role of *pvrl4* in NCC differentiation.

Lastly, loss of *Gldc* (glycine dehydrogenase), a GCS (glycine cleavage system) encoding gene contributes to NTDs in mice and humans (Narisawa, Komatsuzaki et al. 2011). It is hypothesized that individuals carrying mutations in GLDC show poor folate one carbon metabolism (Narisawa, Komatsuzaki et al. 2011), thereby contributing to NTDs (Zhang, Luo et al. 2008, Li, Wahlqvist et al. 2016). However, loss of *gldc* in zebrafish showed no axial defects and craniofacial abnormalities. This might be because the mechanisms underlying neurulation in fish (evagination of a lumen from a solid rod of cells) varies from those seen in mammals (Lowery and Sive 2004), suggesting that *gldc* might play critical roles in the neurulation of mammals and not of fish.

5.5 Conclusion and future directions

Identifying putative *grhl3* targets and determining their function in epithelial development via knockdown/knockout-based experiments will help elucidate the biological mechanisms involved in epithelial homeostasis and barrier formation. This will ultimately help us understand the aetiology of epithelial disorders, birth defects and cancers of epithelial origin, by revealing the genetic pathways being dysregulated. This chapter has examined the functions of putative *grhl* target genes : *pvrl4*, *tbc1d2*, *gldc*, and *tmem54* (Table 5.2), and their relationships with *grhl3* in early embryogenesis. Among these genes, *pvrl4* and *tmem54a* were found to play a key role in axial patterning and craniofacial formation of zebrafish embryos. The next step would be is to identify the mechanism by which they drive craniofacial development and axial formation.

Previous studies had shown substantial similarities in craniofacial abnormalities and axial defects seen in both *pvrl4* and *sox9b* morphants. Likewise, the axial defects and severe jaw defects seen due to loss of *tmem54a* were comparable to that of *hdac1* morphants. Both *sox9b* and *hdac1* genes are involved in the differentiation of NCC to form craniofacial cartilage. Thus, it is critical to determine the expression of neural crest cell specification *(sox9b)* and pharyngeal homing *(dlx2)* marker genes in *pvrl4* and *tmem54a* morphants via in-situ hybridization. A variation in NCC marker gene expression in the *pvrl4* and *tmem54a* morphants will signify that the jaw defects are due to poor

differentiation of NCC. This will shed further light on the role of *tmem54a* and *pvrl4* in craniofacial development.

5.6 Supplementary data

Supplementary table 5.1 Exon 3 sequence of *tbc1d2*^{-/-(+47bp)} *and tbc1d2*^{-/-(-21bp)} mutant embryos.

tbc1d2 exon 3	GTTGTCACTGAACGAATGTGCAAATATAATATTAACTTTACCTCAATCCTCA GAGGGACCCCCACTCCAAGCAGCACTAAACTCTGTGGATACCTCAACAAG CAGGGCGGACCCCTCAAAACCTGGAAGTCCCGTTGGTTTGCATATGAGG AGAAGAGCTGTCAGCTGTTTTACTACCGCATGGCACATGATATTAATTCTC TGGGTAAGGTGGATCTGACTCGGGCCACATTCAGTTA
tbc1d2 (+47bp)	GTTGTCACTGAACGAATGTGCAAATATAATATTAACTTTACCTCAATCCTCA GAGGGACCCCCACTCCAAGCAGCACTAAACTCTGTGGATACCTCAACAAG CAGTCATGGCGTTTAAACCTTAATTAAGCTGTTGTTCCTTTATTTTTGAGG GCGGACCCCTCAAAACCTGGAAGTCCCGTTGGTTTGCATATGAGGAGAAG AGCTGTCAGCTGTTTTACTACCGCATGGCACATGATATTAATTCTCTGGGT AAGGTGGATCTGACTCGGGCCACATTCAGTTA
tbc1d2 (-21bp)	GTTGTCACTGAACGAATGTGCAAATATAATATTAACTTTACCTCAATCCTCA GAGGGACCCCCACTCCAAGCAGCACTAAACTCTGTGGATCTCAAAACCTG GAAGTCCCGTTGGTTTGCATATGAGGAGAAGAGCTGTCAGCTGTTTTACT ACCGCATGGCACATGATATTAATTCTCTGGGTAAGGTGGATCTGACTCGG GCCACATTCAGTTA (-CCTCAACAAGCAGGGCGGACC)

Microinjection of *ovol1a* mRNA in WT and *grhl3⁻ᐟ⁻* embryos
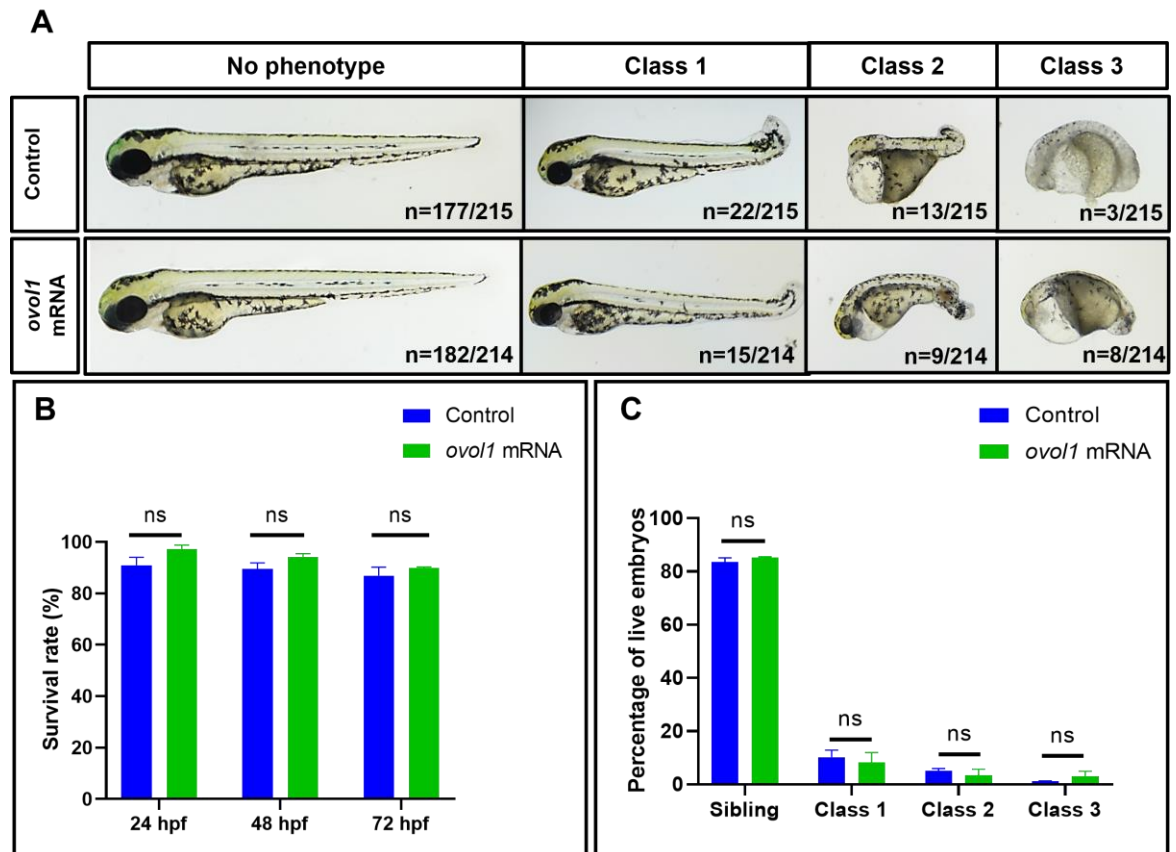
Supplementary figure 5.1 Microinjection of *ovol1a* mRNA (25 ng/µl) in *grhl3⁻ᐟ⁻* embryos.

Embryos derived from inter-crossing *grhl3⁺ᐟ⁻* fish were injected with *ovol1a* mRNA (25 ng/µl) at single cell stage. Control embryos were injected with EGFP (25 ng/µl) at 0 hpf. (**A**) Phenotypes of *ovol1a* mRNA injected *grhl3⁻ᐟ⁻* embryos were observed until 72 hpf and imaged at 72 hpf. (**B**) Survival rate and (**C**) phenotypic incidence of sibling, class 1, class 2, and class 3 phenotypes in *ovol1a* mRNA injected embryos derived from inter-crossing *grhl3⁺ᐟ⁻* fish was quantitated and analysed. Data is represented as mean ± SEM. Statistical significance determined by Multiple t-tests with correction for multiple comparisons using the Holm-Sidak method. ns- non-significant.
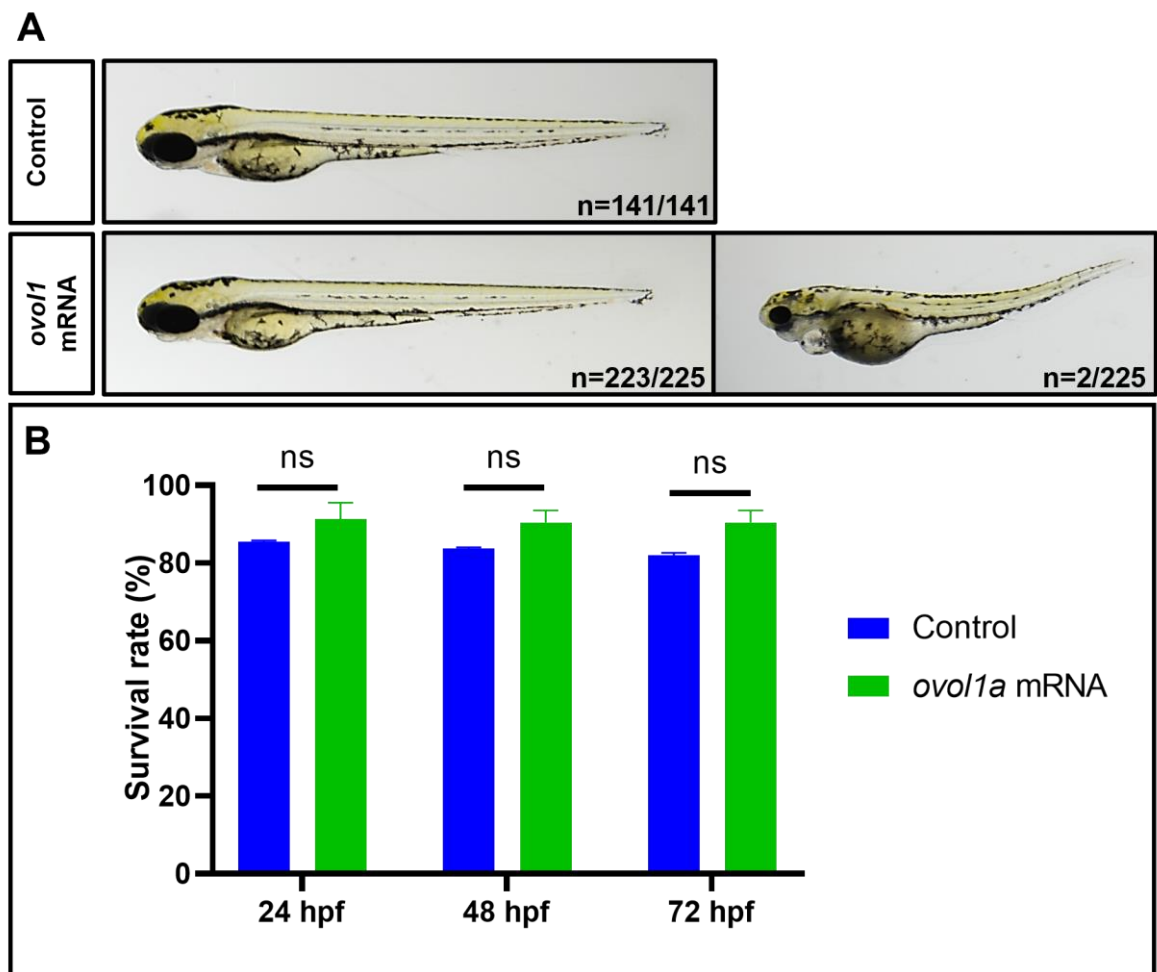
Supplementary figure 5.2 Microinjection of *ovol1a* mRNA (50 ng/µl) in WT embryos.

ovol1a mRNA was injected in single cell stage WT embryos at 50 ng/µl. Control embryos were injected with EGFP (50 ng/µl) at 0 hpf. (**A**) Phenotypes of *ovol1a* mRNA embryos were imaged at 72 hpf. (**B**) Survival rate of injected WT embryos was quantitated and analysed. Data is represented as mean ± SEM. Statistical significance determined by Multiple t-tests with correction for multiple comparisons using the Holm-Sidak method. ns- non-significant.
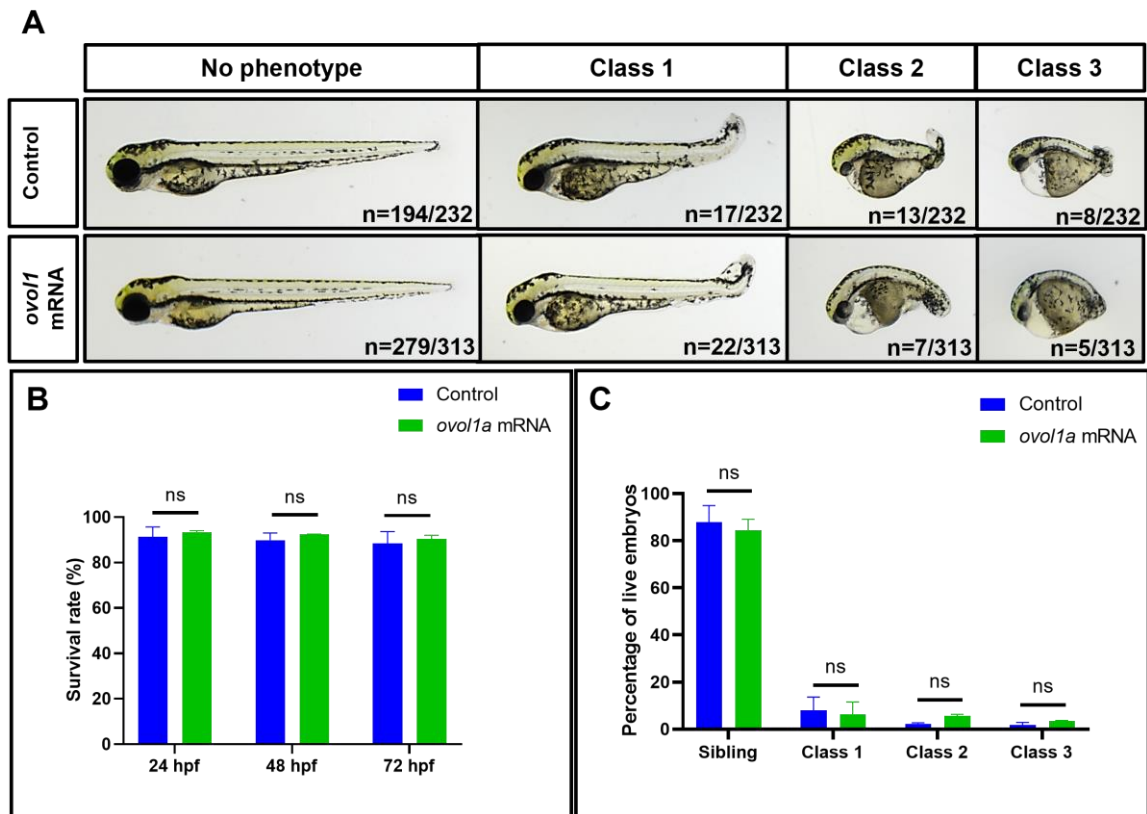
Supplementary figure 5.3 Microinjection of *ovol1a* mRNA (50 ng/µl) in *grhl3-/-* embryos.

Embryos derived from inter-crossing *grhl3+/-* fish were injected with *ovol1a* mRNA (50 ng/µl) at single cell stage**.** Control embryos were injected with EGFP (50 ng/µl) at 0 hpf. (**A**) Phenotypes of *ovol1a* mRNA injected *grhl3-/-* embryos were observed until 72 hpf and imaged at 72 hpf. (**B**) Survival rate and (**C**) phenotypic incidence of sibling, class 1, class 2, and class 3 phenotypes in *ovol1a* mRNA injected embryos derived from inter-crossing *grhl3+/-* fish was quantitated and analysed. Data is represented as mean ± SEM. Statistical significance determined by Multiple t-tests with correction for multiple comparisons using the Holm-Sidak method. ns- non-significant.

Chapter 6: Investigating novel gene-environment interactions (GEI) in epithelial development

6.1 Summary

Identifying environmental factors that may rescue the epithelial defects in *grhl3$^{-/-}$* embryos might provide insight into the therapeutic options for the prevention of *GRHL3*-dependent developmental birth defects in humans. This chapter sought to understand the effect of essential vitamins and minerals (myoinositol, nicotinamide, thiamine, cobalamin, and potassium iodide) and polyphenols (resveratrol, curcumin, and luteolin) on the survival rate and incidence of aberrant phenotypes in *grhl3$^{-/-}$* embryos. At single-cell stage, embryos derived from inter-crossing *grhl3$^{+/-}$* fish were exposed to the drug and monitored for survival until 72 hpf. The percentage of class 1, class 2, and class 3 *grhl3$^{-/-}$* phenotypes were recorded for each dosage and compared with control to determine whether a phenotypic shift takes place when exposed to the drug. Overall, the data in this chapter yielded mixed results. Treatment with myoinositol, nicotinamide, thiamine chloride, and cobalamin, yielded mild phenotypic shift in the severity of *grhl3$^{-/-}$* phenotypes while potassium iodide (at 10 mg/ml), luteolin (at 10 μM and 20 μM) and resveratrol (at 50-200 μM) treatments resulted in increased lethality of *grhl3$^{-/-}$* embryos at high concentrations. Lastly, treatment with curcumin showed phenotypic rescue of *grhl3$^{-/-}$* embryos at concentrations 2 μM and 3 μM, suggesting the importance of curcumin in axial patterning. This could be a prelude to using curcumin in the *curly-tail* mice, having hypomorphic *Grhl3* function to unravel the interaction between curcumin and *Grhl3*. This would then provide viable options for the therapeutic use of curcumin for the prevention of epithelial birth defects in future.

6.2 Introduction

Congenital anomalies including neural tube defects (NTDs), oral clefts and congenital heart defects affect about 8 million infants every year worldwide (Christianson, Howson et al. 2006) and primarily arise from complex and poorly defined interactions of genetic and environmental factors that interfere with normal morphogenetic processes. Therefore, identifying both genetic and non-genetic factors that contribute to birth defects and understanding their interactions (i.e., Gene-Environment Interactions; GxE), will help us understand the biological mechanisms that underlie birth defects and aid in the prevention of congenital anomalies in future.

The *Grhl3* hypomorphic (*curly-tail*) mouse model, as discussed in chapter 1, displays phenotypes such as defects in convergence-extension mediated movements, axial elongation and tail development, and neural-tube defects (NTD) such as spina bifida and exencephaly (Ting, Wilanowski et al. 2003). The incidence of these defects was either exacerbated or alleviated upon exposure to retinoic acid, mitomycin C, temperature, hydroxyurea, and inositol at the appropriate time-point (detailed in chapter 1: Introduction)(Seller, Embury et al. 1979, Seller, Embury et al. 1979, Seller and Perkins 1982, Seller and Perkins 1986, Seller and Perkins-Cole 1987, Greene, Leung et al. 2017). Since the NTDs observed in *curly tail* mouse display high degree of similarity to the NTDs seen in humans, testing, and identifying potential environmental factors that alleviate NTDs in the *curly tail* mice paves way to finding novel factors that can help prevent the incidence of NTDs in humans.

Having understood the significance of *Grhl3* interaction with environmental factors in mouse model, I was interested to screen some key environmental factors in our *grhl3*-deficient zebrafish model to rescue the developmental defects seen in *grhl3$^{-/-}$* embryos. The optical transparency of zebrafish embryos during the early formative stages of gastrulation, epithelial formation and organogenesis allows for effective visualization and enables a greater understanding of the chemical impact on the development of heart, brain, eyes, jaw, notochord, body segmentation and body size. Moreover, *grhl3$^{-/-}$* embryos housed at the Monash Aquatic Facility showing the rupturing phenotype at gastrulation were rescued, and an overall improvement in their survival was observed when these embryos were incubated at 25°C as opposed to temperature, 28.5°C (Miles 2017 unpublished). Thus, I speculate that prevention of rupture in the *grhl3$^{-/-}$* embryos at the La Trobe Aquatic Facility (as described in chapter 1) might be due to the influence of environmental factors such as temperature. Furthermore, preliminary studies from our research group showed that *grhl3$^{-/-}$* embryos, when exposed to 50 μM caffeine exhibited severe axial distension, as opposed to no phenotypes observed in similarly treated WT embryos (Berry, unpublished). These data suggest that the presence of compromised epithelia in *grhl3$^{-/-}$* embryos might make these embryos overtly susceptible to environmental factors. Therefore, *grhl3$^{-/-}$* embryos (showing poor epithelial establishment) might serve as an excellent model system to uncover potential GxE interactions in epithelial development.

Several GxE interactions have been identified using zebrafish embryos, of which, one of the best studied examples in the neural tube closure of zebrafish embryos is the folate pathway (Lee, Bonner et al. 2012). Folate insufficiency during human pregnancies contributes to NTDs in infants (Fleming and Copp 1998, Stover 2004). Likewise, transgenic zebrafish embryos with folate deficiency during early stages, hindered neural crest cell migration, thereby leading to defective neural tube closure (Kao, Chu et al. 2014). These studies thus provide further insight into the underlying cause of NTDs in zebrafish embryos and shed light on the roles of folate in development.

For this study, I explored the significance of other essential vitamins and minerals that play a critical role in growth and development (myoinositol, nicotinamide, thiamine, cobalamin, potassium iodide). The genetic pathways that may interact with these vitamins/minerals during embryogenesis were unknown, making them suitable factors to test in our *grhl3* deficient model. In addition to vitamins and minerals, polyphenols (curcumin, resveratrol and luteolin) were tested on *grhl3*$^{-/-}$ embryos since they enhance epithelial integrity and have been widely used in the treatment of barrier defects (Wang, Wang et al. 2012, Wang, Han et al. 2016, Titto, Ankit et al. 2020), NTDs (associated with maternal diabetes) (Hsieh, Chen et al. 2014, Wu, Wang et al. 2015) and epithelial cancers (Singh, Hu et al. 1998, Yang, Yang et al. 2008, Shankar, Nall et al. 2011, Boyer, Jandova et al. 2012, Liu and Chen 2013, Ahmed, Khan et al. 2019). This chapter will thus explore the effect of vitamins, minerals, and polyphenols on the survival rate of *grhl3*$^{-/-}$ and WT embryos to determine the efficacy of these drugs on zebrafish embryos. Lastly, the phenotypic incidence and severity of *grhl3*$^{-/-}$ embryos was analysed to see whether a rescue in the severity of *grhl3*$^{-/-}$ embryos took place upon exposure to these environmental factors.

6.3 Optimizing the experimental paradigm

6.3.1 Determining the effects of pronase on embryonic development

In order to understand the impact of test chemicals on the early development of embryos, it was critical to dechorionate the embryos first at early embryonic stages (<3 hpf), for better diffusion of the chemical. To this end, I used pronase, a commercially available mixture of proteases, for the chemical degradation of proteins present in the embryonic chorion. Pronase-mediated dechorionation was performed to ensure better penetration of test chemical (myoinositol, nicotinamide, thiamine, cobalamin, potassium iodide,

resveratrol, curcumin, and luteolin) into the developing embryo. Both WT embryos and embryos derived from inter-crossing $grhl3^{+/-}$ adult zebrafish were subjected to treatment with pronase at 2 hpf.

To perform pronase-mediated dechorionation, embryos derived from inter-crossing $grhl3^{+/-}$ fish and WT embryos at 2 hpf were exposed to 0.25 mg/ml, 0.5 mg/ml, and 1 mg/ml pronase for 45 seconds, followed by thorough rinsing of the embryos with embryo medium 3-4 times. The survival rate of pronase treated WT embryos was $33.8 \pm 31.8\%$ at 0.25 mg/ml, $56.6 \pm 14.2\%$ at 0.5 mg/ml and $12.75 \pm 5.2\%$ at 1 mg/ml and that of control was 100% at 72 hpf. A significant decrease in the survival rate of WT embryos (Figure 6.1A) was observed at 1 mg/ml while embryos derived from inter-crossing $grhl3^{+/-}$ fish showed a significant decrease in the survival rate at concentrations 0.25 mg/ml, 0.5 mg/ml, and 1 mg/ml (Figure 6.1B). These results indicate that pronase-mediated dechorionation might not be the preferred option to remove the chorion, particularly in embryos derived from inter-crossing $grhl3^{+/-}$ adult zebrafish.

Figure 6.1 Effects of pronase on embryos derived from inter-crossing *grhl3*^{+/-} adult zebrafish and WT embryos.

Embryos were treated with pronase (0.25 mg/ml, 0.5 mg/ml, and 1 mg/ml) at 2 hpf for 45 seconds, followed by thorough rinsing with embryo medium. **(A)** Survival rate of pronase treated WT embryos relative to control (n=3). **(B)** Survival rate of embryos derived from inter-crossing *grhl3*^{+/-} adult zebrafish following pronase treatment relative to control (n=3). Data is represented as mean ± SEM. Statistical significance determined by Multiple t-tests with correction for multiple comparisons using the Holm-Sidak method; *P < 0.05; **P < 0.01; ***P < 0.005.

6.3.2 Effects of DMSO on embryos derived from inter-crossing $grhl3^{+/-}$ adult zebrafish and WT embryos

0.1 and 0.2% DMSO have been extensively used for better penetration of test vitamins/minerals/polyphenol via the chorion into the embryo. In order to test the safety of DMSO, 0.1% and 0.2% DMSO prepared in embryo medium was administered to WT embryos and embryos derived from inter-crossing $grhl3^{+/-}$ adult zebrafish at the single cell stage. The survival rate and phenotypic incidence of WT embryos and embryos derived from inter-crossing $grhl3^{+/-}$ adult zebrafish was quantitated, and statistical analysis was performed. Survival percentage of 0.1%, 0.2% DMSO treated WT embryos and control was 95.9 ± 0.8%, 94.35 ± 0.1% and 97.7 ± 1.0% respectively at 72 hpf (Figure 6.2A). The survival rate of embryos derived from inter-crossing $grhl3^{+/-}$ fish treated with 0.1% and 0.2% DMSO was 75.8 ± 4.8% and 79.1 ± 6.9% respectively and that of control was 81.6 ± 1.6% (Figure 6.2B). No significant variations were observed in the survival rate of WT embryos and embryos derived from inter-crossing $grhl3^{+/-}$ fish at 24 hpf, 48 hpf and 72 hpf relative to control.

In terms of phenotypic incidence of DMSO treated embryos derived from inter-crossing $grhl3^{+/-}$ adult zebrafish, percentage of siblings and phenotypic mutants (class 1 + class 2 + class 3) were 97.05 ± 1.3% and 2.9 ± 1.3% at 0.1% DMSO and 94.1 ± 0.8% and 5.9 ± 0.8% at 0.2% DMSO respectively. The percentage of siblings and phenotypic mutants in control was 91.0 ± 1.3% (*grhl3* siblings) and 8.9 ± 1.3% (*grhl3* mutants)(Figure 6.2C). Statistical analyses revealed no significant differences in the incidence rate of phenotypic defects observed in $grhl3^{-/-}$ embryos. This suggests that DMSO is relatively safe and can be used in conjunction with the test chemicals for better penetration into the developing embryo.

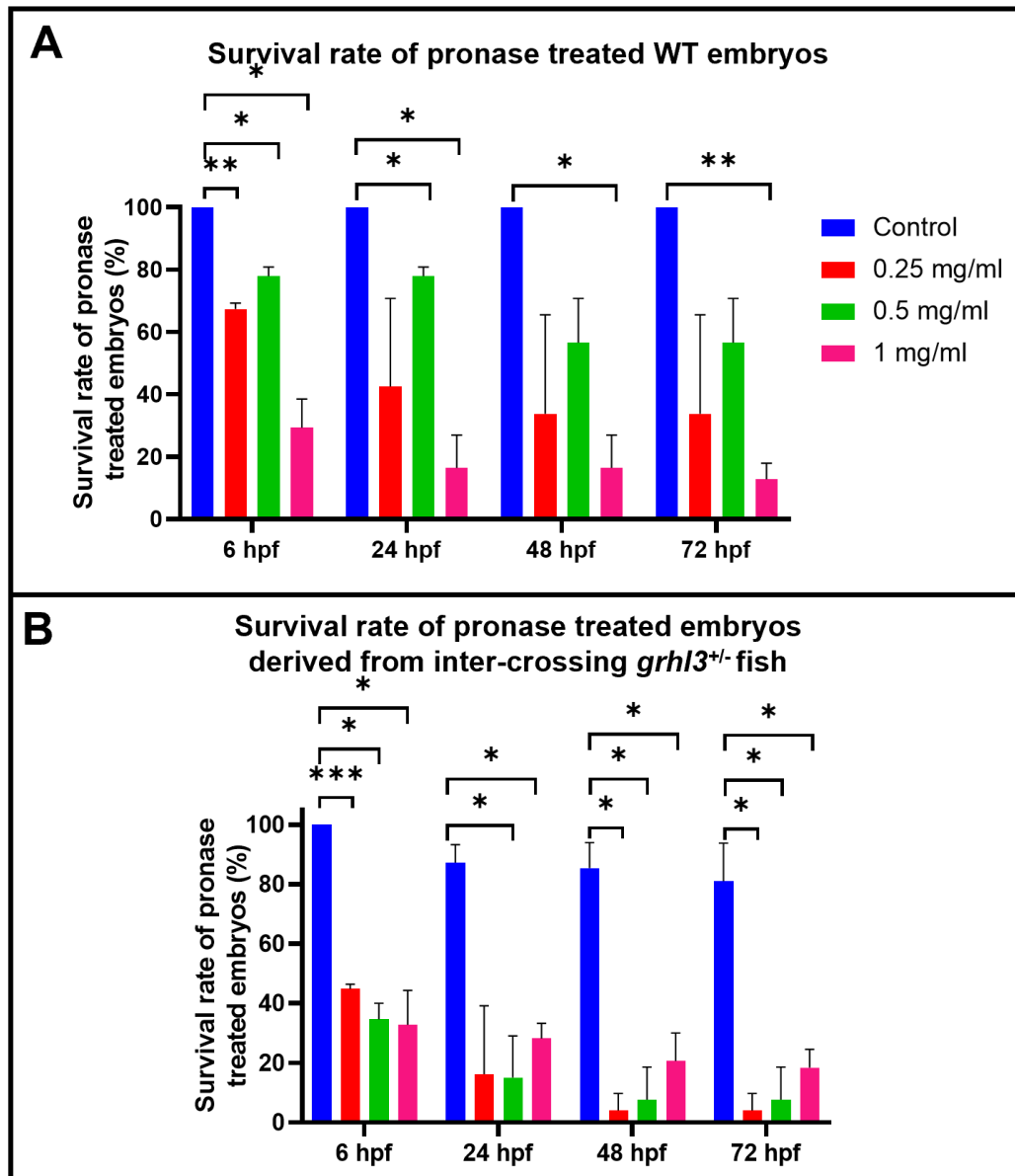**Figure 6.2 Effects of DMSO on embryos derived from inter-crossing *grhl3*^{+/-} adult zebrafish and WT embryos.**

Embryos were exposed to 0.1% and 0.2% DMSO at 0 hpf. **(A)** Survival rate of DMSO treated WT embryos relative to control (n=3). **(B)** Survival rate of embryos derived from inter-crossing *grhl3*^{+/-} adult zebrafish following DMSO treatment relative to control (n=3). **(C)** Phenotypic incidence of class 1, class 2, and class 3 *grhl3*^{-/-} embryos at 72 hpf, post treatment. **(D)** Phenotypes observed in DMSO treated WT and *grhl3*^{+/-} embryos. Data is represented as mean ± SEM. Statistical significance determined by Multiple t-tests with correction for multiple comparisons using the Holm-Sidak method; ns - non-significant.

6.4 Results

6.4.1 Effect of essential vitamins and minerals on embryos derived from inter-crossing *grhl3*^{+/-} adult zebrafish and WT embryos

- *Myoinositol (Vitamin B8)*

Dosage range tested: 6.75 mg/ml, 12.5 mg/ml, 25 mg/ml, 37.5 mg/ml, 50 mg/ml, and 75 mg/ml.

Key findings on survival rates: Myoinositol treatment was performed in triplicate, containing 100 embryos per Petri dish. The survival rate remained consistent (~92-99%) across the wide range of concentrations tested in WT embryos (Figure 6.3A) and embryos derived from inter-crossing *grhl3*^{+/-} adult fish (Figure 6.3B-D). Statistical analyses

revealed no significant differences in the survival rate of embryos derived from inter-crossing *grhl3*$^{+/-}$ adult fish and WT embryos.

Key findings on phenotypic incidence: Percentage of phenotypic mutants at 6.75 mg/ml, 12.5 mg/ml, and 25 mg/ml myoinositol treatment were 19.0 ± 5.35%, 17.9 ± 5.35% and 17.9 ± 5.35% respectively (Figure 6.3E-F). No significant changes in overall phenotypic incidence were observed at these concentrations, relative to control (~14.4 ± 3.0%). When assessing the phenotypic severity in embryos treated with 37.5 mg/ml myoinositol, it was found that the proportion of embryos presented with class 1 (17.5± 3.5%) and class 3 (2.6 ± 4.4%) defects remained unchanged from non-treated *grhl3*$^{-/-}$ embryos, whereas a significant (10.54%; p<0.05) increase in embryos presented with class 2 defects (11.4 ± 3.6%) was seen. Similarly, the class 1 (9.8 ± 81.6%; 12.9 ± 5.7) and class 2 (6.0 ± 0.5%; 7.1 ± 0.8%) phenotypes observed at 50 mg/ml and 75 mg/ml treated embryos remained unchanged, while a decrease (2.1%; p=0.04) in class 3 phenotypes (0.0%) was seen relative to control (2.1 ± 0.8%) (Figure 6.3G). Absence of class 3 embryos and no differences in survival rate at 50 mg/ml and 75 mg/ml signified that class 3 *grhl3*$^{-/-}$ embryos do not die due to toxicity but rather exhibited slight phenotypic shift showing rescue.

Summary: These data show that myoinositol treatment, even at the highest dose tested, does not contribute to lethality. In terms of phenotypic severity of *grhl3*$^{-/-}$ embryos, myoinositol treatment at 50 mg/ml and 75 mg/ml can alleviate the severe defects in class 3 embryos partially, as shown by a slight, albeit significant, phenotypic shift towards class 2. However, this cannot be considered a rescue, as the overall percentage of phenotypic mutants and non-phenotypic siblings does not show significant differences relative to control.
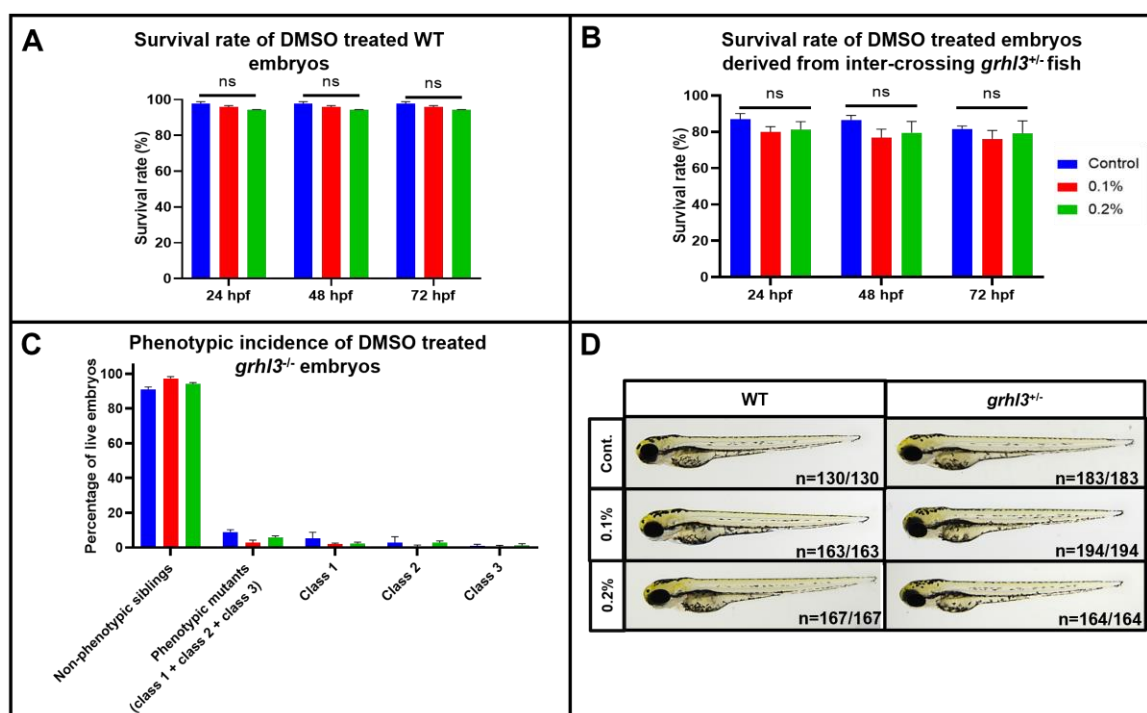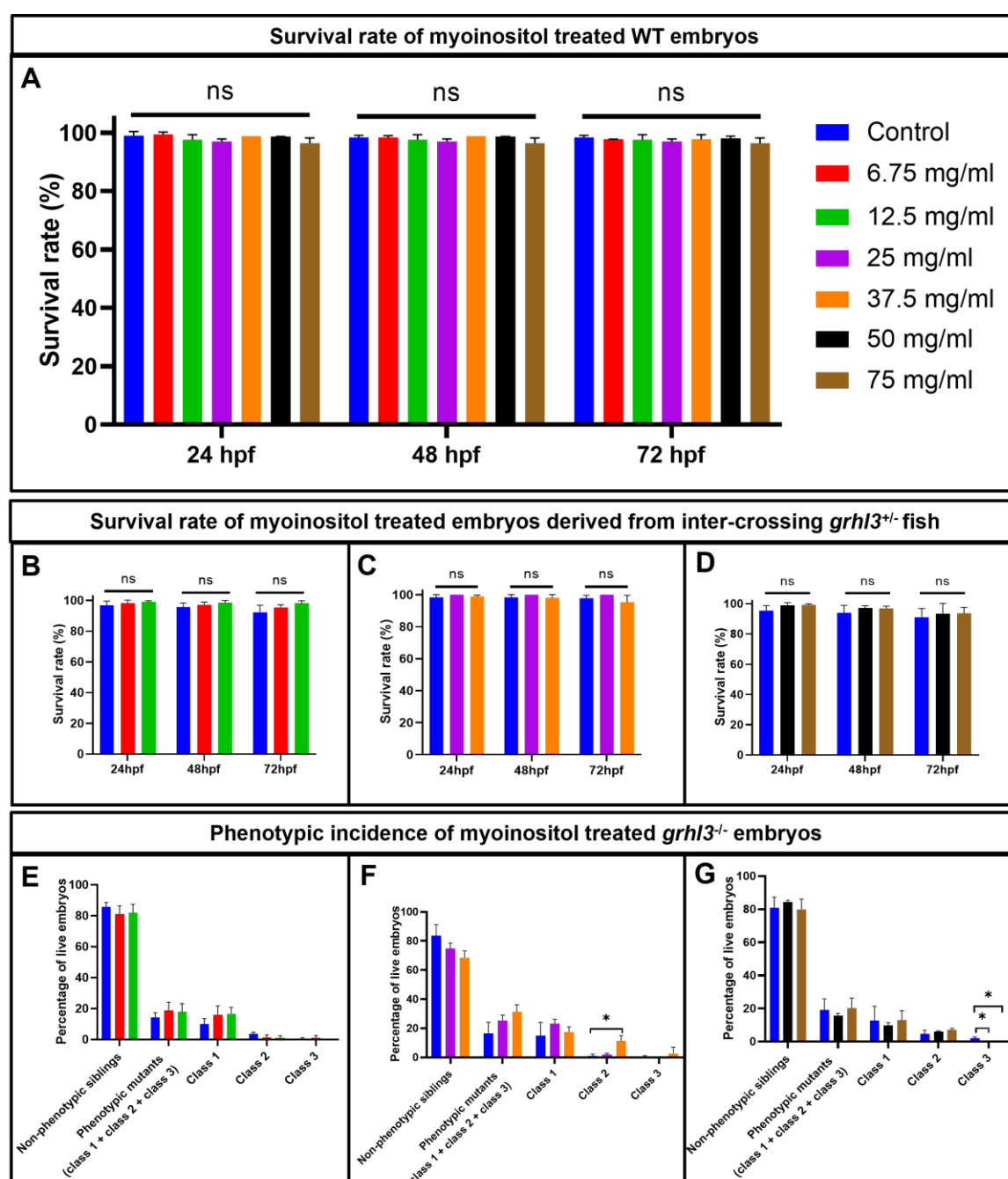
Figure 6.3 Effects of myoinositol on embryos derived from inter-crossing *grhl3$^{+/-}$* adult zebrafish and WT embryos.

Embryos were exposed to myoinositol at 0 hpf (6.75 mg/ml, 12.5 mg/ml, 25 mg/ml, 37.5 mg/ml, 50 mg/ml, and 75 mg/ml). (**A**) Survival rate of myoinositol treated WT embryos relative to control (n=3). (**B, C, D**) Survival rate of embryos derived from inter-crossing *grhl3$^{+/-}$* adult zebrafish following myoinositol treatment relative to control (n=3). (**E, F, G**) Phenotypic incidence of class 1, class 2, and class 3 *grhl3$^{-/-}$* embryos at 72 hpf, post myoinositol treatment. Data is represented as mean ± SEM. Statistical significance determined by Multiple t-tests with correction for multiple comparisons using the Holm-Sidak method*P < 0.05; ns - non-significant.

- ▪ *Nicotinamide (Vitamin B3)*

Dosage range tested: 1 μM, 2.5 μM, 5 μM, 10 μM and 20 μM.

Key findings on survival rates: The survival rate of nicotinamide treated WT embryos and control embryos at all dosages tested, ranged between ~98-100%, indicating no significant differences between treated embryos and control (Figure 6.4A). Embryos derived from inter-crossing *grhl3*$^{+/-}$ adult zebrafish treated with 1 μM, 2.5 μM and 5 μM nicotinamide showed a survival of ~87.5-89% at 72 hpf and that of control was 78.5%. At 10 μM and 20 μM, the survival rate of embryos derived from inter-crossing *grhl3*$^{+/-}$ adult zebrafish was 94.0 ± 0.3% and 99.1 ± 1.3% respectively and the survival rate of control embryos was 92.95 ± 0.1% (Figure 6.4B). Although minor variations in survival rate was noted, no significant differences were found between treated and control embryos.

Key findings on phenotypic incidence: The overall percentage of phenotypic mutants at 1 μM, 2.5 μM, 5 μM and control was 15.0 ± 2.4%, 6.6 ± 0.1%, 11.4 ± 1.0% and 6.9 ± 1.9% respectively. At concentrations 10 μM and 20 μM, the percentage of phenotypic mutants were 25.4 ± 4.5% and 17.6 ± 6.2% respectively and that of control was 21.2 ± 1.7% (Figure 6.4C). No significant variation in the percentage of *grhl3*$^{-/-}$ embryos was observed relative to control.

Summary: These results suggest that nicotinamide is completely safe at the dosage range used and does not alleviate nor exacerbate the phenotypes of *grhl3*$^{-/-}$ embryos.

- ▪ *Thiamine (Vitamin B2)*

Dosage range tested: 1 μM, 2.5 μM, 5 μM, 10 μM and 20 μM.

Key findings on survival rates: Survival rate of WT embryos treated with thiamine (1-20 μM) ranged between 90.5-99% and the survival rate of control embryos was 95.35 ± 4.9% (Figure 6.5A). Embryos derived from inter-crossing *grhl3*$^{+/-}$ adult fish treated with thiamine showed survival percentage of 74.9 ± 2.2% at 1 μM, 77.9 ± 3.8% at 2.5 μM, 86.45 ± 7.1% at 5 μM , 79.8 ± 2.7% at 10 μM and 71.85 ± 0.6% at 20 μM (Figure 6.5B). Statistical analysis revealed no significant variation in the survival rate of embryos derived from inter-crossing *grhl3*$^{+/-}$ adult zebrafish and WT embryos.

Key findings on phenotypic incidence: Percentage of *grhl3* phenotypic mutants upon thiamine treatment was 0% (1 μM), 2.7 ± 2.4% (2.5 μM), 11.0 ± 5.1% (5 μM), 4.2 ± 3.6% (10 μM) and 5.3 ± 2.8% (20 μM) and that of control was 2.9 ± 1.3% (Figure 6.5C). The

overall percentage of *grhl3⁻/⁻* mutants showed no significant differences between treated embryos and control, however class 1 phenotypic population was completely absent when treated at 1 μM and 2.5 μM, showing a significant reduction (p=0.009) when compared to control.

Summary: Thiamine at the dosages tested did not cause lethality of embryos and thus, can be considered safe. Absence of class 1 phenotype at 1 μM and 2.5 μM is not due to toxicity since higher concentrations of thiamine are well-tolerated by the embryos. However, the absence of class 1 cannot be considered a rescue as well, since the overall percentage of phenotypic mutants does not show any statistical difference relative to control. Therefore, class 1 might be absent in this particular clutch of embryos from the beginning prior to the chemical treatment.

Figure 6.4 Effects of nicotinamide on embryos derived from inter-crossing *grhl3⁺/⁻* adult zebrafish and WT embryos.

Embryos were exposed to nicotinamide (1 μM, 2.5 μM, 5 μM, 10 μM and 20 μM) at 0 hpf. **(A)** Survival rate of nicotinamide treated WT embryos relative to control (0.1% DMSO) (n=3). **(B)** Survival rate of embryos derived from inter-crossing *grhl3⁺/⁻* adult zebrafish following nicotinamide treatment relative to control (0.1% DMSO) (n=3). **(C)** Phenotypic incidence of class 1, class 2, and class 3 *grhl3⁻/⁻* embryos at 72 hpf, post nicotinamide treatment. **(D)** Phenotypes observed in nicotinamide (20 μM) treated WT and *grhl3⁺/⁻* embryos. Data is represented as mean ± SEM. Statistical significance determined by Multiple t-tests with correction for multiple comparisons using the Holm-Sidak method. ns – non-significant.
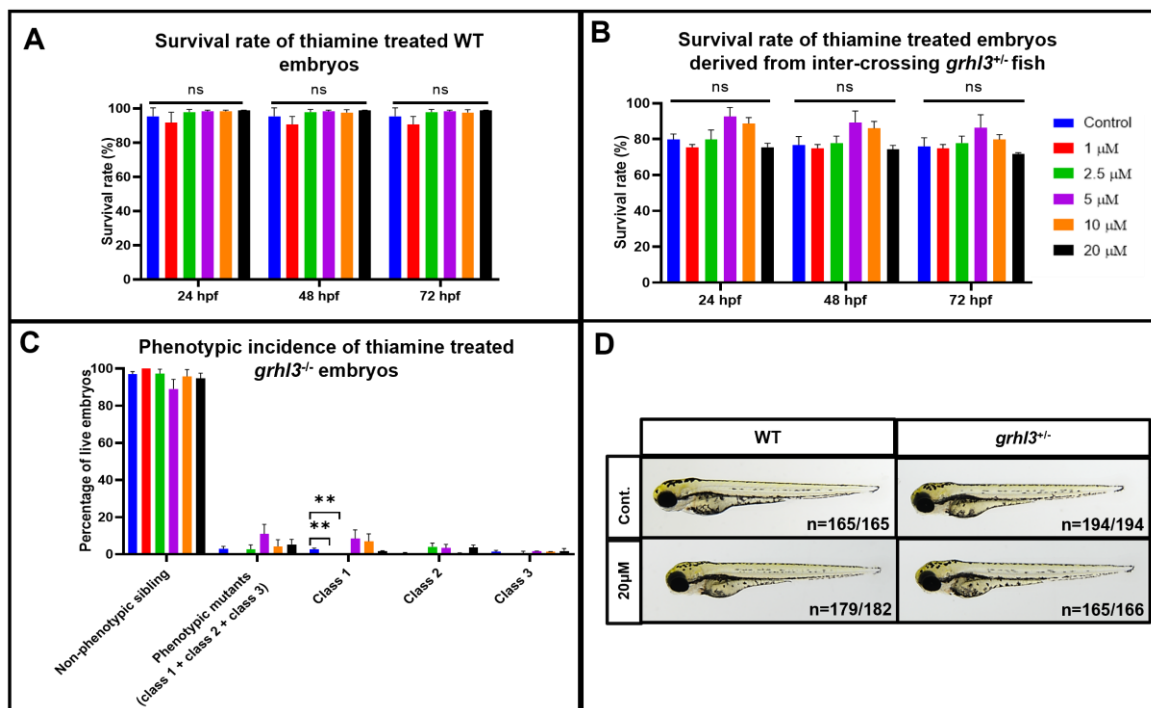
Figure 6.5 Effects of thiamine on embryos derived from inter-crossing *grhl3*⁺/⁻ adult zebrafish and WT embryos.

Embryos were exposed to thiamine (1 μM, 2.5 μM, 5 μM, 10 μM and 20 μM) at 0 hpf. **(A)** Survival rate of thiamine treated WT embryos relative to control (0.1% DMSO) (n=3). **(B)** Survival rate of embryos derived from inter-crossing *grhl3*⁺/⁻ adult zebrafish following thiamine treatment relative to control (0.1% DMSO) (n=3). **(C)** Phenotypic incidence of class 1, class 2, and class 3 *grhl3*⁻/⁻ embryos at 72 hpf, post thiamine treatment. relative to control (0.1% DMSO) **(D)** Phenotypes observed in thiamine (20 μM) treated WT and *grhl3*⁺/⁻ embryos. Data is represented as mean ± SEM. Statistical significance determined by Multiple t-tests with correction for multiple comparisons using the Holm-Sidak method.**P < 0.01; ns- non-significant.

▪ *Cobalamin (Vitamin B12)*

Dosage range tested: 1 μM, 2.5 μM, 5 μM, 10 μM and 20 μM.

Key findings on survival rates: The survival rate of WT embryos treated with cobalamin at concentrations 1-20 μM ranged between ~98-99%, showing no significant differences in comparison to controls (99.2 ± 1.1%)(Figure 6.6A). Thiamine treatment at 1 μM, 2.5 μM, 5 μM, 10 μM and 20 μM on embryos derived from inter-crossing *grhl3*⁺/⁻ adult zebrafish showed survival percentage of 86.0 ± 1.91%, 84.0 ± 1.5%, 87.6 ± 1.6%, 83.5 ± 0.8% and 79.3 ± 4.8% respectively at 72 hpf (Figure 6.6B). From these results, I found that embryos derived from inter-crossing *grhl3*⁺/⁻ adult zebrafish treated with 2.5 μM and 10 μM cobalamin showed a ~3% and 3.8% decrease in survival rate respectively relative to controls.

Key findings on phenotypic incidence: *grhl3* phenotypic mutants were present at $13.1 \pm 1.8\%$, $10.0 \pm 3.2\%$, $16.1 \pm 0.6\%$ and $15.4 \pm 8.6\%$ at concentrations 1 μM, 2.5 μM, 5 μM, 10 μM respectively and $11.8 \pm 3.4\%$ *grhl3* mutants were present in control. At 20 μM and control, *grhl3* phenotypic mutants were present at $2.3 \pm 2.3\%$ and $4.8 \pm 4.8\%$ respectively. Class 3 *grhl3*$^{-/-}$ embryos were absent at 1 μM and 2.5 μM concentrations (Figure 6.6C)**.**

Summary: At 1 μM, since there was no significant reduction in the survival of *grhl3*$^{-/-}$ embryos, thus, the absence of class 3 embryos could mean that a phenotypic shift took place towards the class 1/class 2 phenotypes.
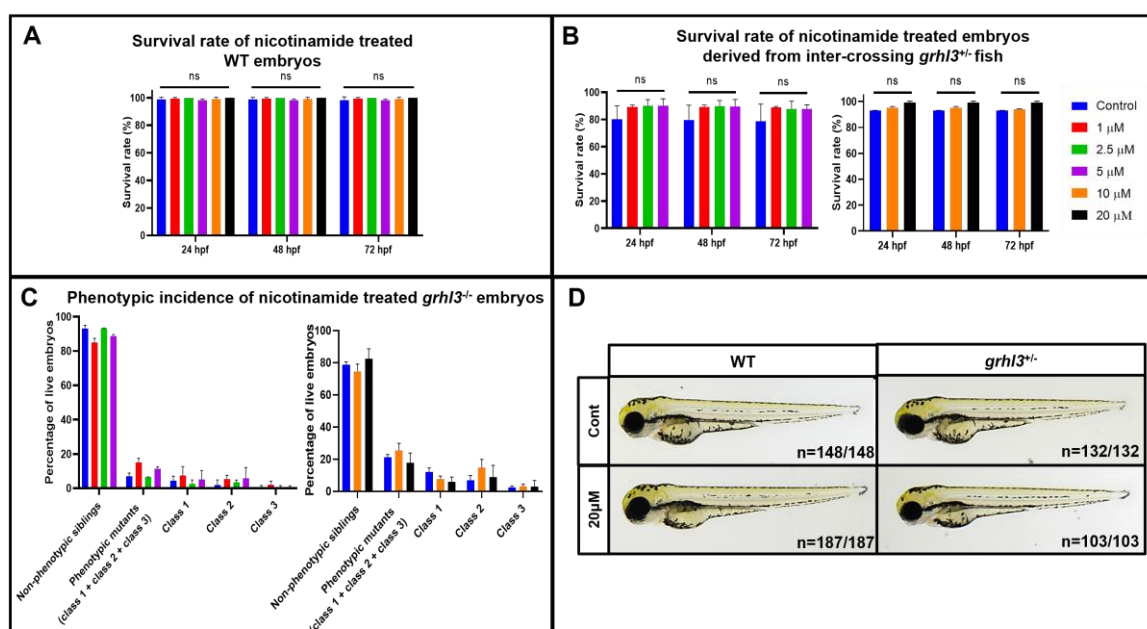

Figure 6.6 Effects of cobalamin on embryos derived from inter-crossing *grhl3*$^{+/-}$ adult zebrafish and WT embryos.

Embryos were exposed to cobalamin (1 μM, 2.5 μM, 5 μM, 10 μM and 20 μM) at 0 hpf. **(A)** Survival rate of cobalamin treated WT embryos relative to control (0.1% DMSO) (n=3). **(B)** Survival rate of embryos derived from inter-crossing *grhl3*$^{+/-}$ adult zebrafish following cobalamin treatment relative to control (0.1% DMSO) (n=3). **(C)** Phenotypic incidence of class 1, class 2, and class 3 *grhl3*$^{-/-}$ embryos at 72 hpf, post cobalamin treatment. **(D)** Phenotypes observed in cobalamin (20 μM) treated *grhl3*$^{+/-}$ vs. WT embryos. Statistical significance determined by Multiple t-tests with correction for multiple comparisons using the Holm-Sidak method; *P < 0.05; ****P < 0.001; ns – non-significant.

▪ *Potassium Iodide*

Dosage range tested: 2.5 mg/ml, 5 mg/ml, and 10 mg/ml.

Key findings on survival rates: Survival rate of WT embryos treated with 2.5 mg/ml, 5 mg/ml, and 10 mg/ml Potassium Iodide (KI) was 99.4 ± 0.85%, 89.6 ± 8.25% and 8.7 ± 12.3% respectively and that of control was 100% (Figure 6.7A). Embryos derived from inter-crossing *grhl3*$^{+/-}$ adult zebrafish treated with 2.5 mg/ml, 5 mg/ml, and 10 mg/ml KI showed survival percentage of 81.6 ± 6.3%, 78.7 ± 9.8% and 40.9 ± 6.8% respectively while survival percentage of control embryos was 97.2 ± 0.27% (Figure 6.7B). Upon statistical analyses it was revealed that administration of KI at 10 mg/ml on WT embryos and embryos derived from inter-crossing *grhl3*$^{+/-}$ adult zebrafish showed a significant decrease in their survival relative to control. Lethality of embryos at 10 mg/ml might be due to toxicity posed by KI at this dosage.

Key findings on phenotypic incidence: The overall percentage of *grhl3* mutants at 2.5 mg/ml, 5 mg/ml, and 10 mg/ml KI treatment was 19.5 ± 6.3%, 4.4 ± 0.9% and 4.6 ± 2.85% respectively and the percentage of *grhl3* mutants in control was 17.7 ± 3.3% (Figure 6.7C). Although no significant difference was seen in the overall percentage of mutants between treated and control embryos, KI treatment at 10 mg/ml on embryos derived from inter-crossing *grhl3*$^{+/-}$ adult zebrafish showed absence of class 2 embryos, thereby showing 4.3% reduction in class 2 in comparison to control.

WT embryos treated with KI (10 mg/ml) showed 2 different phenotypes; poor yolk sac formation along with curvature of body was displayed in 6 out of 12 embryos, while remaining embryos (n=6/12) exhibited defective eye formation along with axial defects. Treatment at 10 mg/ml in *grhl3*$^{+/-}$ embryos displayed 64 out of 68 embryos with normal phenotype while 4/68 embryos showed poor eye development coupled with axial defects (Figure 6.7D).

Summary: Treatment at 10 mg/ml showed lethality in WT embryos and embryos derived from inter-crossing *grhl3*$^{+/-}$ adult zebrafish. Reduction in class 2 *grhl3*$^{-/-}$ can be attributed to toxicity induced at 10 mg/ml. In addition, severe toxicity-induced phenotypes such as axial defects and poor development of eyes were observed in embryos treated with KI at 10 mg/ml. This suggests that KI is toxic to zebrafish embryos at concentrations ≥10 mg/ml.
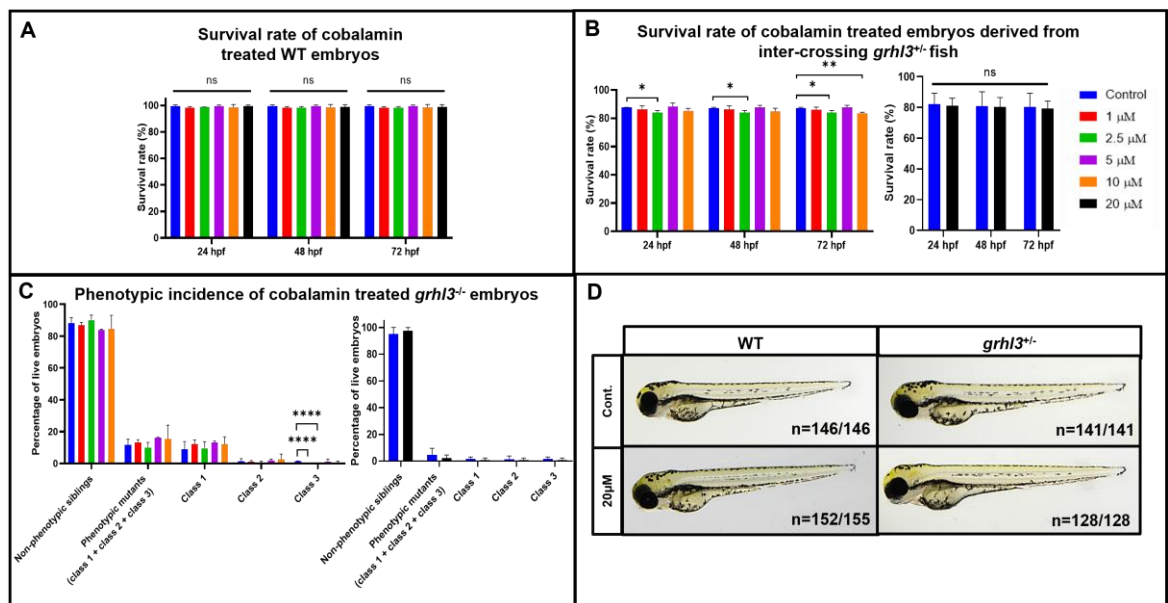
Figure 6.7 Effects of potassium iodide (KI) on embryos derived from inter-crossing *grhl3*$^{+/-}$ adult zebrafish and WT embryos.

Embryos were exposed to KI (2.5 mg/ml, 5 mg/ml, and 10 mg/ml) at 0 hpf. (**A**) Survival rate of KI treated WT embryos relative to control (0.1% DMSO) (n=3). (**B**) Survival rate of embryos derived from inter-crossing *grhl3*$^{+/-}$ adult zebrafish following KI treatment relative to control (n=3). (**C**) Phenotypic incidence of class 1, class 2, and class 3 *grhl3*$^{-/-}$ embryos at 72 hpf, post KI treatment. (**D**) Phenotypes observed in KI (10 mg/ml) treated WT and *grhl3*$^{+/-}$ embryos. Data is represented as mean ± SEM. Statistical significance determined by Multiple t-tests with correction for multiple comparisons using the Holm-Sidak method *P < 0.05.

6.4.2 Effect of natural antioxidants on embryos derived from inter-crossing *grhl3*$^{+/-}$ adult zebrafish and WT embryos

▪ *Resveratrol (RSV)*

Dosage range tested: 50 μM, 100 μM, 150 μM, and 200 μM.

Key findings on survival rates: Survival rate of WT embryos at 50 μM, 100 μM, 150 μM, and 200 μM concentrations were 97.8 ± 1.5%, 87.8 ± 6.0%, 61.3 ± 1.5% and 46.5 ± 5.85% respectively and that of control was 98.2 ± 0.9% (Figure 6.8A). A significant increase in death of WT embryos was observed at concentrations >100 μM. In embryos derived from inter-crossing *grhl3*$^{+/-}$ adult zebrafish, RSV administration at 50 μM, 100 μM, 150 μM, and 200 μM showed survival of 71.15 ± 2.4%, 63.9 ± 8.4%, 67.6 ± 5.7%, and 70.6 ± 8.6% respectively while the survival rate of control embryos was 94.0 ± 2.6%

at 72 hpf (Figure 6.8B). A significant decrease in the survival rate of treated embryos relative to control was noted at concentrations ranging 50 μM - 200 μM.

Key findings on phenotypic incidence: The overall percentage of *grhl3*$^{-/-}$ mutants at 50 μM, 100 μM, 150 μM, and 200 μM were 2.7 ± 2.0%, 1.3 ± 2.2%, 0%, 2.35 ± 1.2% respectively and that of control was 19.8 ± 2.5%. A significant decrease in the overall percentage of phenotypic mutants was noted at concentrations 50 μM - 200 μM. Furthermore, no class 1 phenotypic embryos were observed at concentrations 50 μM, 100 μM, 150 μM, and 200 μM. There was a 3.14% decrease in the percentage of class 2 embryos at concentrations 100 μM and 150 μM compared to the control (0.1% DMSO) (Figure 6.8C)**.** The absence of class 1 and reduction in phenotypic mutants can be attributed to death due to toxicity of RSV. Lastly, WT and *grhl3*$^{+/-}$ embryos treated with 200 μM RSV exhibited poor melanocyte formation and haemorrhage (Figure 6.8D)**.**

Summary: High mortality rate was noted in RSV (50 μM - 200 μM) treated embryos derived from inter-crossing *grhl3*$^{+/-}$adult zebrafish. This might be due to toxicity induced by RSV on *grhl3* mutant embryos (as seen by a reduction in class 1 and class 2 embryos). Lastly, RSV treatment at 200 μM displayed poor melanocyte formation and haemorrhage in both WT and *grhl3*$^{+/-}$ embryos.
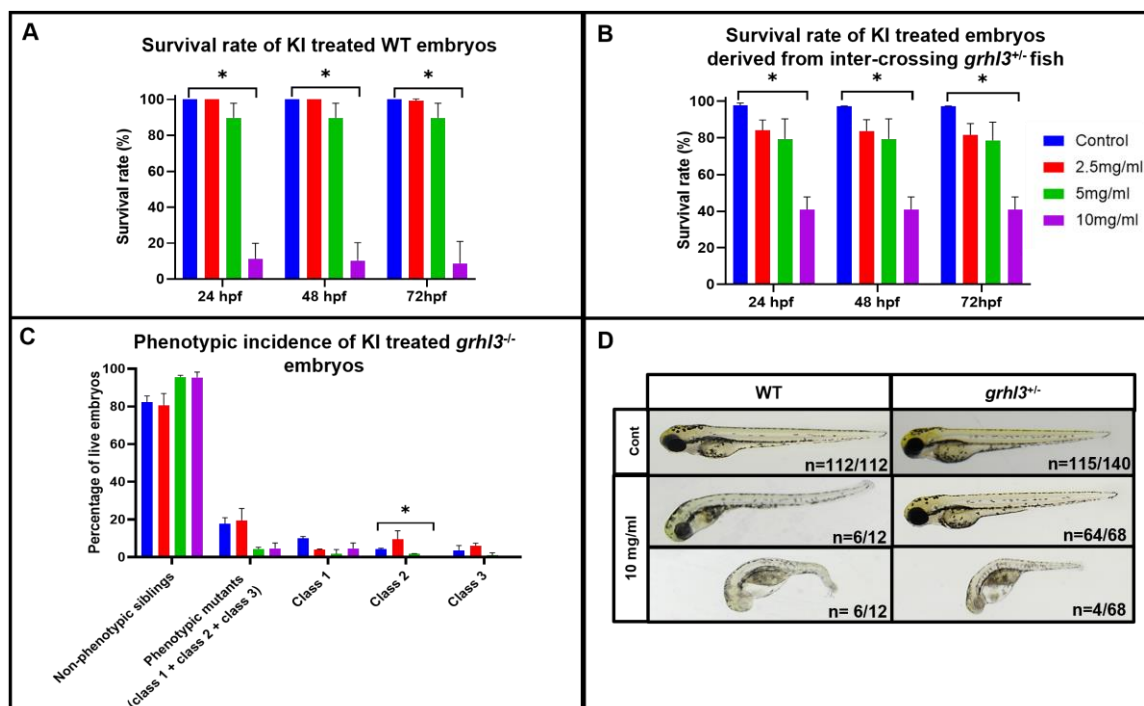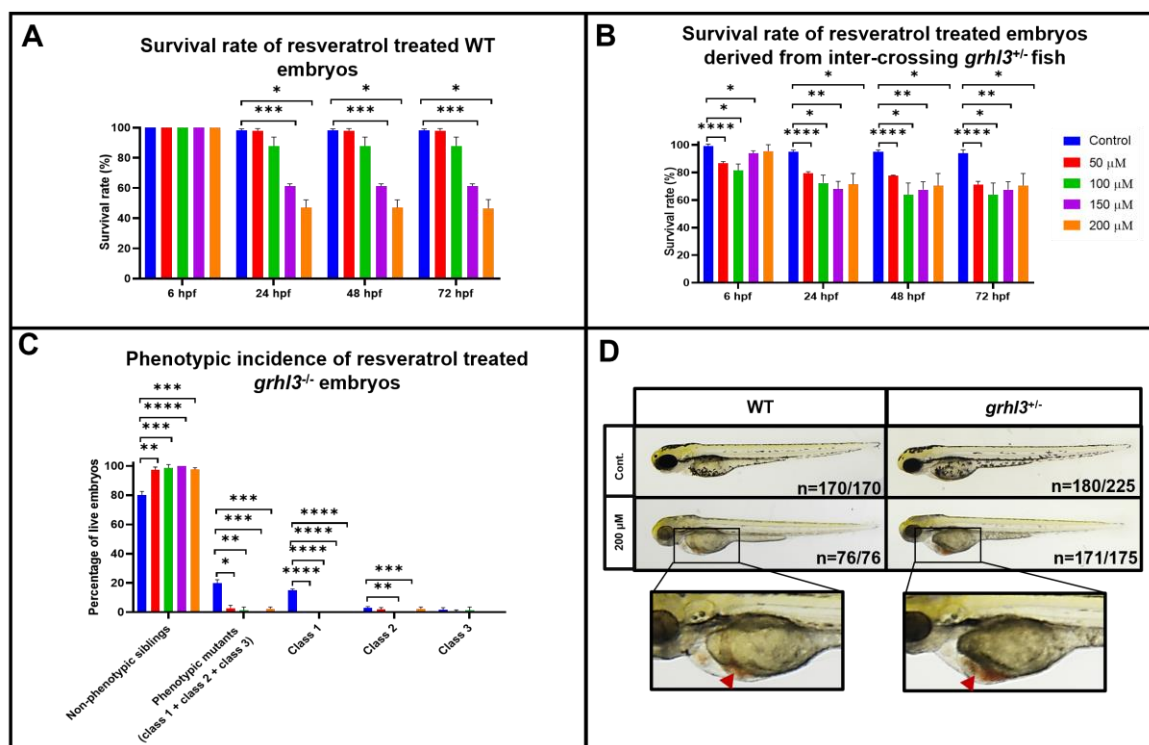
Figure 6.8 Effects of resveratrol on embryos derived from inter-crossing *grhl3*+/- adult zebrafish and WT embryos.

Embryos were exposed to resveratrol (RSV) (1 μM, 2.5 μM, 5 μM, 10 μM and 20 μM) at 0 hpf. **(A)** Survival rate of RSV treated WT embryos relative to control (0.2% DMSO) (n=3). **(B)** Survival rate of RSV treated embryos derived from inter-crossing *grhl3*+/- adult zebrafish relative to control (0.2% DMSO) (n=3). **(C)** Phenotypic incidence of class 1, class 2, and class 3 *grhl3*-/- embryos at 72 hpf, post RSV treatment **(D)** Phenotypes observed in RSV (20 μM) treated *grhl3*+/- vs. WT embryos (red arrow indicates haemorrhage). Data is represented as mean ± SEM. Statistical significance determined by Multiple t-tests with correction for multiple comparisons using the Holm-Sidak method *P < 0.05; **P < 0.01; ***P < 0.005; ****P < 0.001.

- *Curcumin*

Dosage range tested: 1 μM, 2 μM, 3 μM, and 4 μM.

Key findings on survival rates: Curcumin treated at concentrations 1 μM, 2 μM, 3 μM in WT embryos showed survival percentage ranging between ~97.5-99%. At 4 μM high lethality was observed with only 52.8 ± 7.15% embryos surviving (Figure 6.9A). No significant differences in survival rate was seen at 1-3 μM concentrations, however a significant reduction in survival rate was observed at 4 μM curcumin treatment relative to control (~96%).

Embryos derived from inter-crossing *grhl3*+/-(1-Δ4) fish showed survival rate ranging 79.5% - 84% at 1-3 μM while control embryos showed survival of 81.1 ± 3.1%. At 4 μM, embryos showed survival of 46.05 ± 2.7%, thereby showing significant lethality

(p=0.0004) in comparison to controls (Figure 6.9B). Similarly, at 4 μM curcumin treatment, embryos derived from inter-crossing *grhl3*$^{+/-(-31bp)}$ fish displayed significant lethality with only 9.8 ± 2.1% of embryos surviving until 72 hpf. The survival rate of embryos derived from inter-crossing *grhl3*$^{+/-(-31bp)}$ fish at 1 μM, 2 μM, and 3 μM were 81.9 ± 5.65%, 75.8 ± 1.1% and 54.8 ± 6.0% respectively and showed no significant differences relative to controls (73.9 ± 1.1%) (Figure 6.9C). Therefore, administration of curcumin at 4 μM poses toxicity to WT, *grhl3*$^{-/-(-31bp)}$ and *grhl3*$^{-/-(1-Δ4)}$ embryos.

Key findings on phenotypic incidence: The overall phenotypic incidence of *grhl3*$^{-/-(1-Δ4)}$ mutants at 1 μM, 2 μM, 3 μM and 4 μM curcumin treatment was 11.7 ± 6.8%, 10.7 ± 2.8%, 4.9 ± 4.2% and 7.0 ± 5.1% respectively and % of *grhl3*$^{-/-(1-Δ4)}$ mutants in control was 15.7 ± 6.0% (Figure 6.10B). 8.2 ± 6.9%, 0%, 16.7 ± 27.9%, 52.8 ± 3.9% and 9.0 ± 2.1% of *grhl3*$^{-/-(-31bp)}$ phenotypic mutants was observed at 1 μM, 2 μM, 3 μM, 4 μM concentrations of curcumin and control respectively (Figure 6.10A).

Statistical analysis showed that curcumin treatment at 3 μM in *grhl3*$^{-/-(1-Δ4)}$ embryos led to a 10% increase in non-phenotypic siblings and 10.76% reduction in phenotypic mutants relative to controls. Likewise, curcumin administration at 2 μM in *grhl3*$^{-/-(-31bp)}$ embryos showed an 9.03% increase in non-phenotypic siblings and a 9.03% decrease in phenotypic mutants when compared to control. No *grhl3*$^{-/-(-31bp)}$ embryos with class 1, class 2 and class 3 phenotypes were reported when treated at 2 μM. A fall in the number of both class 1 and non-phenotypic embryos was observed at 4 μM treatment, possibly due the lethal effect of curcumin at high dosages (Figure 6.10A-B).

WT and *grhl3*$^{+/-}$ embryos treated at 4 μM showed an array of distinct phenotypes. Approximately 2% of the WT and 25% of *grhl3*$^{+/-}$ treated embryos showed a "hook-like"-tail phenotype similar to class 1 phenotype of *grhl3*$^{-/-}$ embryos; 14% of the WT embryos displayed severe resorption of yolk sac and no development past the yolk sac, phenotype comparable to class 3 phenotype of *grhl3*$^{-/-}$ embryos and about 55%-62% of the WT and *grhl3*$^{+/-}$ larvae exhibited deposition of curcumin in their yolk sac and rest of the body (Figure 6.10C).

Figure 6.9 Effects of curcumin on the survival rate of embryos derived from inter-crossing *grhl3*^{+/-} adult zebrafish and WT embryos.

Embryos were exposed to curcumin (1 μM, 2 μM, 3 μM, and 4 μM) at 0 hpf. **(A)** Survival rate of curcumin treated WT embryos relative to control (0.1% DMSO) (n=3). **(B)** Survival rate of embryos derived from inter-crossing *grhl3*$^{+/-(1-Δ4)}$ adult zebrafish following curcumin treatment relative to control (0.1% DMSO) (n=3). **(C)** Survival rate of embryos derived from inter-crossing *grhl3*$^{+/-(-31bp)}$ adult zebrafish following curcumin treatment. Data is represented as mean ± SEM. Statistical significance determined by Multiple t-tests with correction for multiple comparisons using the Holm-Sidak method; *$P < 0.05$; ***$P < 0.005$; ****$P < 0.001$; ns – non-significant.
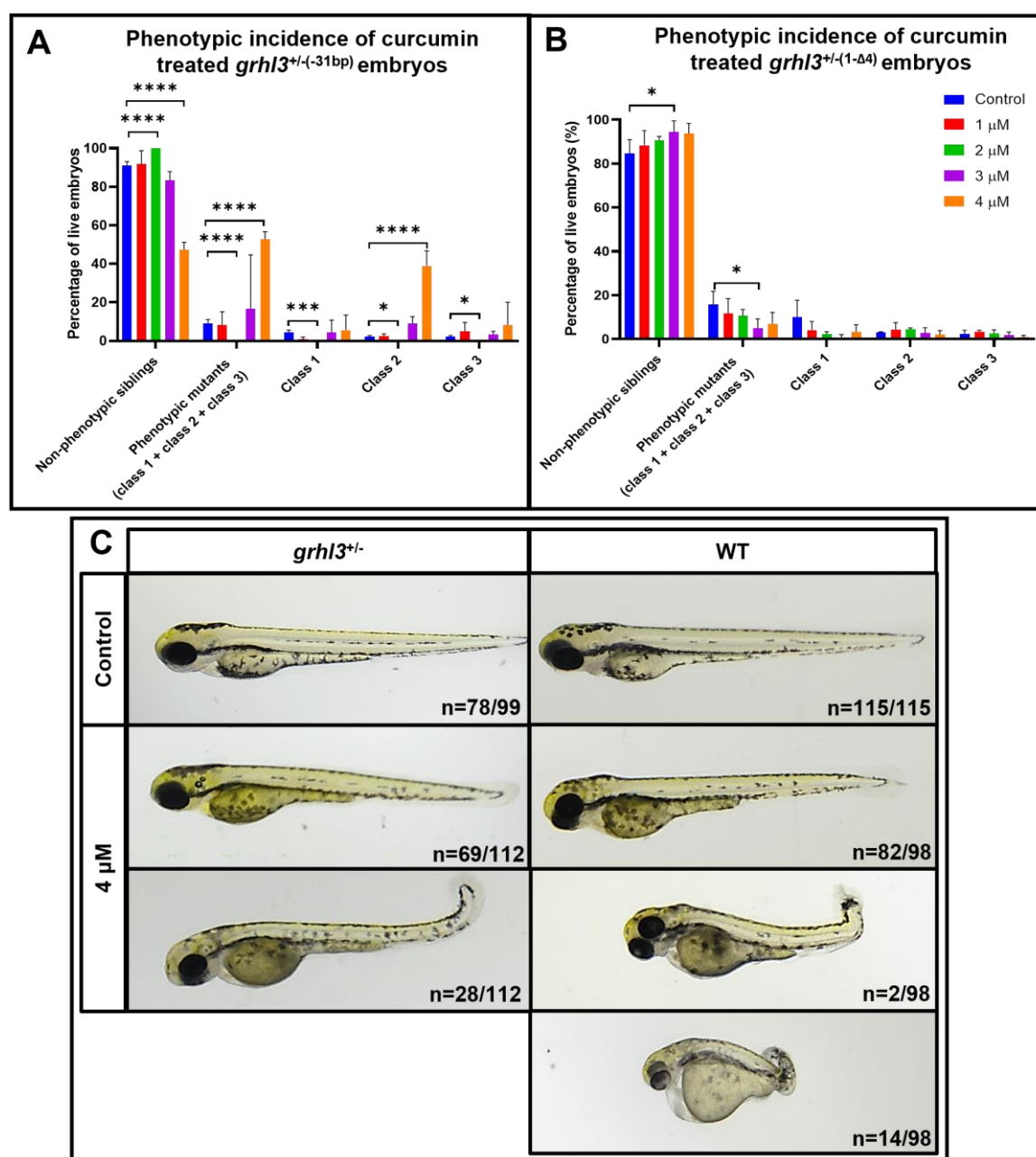
Figure 6.10 Effect of curcumin on the phenotypic incidence of embryos derived from inter-crossing *grhl3*^{+/-} adult zebrafish.

(A-B) Phenotypic incidence of class 1, class 2, and class 3 *grhl3*$^{-/-(1-Δ4)}$ and *grhl3*$^{-/-(-31bp)}$ embryos at 72 hpf, post curcumin treatment (n=3). (C) Phenotypes observed in curcumin (4 μM) treated WT embryos vs. *grhl3*$^{+/-}$ embryos. Data is represented as mean ± SEM. Statistical significance determined by Multiple t-tests with correction for multiple comparisons using the Holm-Sidak method *P < 0.05; ***P < 0.005; ****P < 0.001.

Summary: Curcumin treatment at concentrations of 2 μM and 3 μM showed an overall increase in non-phenotypic siblings and a decrease in phenotypic mutants, thereby showing a rescue in the severity of phenotypes. However, lethality and toxicity-induced aberrant phenotypes were observed at 4 μM in both embryos derived from inter-crossing

$grhl3^{+/-}$ adult zebrafish and WT embryos, suggesting that high concentrations ($\geq$ 4 μM) of curcumin may pose toxicity to the development of embryos.

▪ *Luteolin*

Dosage range tested: 1 μM, 2.5 μM, 5 μM, 10 μM and 20 μM.

Key findings on survival rates: Survival rate of WT treated embryos at dosages 1 μM – 20 μM ranged between ~98-100% while that of control was 94.3% (Figure 6.11A). Embryos derived from inter-crossing $grhl3^{+/-}$ adult zebrafish treated with 1 μM, 2.5 μM, 5 μM, 10 μM and 20 μM showed survival percentage of 82.65 $\pm$ 9.3%, 81.7 $\pm$ 5.7%, 75.7 $\pm$ 4.4%, 68.1 $\pm$ 1.0%, and 69.4 $\pm$ 1.9% respectively and control embryos showed survival % of 87.9 $\pm$ 2.1% (Figure 6.11B). Upon statistical analysis, it was found that the survival rate of treated WT embryos was significantly greater than that of control at 72 hpf. In contrast, treatment at 5 μM, 10 μM and 20 μM, showed a drop in the survival rate of embryos derived from inter-crossing $grhl3^{+/-}$ adult zebrafish.

Key findings on phenotypic incidence: The overall phenotypic incidence of $grhl3^{-/-}$ mutants at 1 μM, 2.5 μM, and 5 μM concentrations was 14.9 $\pm$ 9.1%, 12.8 $\pm$ 3.8%, and 8.9 $\pm$ 2.3% respectively. In control embryos, 10.2 $\pm$ 8.8% $grhl3^{-/-}$ mutants was present (Figure 6.11C). At dosages of 10 μM and 20 μM, the phenotypic mutants were completely absent. Although class 1 and class 3 mutants were absent at 10 μM and 20 μM luteolin treatments, statistical analysis revealed no significant difference relative to controls. However, absence of class 2 phenotypic mutants showed significant decline (3.08%) in their percentage when compared to controls.

Summary: High mortality was seen in embryos derived from inter-crossing $grhl3^{+/-}$ adult zebrafish, while WT embryos showed improved survival. Furthermore, it is clear from the studies conducted that the embryos dying are primarily $grhl3^{-/-}$ mutants since they are completely absent at 10 μM and 20 μM, suggesting the toxic effects of luteolin on $grhl3^{-/-}$ embryos.
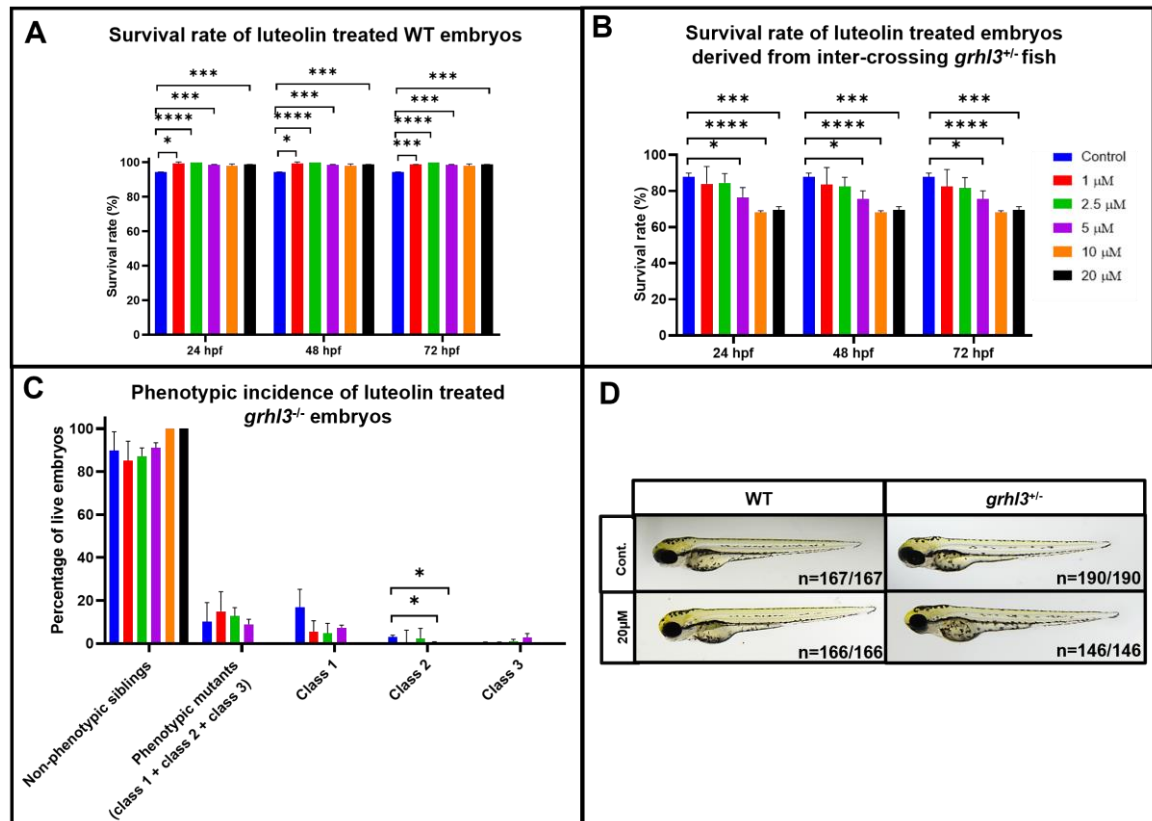
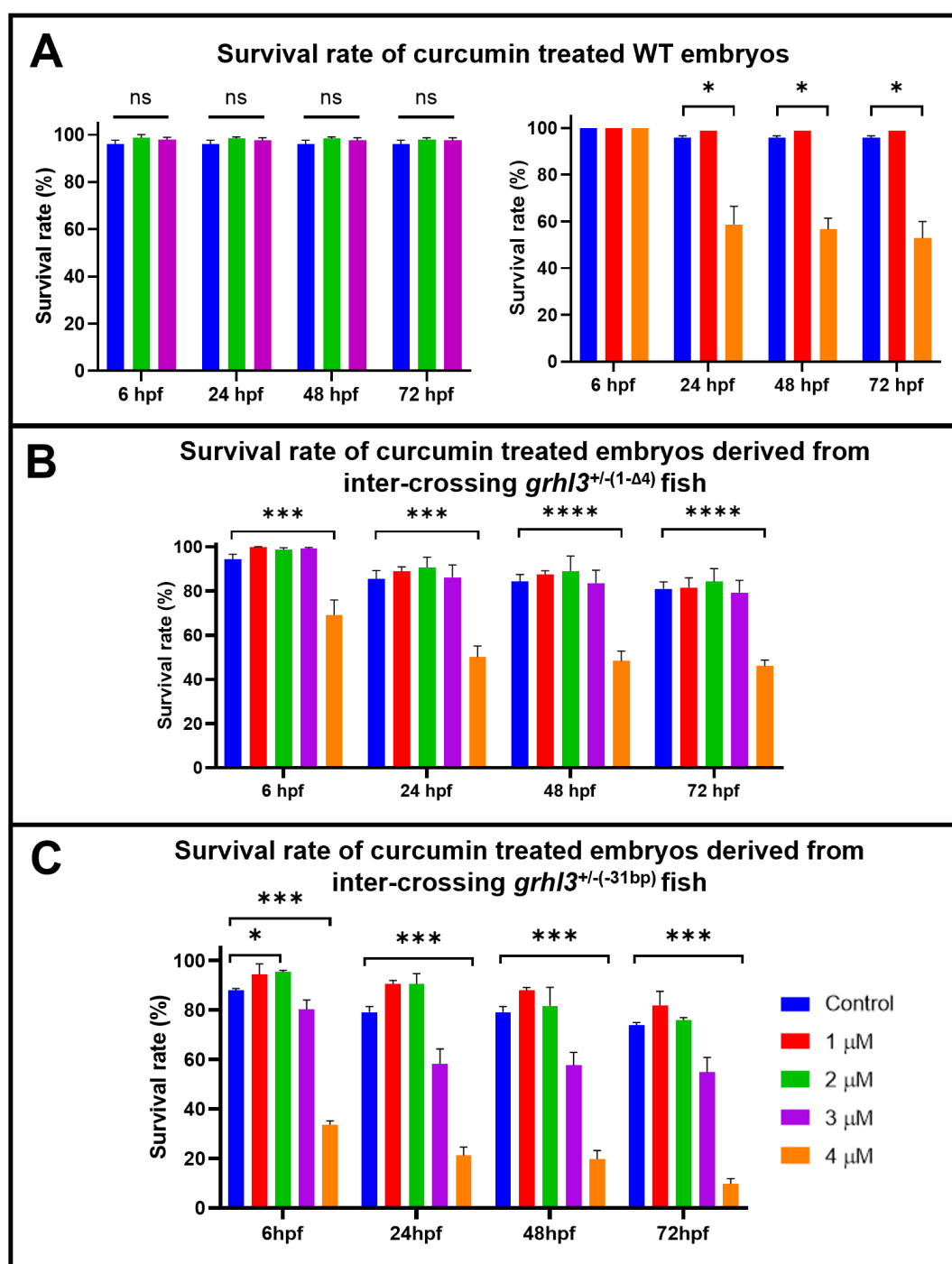**Figure 6.11 Effects of luteolin on embryos derived from inter-crossing *grhl3*^+/- adult zebrafish and WT embryos.**

Embryos were exposed to luteolin (1 μM, 2.5 μM, 5 μM, 10 μM and 20 μM) at 0 hpf. **(A)** Survival rate of luteolin treated WT embryos relative to control (0.2% DMSO) (n=3). **(B)** Survival rate of embryos derived from inter-crossing *grhl3*^+/-adult zebrafish following luteolin treatment relative to control (0.2% DMSO) (n=3). **(C)** Phenotypic incidence of class 1, class 2, and class 3 *grhl3*^-/-embryos at 72 hpf, post luteolin treatment **(D)** Phenotypes observed in luteolin (20 μM) treated *grhl3*^+/ - vs. WT embryos. Data is represented as mean ± SEM. Statistical significance determined by Multiple t-tests with correction for multiple comparisons using the Holm-Sidak method; *P < 0.05; ***P < 0.005; ****P < 0.001.

6.5 Discussion

Altering the chorion permeability for the passage of chemicals

Zebrafish embryos are surrounded by a chorion during the early stages of development. This 1.5-2.5 μm thick acellular envelope comprises numerous canals, the pore size of which is approximately 0.6-0.7 μm. Numerous studies have suggested that chorion may act as a barrier to the entry of chemicals into the developing embryo (Kais, Schneider et al. 2013). Furthermore, the narrow diameter of the canals has been hypothesized to prevent the uptake of compounds depending on their size (Rawson, Zhang et al. 2000).

Several attempts have been made to eliminate the chorion prior to 24 hpf, but this has often resulted in poor survival rate. Therefore, most studies continue to perform chemical screens on embryos with the chorion still intact (Henn and Braunbeck 2011). The major setback is that it leads to substantial limitations on chemical access to the embryo, posed by the permeability of chorion. Furthermore, compounds that interfere with the hatching of embryos can also cause secondary phenotypic responses due to the restricted development of embryos within the chorion (Zhou, Dong et al. 2009). Thus, there is a greater incidence of generating false negative results in chemical toxicity assays due to the presence of chorion.

Enzyme-supported dechorionation of zebrafish embryos using pronase (1 mg/ml) is generally recommended for embryos at 24 hpf or older (Westerfield 2000). Pronase administration at 1 mg/ml on embryos derived from inter-crossing $grhl3^{+/-}$ adult zebrafish and WT embryos, performed at ~2 hpf resulted in increased incidence of embryonic death, with only about 20% of embryos surviving, consistent with previous observations made by Henn and Braunbeck 2011. When dosages lower than 1 mg/ml were tested (0.25 mg/ml and 0.5 mg/ml), embryos derived from inter-crossing $grhl3^{+/-}$ adult zebrafish again showed an increased lethality rate with <10% embryos surviving at 72 hpf. Thus, pronase mediated dechorionation is not a suitable option for removal of chorion in embryos <24 hpf.

The difficulties faced in chorion removal has encouraged researchers to identify solvents that alter chorion permeability. DMSO, a commonly used solvent to dissolve chemicals has been found to compromise chorion barrier function (Rammler and Zaffaroni 1967) at concentrations 0.1%-1% (Kais, Schneider et al. 2013). As an effective solvent carrier, DMSO transports test chemicals across the chorion to the developing embryo but not for

further passage into the embryo (Kais, Schneider et al. 2013). For the effective passage of environmental factors used in this study, I dissolved the vitamins/polyphenols at low DMSO concentrations of 0.1% and 0.2%. Hence, treatment of DMSO at 0.1% and 0.2% was done to evaluate its safety on WT and *grhl3*^{-/-} embryos. No toxicity was seen and no significant variation in phenotypic incidence in *grhl3*^{-/-} embryos was observed when compared to untreated controls. These data show that DMSO is safe and poses no toxicity related effects (LC10: 30g/L (0.3%) (Hallare, Nagel et al. 2006, Maes, Verlooy et al. 2012).

Increased chorion permeability by DMSO has been observed only until 26 hpf (Kais, Schneider et al. 2013). Beyond this developmental stage, a structural change in chorion takes place due to the proteolytic activities in pre-hatching stages (Kim, Sun et al. 2004). Furthermore, other factors such as molecular mass of the test chemical also plays a critical role in the transport across the chorion, since the movement of bulky chemical molecules has been restricted even when dissolved in DMSO (Kais, Schneider et al. 2013). Keeping the above limitations in mind, test chemicals dissolved in DMSO were treated at 0 hpf for better penetration of chemicals and chemicals with large molecular size were avoided for the study.

Significance of vitamins, minerals, and polyphenols on the epithelial establishment of *grhl3*^{-/-} embryos

Myoinositol (vitamin B8) administration (6.75-37.5 mg/ml) did not alleviate, nor did it exacerbate the severity of phenotypes in *grhl3*^{-/-} treated zebrafish embryos. Absence of *grhl3* in zebrafish embryos causes myoinositol to not offer protective effects from NTDs, as seen in the *Grhl3*^{-/-} mouse model (Ting, Wilanowski et al. 2003). However, *curly tail* mouse with hypomorphic *Grhl3* function showed a rescue with inositol treatment. The discrepancies in the effects of myoinositol might be because of the greater severity of NTDs observed in *Grhl3* null mice as opposed to *curly tail* mice. Furthermore, phosphorylation of inositol produces an array of phosphoinositide having a range of cellular functions in signalling and membrane dynamics (Di Paolo and De Camilli 2006). This key process is integral for prevention of NTDs in *curly tail* strains as any hindrance in phosphate recycling deters the protective effect it has to offer (Greene and Copp 1997). There is a likelihood that *grhl3* mutation causes poor expression of genes responsible for the phosphorylation of inositol, thereby showing no visible effect on the *grhl3*^{-/-} zebrafish model.

Nicotinamide/niacin is crucial for cholesterol-lipoprotein metabolism (Huang, Voyiaziakis et al. 1995) and impaired biosynthesis of cholesterol contributes to severe growth retardation and defective neural tube closure (Tozawa, Ishibashi et al. 1999). However, niacin treatment like myoinositol showed neither exacerbation nor amelioration of axial defects in *grhl3*^{-/-} embryos. Since there were no studies done on niacin supplementation in zebrafish embryos, I performed dosage studies at low concentrations ranging between 1 μM -20 μM. Thus, the dose range administered may not be adequate to produce any obvious results and studies in future should employ higher dosages to determine the efficacy of niacin in rescuing the *grhl3*^{-/-} phenotypes.

Studies have claimed that niacin in conjunction with thiamine and pyridoxine prevents orofacial clefts (Krapels, van Rooij et al. 2004). However, the mechanism by which they prevent orofacial defects is uncertain. These vitamins are critical to breakdown fats, carbohydrates, and proteins for energy supply to cells. Supply of energy to cells is integral for development of lip/palate and other organs (Krapels, van Rooij et al. 2004). Because of the strong correlation between niacin, thiamine and pyridoxine in epithelial development, future studies with concomitant supplementation of these B vitamins in *grhl3*^{-/-} embryos must be performed to see whether there is a rescue observed in jaw defects of *grhl3*^{-/-} embryos when opposed to thiamine or niacin being used individually.

Similarly, future studies must incorporate both B_{12} and folate to rescue the phenotypes observed in *grhl3*^{-/-} embryos, since B_{12} treatment alone, only showed a slight phenotypic shift in the severity of *grhl3*^{-/-} embryos. This is because B_{12} (cobalamin) is metabolically related to folate, and when supplemented in conjunction with folate during pregnancy, it was found to further decrease the incidence of NTDs in infants (Candito, Rivet et al. 2008). As a co-factor to enzyme methionine synthase, cobalamin converts homocysteine to methionine (Banerjee 1999). Folate derived methyl groups are then converted into several by-products including methyl DNA and methylated proteins, that are critical to drive differential gene expression (Rochtus, Izzi et al. 2015). Furthermore, B_{12} plays a critical role in the incorporation of folates into the cellular pool and the flux of folate derived 1-carbon units during DNA synthesis or methylation reactions (Molloy, Kirke et al. 2009). DNA synthesis is essential for embryonic development, and the disruption of these processes can contribute to folate or B12 responsive NTDs.

Potassium iodide used in lower dosages prevents oxidative damage of membrane lipids in porcine thyroid gland (Milczarek, Stępniak et al. 2013). However, excess iodine can

cause toxicity due to its pro-oxidative action (Joanta, Joanta et al. 2006, Xia, Qu et al. 2013). This might explain why we see increased death in embryos derived from *grhl3*^{+/-} fish and WT embryos at 10 mg/ml. Similarly, high concentration of RSV acts as a pro-oxidant, contributing to DNA damage and activation of cytotoxic and apoptotic pathways (De La Lastra and Villegas 2007, Liu, Wu et al. 2017), primary reason for the significant lethality seen in RSV treated embryos. Another interesting point to note is that RSV acts as a hypo pigmenting agent preventing keratinocyte induced melanocyte stimulation (Na, Shin et al. 2019), which is probably why we see poor melanocyte formation when embryos were subjected to treatment at 200 μM.

Curcumin strengthens and maintains epithelial integrity (Wang, Wang et al. 2012, Titto, Ankit et al. 2020). Studies on zebrafish embryos indicated that embryos survived well following treatment with 5 μM curcumin but showed several developmental defects like hook-like tail, retarded yolk sac resorption, bent tail and shorter body length (Wu, Lin et al. 2007). Observations from my study on both WT embryos and embryos derived from inter-crossing *grhl3*[+/-]adult zebrafish indicate toxicity at 4 μM causing lethality of treated embryos along with the above-mentioned developmental defects. Toxicity and the developmental defects owing to curcumin exposure could be attributed to dysregulation of several genes. One such gene is sarco-/endoplasmic reticulum Ca^{2+} ATPase (SERCA), crucial to maintain low Ca^{2+} concentration within cells (Bilmen, Khan et al. 2001). In addition, higher dosage of curcumin increases the cellular reactive oxygen species (ROS) such as superoxide anion and hydrogen peroxide (Cao, Jia et al. 2006, McNally, Harrison et al. 2007, López-Lázaro 2008). ROS can induce cell malignant transformation and possibly cause death of the cell (Suh, Arnold et al. 1999, Arnold, Shi et al. 2001). Thus, it is critical to identify an optimum concentration of curcumin to prevent death due to toxicity.

Loss of *grhl3* in our zebrafish model causes an increase in oxidative stress (we have shown that the genes responsible for reducing hydroperoxide activity, *gpx4a* and *gpx4b* are over-expressed [*our unpublished data*]). I, therefore, speculate that curcumin acts as an antioxidant during early developmental phases to reduce the hydroperoxide activity, thereby alleviating the phenotypic severity seen in *grhl3*^{-/-} embryos. Therefore, we see a phenotypic rescue in *grhl3*^{-/-} embryos when treated with 2 μM and 3 μM curcumin. Similarly, luteolin acts as an antioxidant (Shimoi, Masuda et al. 1994, Romanova, Vachalkova et al. 2001) during early developmental phases thereby showing improved

survival of WT embryos. Thus, polyphenols at optimum concentration act as excellent antioxidants during the early developmental phases.

6.6 Conclusion and future directions

Determining environmental factors that interact with abrogated *grhl3* function is likely to uncover viable therapeutic options for the prevention of *Grhl3*-dependent epithelial birth defects. Few of these chemicals had no effect, possibly because of the poor metabolism of chemicals due to unique therapeutic indices and routes of administration. Furthermore, the molecular size of the drug might be difficult to permeate the chorion. Thus, it is critical to quantitate the molecular size of the compound via gel permeation chromatography or size exclusion chromatography. Lastly, mass spectrometric analysis of the treated embryos must be performed to confirm the entry of drug into the embryo. Overcoming these limitations in future might help us understand the effects of these vitamins better on the development of *grhl3*$^{-/-}$ zebrafish embryos.

Curcumin was the only compound to show a rescue in the phenotypic severity of *grhl3*$^{-/-}$ embryos. In future, it may be worthwhile to explore the mechanism of curcumin action on *grhl3*$^{-/-}$ embryos and understand the possible interaction between *grhl3* and curcumin. Curcumin can then be tested on the *curly tail* mouse model as a prelude to using curcumin in the maternal diet during pregnancy for the prevention of epithelial birth defects. Identifying such novel therapeutic agents can help prevent the incidence of epithelial birth defects in future.

Table 6.1 Summary of chapter 6 findings

	Concentration	Effect on survival rate	Effect on phenotypic severity	Phenotypes in *grhl3*^{+/-} embryos
Vitamin/Mineral				
Myoinositol	6.75 mg/ml, 12.5 mg/ml, 25 mg/ml, 37.5 mg/ml, 50 mg/ml, 75 mg/ml.	None	37.5 mg/ml: ↑ class 2 *grhl3*^{-/-} embryos. 50 mg/ml and 75 mg/ml : ↓ class 3 *grhl3*^{-/-} embryos.	No aberrant phenotype.
Nicotinamide	1 µM, 2.5 µM, 5 µM, 10 µM, 20 µM.	None	None	No aberrant phenotype.
Thiamine chloride	1 µM, 2.5 µM, 5 µM, 10 µM, 20 µM.	None	1 µM and 2.5 µM: ↓ class 1 *grhl3*^{-/-} embryos.	No aberrant phenotype.
Cobalamin	1 µM, 2.5 µM, 5 µM, 10 µM, 20 µM.	2.5 µM: ↓ survival of *grhl3*^{-/-} and *grhl3*[+/?] embryos. 10 µM: ↓ survival of *grhl3*^{-/-} and *grhl3*[+/?] embryos (only at 72 hpf)	1 µM and 2.5 µM: class 3 *grhl3*^{-/-} embryos absent.	No aberrant phenotype.
Potassium Iodide	2.5 mg/ml, 5 mg/ml, 10 mg/ml.	10 mg/ml : ↓ survival of *grhl3*^{-/-} and *grhl3*[+/?] embryos.	10 mg/ml : absence of class 2 embryos	poor eye development, axial defects
Polyphenol				
Resveratrol	50 µM, 100 µM, 150 µM, 200 µM.	50 µM - 200µM: ↓ survival of *grhl3*^{-/-} / *grhl3*[+/?] embryos.	50 µM, 100 µM, 150 µM, and 200 µM : class 1 *grhl3*^{-/-} embryos absent. 100 µM and 150 µM: ↓ class 2 *grhl3*^{-/-} embryos.	Poor melanocyte formation and haemorrhage at 200 µM.
Curcumin	1 µM, 2 µM, 3 µM, 4 µM.	4 µM: ↓ survival of *grhl3*^{-/-} and *grhl3*[+/?] embryos.	2 µM : *grhl3*[-/-(-31bp)] embryos with class 1, class 2 and class 3 phenotypes absent. 3 µM : ↑ non-phenotypic siblings and ↓ phenotypic *grhl3*[-/-(1-Δ4)] embryos. 4 µM : ↓ class 1 *grhl3*^{-/-} and non-phenotypic embryos.	Hook-like-tail; severe resorption of yolk sac and no development past the yolk sac; deposition of curcumin.
Luteolin	1 µM, 2.5 µM, 5 µM, 10 µM, 20 µM.	1µM -20 µM: ↓ survival of *grhl3*^{-/-} / *grhl3*[+/?] embryos.	10 µM and 20 µM: ↓ in class 2 *grhl3*^{-/-} embryos.	No aberrant phenotype.

Chapter 7: General discussion and concluding remarks

7.1 Introduction

Epithelial establishment relies on the complex synergies of numerous molecular pathways, comprising hundreds of genes. One such critical epithelial gene pathway is that controlled by *grhl3*, a gene that regulates the homeostatic maintenance of epithelial formation and repair (Bray and Kafatos 1991, Wilanowski, Tuckfield et al. 2002, Ting, Wilanowski et al. 2003, Auden, Caddy et al. 2006, Miles, Darido et al. 2017). The work presented in this thesis characterises the genetic pathways regulated by *grhl3* in epithelial development, and the environmental factors that can impart both positive and negative consequences to epithelial development in the context of impaired *grhl3* function.

To understand the role of *grhl3* in epithelial homeostasis, a CRISPR/Cas9-mediated zebrafish *grhl3* knockout model was generated. Characterization of *grhl3*^{-/-} embryos showed axial phenotypes, craniofacial abnormalities, and aberrant formation of intestinal epithelia (at 7 dpf). Together, these data highlight the roles of *grhl3* in epithelial development of zebrafish embryos as revealed in chapter 3.

As TFs, *grh/Grhl* proteins bind to promoters of target genes to regulate transcription. In-silico and meta-analysis approach described in chapter 4 identified several genes that showed differential expression following *grhl3* de-regulation. From the genes identified via bioinformatic analysis, 4 genes, *pvrl4*, *tbc1d2*, *gldc*, and *tmem54* were selected for knockout/knockdown and rescue experiments in chapter 5. From these experiments, *tmem54a* and *pvrl4* were revealed to be critical in orofacial development and axial patterning. Furthermore, *pvrl4* was identified to partially rescue the phenotypic severity of *grhl3*^{-/-} embryos, signifying the importance of *grhl3-pvrl4* pathway in epithelial establishment. Thus, in chapter 4 and 5, I found *pvrl4* and *tmem54a* genes to be critical drivers of epithelial formation and craniofacial development, paving way for future experiments with these genes in higher model organisms.

Apart from genetic factors that interact with *Grhl3* during epithelial homeostasis, *Grhl3*-deficiency in mice has been found to be significantly influenced by environmental factors (Seller, Embury et al. 1979, Seller and Perkins 1982, Seller and Perkins-Cole 1987, Greene, Leung et al. 2017). In chapter 5, a rescue was seen in the phenotypic severity of *grhl3*^{-/-} embryos upon exposure to curcumin (2-3 µm). Screening such environmental factors that rescue epithelial defects in *grhl3*^{-/-} embryos paves way to identifying therapeutic factors that can be used in humans to prevent developmental defects.

This final chapter will discuss the findings from this thesis within the context of current literature and provide insights into where this work might be applicable in future.

7.2 Unravelling the functions of *grhl3*

In chapter 3, using *grhl3*$^{-/-}$ zebrafish embryos, I characterised several roles of *grhl3* in epithelial establishment. To characterize the *grhl3*$^{-/-}$ embryos, *grhl3*$^{+/-}$ fish lines were inter-crossed and null embryos were collected. *grhl3*$^{-/-}$ embryos were then screened for the presence of phenotypic defects via light microscopy. At 48 hpf, 3 different phenotypes showing varying degrees of axial defects were observed. Based on their severity they were classified as class 1, class 2, and class 3, with class 1 showing a less severe axial defect and class 3 showing an extremely severe phenotype. Furthermore, quantitation of the body length of these null embryos showed significant reduction in the body length relative to controls. Thus, the axial defects along with the reduction in body length seen in *grhl3*$^{-/-}$ embryos signifies the importance of *grhl3* in axial patterning.

Secondly, cartilage staining (using Alcian Blue) was performed to visualize the craniofacial cartilage in *grhl3*$^{-/-}$ embryos (4 dpf). *grhl3*$^{-/-}$ embryos were presented with loss of ceratobranchials and showed reduction in the length between (a) upper and lower jaw and (b) Meckel's cartilage and ceratohyal. In addition, histological examination of sections taken along the orofacial region of *grhl3*$^{-/-}$ embryos at 7 dpf showed a reduction in the size of orofacial cavity. These findings suggest that *grhl3* is critical for the formation of craniofacial cartilage in zebrafish larvae.

Lastly, histological examination was performed in the gut epithelia at 5 dpf and 7 dpf *grhl3*$^{-/-}$ embryos. No intestinal epithelial defects were detected at 5 dpf, however, at 7 dpf, the intestinal epithelial cells were highly disorganized and the apical and basement membranes were poorly established, suggesting a link between *grhl3* and the formation of intestinal epithelia. Thus, from this study I concluded that *grhl3* plays an integral role in axial patterning, craniofacial development, and intestinal epithelial homeostasis of zebrafish embryos. However, the mechanisms by which *grhl3* regulate some of these processes still remain unclear and could not be explored due to time constraints.

In mammals, convergent-extension (CE) mediated cell movements during axial patterning is largely dependent on the establishment of correct planar cell polarity brought about by the genetic interaction of *Grhl3* with Planar Cell Polarity (PCP) genes (Caddy,

Wilanowski et al. 2010). Although the mechanism of neural tube closure in zebrafish differs from that of mammals, the convergent-extension movements of the pre-tubular plate, i.e., 'primary neurulation' has been found to be similar in fish and other vertebrates (Lowery and Sive 2004). Therefore, I believe the deregulation of PCP genes contributes to axial defect in *grhl3*^{-/-} embryos. Determining the localisation of PCP proteins (i.e., disrupted polarity of cells), via immunostaining of PCP antibodies (i.e., anti-v*angl2*, anti-*Celsr1* and anti-*Scrb*) on *grhl3*^{-/-} embryos will help elucidate the mechanism involved in neurulation and axial patterning of *grhl3*^{-/-} embryos.

The pathway underlying craniofacial development has been well studied in *grhl3* morphants (Dworkin, Simkin et al. 2014), however, I am yet to validate the pathway involved in CRISPR generated *grhl3* knockout embryos. The craniofacial abnormalities seen in *grhl3*^{-/-} mutants include absence of ceratobranchials and basihyal strikingly similar to the jaw deformities observed in *grhl3* morphants (discussed in chapter 3). Thus, I believe that disrupted *edn1/dlx3/hand2* signalling in pharynx contributes to apoptosis of NCCs causing craniofacial defects in *grhl3*^{-/-} embryos as observed in *grhl3* morphants (Dworkin, Simkin et al. 2014). *edn1*, a direct target of *grhl3* (Dworkin, Simkin et al. 2014) regulates its downstream effectors, *dlx3* and *hand2* for the survival and proliferation of NCCs to form the craniofacial cartilage (Dworkin, Simkin et al. 2014). It is thus important to perform apoptotic analysis (TUNEL assays) along the pharyngeal arches and evaluate the expression of *edn1*, and its downstream targets *dlx3* and *hand2* in *grhl3*^{-/-} embryos via in-situ hybridization to confirm my hypothesis.

Lastly, preliminary studies identified the presence of intestinal epithelial deformities at 7 dpf in *grhl3*^{-/-} embryos. It is hypothesized that craniofacial defects lead to poor consumption of rotifers (microscopic planktonic aquatic animals). Thus, lack of nutrients contributes to poor development of intestine (Watts, Powell et al. 2012). Firstly, to verify the presence of intestinal epithelial defects, expression of epithelial markers such as vimentin (*vim*), epithelial cellular adhesion molecule (*epcam*) and e-cadherin (*cdh1*) must be evaluated (via immunohistochemistry) on intestinal sections. Abnormal expression of these markers confirms the presence of EMT defects in the intestine. In addition, in-situ hybridization must be performed to determine the expression of intestinal formation genes such as hes (Ueo, Imayoshi et al. 2012) and hox-family (Beck 2002) of genes. This would suggest the mechanism involved in the aberrant formation of intestinal epithelia in *grhl3*^{-/-} embryos . Lastly, to test my hypothesis, I must determine the acquisition of microbiota in

grhl3^{-/-} mutants vs. control. To do this, fluorescence in-situ hybridization with oligonucleotides targeting sequences of bacterial 16s RNA ribosomal genes must be performed (Bates, Mittge et al. 2006). Absence of colonization of microbiota at 7 dpf in *grhl3* mutants suggests that poor consumption of nutrients results in intestinal defects.

7.3 Significance of potential targets of *grhl3*

In-silico analysis and meta-analysis of published *grhl* RNA-Seq datasets identified potential targets of *Grhl* signalling. For in-silico analysis, the promoters of all mammalian genes were aligned and searched for the *grhl* binding site as stated earlier. The candidate genes identified via this method, were compared with the genes differentially regulated in the 1st pharyngeal arch of *Grhl2* mouse. 21 genes were found to be both a predicted target (PHYLO-PROM), and a differentially regulated (1st pharyngeal arch RNA-SEQ data dataset) gene of *Grhl*. In our meta-analysis approach, 41 *grh/Grhl* RNA-Seq datasets were collated and genes that were differentially expressed following *grhl* loss across disparate contexts as well as those having roles in specific processes such as that of epithelial development were identified. In primary epithelia, 10/18 *grhl* differentially regulated genes showed significant differences in expression between *grhl3*^{-/-} and WT zebrafish embryos following Q-RT-PCR from 48 hpf embryos, signifying the strong predictive power of this approach. Furthermore, 30% of the genes differentially regulated following down-regulation of *Grhl* across all tissues and cell lines were found to be bound by *grh/Grhl* factors from published ChIP seq datasets (Mathiyalagan, Miles et al. 2019), demonstrating the reliability of this approach.

ChIP Seq identifies the transcription factors that bind to the *Grhl* factor in a particular tissue/cell line (Park 2009). In this technique, cross links are initially made between the protein of interest and DNA, followed by shearing of DNA and addition of antibodies to immunoprecipitate the target protein. Finally, the proteins are precipitated, and the DNA is purified and sequenced (Mardis 2007). This will identify *grhl3* targets and help understand the transcriptional regulation by *grhl3* of its targets in various biological processes. Thus, in future, to conclusively state the gene identified as a target of *grhl*, it is necessary to validate the protein-DNA interactions using assays such as Chromatin Immunoprecipitation (ChIP), promoter pull down assays and DNA electrophoretic mobility shift assay (EMSA). Identifying the targets of *grhl3* will help delineate the molecular pathways involved in epithelial homeostasis.

Knockout/knockdown-based experiments of potential targets of *grhl3* i.e., *tbc1d2, pvrl4, gldc* and *tmem54* identified in chapter 4 were performed to determine their role in epithelial formation. Among the 4 genes, *tmem54a* and *pvrl4* were found to play integral roles in craniofacial formation and axial patterning.

tmem54a, one of the two zebrafish orthologues of the *tmem54* gene, encodes for a transmembrane protein. Their implications in human diseases and functions are unknown and this is the first ever study done investigating the function of this gene. Not only was *tmem54a* down-regulated following *Grhl* loss, but large-scale ChIP-Seq analysis has also confirmed that *Grhl2* binds to the promoter of this gene (Aue, Hinze et al. 2015, Walentin, Hinze et al. 2015), confirming that this gene is indeed a direct target of *grhl*-signalling. Loss of *tmem54a* contributed to curvature of body axis and severe craniofacial defects, with most of the jaw structures being completely absent. A similar degree of severe jaw deformity has been identified in zebrafish embryos lacking *hdac1*, a gene integral for the maintenance of NCC to form the craniofacial cartilage in zebrafish embryos (Ignatius, Unal Eroglu et al. 2013). *tmem54a* has been found to interact with *hdac1*, and thus, I hypothesise that the craniofacial defect observed in *tmem54a* morphants might also be due to defect in *hdac1*-dependent NCC differentiation. Evaluating the expression of NCC markers in *tmem54a* morphants, as well as robustly characterising the spatiotemporal expression pattern of *tmem54a*, will help reveal the mechanisms involved in craniofacial development. Furthermore, since I only performed gross morphology studies, it is critical to perform histological studies of various organs to more closely and completely characterise epithelial formation. In addition, generating a *tmem54a* CRISPR knockout fish will be the next step to determine the functions of *tmem54a* at later developmental points. Lastly, knockout of *tmem54* must be performed in mice and higher vertebrate model organisms to understand their epithelial function and determine whether their function is evolutionarily conserved. All these studies will shed light on the significance of *tmem54* in epithelial homeostasis.

Rescue experiments expressing mRNA of potential targets of *grhl (tbc1d2* and *pvrl4)* was performed to rescue the axial defects observed in *grhl3*^{-/-} embryos. One of the interesting findings was the decrease in class 2 *grhl3*^{-/-} embryos and an increase in *grhl3* sibling population upon injection of *pvrl4* mRNA (at 50 ng/µl) in embryos derived from *grhl3*^{+/-} fish, signifying a partial phenotypic rescue in the severity of *grhl3*^{-/-} embryos. Thus, the loss of *grhl3* can be compensated by expression of *pvrl4* mRNA, signifying its key

function in axial patterning and suggesting that *pvrl4* might be a downstream effector of *grhl3* in axial patterning.

PVRL4 is mainly implicated in the formation of e-cadherin based adherans junctions (Brancati, Fortugno et al. 2010). *E- Cadherin (cdh1)*, integral for the formation of adherans junctions (Coopman and Djiane 2016) acts downstream of *grhl3* (Phatak, Kulkarni et al. 2021). Therefore, in the absence of *grhl3*, *cdh1* is downregulated possibly contributing to epithelial defects. Microinjection with *pvrl4* mRNA possibly upregulates the expression of *cdh1,* thereby rescuing the axial defects seen in *grhl3⁻/⁻* embryos. To test this hypothesis, it is necessary to determine the expression of *cdh1* in *grhl3⁻/⁻* embryos injected with *pvrl4* mRNA vs. control at 72 hpf via Q-RT-PCR. Furthermore, ChIP assays must be performed, as this will shed light on whether *pvrl4* is a target of *grhl3* in epithelial homeostasis.

Having seen the ability of *pvrl4* to rescue *grhl3⁻/⁻* phenotypes, I investigated its role in axial patterning and craniofacial formation. MO-mediated knockdown of *pvrl4* contributed to axial defects along with pericardial edema and craniofacial defects in ~20% of embryos while rest of the embryos showed normal phenotypes. Since these phenotypes were seen only in a small proportion of embryos, I hypothesize that this may be due to non-specific phenotypic effects of morpholino rather than due to loss of *pvrl4*. Thus, generating a CRISPR knockout of *pvrl4* and characterizing this line might be the next step in unravelling the role of *pvrl4*.

7.4 Environmental factors that impact development of *grhl3*- deficient embryos

As described in chapter 1, *grhl3⁻/⁻* embryos at 11 hpf displayed rupturing of the enveloping layer during gastrulation, resulting in embryonic lethality (Miles, Dworkin et al. 2017) when housed at Monash University, Australia. However, transfer of *grhl3* lines to the La Trobe Animal Research and Teaching Facility (LARTF), Bundoora, Australia no longer showed the rupturing phenotype in *grhl3⁻/⁻* embryos. Furthermore, pilot studies in the lab showed no EVL rupture when incubation temperature was decreased from 28.5°C to 25°C, suggesting a possible rescue and improved viability of *grhl3⁻/⁻* embryos when incubated at 25°C (Miles, et.al unpublished). Hence, I presume the improved survival of *grhl3⁻/⁻* embryos at LARTF might be attributed to environmental factors such as pH, temperature, and water quality. All these factors are currently being investigated

by our research group to determine the factors that may play a key role in improving the viability of *grhl3*^{-/-} embryos.

An intact epithelium overlying the WT embryos might act as a barrier preventing the penetration of environmental factors. However, in the *grhl3* deficient embryos the presence of compromised epithelia makes them exceptionally susceptible to environmental insults, hence they act as excellent model systems to understand the effect of environmental factors. Chapter 6 discussed the effect of essential vitamins, minerals, and polyphenols on *grhl3*^{-/-} embryos. Of all the factors tested, curcumin (2-3 µM) was the only one to show a rescue in the phenotypes observed in *grhl3*^{-/-} embryos. An overall increase in the non-phenotypic sibling population and a decrease in the phenotypic mutants was observed upon curcumin treatment at concentrations 2 µM and 3 µM, signifying a rescue in the phenotypic severity of *grhl3*^{-/-} embryos. To confirm their role in the epithelial homeostasis, it is critical to investigate the formation of craniofacial cartilage and explore the epithelial histology of intestinal epithelia at 7 dpf in *grhl3*^{-/-} embryos and observe whether these defects are rescued following curcumin treatment, much like the axial phenotypes.

Once the role of curcumin in epithelial formation is established, the mechanism of curcumin action on *grhl3*^{-/-} embryos must be defined. Preliminary studies done previously in the lab showed an increase in oxidative stress in *grhl3*^{-/-} embryos (Rushton, unpublished). Since curcumin is an excellent antioxidant, it is hypothesised that curcumin acts during the early developmental phases to reduce the oxidative stress. Thus, I was inclined to carry out assays to quantify the ROS levels in curcumin treated *grhl3*^{-/-} embryos vs. control (Deng, Yu et al. 2009, Liu, Sheng et al. 2015). Understanding this is critical to determine the mechanism of curcumin action in rescuing the axial phenotypes in *grhl3*^{-/-} embryos. Unfortunately, all these hypotheses could not be tested due to the substantial impact of COVID-19 lockdown restrictions in 2020-21.
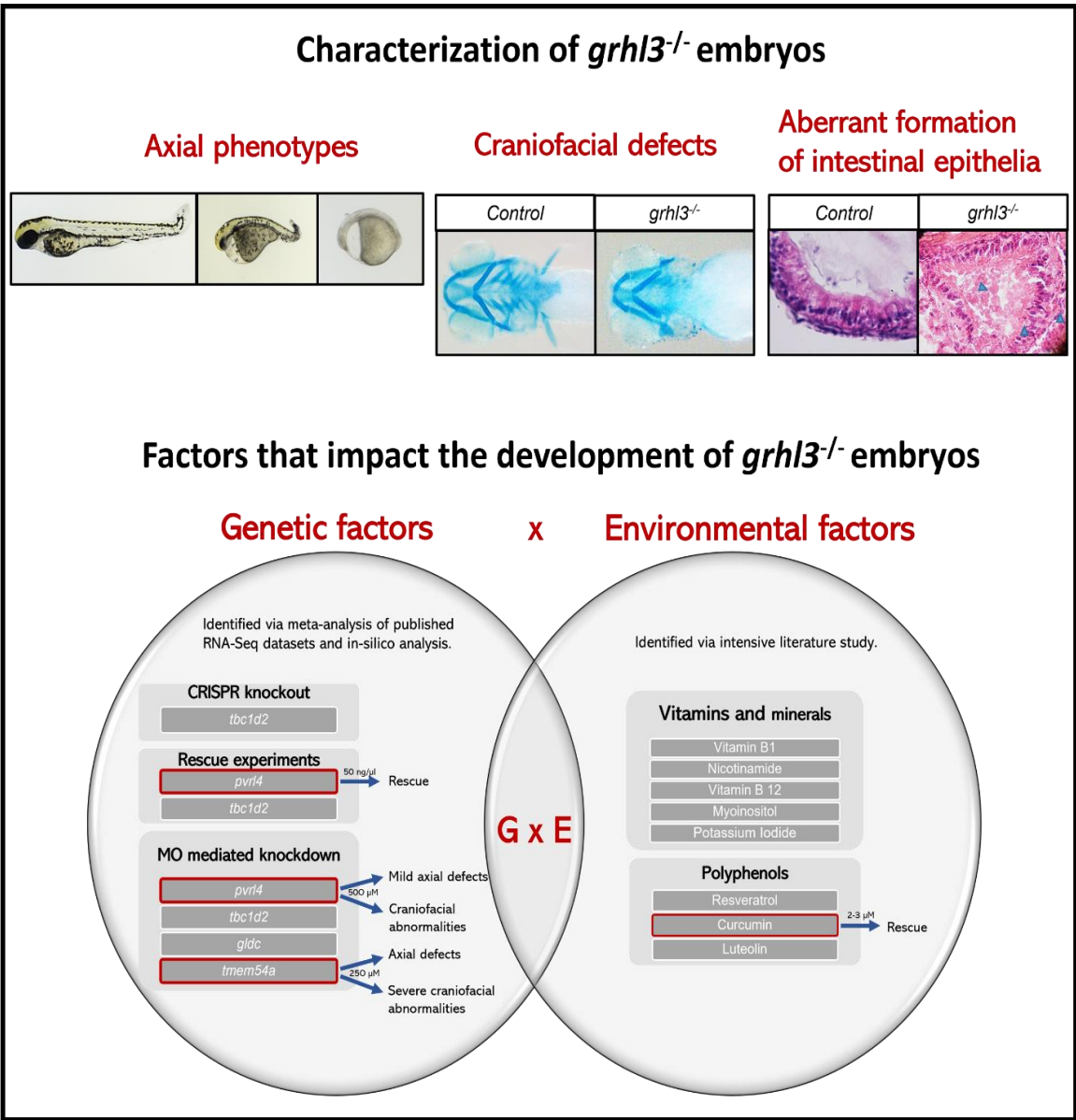
Figure 7.1 Summary of thesis findings.

In this thesis, I have demonstrated the role of *grhl3* in axial patterning, craniofacial development, and intestinal epithelial establishment. In addition, I identified potential targets of *grhl3* via meta-analysis and in-silico analysis. Of which *pvrl4, tbc1d2, gldc* and *tmem54* were selected for rescue, knockout, and knockdown based experiments. Lastly, vitamins, minerals and polyphenols were treated on *grhl3*^-/- embryos, and their impact was seen on the development of *grhl3*^-/- embryos.

7.5 Final reflections and conclusion

Congenital anomalies of epithelia are among the most frequent and debilitating birth defects. Therefore, it is critical to gain insight into the aetiology of congenital anomalies of epithelia by elucidating the genetic and environmental pathways involved in epithelial establishment. The work presented in this thesis described the role of *grhl3* and its gene regulatory network along with the environmental factors that impact *grhl3*-mediated epithelial development. Some of the key highlights of this research are described below.

Firstly, *grhl3* has been established as a critical driver in axial patterning and craniofacial development of zebrafish embryos. I speculate the axial defect seen in *grhl3$^{-/-}$* embryos to be caused by dysregulation of the PCP pathway, a pathway critical for developmental processes such as neural tube closure and gastrulation (Caddy, Wilanowski et al. 2010). Like the PCP pathway, *edn1* signalling (regulated by *grhl3*) in pharynx is essential for NCC differentiation to form craniofacial cartilage (Dworkin, Simkin et al. 2014). Thus, future studies must analyse the localisation of PCP proteins and evaluate the expression of NCC markers in *grhl3$^{-/-}$* embryos to determine the interaction of these pathways with *grhl3* gene.

Secondly, it was shown that loss of *tmem54a* to leads to severe craniofacial deformities and axial defects, signifying its importance in craniofacial formation and axial patterning. Since the jaw defects in *hdac1* mutants is analogous to that of *tmem54a* morphants, it is speculated that *grhl3* interacts with *hdac1* to drive NCC differentiation for the formation of craniofacial cartilage (Ignatius, Unal Eroglu et al. 2013). Understanding the functions of this gene using higher vertebrate model organisms will shed more light on the functions of *tmem54* and determine whether they are evolutionarily conserved across the animal kingdom.

Lastly, curcumin was found to rescue the phenotypic severity of *grhl3$^{-/-}$* embryos. The increased ROS levels in *grhl3$^{-/-}$* embryos (Rushton, unpublished) is proposed to be reduced by the antioxidant effects of curcumin during early embryonic development, thereby rescuing the phenotypes observed. Translating this research to *curly-tail* (hypomorphic *grhl3*) mouse will help establish the genetic interaction between *grhl3* and curcumin.

Curly-tail mouse as described in chapter 1 displays an array of defects including exencephaly, spina bifida and curled tail (Ting, Wilanowski et al. 2003).This model system shows hypomorphic *grhl3* function which was why a rescue was observed in the NTDs in *curly-tail* mice upon inositol exposure, suggesting that neurulation brought about by inositol is *grhl3* dependent (Ting, Wilanowski et al. 2003). Similarly, by exposing curcumin to *curly-tail* mice it can be determined whether an interaction exists between *grhl3* and curcumin. This is critical to understand the mechanism of curcumin mediated neural tube closure.

Overall, this study has identified novel genes and environmental factors involved in epithelial development and future studies will help us understand the mechanisms underlying epithelial establishment mediated by these genetic and environmental factors.

References

(2017). Chapter 31 - Intercellular Junctions. <u>Cell Biology (Third Edition)</u>. T. D. Pollard, W. C. Earnshaw, J. Lippincott-Schwartz and G. T. Johnson, Elsevier**:** 543-553.

Abba, Y., H. Hassim, H. Hamzah and M. M. Noordin (2015). "Antiviral activity of resveratrol against human and animal viruses." <u>Advances in virology</u> **2015**.

Adams, M. J., Jr., M. J. Khoury, K. S. Scanlon, R. E. Stevenson, G. J. Knight, J. E. Haddow, G. C. Sylvester, J. E. Cheek, J. P. Henry, S. P. Stabler and et al. (1995). "Elevated midtrimester serum methylmalonic acid levels as a risk factor for neural tube defects." <u>Teratology</u> **51**(5): 311-317.

Adinolfi, M., S. Beck, S. Embury, P. E. Polani and M. J. Seller (1976). "Levels of alpha-fetoprotein in amniotic fluids of mice (curly-tail) with neural tube defects." <u>J Med Genet</u> **13**(6): 511-513.

Afman, L. A., H. J. Blom, N. M. Van der Put and H. W. Van Straaten (2003). "Homocysteine interference in neurulation: a chick embryo model." <u>Birth Defects Res A Clin Mol Teratol</u> **67**(6): 421-428.

Aggarwal, B. B., A. Kumar and A. C. Bharti (2003). "Anticancer potential of curcumin: preclinical and clinical studies." <u>Anticancer research</u> **23**(1/A): 363-398.

Ahmed, S., H. Khan, D. Fratantonio, M. M. Hasan, S. Sharifi, N. Fathi, H. Ullah and L. Rastrelli (2019). "Apoptosis induced by luteolin in breast cancer: Mechanistic and therapeutic perspectives." <u>Phytomedicine</u> **59**: 152883.

Albani, D., L. Polito, A. Signorini and G. Forloni (2010). "Neuroprotective properties of resveratrol in different neurodegenerative disorders." <u>Biofactors</u> **36**(5): 370-376.

Almeida, M. S. and S. J. Bray (2005). "Regulation of post-embryonic neuroblasts by Drosophila Grainyhead." <u>Mechanisms of development</u> **122**(12): 1282-1293.

Almouzni, G., S. Khochbin, S. Dimitrov and A. P. Wolffe (1994). "Histone acetylation influences both gene expression and development of Xenopus laevis." <u>Developmental biology</u> **165**(2): 654-669.

Alotaibi, H., M. F. Basilicata, H. Shehwana, T. Kosowan, I. Schreck, C. Braeutigam, O. Konu, T. Brabletz and M. P. Stemmler (2015). "Enhancer cooperativity as a novel mechanism underlying the transcriptional regulation of E-cadherin during mesenchymal to epithelial transition." <u>Biochimica et Biophysica Acta (BBA) - Gene Regulatory Mechanisms</u> **1849**(6): 731-742.

Ammon, H. P. and M. A. Wahl (1991). "Pharmacology of Curcuma longa." <u>Planta medica</u> **57**(01): 1-7.

Andl, T., K. Ahn, A. Kairo, E. Y. Chu, L. Wine-Lee, S. T. Reddy, N. J. Croft, J. A. Cebra-Thomas, D. Metzger and P. Chambon (2004). "Epithelial Bmpr1a regulates differentiation and proliferation in postnatal hair follicles and is essential for tooth development." Development **131**(10): 2257-2268.

Arnold, R. S., J. Shi, E. Murad, A. M. Whalen, C. Q. Sun, R. Polavarapu, S. Parthasarathy, J. A. Petros and J. D. Lambeth (2001). "Hydrogen peroxide mediates the cell growth and transformation caused by the mitogenic oxidase Nox1." Proc Natl Acad Sci U S A **98**(10): 5550-5555.

Artavanis-Tsakonas, S., M. D. Rand and R. J. Lake (1999). "Notch Signaling: Cell Fate Control and Signal Integration in Development." Science **284**(5415): 770-776.

Attardi, L. D. and R. Tjian (1993). "Drosophila tissue-specific transcription factor NTF-1 contains a novel isoleucine-rich activation motif." Genes & Development **7**(7b): 1341-1353.

Atten, M. J., E. Godoy-Romero, B. M. Attar, T. Milson, M. Zopel and O. Holian (2005). "Resveratrol regulates cellular PKC α and δ to inhibit growth and induce apoptosis in gastric cancer cells." Investigational new drugs **23**(2): 111-119.

Au - Rosen, J. N., M. F. Au - Sweeney and J. D. Au - Mably (2009). "Microinjection of Zebrafish Embryos to Analyze Gene Function." JoVE(25): e1115.

Auden, A., J. Caddy, T. Wilanowski, S. B. Ting, J. M. Cunningham and S. M. Jane (2006). "Spatial and temporal expression of the Grainyhead-like transcription factor family during murine development." Gene Expr Patterns **6**(8): 964-970.

Aue, A., C. Hinze, K. Walentin, J. Ruffert, Y. Yurtdas, M. Werth, W. Chen, A. Rabien, E. Kilic, J.-D. Schulzke, M. Schumann and K. M. Schmidt-Ott (2015). "A Grainyhead-Like 2/Ovo-Like 2 Pathway Regulates Renal Epithelial Barrier Function and Lumen Expansion." Journal of the American Society of Nephrology **26**(11): 2704.

Augustine-Rauch, K., C. X. Zhang and J. M. Panzica-Kelly (2010). "In vitro developmental toxicology assays: A review of the state of the science of rodent and zebrafish whole embryo culture and embryonic stem cell assays." Birth Defects Research Part C: Embryo Today: Reviews **90**(2): 87-98.

Autuori, M. C., Y. J. Pai, D. J. Stuckey, D. Savery, A. M. Marconi, V. Massa, M. F. Lythgoe, A. J. Copp, A. L. David and N. D. Greene (2017). "Use of high-frequency ultrasound to study the prenatal development of cranial neural tube defects and hydrocephalus in Gldc-deficient mice." Prenatal diagnosis **37**(3): 273-281.

Bakker, S. J. L., J. C. t. Maaten and R. O. B. Gans (2000). "Thiamine supplementation to prevent induction of low birth weight by conventional therapy for gestational diabetes mellitus." Medical Hypotheses **55**(1): 88-90.

Balda, M. S. and K. Matter (1998). "Tight junctions." Journal of cell science **111**(5): 541-547.

Banerjee, R. (1999). Chemistry and Biochemistry of B12, John Wiley & Sons.

Bates, J. M., E. Mittge, J. Kuhlman, K. N. Baden, S. E. Cheesman and K. Guillemin (2006). "Distinct signals from the microbiota promote different aspects of zebrafish gut differentiation." Dev Biol **297**(2): 374-386.

Baxter, R. A. (2008). "Anti-aging properties of resveratrol: review and report of a potent new antioxidant skin care formulation." Journal of cosmetic dermatology **7**(1): 2-7.

Beachy, P. A., S. S. Karhadkar and D. M. Berman (2004). "Tissue repair and stem cell renewal in carcinogenesis." Nature **432**(7015): 324-331.

Beck, F. (2002). "Homeobox genes in gut development." Gut **51**(3): 450-454.

Bell, S. M., L. Zhang, A. Mendell, Y. Xu, H. M. Haitchi, J. L. Lessard and J. A. Whitsett (2011). "Kruppel-like factor 5 is required for formation and differentiation of the bladder urothelium." Dev Biol **358**(1): 79-90.

Ben, J., E. W. Jabs and S. S. Chong (2005). "Genomic, cDNA and embryonic expression analysis of zebrafish IRF6, the gene mutated in the human oral clefting disorders Van der Woude and popliteal pterygium syndromes." Gene Expr Patterns **5**(5): 629-638.

Bereswill, S., M. Muñoz, A. Fischer, R. Plickert, L.-M. Haag, B. Otto, A. A. Kühl, C. Loddenkemper, U. B. Göbel and M. M. Heimesaat (2010). "Anti-inflammatory effects of resveratrol, curcumin and simvastatin in acute small intestinal inflammation." PloS one **5**(12): e15099.

Bhandari, A., W. Gordon, D. Dizon, A. S. Hopkin, E. Gordon, Z. Yu and B. Andersen (2013). "The Grainyhead transcription factor Grhl3/Get1 suppresses miR-21 expression and tumorigenesis in skin: modulation of the miR-21 target MSH2 by RNA-binding protein DND1." Oncogene **32**(12): 1497-1507.

Bienengräber, V., J. Fanghänel, F. A. Malek and G. Kundt (1997). "Application of Thiamine in Preventing Malformations, Specifically Cleft Alveolus and Palate, during the Intrauterine Development of Rats." The Cleft Palate-Craniofacial Journal **34**(4): 318-324.

Bilmen, J. G., S. Z. Khan, M. H. Javed and F. Michelangeli (2001). "Inhibition of the SERCA Ca2+ pumps by curcumin. Curcumin putatively stabilizes the interaction between the nucleotide-binding and phosphorylation domains in the absence of ATP." Eur J Biochem **268**(23): 6318-6327.

Boglev, Y., T. Wilanowski, J. Caddy, V. Parekh, A. Auden, C. Darido, N. R. Hislop, M. Cangkrama, S. B. Ting and S. M. Jane (2011). "The unique and cooperative roles of the Grainy head-like transcription factors in epidermal development reflect unexpected target gene specificity." Dev Biol **349**(2): 512-522.

Borradori, L. and A. Sonnenberg (1999). "Structure and Function of Hemidesmosomes: More Than Simple Adhesion Complexes." Journal of Investigative Dermatology **112**(4): 411-418.

Botchkarev, V. A., N. V. Botchkareva, M. Nakamura, O. Huber, K. Funa, R. Lauster, R. Paus and B. A. Gilchrest (2001). "Noggin is required for induction of the hair follicle growth phase in postnatal skin." The FASEB Journal **15**(12): 2205-2214.

Botti, E., G. Spallone, F. Moretti, B. Marinari, V. Pinetti, S. Galanti, P. D. De Meo, F. De Nicola, F. Ganci, T. Castrignanò, G. Pesole, S. Chimenti, L. Guerrini, M. Fanciulli, G. Blandino, M. Karin and A. Costanzo (2011). "Developmental factor IRF6 exhibits tumor suppressor activity in squamous cell carcinomas." Proc Natl Acad Sci U S A **108**(33): 13710-13715.

Boyer, J. Z., J. Jandova, J. Janda, F. R. Vleugels, D. A. Elliott and J. E. Sligh (2012). "Resveratrol-sensitized UVA induced apoptosis in human keratinocytes through mitochondrial oxidative stress and pore opening." Journal of Photochemistry and Photobiology B: Biology **113**: 42-50.

Brancati, F., P. Fortugno, I. Bottillo, M. Lopez, E. Josselin, O. Boudghene-Stambouli, E. Agolini, L. Bernardini, E. Bellacchio, M. Iannicelli, A. Rossi, A. Dib-Lachachi, L. Stuppia, G. Palka, S. Mundlos, S. Stricker, U. Kornak, G. Zambruno and B. Dallapiccola (2010). "Mutations in PVRL4, Encoding Cell Adhesion Molecule Nectin-4, Cause Ectodermal Dysplasia-Syndactyly Syndrome." The American Journal of Human Genetics **87**(2): 265-273.

Bray, S. J. and F. C. Kafatos (1991). "Developmental function of Elf-1: an essential transcription factor during embryogenesis in Drosophila." Genes Dev **5**(9): 1672-1683.

Brynczka, C., P. Labhart and B. A. Merrick (2007). "NGF-mediated transcriptional targets of p53 in PC12 neuronal differentiation." BMC Genomics **8**: 139.

Brynczka, C., P. Labhart and B. A. Merrick (2007). "NGF-mediated transcriptional targets of p53 in PC12 neuronal differentiation." BMC genomics **8**(1): 139.

Butali, A., P. A. Mossey, W. L. Adeyemo, M. A. Eshete, L. A. Gaines, D. Even, R. O. Braimah, B. S. Aregbesola, J. V. Rigdon and C. I. Emeka (2014). "Novel IRF6 mutations in families with Van Der Woude syndrome and popliteal pterygium syndrome from sub-Saharan Africa." Molecular genetics & genomic medicine **2**(3): 254-260.

Butz, H., P. M. Szabó, R. Nofech-Mozes, F. Rotondo, K. Kovacs, L. Mirham, H. Girgis, D. Boles, A. Patocs and G. M. Yousef (2014). "Integrative Bioinformatics Analysis Reveals New Prognostic Biomarkers of Clear Cell Renal Cell Carcinoma." Clinical Chemistry **60**(10): 1314-1326.

Caddy, J., T. Wilanowski, C. Darido, S. Dworkin, S. B. Ting, Q. Zhao, G. Rank, A. Auden, S. Srivastava, T. A. Papenfuss, J. N. Murdoch, P. O. Humbert, V. Parekh, N. Boulos, T. Weber, J. Zuo, J. M. Cunningham and S. M. Jane (2010). "Epidermal wound repair is regulated by the planar cell polarity signaling pathway." Dev Cell **19**(1): 138-147.

Cai, X., T. Ye, C. Liu, W. Lu, M. Lu, J. Zhang, M. Wang and P. Cao (2011). "Luteolin induced G2 phase cell cycle arrest and apoptosis on non-small cell lung cancer cells." Toxicology in Vitro **25**(7): 1385-1391.

Candito, M., R. Rivet, B. Herbeth, C. Boisson, R.-C. Rudigoz, D. Luton, H. Journel, J.-F. Oury, F. Roux, R. Saura, I. Vernhet, P. Gaucherand, F. Muller, B. Guidicelli, H. Heckenroth, P. Poulain, M. Blayau, C. Francannet, L. Roszyk, C. Brustié, P. Staccini, P. Gérard, N. Fillion-Emery, R.-M. Guéant-Rodriguez, E. Van Obberghen and J.-L. Guéant (2008). "Nutritional and genetic determinants of vitamin B and homocysteine metabolisms in neural tube defects: A multicenter case–control study." American Journal of Medical Genetics Part A **146A**(9): 1128-1133.

Cangkrama, M., C. Darido, S. R. Georgy, D. Partridge, A. Auden, S. Srivastava, T. Wilanowski and S. M. Jane (2016). "Two Ancient Gene Families Are Critical for Maintenance of the Mammalian Skin Barrier in Postnatal Life." J Invest Dermatol **136**(7): 1438-1448.

Cao, J., L. Jia, H. M. Zhou, Y. Liu and L. F. Zhong (2006). "Mitochondrial and nuclear DNA damage induced by curcumin in human hepatoma G2 cells." Toxicol Sci **91**(2): 476-483.

Cao, X.-Y., X.-M. Jiang, Z.-H. Dou, M. A. Rakeman, M.-L. Zhang, K. O'Donnell, T. Ma, K. Amette, N. DeLong and G. R. DeLong (1994). "Timing of vulnerability of the brain to iodine deficiency in endemic cretinism." New England journal of medicine **331**(26): 1739-1744.

Cavalli, P. and A. Copp (2002). "Inositol and folate resistant neural tube defects." Journal of medical genetics **39**(2): e5-e5.

Cavalli, P., G. Tonni, E. Grosso and C. Poggiani (2011). "Effects of inositol supplementation in a cohort of mothers at risk of producing an NTD pregnancy." Birth Defects Research Part A: Clinical and Molecular Teratology **91**(11): 962-965.

Cenci, C. and A. P. Gould (2005). "Drosophila Grainyhead specifies late programmes of neural proliferation by regulating the mitotic activity and Hox-dependent apoptosis of neuroblasts." Development **132**(17): 3835-3845.

Ceyhan, S. T., C. Beyan, V. Atay, H. Yaman, I. Alanbay, K. Kaptan and I. Başer (2010). "Serum vitamin B12 and homocysteine levels in pregnant women with neural tube defect." Gynecol Endocrinol **26**(8): 578-581.

Chang, W. J. and P. P. Hwang (2011). "Development of zebrafish epidermis." Birth Defects Res C Embryo Today **93**(3): 205-214.

Cheung, M. and J. Briscoe (2003). "Neural crest development is regulated by the transcription factor Sox9." Development **130**(23): 5681-5693.

Christianson, A. L., C. P. Howson and B. Modell (2006). Global report on birth defects: the hidden toll of dying and disabled children, March of Dimes Birth Defects Foundation.

Chung, V. Y., T. Z. Tan, M. Tan, M. K. Wong, K. T. Kuay, Z. Yang, J. Ye, J. Muller, C. M. Koh, E. Guccione, J. P. Thiery and R. Y. Huang (2016). "GRHL2-miR-200-ZEB1 maintains the epithelial status of ovarian cancer through transcriptional regulation and histone modification." Sci Rep **6**: 19943.

Cieply, B., J. Farris, J. Denvir, H. L. Ford and S. M. Frisch (2013). "Epithelial–mesenchymal transition and tumor suppression are controlled by a reciprocal feedback loop between ZEB1 and Grainyhead-like-2." Cancer research **73**(20): 6299-6309.

Cieply, B., P. Riley, P. M. Pifer, J. Widmeyer, J. B. Addison, A. V. Ivanov, J. Denvir and S. M. Frisch (2012). "Suppression of the Epithelial–Mesenchymal Transition by Grainyhead-like-2." Cancer Research **72**(9): 2440-2453.

Citi, S., D. Guerrera, D. Spadaro and J. Shah (2014). "Epithelial junctions and Rho family GTPases: the zonular signalosome." Small GTPases **5**(4): 1-15.

Cockroft, D., F. Brook and A. Copp (1992). "Inositol deficiency increases the susceptibility to neural tube defects of genetically predisposed (curly tail) mouse embryos in vitro." Teratology **45**(2): 223-232.

Cogram, P., S. Tesh, J. Tesh, A. Wade, G. Allan, N. D. Greene and A. J. Copp (2002). "D-chiro-inositol is more effective than myo-inositol in preventing folate-resistant mouse neural tube defects." Human Reproduction **17**(9): 2451-2458.

Cohly, H. H. P., A. Taylor, M. F. Angel and A. K. Salahudeen (1998). "Effect of Turmeric, Turmerin and Curcumin on H2O2-Induced Renal Epithelial (LLC-PK1) Cell Injury." Free Radical Biology and Medicine **24**(1): 49-54.

Control, C. f. D. (1991). "Use of folic acid for prevention of spina bifida and other neural tube defects--1983-1991." MMWR. Morbidity and mortality weekly report **40**(30): 513.

Coopman, P. and A. Djiane (2016). "Adherens Junction and E-Cadherin complex regulation by epithelial polarity." Cellular and Molecular Life Sciences **73**(18): 3535-3553.

Copp, A. J., F. A. Brook and H. J. Roberts (1988). "A cell-type-specific abnormality of cell proliferation in mutant (curly tail) mouse embryos developing spinal neural tube defects." Development **104**(2): 285-295.

Curtin, J. A., E. Quint, V. Tsipouri, R. M. Arkell, B. Cattanach, A. J. Copp, D. J. Henderson, N. Spurr, P. Stanier and E. M. Fisher (2003). "Mutation of Celsr1 disrupts planar polarity of inner ear hair cells and causes severe neural tube defects in the mouse." Current Biology **13**(13): 1129-1133.

D'Atri, F. and S. Citi (2001). "Cingulin interacts with F-actin in vitro." FEBS Lett **507**(1): 21-24.

Dai, X., C. Schonbaum, L. Degenstein, W. Bai, A. Mahowald and E. Fuchs (1998). "The ovo gene required for cuticle formation and oogenesis in flies is involved in hair formation and spermatogenesis in mice." Genes & development **12**(21): 3452-3463.

Danila, D. C., A. Anand, N. Schultz, G. Heller, M. Wan, C. C. Sung, C. Dai, R. Khanin, M. Fleisher, H. Lilja and H. I. Scher (2014). "Analytic and clinical validation of a prostate cancer-enhanced messenger RNA detection assay in whole blood as a prognostic biomarker for survival." Eur Urol **65**(6): 1191-1197.

Darido, C., S. R. Georgy, T. Wilanowski, S. Dworkin, A. Auden, Q. Zhao, G. Rank, S. Srivastava, M. J. Finlay, A. T. Papenfuss, P. P. Pandolfi, R. B. Pearson and S. M. Jane (2011). "Targeting of the tumor suppressor GRHL3 by a miR-21-dependent proto-oncogenic network results in PTEN loss and tumorigenesis." <u>Cancer Cell</u> **20**(5): 635-648.

Das, S. and D. K. Das (2007). "Anti-inflammatory responses of resveratrol." <u>Inflammation & Allergy-Drug Targets (Formerly Current Drug Targets-Inflammation & Allergy)(Discontinued)</u> **6**(3): 168-173.

De Castro, S. C., C. S. Hirst, D. Savery, A. Rolo, H. Lickert, B. Andersen, A. J. Copp and N. D. Greene (2018). "Neural tube closure depends on expression of Grainyhead-like 3 in multiple tissues." <u>Developmental biology</u> **435**(2): 130-137.

De Escobar, G. M., M. J. Obregón and F. E. Del Rey (2007). "Iodine deficiency and brain development in the first half of pregnancy." <u>Public health nutrition</u> **10**(12A): 1554-1570.

de la Garza, G., J. R. Schleiffarth, M. Dunnwald, A. Mankad, J. L. Weirather, G. Bonde, S. Butcher, T. A. Mansour, Y. A. Kousa, C. F. Fukazawa, D. W. Houston, J. R. Manak, B. C. Schutte, D. S. Wagner and R. A. Cornell (2013). "Interferon Regulatory Factor 6 Promotes Differentiation of the Periderm by Activating Expression of Grainyhead-Like 3." <u>Journal of Investigative Dermatology</u> **133**(1): 68-77.

De La Lastra, C. A. and I. Villegas (2007). "Resveratrol as an antioxidant and pro-oxidant agent: mechanisms and clinical implications." <u>Biochemical Society Transactions</u> **35**(5): 1156-1160.

de Vries, M., M. Carpinelli, E. Rutland, A. Hatzipantelis, D. Partridge, A. Auden, P. J. Anderson, B. De Groef, H. Wu, M. Osterwalder, A. Visel, S. M. Jane and S. Dworkin (2020). "Interrogating the Grainyhead-like 2 (Grhl2) genomic locus identifies an enhancer element that regulates palatogenesis in mouse." <u>Developmental Biology</u> **459**(2): 194-203.

Delange, F. (2000). "The role of iodine in brain development." <u>Proceedings of the nutrition society</u> **59**(1): 75-79.

Deng, J., L. Yu, C. Liu, K. Yu, X. Shi, L. W. Y. Yeung, P. K. S. Lam, R. S. S. Wu and B. Zhou (2009). "Hexabromocyclododecane-induced developmental toxicity and apoptosis in zebrafish embryos." <u>Aquatic Toxicology</u> **93**(1): 29-36.

Devuyst, O. (2012). <u>Physiopathology and diagnosis of nephrogenic diabetes insipidus</u>. Annales d'endocrinologie, Elsevier.

Di Paolo, G. and P. De Camilli (2006). "Phosphoinositides in cell regulation and membrane dynamics." <u>Nature</u> **443**(7112): 651-657.

Dieckgraefe, B. K. and D. M. Weems (1999). "Epithelial injury induces egr-1 and fos expression by a pathway involving protein kinase C and ERK." <u>American Journal of Physiology-Gastrointestinal and Liver Physiology</u> **276**(2): G322-G330.

Ding, X.-Z. and T. E. Adrian (2002). "Resveratrol inhibits proliferation and induces apoptosis in human pancreatic cancer cells." <u>Pancreas</u> **25**(4): e71-e76.

Do, G. M., U. J. Jung, H. J. Park, E. Y. Kwon, S. M. Jeon, R. A. McGregor and M. S. Choi (2012). "Resveratrol ameliorates diabetes-related metabolic changes via activation of AMP-activated protein kinase and its downstream targets in db/db mice." <u>Mol Nutr Food Res</u> **56**(8): 1282-1291.

Dworkin, S., Y. Boglev, H. Owens and S. J. Goldie (2016). "The Role of Sonic Hedgehog in Craniofacial Patterning, Morphogenesis and Cranial Neural Crest Survival." <u>J Dev Biol</u> **4**(3).

Dworkin, S., C. Darido, S. R. Georgy, T. Wilanowski, S. Srivastava, F. Ellett, L. Pase, Y. Han, A. Meng, J. K. Heath, G. J. Lieschke and S. M. Jane (2012). "Midbrain-hindbrain boundary patterning and morphogenesis are regulated by diverse grainy head-like 2-dependent pathways." <u>Development</u> **139**(3): 525-536.

Dworkin, S., J. Simkin, C. Darido, D. D. Partridge, S. R. Georgy, J. Caddy, T. Wilanowski, G. J. Lieschke, K. Doggett, J. K. Heath and S. M. Jane (2014). "Grainyhead-like 3 regulation of endothelin-1 in the pharyngeal endoderm is critical for growth and development of the craniofacial skeleton." <u>Mech Dev</u> **133**: 77-90.

Eisen, J. S. and J. C. Smith (2008). "Controlling morpholino experiments: don't stop making antisense." <u>Development</u> **135**(10): 1735-1743.

El-Brolosy, M. A. and D. Y. R. Stainier (2017). "Genetic compensation: A phenomenon in search of mechanisms." <u>PLOS Genetics</u> **13**(7): e1006780.

Elshaer, M., Y. Chen, X. J. Wang and X. Tang (2018). "Resveratrol: An overview of its anti-cancer mechanisms." <u>Life sciences</u> **207**: 340-349.

Embury, S., M. J. Seller, M. Adinolfi and P. E. Polani (1979). "Neural tube defects in curly-tail mice. I. Incidence, expression and similarity to the human condition." <u>Proceedings of the Royal Society of London. Series B. Biological Sciences</u> **206**(1162): 85-94.

Evans, W. H. and P. E. Martin (2002). "Gap junctions: structure and function." <u>Molecular membrane biology</u> **19**(2): 121-136.

Fabian, J., M. Lodrini, I. Oehme, M. C. Schier, T. M. Thole, T. Hielscher, A. Kopp-Schneider, L. Opitz, D. Capper, A. von Deimling, I. Wiegand, T. Milde, U. Mahlknecht, F. Westermann, O. Popanda, F. Roels, B. Hero, F. Berthold, M. Fischer, A. E. Kulozik, O. Witt and H. E. Deubzer (2014). "GRHL1 acts as tumor suppressor in neuroblastoma and is negatively regulated by MYCN and HDAC3." <u>Cancer Res</u> **74**(9): 2604-2616.

Fänge, R. (1966). "Physiology of the swimbladder." <u>Physiological reviews</u> **46**(2): 299-322.

Fanning, A. S., B. J. Jameson, L. A. Jesaitis and J. M. Anderson (1998). "The tight junction protein ZO-1 establishes a link between the transmembrane protein occludin and the actin cytoskeleton." <u>J Biol Chem</u> **273**(45): 29745-29753.

Farber, S. A., M. Pack, S. Y. Ho, I. D. Johnson, D. S. Wagner, R. Dosch, M. C. Mullins, H. S. Hendrickson, E. K. Hendrickson and M. E. Halpern (2001). "Genetic analysis of digestive physiology using fluorescent phospholipid reporters." Science **292**(5520): 1385-1388.

Farris, J. C., P. M. Pifer, L. Zheng, E. Gottlieb, J. Denvir and S. M. Frisch (2016). "Grainyhead-like 2 Reverses the Metabolic Changes Induced by the Oncogenic Epithelial-Mesenchymal Transition: Effects on Anoikis." Mol Cancer Res **14**(6): 528-538.

Ferreira, V. H., A. Nazli, S. E. Dizzell, K. Mueller and C. Kaushic (2015). "The anti-inflammatory activity of curcumin protects the genital mucosal epithelial barrier from disruption and blocks replication of HIV-1 and HSV-2." PloS one **10**(4): e0124903.

Filardo, S., M. Di Pietro, P. Mastromarino and R. Sessa (2020). "Therapeutic potential of resveratrol against emerging respiratory viral infections." Pharmacology & therapeutics **214**: 107613.

Finney, J. L., G. N. Robertson, C. A. McGee, F. M. Smith and R. P. Croll (2006). "Structure and autonomic innervation of the swim bladder in the zebrafish (Danio rerio)." Journal of comparative neurology **495**(5): 587-606.

Fleming, A. and A. J. Copp (1998). "Embryonic folate metabolism and mouse neural tube defects." Science **280**(5372): 2107-2109.

Frasa, M. A., F. C. Maximiano, K. Smolarczyk, R. E. Francis, M. E. Betson, E. Lozano, J. Goldenring, M. C. Seabra, A. Rak, M. R. Ahmadian and V. M. Braga (2010). "Armus is a Rac1 effector that inactivates Rab7 and regulates E-cadherin degradation." Curr Biol **20**(3): 198-208.

Fraser, F. C. and T. Fainstat (1951). "Production of congenital defects in the offspring of pregnant mice treated with cortisone: progress report." Pediatrics **8**(4): 527-533.

Fukazawa, C., C. Santiago, K. M. Park, W. J. Deery, S. G. de la Torre Canny, C. K. Holterhoff and D. S. Wagner (2010). "poky/chuk/ikk1 is required for differentiation of the zebrafish embryonic epidermis." Developmental biology **346**(2): 272-283.

Ganz, T. (2002). "Epithelia: Not just physical barriers." Proceedings of the National Academy of Sciences **99**(6): 3357-3358.

Gao, X., C. M. Vockley, F. Pauli, K. M. Newberry, Y. Xue, S. H. Randell, T. E. Reddy and B. L. Hogan (2013). "Evidence for multiple roles for grainyheadlike 2 in the establishment and maintenance of human mucociliary airway epithelium." Proc Natl Acad Sci U S A **110**(23): 9356-9361.

Garrod, D. and M. Chidgey (2008). "Desmosome structure, composition and function." Biochimica et Biophysica Acta (BBA) - Biomembranes **1778**(3): 572-587.

Gautam, S., Y. Xu, M. Dumaguin, N. Janakiraman and R. Chapman (2000). "Resveratrol selectively inhibits leukemia cells: a prospective agent for ex vivo bone marrow purging." <u>Bone marrow transplantation</u> **25**(6): 639-645.

Georgy, S. R., M. Cangkrama, S. Srivastava, D. Partridge, A. Auden, S. Dworkin, C. A. McLean, S. M. Jane and C. Darido (2015). "Identification of a Novel Proto-oncogenic Network in Head and Neck Squamous Cell Carcinoma." <u>J Natl Cancer Inst</u> **107**(9).

Getsios, S., C. L. Simpson, S. Kojima, R. Harmon, L. J. Sheu, R. L. Dusek, M. Cornwell and K. J. Green (2009). "Desmoglein 1-dependent suppression of EGFR signaling promotes epidermal differentiation and morphogenesis." <u>J Cell Biol</u> **185**(7): 1243-1258.

Goldie, S. (2018). "Loss of GRHL3 leads to TARC/CCL17- mediated keratinocyte proliferation in the epidermis." <u>Cell Death & Disease</u> **9**: 1072.

Goldie, S. J., B. D. Arhatari, P. Anderson, A. Auden, D. D. Partridge, S. M. Jane and S. Dworkin (2016). "Mice lacking the conserved transcription factor Grainyhead-like 3 (Grhl3) display increased apposition of the frontal and parietal bones during embryonic development." <u>BMC Dev Biol</u> **16**(1): 37.

Goldie, S. J., D. L. Cottle, F. H. Tan, S. Roslan, S. Srivastava, R. Brady, D. D. Partridge, A. Auden, I. M. Smyth, S. M. Jane, S. Dworkin and C. Darido (2018). "Loss of GRHL3 leads to TARC/CCL17-mediated keratinocyte proliferation in the epidermis." <u>Cell Death Dis</u> **9**(11): 1072.

Goodenough, D. A. and D. L. Paul (2009). "Gap junctions." <u>Cold Spring Harbor perspectives in biology</u> **1**(1): a002576.

Gordon, C. T., T. Y. Tan, S. Benko, D. FitzPatrick, S. Lyonnet and P. G. Farlie (2009). "Long-range regulation at the SOX9 locus in development and disease." <u>Journal of medical genetics</u> **46**(10): 649-656.

Gordon, W. M., M. D. Zeller, R. H. Klein, W. R. Swindell, H. Ho, F. Espetia, J. E. Gudjonsson, P. F. Baldi and B. Andersen (2014). "A GRHL3-regulated repair pathway suppresses immune-mediated epidermal hyperplasia." <u>J Clin Invest</u> **124**(12): 5205-5218.

Greene, N. D. and A. J. Copp (1997). "Inositol prevents folate-resistant neural tube defects in the mouse." <u>Nature medicine</u> **3**(1): 60-66.

Greene, N. D. and A. J. Copp (2014). "Neural tube defects." <u>Annual review of neuroscience</u> **37**: 221-242.

Greene, N. D., K.-Y. Leung, V. Gay, K. Burren, K. Mills, L. S. Chitty and A. J. Copp (2016). "Inositol for the prevention of neural tube defects: a pilot randomised controlled trial." <u>British Journal of Nutrition</u> **115**(6): 974-983.

Greene, N. D., K. Y. Leung and A. J. Copp (2017). "Inositol, neural tube closure and the prevention of neural tube defects." <u>Birth Defects Res</u> **109**(2): 68-80.

Greene, N. D. E. and A. J. Copp (1997). "Inositol prevents folate-resistant neural tube defects in the mouse." <u>Nature Medicine</u> **3**(1): 60-66.

Greene, N. D. E. and A. J. Copp (2005). "Mouse models of neural tube defects: Investigating preventive mechanisms." <u>American Journal of Medical Genetics Part C: Seminars in Medical Genetics</u> **135C**(1): 31-41.

Groenen, P. M. W., I. A. L. M. van Rooij, P. G. M. Peer, M. C. Ocké, G. A. Zielhuis and R. g. P. M. Steegers-Theunissen (2004). "Low Maternal Dietary Intakes of Iron, Magnesium, and Niacin Are Associated with Spina Bifida in the Offspring." <u>The Journal of Nutrition</u> **134**(6): 1516-1522.

Gruneberg, H. (1954). "Genetical studies on the skeleton of the mouse. VIII. Curly tail." <u>J. Genet</u> **52**: 52-67.

Gustavsson, P., N. D. Greene, D. Lad, E. Pauws, S. C. de Castro, P. Stanier and A. J. Copp (2007). "Increased expression of Grainyhead-like-3 rescues spina bifida in a folate-resistant mouse model." <u>Hum Mol Genet</u> **16**(21): 2640-2646.

Hallare, A., K. Nagel, H. R. Köhler and R. Triebskorn (2006). "Comparative embryotoxicity and proteotoxicity of three carrier solvents to zebrafish (Danio rerio) embryos." <u>Ecotoxicol Environ Saf</u> **63**(3): 378-388.

Han, Y., Y. Mu, X. Li, P. Xu, J. Tong, Z. Liu, T. Ma, G. Zeng, S. Yang, J. Du and A. Meng (2011). "Grhl2 deficiency impairs otic development and hearing ability in a zebrafish model of the progressive dominant hearing loss DFNA28." <u>Hum Mol Genet</u> **20**(16): 3213-3226.

Heasman, J. (2002). "Morpholino Oligos: Making Sense of Antisense?" <u>Developmental Biology</u> **243**(2): 209-214.

Hemphala, J., A. Uv, R. Cantera, S. Bray and C. Samakovlis (2003). "Grainy head controls apical membrane growth and tube elongation in response to Branchless/FGF signalling." <u>Development</u> **130**(2): 249-258.

Henn, K. and T. Braunbeck (2011). "Dechorionation as a tool to improve the fish embryo toxicity test (FET) with the zebrafish (Danio rerio)." <u>Comparative Biochemistry and Physiology Part C: Toxicology & Pharmacology</u> **153**(1): 91-98.

Hinze, C., J. Ruffert, K. Walentin, N. Himmerkus, E. Nikpey, O. Tenstad, H. Wiig, K. Mutig, Z. Y. Yurtdas and J. D. Klein (2018). "GRHL2 is required for collecting duct epithelial barrier function and renal osmoregulation." <u>Journal of the American Society of Nephrology</u> **29**(3): 857-868.

Hislop, N. R., J. Caddy, S. B. Ting, A. Auden, S. Vasudevan, S. L. King, G. J. Lindeman, J. E. Visvader, J. M. Cunningham and S. M. Jane (2008). "Grhl3 and Lmo4 play coordinate roles in epidermal migration." <u>Dev Biol</u> **321**(1): 263-272.

Hoffman, T. L., A. L. Javier, S. A. Campeau, R. D. Knight and T. F. Schilling (2007). "Tfap2 transcription factors in zebrafish neural crest development and ectodermal evolution." J Exp Zool B Mol Dev Evol **308**(5): 679-691.

Hopkin, A. S., W. Gordon, R. H. Klein, F. Espitia, K. Daily, M. Zeller, P. Baldi and B. Andersen (2012). "GRHL3/GET1 and trithorax group members collaborate to activate the epidermal progenitor differentiation program." PLoS Genet **8**(7): e1002829.

Horinaka, M., T. Yoshida, T. Shiraishi, S. Nakata, M. Wakada, R. Nakanishi, H. Nishino, H. Matsui and T. Sakai (2005). "Luteolin induces apoptosis via death receptor 5 upregulation in human malignant tumor cells." Oncogene **24**(48): 7180-7189.

Hsieh, C.-L., K.-C. Chen, P.-X. Lin, C.-C. Peng and R. Y. Peng (2014). "Resveratrol and vitamin E rescue valproic acid-induced teratogenicity: The mechanism of action." Clinical and Experimental Pharmacology and Physiology **41**(3): 210-219.

Huang, F.-J., K.-C. Lan, H.-Y. Kang, Y.-C. Liu, Y.-D. Hsuuw, W.-H. Chan and K.-E. Huang (2013). "Effect of curcumin on in vitro early post-implantation stages of mouse embryo development." European Journal of Obstetrics & Gynecology and Reproductive Biology **166**(1): 47-51.

Huang, L.-S., E. Voyiaziakis, D. F. Markenson, K. A. Sokol, T. Hayek and J. L. Breslow (1995). "apo B gene knockout in mice results in embryonic lethality in homozygotes and neural tube defects, male infertility, and reduced HDL cholesterol ester and apo AI transport rates in heterozygotes." The Journal of clinical investigation **96**(5): 2152-2161.

Huang, M.-T., Y.-R. Lou, W. Ma, H. L. Newmark, K. R. Reuhl and A. H. Conney (1994). "Inhibitory effects of dietary curcumin on forestomach, duodenal, and colon carcinogenesis in mice." Cancer research **54**(22): 5841-5847.

Huang, M.-T., T. Lysz, T. Ferraro, T. F. Abidi, J. D. Laskin and A. H. Conney (1991). "Inhibitory effects of curcumin on in vitro lipoxygenase and cyclooxygenase activities in mouse epidermis." Cancer research **51**(3): 813-819.

Huber, M., I. Rettler, K. Bernasconi, E. Frenk, S. Lavrijsen, M. Ponec, A. Bon, S. Lautenschlager, D. Schorderet and D. Hohl (1995). "Mutations of keratinocyte transglutaminase in lamellar ichthyosis." Science **267**(5197): 525-528.

Hunt, D. M., L. Rickman, N. V. Whittock, R. A. Eady, D. Simrak, P. J. Dopping-Hepenstal, H. P. Stevens, D. K. Armstrong, H. C. Hennies, W. Küster, A. E. Hughes, J. Arnemann, I. M. Leigh, J. A. McGrath, D. P. Kelsell and R. S. Buxton (2001). "Spectrum of dominant mutations in the desmosomal cadherin desmoglein 1, causing the skin disease striate palmoplantar keratoderma." Eur J Hum Genet **9**(3): 197-203.

Ignatius, M. S., A. Unal Eroglu, S. Malireddy, G. Gallagher, R. M. Nambiar and P. D. Henion (2013). "Distinct Functional and Temporal Requirements for Zebrafish Hdac1 during Neural Crest-Derived Craniofacial and Peripheral Neuron Development." PLOS ONE **8**(5): e63218.

Ingraham, C. R., A. Kinoshita, S. Kondo, B. Yang, S. Sajan, K. J. Trout, M. I. Malik, M. Dunnwald, S. L. Goudy, M. Lovett, J. C. Murray and B. C. Schutte (2006). "Abnormal skin, limb and craniofacial morphogenesis in mice deficient for interferon regulatory factor 6 (Irf6)." <u>Nature Genetics</u> **38**(11): 1335-1340.

Jaber, N., N. Mohd-Naim, Z. Wang, J. L. DeLeon, S. Kim, H. Zhong, N. Sheshadri, Z. Dou, A. L. Edinger, G. Du, V. M. M. Braga and W.-X. Zong (2016). "Vps34 regulates Rab7 and late endocytic trafficking through recruitment of the GTPase-activating protein Armus." <u>Journal of cell science</u> **129**(23): 4424-4435.

Jang, J. Y., D. Park, S. Shin, J. H. Jeon, B. I. Choi, S. S. Joo, S. Y. Hwang, S. S. Nahm and Y. B. Kim (2008). "Antiteratogenic effect of resveratrol in mice exposed in utero to 2,3,7,8-tetrachlorodibenzo-p-dioxin." <u>Eur J Pharmacol</u> **591**(1-3): 280-283.

Janicke, M., B. Renisch and M. Hammerschmidt (2010). "Zebrafish grainyhead-like1 is a common marker of different non-keratinocyte epidermal cell lineages, which segregate from each other in a Foxi3-dependent manner." <u>Int J Dev Biol</u> **54**(5): 837-850.

Jensen, H., L. Andersen and J. Hau (1991). "Fetal malformations and maternal alpha-fetoprotein levels in curly tail (ct) mice." <u>INTERNATIONAL JOURNAL OF FETOMATERNAL MEDICINE</u> **4**: 205-205.

Jiang, F. and J. A. Doudna (2017). "CRISPR–Cas9 structures and mechanisms." <u>Annual review of biophysics</u> **46**: 505-529.

Joanta, A., A. Joanta, A. Joanta, A. Joanta, A. Filip, A. Filip, A. Filip, A. Filip, S. Clichici and S. Clichici (2006). "Iodide excess exerts oxidative stress in some target tissues of the thyroid hormones< p." <u>Acta Physiologica Hungarica</u> **93**(4): 347-360.

Joung, J. K. and J. D. Sander (2013). "TALENs: a widely applicable technology for targeted genome editing." <u>Nature reviews Molecular cell biology</u> **14**(1): 49-55.

Joyner, A. L., K. Herrup, B. A. Auerbach, C. A. Davis and J. Rossant (1991). "Subtle cerebellar phenotype in mice homozygous for a targeted deletion of the En-2 homeobox." <u>Science</u> **251**(4998): 1239-1243.

Kais, B., K. E. Schneider, S. Keiter, K. Henn, C. Ackermann and T. Braunbeck (2013). "DMSO modifies the permeability of the zebrafish (Danio rerio) chorion-Implications for the fish embryo test (FET)." <u>Aquatic Toxicology</u> **140-141**: 229-238.

Kao, T.-T., C.-Y. Chu, G.-H. Lee, T.-H. Hsiao, N.-W. Cheng, N.-S. Chang, B.-H. Chen and T.-F. Fu (2014). "Folate deficiency-induced oxidative stress contributes to neuropathy in young and aged zebrafish — Implication in neural tube defects and Alzheimer's diseases." <u>Neurobiology of Disease</u> **71**: 234-244.

Kasdallah-Grissa, A., B. Mornagui, E. Aouani, M. Hammami, M. El May, N. Gharbi, A. Kamoun and S. El-Fazaâ (2007). "Resveratrol, a red wine polyphenol, attenuates ethanol-induced oxidative stress in rat liver." <u>Life Sciences</u> **80**(11): 1033-1039.

Kersbergen, A., S. A. Best, S. Dworkin, C. Ah-Cann, M. E. de Vries, M. L. Asselin-Labat, M. E. Ritchie, S. M. Jane and K. D. Sutherland (2018). "Lung morphogenesis is orchestrated through Grainyhead-like 2 (Grhl2) transcriptional programs." Dev Biol **443**(1): 1-9.

Kibar, Z., K. J. Vogan, N. Groulx, M. J. Justice, D. A. Underhill and P. Gros (2001). "Ltap, a mammalian homolog of Drosophila Strabismus/Van Gogh, is altered in the mouse neural tube mutant Loop-tail." Nature genetics **28**(3): 251-255.

Kim, D.-H., Y. Sun, S. Yun, B. Kim, C. N. Hwang, S. H. Lee and B. J. Nelson (2004). Mechanical property characterization of the zebrafish embryo chorion. The 26th Annual International Conference of the IEEE Engineering in Medicine and Biology Society, IEEE.

Kim, M. and W. McGinnis (2011). "Phosphorylation of Grainy head by ERK is essential for wound-dependent regeneration but not for development of an epidermal barrier." Proceedings of the National Academy of Sciences **108**(2): 650-655.

Kimmel, C. B., R. M. Warga and T. F. Schilling (1990). "Origin and organization of the zebrafish fate map." Development **108**(4): 581-594.

Kirke, P. N., A. M. Molloy, L. E. Daly, H. Burke, D. G. Weir and J. M. Scott (1993). "Maternal plasma folate and vitamin B12 are independent risk factors for neural tube defects." Q J Med **86**(11): 703-708.

Knight, R. D., S. Nair, S. S. Nelson, A. Afshar, Y. Javidan, R. Geisler, G. J. Rauch and T. F. Schilling (2003). "lockjaw encodes a zebrafish tfap2a required for early neural crest development." Development **130**(23): 5755-5768.

Komiya, Y., L.-T. Su, H.-C. Chen, R. Habas and L. W. Runnels (2014). "Magnesium and embryonic development." Magnesium research **27**(1): 1-8.

Kousa, Y. A., H. Zhu, W. D. Fakhouri, Y. Lei, A. Kinoshita, R. R. Roushangar, N. K. Patel, A. J. Agopian, W. Yang, E. J. Leslie, T. D. Busch, T. A. Mansour, X. Li, A. L. Smith, E. B. Li, D. B. Sharma, T. J. Williams, Y. Chai, B. A. Amendt, E. C. Liao, L. E. Mitchell, A. G. Bassuk, S. Gregory, A. Ashley-Koch, G. M. Shaw, R. H. Finnell and B. C. Schutte (2019). "The TFAP2A-IRF6-GRHL3 genetic pathway is conserved in neurulation." Hum Mol Genet **28**(10): 1726-1737.

Krapels, I. P., I. A. van Rooij, M. C. Ocké, B. A. van Cleef, A. M. Kuijpers-Jagtman and R. P. Steegers-Theunissen (2004). "Maternal dietary B vitamin intake, other than folate, and the association with orofacial cleft in the offspring." Eur J Nutr **43**(1): 7-14.

Krapels, I. P. C., I. A. L. M. van Rooij, M. C. Ocké, B. A. G. L. van Cleef, A.-M. M. Kuijpers-Jagtman and R. P. M. Steegers-Theunissen (2004). "Maternal dietary B vitamin intake,other than folate, and the association with orofacial cleft inthe offspring." European Journal of Nutrition **43**(1): 7-14.

Kudryavtseva, E. I., T. M. Sugihara, N. Wang, R. J. Lasso, J. F. Gudnason, S. M. Lipkin and B. Andersen (2003). "Identification and characterization of Grainyhead-like epithelial

transactivator (GET-1), a novel mammalian Grainyhead-like factor." <u>Developmental Dynamics</u> **226**(4): 604-617.

Kurbel, S., K. Dodig and R. Radic (2002). "The osmotic gradient in kidney medulla: a retold story." <u>Advances in physiology education</u> **26**(4): 278-281.

Lee, H. and D. Kimelman (2002). "A dominant-negative form of p63 is required for epidermal proliferation in zebrafish." <u>Dev Cell</u> **2**(5): 607-616.

Lee, M. S., J. R. Bonner, D. J. Bernard, E. L. Sanchez, E. T. Sause, R. R. Prentice, S. M. Burgess and L. C. Brody (2012). "Disruption of the folate pathway in zebrafish causes developmental defects." <u>BMC Developmental Biology</u> **12**(1): 12.

Lemay, P., P. De Marco, A. Emond, D. Spiegelman, A. Dionne-Laporte, S. Laurent, E. Merello, A. Accogli, G. A. Rouleau, V. Capra and Z. Kibar (2017). "Rare deleterious variants in GRHL3 are associated with human spina bifida." <u>Human Mutation</u> **38**(6): 716-724.

Leslie, E. J., H. Liu, J. C. Carlson, J. R. Shaffer, E. Feingold, G. Wehby, C. A. Laurie, D. Jain, C. C. Laurie and K. F. Doheny (2016). "A genome-wide association study of nonsyndromic cleft palate identifies an etiologic missense variant in GRHL3." <u>The American Journal of Human Genetics</u> **98**(4): 744-754.

Li, K., M. L. Wahlqvist and D. Li (2016). "Nutrition, one-carbon metabolism and neural tube defects: a review." <u>Nutrients</u> **8**(11): 741.

Li, M., C. Zhao, Y. Wang, Z. Zhao and A. Meng (2002). "Zebrafish sox9b is an early neural crest marker." <u>Dev Genes Evol</u> **212**(4): 203-206.

Li, X., H. Weng, E. A. Reece and P. Yang (2011). "SOD1 overexpression in vivo blocks hyperglycemia-induced specific PKC isoforms: substrate activation and consequent lipid peroxidation in diabetic embryopathy." <u>American journal of obstetrics and gynecology</u> **205**(1): 84. e81-84. e86.

Li, Z., Y. Zhang, L. Chen and H. Li (2018). "The dietary compound luteolin inhibits pancreatic cancer growth by targeting BCL-2." <u>Food & function</u> **9**(5): 3018-3027.

Lin, Y. S., P. H. Tsai, C. C. Kandaswami, C. H. Cheng, F. C. Ke, P. P. Lee, J. J. Hwang and M. T. Lee (2011). "Effects of dietary flavonoids, luteolin, and quercetin on the reversal of epithelial–mesenchymal transition in A431 epidermal cancer cells." <u>Cancer science</u> **102**(10): 1829-1839.

Lindsey, B. W., F. M. Smith and R. P. Croll (2010). "From inflation to flotation: contribution of the swimbladder to whole-body density and swimming depth during development of the zebrafish (Danio rerio)." <u>Zebrafish</u> **7**(1): 85-96.

Liu, D. and Z. Chen (2013). "The effect of curcumin on breast cancer cells." <u>Journal of breast cancer</u> **16**(2): 133.

Liu, F., F. Yang, D. Wen, W. Xia, L. Hao, J. Hu, J. Zong, X. Shen, J. Ma, N. Jiang, S. Sun, J. Zhang, H. Wang, X. Wang, Z. Ma and D. Ma (2015). "Grhl1 deficiency affects inner ear development in zebrafish." Int J Dev Biol **59**(10-12): 417-423.

Liu, H., N. Sheng, W. Zhang and J. Dai (2015). "Toxic effects of perfluorononanoic acid on the development of Zebrafish (Danio rerio) embryos." Journal of Environmental Sciences **32**: 26-34.

Liu, K. J., J. R. Arron, K. Stankunas, G. R. Crabtree and M. T. Longaker (2007). "Chemical rescue of cleft palate and midline defects in conditional GSK-3beta mice." Nature **446**(7131): 79-82.

Liu, Y., X. Wu, X. Hu, Z. Chen, H. Liu, S. Takeda and Y. Qing (2017). "Multiple repair pathways mediate cellular tolerance to resveratrol-induced DNA damage." Toxicology In Vitro **42**: 130-138.

López-Lázaro, M. (2008). "Anticancer and carcinogenic properties of curcumin: considerations for its clinical development as a cancer chemopreventive and chemotherapeutic agent." Mol Nutr Food Res **52 Suppl 1**: S103-127.

Lowery, L. A. and H. Sive (2004). "Strategies of vertebrate neurulation and a re-evaluation of teleost neural tube formation." Mechanisms of Development **121**(10): 1189-1197.

Lu, X., A. G. Borchers, C. Jolicoeur, H. Rayburn, J. C. Baker and M. Tessier-Lavigne (2004). "PTK7/CCK-4 is a novel regulator of planar cell polarity in vertebrates." Nature **430**(6995): 93-98.

Luo, X., L. Zhang, H. Wei, W. Liu, M. Wang and Q. Ning (2004). "Methylmalonic acid in amniotic fluid and maternal urine as a marker for neural tube defects." J Huazhong Univ Sci Technolog Med Sci **24**(2): 166-169.

Mace, K. A., J. C. Pearson and W. McGinnis (2005). "An epidermal barrier wound repair pathway in Drosophila is mediated by grainy head." Science **308**(5720): 381-385.

Mackay, D. R., M. Hu, B. Li, C. Rhéaume and X. Dai (2006). "The Mouse Ovol2 Gene Is Required for Cranial Neural Tube Development." Developmental biology **291**(1): 38-52.

Madison, B. B., K. Braunstein, E. Kuizon, K. Portman, X. T. Qiao and D. L. Gumucio (2005). "Epithelial hedgehog signals pattern the intestinal crypt-villus axis." Development **132**(2): 279-289.

Maes, J., L. Verlooy, O. E. Buenafe, P. A. M. de Witte, C. V. Esguerra and A. D. Crawford (2012). "Evaluation of 14 Organic Solvents and Carriers for Screening Applications in Zebrafish Embryos and Larvae." PLOS ONE **7**(10): e43850.

Mahyar-Roemer, M., A. Katsen, P. Mestres and K. Roemer (2001). "Resveratrol induces colon tumor cell apoptosis independently of p53 and precede by epithelial differentiation, mitochondrial proliferation and membrane potential collapse." International Journal of Cancer **94**(5): 615-622.

Mangold, E., A. C. Bohmer, N. Ishorst, A. K. Hoebel, P. Gultepe, H. Schuenke, J. Klamt, A. Hofmann, L. Golz, R. Raff, P. Tessmann, S. Nowak, H. Reutter, A. Hemprich, T. Kreusch, F. J. Kramer, B. Braumann, R. Reich, G. Schmidt, A. Jager, R. Reiter, S. Brosch, J. Stavusis, M. Ishida, R. Seselgyte, G. E. Moore, M. M. Nothen, G. Borck, K. A. Aldhorae, B. Lace, P. Stanier, M. Knapp and K. U. Ludwig (2016). "Sequencing the GRHL3 Coding Region Reveals Rare Truncating Mutations and a Common Susceptibility Variant for Nonsyndromic Cleft Palate." Am J Hum Genet **98**(4): 755-762.

Mannervik, M. and M. Levine (1999). "The Rpd3 histone deacetylase is required for segmentation of the Drosophila embryo." Proceedings of the National Academy of Sciences **96**(12): 6797-6801.

Mardis, E. R. (2007). "ChIP-seq: welcome to the new frontier." Nature Methods **4**(8): 613-614.

Marrs, J. A., S. G. Clendenon, D. R. Ratcliffe, S. M. Fielding, Q. Liu and W. F. Bosron (2010). "Zebrafish fetal alcohol syndrome model: effects of ethanol are rescued by retinoic acid supplement." Alcohol **44**(7): 707-715.

Massa, V., B. Wlodarczyk, E. Giavini and R. H. Finnell (2006). "Myo-inositol enhances teratogenicity of valproic acid in the mouse." Birth Defects Research Part A: Clinical and Molecular Teratology **76**(3): 200-204.

Mathiyalagan, N., L. B. Miles, P. J. Anderson, T. Wilanowski, B. L. Grills, S. J. McDonald, M. C. Keightley, A. Charzynska, M. Dabrowski and S. Dworkin (2019). "Meta-Analysis of Grainyhead-Like Dependent Transcriptional Networks: A Roadmap for Identifying Novel Conserved Genetic Pathways." Genes **10**(11): 876.

McGraw, S., C. Robert, L. Massicotte and M.-A. Sirard (2003). "Quantification of histone acetyltransferase and histone deacetylase transcripts during early bovine embryo development." Biology of Reproduction **68**(2): 383-389.

McNally, S. J., E. M. Harrison, J. A. Ross, O. J. Garden and S. J. Wigmore (2007). "Curcumin induces heme oxygenase 1 through generation of reactive oxygen species, p38 activation and phosphatase inhibition." Int J Mol Med **19**(1): 165-172.

Menke, C., M. Cionni, T. Siggers, M. L. Bulyk, D. R. Beier and R. W. Stottmann (2015). "Grhl2 is required in nonneural tissues for neural progenitor survival and forebrain development." Genesis.

Michels, G., W. Wätjen, N. Weber, P. Niering, Y. Chovolou, A. Kampkötter, P. Proksch and R. Kahl (2006). "Resveratrol induces apoptotic cell death in rat H4IIE hepatoma cells but necrosis in C6 glioma cells." Toxicology **225**(2-3): 173-182.

Milczarek, M., J. Stępniak, A. Lewiński and M. Karbownik-Lewińska (2013). "Potassium iodide, but not potassium iodate, as a potential protective agent against oxidative damage to membrane lipids in porcine thyroid." Thyroid Res **6**(1): 10.

Miles, L. B., C. Darido, J. Kaslin, J. K. Heath, S. M. Jane and S. Dworkin (2017). "Mis-expression of grainyhead-like transcription factors in zebrafish leads to defects in enveloping layer (EVL) integrity, cellular morphogenesis and axial extension." Sci Rep **7**(1): 17607.

Miles, L. B., S. Dworkin and C. Darido (2017). "Alternative splicing and start sites: Lessons from the Grainyhead-like family." Dev Biol **429**(1): 12-19.

Mills, J. L., Y. Lee, M. Conley, P. Kirke, J. McPartlin, D. G. Weir and J. M. Scott (1995). "Homocysteine metabolism in pregnancies complicated by neural-tube defects." The Lancet **345**(8943): 149-151.

Milstone, Z. J., G. Lawson and C. M. Trivedi (2017). "Histone deacetylase 1 and 2 are essential for murine neural crest proliferation, pharyngeal arch development, and craniofacial morphogenesis." Dev Dyn **246**(12): 1015-1026.

Miura, D., Y. Miura and K. Yagasaki (2004). "Resveratrol inhibits hepatoma cell invasion by suppressing gene expression of hepatocyte growth factor via its reactive oxygen species-scavenging property." Clinical & experimental metastasis **21**(5): 445-451.

Mlacki, M., C. Darido, S. M. Jane and T. Wilanowski (2014). "Loss of Grainy head-like 1 is associated with disruption of the epidermal barrier and squamous cell carcinoma of the skin." PLoS One **9**(2): e89247.

Mohandas, K. and D. Desai (1999). "Epidemiology of digestive tract cancers in India. V. Large and small bowel." Indian journal of gastroenterology: official journal of the Indian Society of Gastroenterology **18**(3): 118.

Molloy, A. M., P. N. Kirke, J. F. Troendle, H. Burke, M. Sutton, L. C. Brody, J. M. Scott and J. L. Mills (2009). "Maternal vitamin B12 status and risk of neural tube defects in a population with high neural tube defect prevalence and no folic Acid fortification." Pediatrics **123**(3): 917-923.

Mork, L. and G. Crump (2015). "Zebrafish Craniofacial Development: A Window into Early Patterning." Current topics in developmental biology **115**: 235-269.

Mottus, R., R. E. Sobel and T. A. Grigliatti (2000). "Mutational analysis of a histone deacetylase in Drosophila melanogaster: missense mutations suppress gene silencing associated with position effect variegation." Genetics **154**(2): 657-668.

Mousa, S. S., S. S. Mousa and S. A. Mousa (2005). "Effect of resveratrol on angiogenesis and platelet/fibrin-accelerated tumor growth in the chick chorioallantoic membrane model." Nutrition and cancer **52**(1): 59-65.

Na, J.-I., J.-W. Shin, H.-R. Choi, S.-H. Kwon and K.-C. Park (2019). "Resveratrol as a Multifunctional Topical Hypopigmenting Agent." International Journal of Molecular Sciences **20**(4): 956.

Nambiar, R. M. and P. D. Henion (2004). "Sequential antagonism of early and late Wnt-signaling by zebrafish colgate promotes dorsal and anterior fates." Dev Biol **267**(1): 165-180.

Nambiar, R. M., M. S. Ignatius and P. D. Henion (2007). "Zebrafish colgate/hdac1 functions in the non-canonical Wnt pathway during axial extension and in Wnt-independent branchiomotor neuron migration." Mechanisms of development **124**(9-10): 682-698.

Narisawa, A., S. Komatsuzaki, A. Kikuchi, T. Niihori, Y. Aoki, K. Fujiwara, M. Tanemura, A. Hata, Y. Suzuki, C. L. Relton, J. Grinham, K.-Y. Leung, D. Partridge, A. Robinson, V. Stone, P. Gustavsson, P. Stanier, A. J. Copp, N. D. E. Greene, T. Tominaga, Y. Matsubara and S. Kure (2011). "Mutations in genes encoding the glycine cleavage system predispose to neural tube defects in mice and humans." Human Molecular Genetics **21**(7): 1496-1503.

Negrete, H., J. Lavelle, J. Berg, S. Lewis and M. Zeidel (1996). "Permeability properties of the intact mammalian bladder epithelium." American Journal of Physiology-Renal Physiology **271**(4): F886-F894.

Neumann, P. E., W. N. Frankel, V. A. Letts, J. M. Coffin, A. J. Copp and M. Bernfield (1994). "Multifactorial inheritance of neural tube defects: localization of the major gene and recognition of modifiers in ct mutant mice." Nat Genet **6**(4): 357-362.

Nevil, M., E. R. Bondra, K. N. Schulz, T. Kaplan and M. M. Harrison (2017). "Stable Binding of the Conserved Transcription Factor Grainy Head to its Target Genes Throughout Drosophila melanogaster Development." Genetics **205**(2): 605-620.

Niessen, C. M. (2007). "Tight Junctions/Adherens Junctions: Basic Structure and Function." Journal of Investigative Dermatology **127**(11): 2525-2532.

O'Sullivan-Coyne, G., G. C. O'Sullivan, T. R. O'Donovan, K. Piwocka and S. L. McKenna (2009). "Curcumin induces apoptosis-independent death in oesophageal cancer cells." British Journal of Cancer **101**(9): 1585-1595.

Oetari, S., M. Sudibyo, J. N. Commandeur, R. Samhoedi and N. P. Vermeulen (1996). "Effects of curcumin on cytochrome P450 and glutathione S-transferase activities in rat liver." Biochemical pharmacology **51**(1): 39-45.

Ornoy, A. and Z. Ergaz (2010). "Alcohol abuse in pregnant women: effects on the fetus and newborn, mode of action and maternal treatment." International journal of environmental research and public health **7**(2): 364-379.

Pai, Y. J., K.-Y. Leung, D. Savery, T. Hutchin, H. Prunty, S. Heales, M. E. Brosnan, J. T. Brosnan, A. J. Copp and N. D. Greene (2015). "Glycine decarboxylase deficiency causes neural tube defects and features of non-ketotic hyperglycinemia in mice." Nature communications **6**(1): 1-11.

Paltoglou, S., R. Das, S. L. Townley, T. E. Hickey, G. A. Tarulli, I. Coutinho, R. Fernandes, A. R. Hanson, I. Denis, J. S. Carroll, S. M. Dehm, G. V. Raj, S. R. Plymate, W. D. Tilley and L. A. Selth (2017). "Novel Androgen Receptor Coregulator GRHL2 Exerts

Both Oncogenic and Antimetastatic Functions in Prostate Cancer." <u>Cancer Res</u> **77**(13): 3417-3430.

Pandurangan, A. K., P. Dharmalingam, S. K. A. Sadagopan, M. Ramar and A. Munusamy (2013). "Luteolin induces growth arrest in colon cancer cells through involvement of Wnt/β-catenin/GSK-3β signaling." <u>Journal of Environmental Pathology, Toxicology and Oncology</u> **32**(2).

Panis, C., L. Pizzatti, A. C. Herrera, R. Cecchini and E. Abdelhay (2013). "Putative circulating markers of the early and advanced stages of breast cancer identified by high-resolution label-free proteomics." <u>Cancer Letters</u> **330**(1): 57-66.

Paré, A., M. Kim, M. T. Juarez, S. Brody and W. McGinnis (2012). "The Functions of Grainy Head-Like Proteins in Animals and Fungi and the Evolution of Apical Extracellular Barriers." <u>PLOS ONE</u> **7**(5): e36254.

Park, P. J. (2009). "ChIP–seq: advantages and challenges of a maturing technology." <u>Nature Reviews Genetics</u> **10**(10): 669-680.

Peeters, M. C., B. Schutte, M. H. J. Lenders, J. W. Hekking, J. Drukker and H. W. V. Straaten (1998). "Role of differential cell proliferation in the tail bud in aberrant mouse neurulation." <u>Developmental dynamics: an official publication of the American Association of Anatomists</u> **211**(4): 382-389.

Peker, E., N. Demir, O. Tuncer, L. Üstyol, R. Balahoroğlu, S. Kaba and K. Karaman (2016). "The levels of vitamın B12, folate and homocysteine in mothers and their babies with neural tube defects." <u>J Matern Fetal Neonatal Med</u> **29**(18): 2944-2948.

Pérez-lópez, F. R. (2007). "Iodine and thyroid hormones during pregnancy and postpartum." <u>Gynecological Endocrinology</u> **23**(7): 414-428.

Petrof, G., A. Nanda, J. Howden, T. Takeichi, J. R. McMillan, S. Aristodemou, L. Ozoemena, L. Liu, A. P. South, C. Pourreyron, D. Dafou, L. E. Proudfoot, H. Al-Ajmi, M. Akiyama, W. H. McLean, M. A. Simpson, M. Parsons and J. A. McGrath (2014). "Mutations in GRHL2 result in an autosomal-recessive ectodermal Dysplasia syndrome." <u>Am J Hum Genet</u> **95**(3): 308-314.

Peyrard-Janvid, M., E. J. Leslie, Y. A. Kousa, T. L. Smith, M. Dunnwald, M. Magnusson, B. A. Lentz, P. Unneberg, I. Fransson, H. K. Koillinen, J. Rautio, M. Pegelow, A. Karsten, L. Basel-Vanagaite, W. Gordon, B. Andersen, T. Svensson, J. C. Murray, R. A. Cornell, J. Kere and B. C. Schutte (2014). "Dominant mutations in GRHL3 cause Van der Woude Syndrome and disrupt oral periderm development." <u>Am J Hum Genet</u> **94**(1): 23-32.

Phatak, M., S. Kulkarni, L. B. Miles, N. Anjum, S. Dworkin and M. Sonawane (2021). "Grhl3 promotes retention of epidermal cells under endocytic stress to maintain epidermal architecture in zebrafish." <u>PLoS Genetics</u> **17**(9): e1009823.

Pillai, R., L. E. Coverdale, G. Dubey and C. C. Martin (2004). "Histone deacetylase 1 (HDAC-1) required for the normal formation of craniofacial cartilage and pectoral fins of the zebrafish." Developmental Dynamics **231**(3): 647-654.

Piotrowski, T. and C. Nüsslein-Volhard (2000). "The endoderm plays an important role in patterning the segmented pharyngeal region in zebrafish (Danio rerio)." Developmental biology **225**(2): 339-356.

Pitkin, R. M. (2007). "Folate and neural tube defects." The American journal of clinical nutrition **85**(1): 285S-288S.

Presland, R. and R. Jurevic (2002). "Making sense of the epithelial barrier: what molecular biology and genetics tell us about the functions of oral mucosal and epidermal tissues." Journal of Dental Education **66**(4): 564-574.

Pyrgaki, C., A. Liu and L. Niswander (2011). "Grainyhead-like 2 regulates neural tube closure and adhesion molecule expression during neural fold fusion." Dev Biol **353**(1): 38-49.

Rammler, D. H. and A. Zaffaroni (1967). "BIOLOGICAL IMPLICATIONS OF DMSO BASED ON A REVIEW OF ITS CHEMICAL PROPERTIES*." Annals of the New York Academy of Sciences **141**(1): 13-23.

Rawson, D. M., T. Zhang, D. Kalicharan and W. L. Jongebloed (2000). "Field emission scanning electron microscopy and transmission electron microscopy studies of the chorion, plasma membrane and syncytial layers of the gastrula-stage embryo of the zebrafish Brachydanio rerio: a consideration of the structural and functional relationships with respect to cryoprotectant penetration." Aquaculture Research **31**(3): 325-336.

Ray, H. J. and L. A. Niswander (2016). "Grainyhead-like 2 downstream targets act to suppress epithelial-to-mesenchymal transition during neural tube closure." Development **143**(7): 1192-1204.

Ray, J. G., C. Meier, M. J. Vermeulen, S. Boss, P. R. Wyatt and D. E. Cole (2002). "Association of neural tube defects and folic acid food fortification in Canada." The Lancet **360**(9350): 2047-2048.

Reya, T. and H. Clevers (2005). "Wnt signalling in stem cells and cancer." Nature **434**(7035): 843-850.

Richardson, R. J., N. L. Hammond, P. A. Coulombe, C. Saloranta, H. O. Nousiainen, R. Salonen, A. Berry, N. Hanley, D. Headon, R. Karikoski and M. J. Dixon (2014). "Periderm prevents pathological epithelial adhesions during embryogenesis." The Journal of clinical investigation **124**(9): 3891-3900.

Rickman, L., D. Simrak, H. P. Stevens, D. M. Hunt, I. A. King, S. P. Bryant, R. A. Eady, I. M. Leigh, J. Arnemann, A. I. Magee, D. P. Kelsell and R. S. Buxton (1999). "N-terminal deletion in a desmosomal cadherin causes the autosomal dominant skin disease striate palmoplantar keratoderma." Hum Mol Genet **8**(6): 971-976.

Rieder, M. J. (1994). "Prevention of neural tube defects with periconceptional folic acid." Clinics in perinatology **21**(3): 483-503.

Rifat, Y., V. Parekh, T. Wilanowski, N. R. Hislop, A. Auden, S. B. Ting, J. M. Cunningham and S. M. Jane (2010). "Regional neural tube closure defined by the Grainy head-like transcription factors." Developmental Biology **345**(2): 237-245.

Rochtus, A., B. Izzi, E. Vangeel, S. Louwette, C. Wittevrongel, D. Lambrechts, Y. Moreau, R. Winand, C. Verpoorten and K. Jansen (2015). "DNA methylation analysis of Homeobox genes implicates HOXB7 hypomethylation as risk factor for neural tube defects." Epigenetics **10**(1): 92-101.

Romanova, D., A. Vachalkova, L. Cipak, Z. Ovesna and P. Rauko (2001). "Study of antioxidant effect of apigenin, luteolin and quercetin by DNA protective method." Neoplasma **48**(2): 104-107.

Russell, L. J., J. J. DiGiovanna, G. R. Rogers, P. M. Steinert, N. Hashem, J. G. Compton and S. J. Bale (1995). "Mutations in the gene for transglutaminase 1 in autosomal recessive lamellar ichthyosis." Nature Genetics **9**(3): 279-283.

Sah, V. P., L. D. Attardi, G. J. Mulligan, B. O. Williams, R. T. Bronson and T. Jacks (1995). "A subset of p53-deficient embryos exhibit exencephaly." Nature Genetics **10**(2): 175-180.

Samuelson, D. A. (2007). Textbook of veterinary histology.

Sancho, E., E. Batlle and H. Clevers (2004). "Signaling pathways in intestinal development and cancer." Annu. Rev. Cell Dev. Biol. **20**: 695-723.

Schmidt, R. J., P. A. Romitti, T. L. Burns, M. L. Browne, C. M. Druschel, R. S. Olney and S. National Birth Defects Prevention (2009). "Maternal Caffeine Consumption and Risk of Neural Tube Defects." Birth defects research. Part A, Clinical and molecular teratology **85**(11): 879-889.

Schwerte, T. (2010). "Skin epithelium of zebrafish may work as an airway epithelia analogue model to evaluate systemic effects of micro-and nano-particles." Thrombosis and haemostasis **103**(04): 692-693.

Seller, M. and K. Perkins-Cole (1987). "Hyperthermia and neural tube defects of the curly-tail mouse." Journal of craniofacial genetics and developmental biology **7**(4): 321-330.

Seller, M. J., S. Embury, P. E. Polani and M. Adinolfi (1979). "Neural tube defects in curly-tail mice. II. Effect of maternal administration of vitamin A." Proc R Soc Lond B Biol Sci **206**(1162): 95-107.

Seller, M. J., S. Embury, P. E. Polani and M. Adinolfi (1979). "Neural tube defects in curly-tail mice. II. Effect of maternal administration of vitamin A." Proceedings of the Royal Society of London. Series B. Biological Sciences **206**(1162): 95-107.

References

Seller, M. J. and K. J. Perkins-Cole (1987). "Sex difference in mouse embryonic development at neurulation." <u>J Reprod Fertil</u> **79**(1): 159-161.

Seller, M. J. and K. J. Perkins (1982). "Prevention of neural tube defects in curly-tail mice by maternal administration of vitamin A." <u>Prenat Diagn</u> **2**(4): 297-300.

Seller, M. J. and K. J. Perkins (1983). "Effect of hydroxyurea on neural tube defects in the curly-tail mouse." <u>Journal of craniofacial genetics and developmental biology</u> **3**(1): 11-17.

Seller, M. J. and K. J. Perkins (1986). "Effect of mitomycin C on the neural tube defects of the curly-tail mouse." <u>Teratology</u> **33**(3): 305-309.

Shankar, S., D. Nall, S.-N. Tang, D. Meeker, J. Passarini, J. Sharma and R. K. Srivastava (2011). "Resveratrol inhibits pancreatic cancer stem cell characteristics in human and Kras G12D transgenic mice by inhibiting pluripotency maintaining factors and epithelial-mesenchymal transition." <u>PloS one</u> **6**(1): e16530.

Shi, M., G. L. Wehby and J. C. Murray (2008). "Review on genetic variants and maternal smoking in the etiology of oral clefts and other birth defects." <u>Birth Defects Research Part C: Embryo Today: Reviews</u> **84**(1): 16-29.

Shimoi, K., S. Masuda, M. Furugori, S. Esaki and N. Kinae (1994). "Radioprotective effect of antioxidative flavonoids in γ-ray irradiated mice." <u>Carcinogenesis</u> **15**(11): 2669-2672.

Singh, C. K., A. Kumar, D. B. Hitchcock, D. Fan, R. Goodwin, H. A. LaVoie, P. Nagarkatti, D. J. DiPette and U. S. Singh (2011). "Resveratrol prevents embryonic oxidative stress and apoptosis associated with diabetic embryopathy and improves glucose and lipid profile of diabetic dam." <u>Mol Nutr Food Res</u> **55**(8): 1186-1196.

Singh, C. K., A. Kumar, H. A. LaVoie, D. J. DiPette and U. S. Singh (2012). "Resveratrol Prevents Impairment in Activation of Retinoic Acid Receptors and MAP Kinases in the Embryos of a Rodent Model of Diabetic Embryopathy." <u>Reproductive Sciences</u> **19**(9): 949-961.

Singh, S. V., X. Hu, S. K. Srivastava, M. Singh, H. Xia, J. L. Orchard and H. A. Zaren (1998). "Mechanism of inhibition of benzo [a] pyrene-induced forestomach cancer in mice by dietary curcumin." <u>Carcinogenesis</u> **19**(8): 1357-1360.

Smedts, H. P. M., M. Rakhshandehroo, A. C. Verkleij-Hagoort, J. H. M. de Vries, J. Ottenkamp, E. A. P. Steegers and R. P. M. Steegers-Theunissen (2008). "Maternal intake of fat, riboflavin and nicotinamide and the risk of having offspring with congenital heart defects." <u>European Journal of Nutrition</u> **47**(7): 357-365.

Sonal, J. Sidhaye, M. Phatak, S. Banerjee, A. Mulay, O. Deshpande, S. Bhide, T. Jacob, I. Gehring, C. Nuesslein-Volhard and M. Sonawane (2014). "Myosin Vb Mediated Plasma Membrane Homeostasis Regulates Peridermal Cell Size and Maintains Tissue Homeostasis in the Zebrafish Epidermis." <u>PLOS Genetics</u> **10**(9): e1004614.

Sonawane, M., H. Martin-Maischein, H. Schwarz and C. Nusslein-Volhard (2009). "Lgl2 and E-cadherin act antagonistically to regulate hemidesmosome formation during epidermal development in zebrafish." Development **136**(8): 1231-1240.

Song, W. B., Y. Y. Wang, F. S. Meng, Q. H. Zhang, J. Y. Zeng, L. P. Xiao, X. P. Yu, D. D. Peng, L. Su, B. Xiao and Z. S. Zhang (2010). "Curcumin protects intestinal mucosal barrier function of rat enteritis via activation of MKP-1 and attenuation of p38 and NF-κB activation." PLoS One **5**(9): e12969.

Srivivasan, A., V. P. Menon, V. Periaswamy and K. Rajasekaran (2003). "Protection of pancreatic beta-cell by the potential antioxidant bis-o-hydroxycinnamoyl methane, analogue of natural curcuminoid in experimental diabetes." J Pharm Pharm Sci **6**(3): 327-333.

Stainier, D. Y. R., E. Raz, N. D. Lawson, S. C. Ekker, R. D. Burdine, J. S. Eisen, P. W. Ingham, S. Schulte-Merker, D. Yelon, B. M. Weinstein, M. C. Mullins, S. W. Wilson, L. Ramakrishnan, S. L. Amacher, S. C. F. Neuhauss, A. Meng, N. Mochizuki, P. Panula and C. B. Moens (2017). "Guidelines for morpholino use in zebrafish." PLOS Genetics **13**(10): e1007000.

Stover, P. J. (2004). "Physiology of folate and vitamin B 12 in health and disease." Nutrition reviews **62**(suppl_1): S3-S12.

Suarez, L., M. Felkner, J. D. Brender, M. Canfield and K. Hendricks (2008). "Maternal exposures to cigarette smoke, alcohol, and street drugs and neural tube defect occurrence in offspring." Maternal and child health journal **12**(3): 394-401.

Suh, Y. A., R. S. Arnold, B. Lassegue, J. Shi, X. Xu, D. Sorescu, A. B. Chung, K. K. Griendling and J. D. Lambeth (1999). "Cell transformation by the superoxide-generating oxidase Mox1." Nature **401**(6748): 79-82.

Sun, D.-W., H.-D. Zhang, L. Mao, C.-F. Mao, W. Chen, M. Cui, R. Ma, H.-X. Cao, C.-W. Jing and Z. Wang (2015). "Luteolin inhibits breast cancer development and progression in vitro and in vivo by suppressing notch signaling and regulating MiRNAs." Cellular Physiology and Biochemistry **37**(5): 1693-1711.

Sun, X., Z. Li, Y. Niu, L. Zhao, Y. Huang, Q. Li, S. Zhang, T. Chen, T. Fu, T. Yang, X. An, Y. Jiang and J. Zhang (2019). "Jarid1b promotes epidermal differentiation by mediating the repression of Ship1 and activation of the AKT/Ovol1 pathway." Cell Proliferation **52**(5): e12638.

Surh, Y.-J., Y.-J. Hurh, J.-Y. Kang, E. Lee, G. Kong and S. J. Lee (1999). "Resveratrol, an antioxidant present in red wine, induces apoptosis in human promyelocytic leukemia (HL-60) cells." Cancer letters **140**(1-2): 1-10.

Sztal, T. E., E. A. McKaige, C. Williams, A. A. Ruparelia and R. J. Bryson-Richardson (2018). "Genetic compensation triggered by actin mutation prevents the muscle damage caused by loss of actin protein." PLOS Genetics **14**(2): e1007212.

Tan, R.-R., S.-J. Zhang, B. Tsoi, W.-S. Huang, X.-J. Zhuang, X.-Y. Chen, N. Yao, Z.-F. Mao, L.-P. Tang, Q. Wang, H. Kurihara, Y.-F. Li and R.-R. He (2015). "A natural product, resveratrol, protects against high-glucose-induced developmental damage in chicken embryo." Journal of Asian Natural Products Research **17**(5): 586-594.

Tanaka, Y., F. Kanai, M. Tada, R. Tateishi, M. Sanada, Y. Nannya, M. Ohta, Y. Asaoka, M. Seto, S. Shiina, H. Yoshida, T. Kawabe, O. Yokosuka, S. Ogawa and M. Omata (2008). "Gain of GRHL2 is associated with early recurrence of hepatocellular carcinoma." J Hepatol **49**(5): 746-757.

Tao, J., E. Kuliyev, X. Wang, X. Li, T. Wilanowski, S. M. Jane, P. E. Mead and J. M. Cunningham (2005). "BMP4-dependent expression of Xenopus Grainyhead-like 1 is essential for epidermal differentiation." Development **132**(5): 1021-1034.

Teng, A., M. Nair, J. Wells, J. A. Segre and X. Dai (2007). "Strain-dependent perinatal lethality of Ovol1-deficient mice and identification of Ovol2 as a downstream target of Ovol1 in skin epidermis." Biochimica et Biophysica Acta (BBA) - Molecular Basis of Disease **1772**(1): 89-95.

Tian, S., R. Guo, S. Wei, Y. Kong, X. Wei, W. Wang, X. Shi and H. Jiang (2016). "Curcumin protects against the intestinal ischemia-reperfusion injury: involvement of the tight junction protein ZO-1 and TNF-α related mechanism." Korean J Physiol Pharmacol **20**(2): 147-152.

Ting, S. B., J. Caddy, N. Hislop, T. Wilanowski, A. Auden, L. L. Zhao, S. Ellis, P. Kaur, Y. Uchida, W. M. Holleran, P. M. Elias, J. M. Cunningham and S. M. Jane (2005). "A homolog of Drosophila grainy head is essential for epidermal integrity in mice." Science **308**(5720): 411-413.

Ting, S. B., T. Wilanowski, A. Auden, M. Hall, A. K. Voss, T. Thomas, V. Parekh, J. M. Cunningham and S. M. Jane (2003). "Inositol- and folate-resistant neural tube defects in mice lacking the epithelial-specific factor Grhl-3." Nat Med **9**(12): 1513-1519.

Ting, S. B., T. Wilanowski, L. Cerruti, L. L. Zhao, J. M. Cunningham and S. M. Jane (2003). "The identification and characterization of human Sister-of-Mammalian Grainyhead (SOM) expands the grainyhead-like family of developmental transcription factors." Biochem J **370**(Pt 3): 953-962.

Titto, M., T. Ankit, B. Saumya, A. Gausal and S. Sarada (2020). "Curcumin prophylaxis refurbishes alveolar epithelial barrier integrity and alveolar fluid clearance under hypoxia." Respiratory physiology & neurobiology **274**: 103336.

Tozawa, R.-i., S. Ishibashi, J.-i. Osuga, H. Yagyu, T. Oka, Z. Chen, K. Ohashi, S. Perrey, F. Shionoiri and N. Yahagi (1999). "Embryonic lethality and defective neural tube closure in mice lacking squalene synthase." Journal of Biological Chemistry **274**(43): 30843-30848.

Triggiani, V., E. Tafaro, V. A. Giagulli, C. Sabbà, F. Resta, B. Licchelli and E. Guastamacchia (2009). "Role of iodine, selenium and other micronutrients in thyroid function and disorders." Endocrine, Metabolic & Immune Disorders-Drug Targets

(Formerly Current Drug Targets-Immune, Endocrine & Metabolic Disorders) **9**(3): 277-294.

Tu, C.-t., B. Han, H.-c. Liu and S.-c. Zhang (2011). "Curcumin protects mice against concanavalin A-induced hepatitis by inhibiting intrahepatic intercellular adhesion molecule-1 (ICAM-1) and CXCL10 expression." Molecular and cellular biochemistry **358**(1-2): 53-60.

Tuckfield, A., D. R. Clouston, T. M. Wilanowski, L. L. Zhao, J. M. Cunningham and S. M. Jane (2002). "Binding of the RING polycomb proteins to specific target genes in complex with the grainyhead-like family of developmental transcription factors." Molecular and cellular biology **22**(6): 1936-1946.

Ueo, T., I. Imayoshi, T. Kobayashi, T. Ohtsuka, H. Seno, H. Nakase, T. Chiba and R. Kageyama (2012). "The role of Hes genes in intestinal development, homeostasis and tumor formation." Development **139**(6): 1071-1082.

Uslu, V. V., M. Petretich, S. Ruf, K. Langenfeld, N. A. Fonseca, J. C. Marioni and F. Spitz (2014). "Long-range enhancers regulating Myc expression are required for normal facial morphogenesis." Nature genetics **46**(7): 753-758.

Uv, A. E., C. Thompson and S. J. Bray (1994). "The Drosophila tissue-specific factor Grainyhead contains novel DNA-binding and dimerization domains which are conserved in the human protein CP2." Molecular and cellular biology **14**(6): 4020-4031.

van Straaten, H. W. and A. J. Copp (2001). "Curly tail: a 50-year history of the mouse spina bifida model." Anatomy and embryology **203**(4): 225-237.

Vasioukhin, V., C. Bauer, L. Degenstein, B. Wise and E. Fuchs (2001). "Hyperproliferation and defects in epithelial polarity upon conditional ablation of α-catenin in skin." Cell **104**(4): 605-617.

Veldman, M. B. and S. Lin (2008). "Zebrafish as a Developmental Model Organism for Pediatric Research." Pediatric Research **64**: 470.

Venkatesan, K., H. R. McManus, C. C. Mello, T. F. Smith and U. Hansen (2003). "Functional conservation between members of an ancient duplicated transcription factor family, LSF/Grainyhead." Nucleic Acids Research **31**(15): 4304-4316.

Verkleij-Hagoort, A. C., J. H. M. de Vries, N. T. C. Ursem, R. de Jonge, W. C. J. Hop and R. P. M. Steegers-Theunissen (2006). "Dietary intake of B-vitamins in mothers born a child with a congenital heart defect." European Journal of Nutrition **45**(8): 478-486.

Walentin, K., C. Hinze, M. Werth, N. Haase, S. Varma, R. Morell, A. Aue, E. Potschke, D. Warburton, A. Qiu, J. Barasch, B. Purfurst, C. Dieterich, E. Popova, M. Bader, R. Dechend, A. C. Staff, Z. Y. Yurtdas, E. Kilic and K. M. Schmidt-Ott (2015). "A Grhl2-dependent gene network controls trophoblast branching morphogenesis." Development **142**(6): 1125-1136.

Wallace, K. N., S. Akhter, E. M. Smith, K. Lorent and M. Pack (2005). "Intestinal growth and differentiation in zebrafish." <u>Mech Dev</u> **122**(2): 157-173.

Wang, L., W. Li, M. Lin, M. Garcia, D. Mulholland, M. Lilly and M. Martins-Green (2014). "Luteolin, ellagic acid and punicic acid are natural products that inhibit prostate cancer metastasis." <u>Carcinogenesis</u> **35**(10): 2321-2330.

Wang, N., Q. Han, G. Wang, W.-P. Ma, J. Wang, W.-X. Wu, Y. Guo, L. Liu, X.-Y. Jiang and X.-L. Xie (2016). "Resveratrol protects oxidative stress-induced intestinal epithelial barrier dysfunction by upregulating heme oxygenase-1 expression." <u>Digestive diseases and sciences</u> **61**(9): 2522-2534.

Wang, N., G. Wang, J. Hao, J. Ma, Y. Wang, X. Jiang and H. Jiang (2012). "Curcumin ameliorates hydrogen peroxide-induced epithelial barrier disruption by upregulating heme oxygenase-1 expression in human intestinal epithelial cells." <u>Digestive diseases and sciences</u> **57**(7): 1792-1801.

Wang, Q., H. Wang, Y. Jia, H. Pan and H. Ding (2017). "Luteolin induces apoptosis by ROS/ER stress and mitochondrial dysfunction in gliomablastoma." <u>Cancer chemotherapy and pharmacology</u> **79**(5): 1031-1041.

Wang, Y., Y. Sun, Y. Huang, Y. Pan, Z. Jia, L. Ma, L. Ma, F. Lan, Y. Zhou, J. Shi, X. Yang, L. Zhang, H. Jiang, M. Jiang, A. Yin, J. Cheng, L. Wang, Y. Yang and B. Shi (2016). "Association study between Van der Woude Syndrome causative gene GRHL3 and nonsyndromic cleft lip with or without cleft palate in a Chinese cohort." <u>Gene</u> **588**(1): 69-73.

Watts, S. A., M. Powell and L. R. D'Abramo (2012). "Fundamental approaches to the study of zebrafish nutrition." <u>ILAR journal</u> **53**(2): 144-160.

Werner, S., S. Frey, S. Riethdorf, C. Schulze, M. Alawi, L. Kling, V. Vafaizadeh, G. Sauter, L. Terracciano and U. Schumacher (2013). "Dual roles of the transcription factor grainyhead-like 2 (GRHL2) in breast cancer." <u>Journal of biological chemistry</u> **288**(32): 22993-23008.

Werth, M., K. Walentin, A. Aue, J. Schonheit, A. Wuebken, N. Pode-Shakked, L. Vilianovitch, B. Erdmann, B. Dekel, M. Bader, J. Barasch, F. Rosenbauer, F. C. Luft and K. M. Schmidt-Ott (2010). "The transcription factor grainyhead-like 2 regulates the molecular composition of the epithelial apical junctional complex." <u>Development</u> **137**(22): 3835-3845.

Westerfield, M. (2000). "The zebrafish book: a guide for the laboratory use of zebrafish." <u>http://zfin. org/zf_info/zfbook/zfbk. html</u>.

Wettstein, D. A., D. L. Turner and C. Kintner (1997). "The Xenopus homolog of Drosophila Suppressor of Hairless mediates Notch signaling during primary neurogenesis." <u>Development</u> **124**(3): 693-702.

Wilanowski, T., J. Caddy, S. B. Ting, N. R. Hislop, L. Cerruti, A. Auden, L. L. Zhao, S. Asquith, S. Ellis, R. Sinclair, J. M. Cunningham and S. M. Jane (2008). "Perturbed

desmosomal cadherin expression in grainy head-like 1-null mice." EMBO J **27**(6): 886-897.

Wilanowski, T., A. Tuckfield, L. Cerruti, S. O'Connell, R. Saint, V. Parekh, J. Tao, J. M. Cunningham and S. M. Jane (2002). "A highly conserved novel family of mammalian developmental transcription factors related to Drosophila grainyhead." Mech Dev **114**(1-2): 37-50.

Wilson, J. G. (1977). "Teratogenic effects of environmental chemicals." Fed Proc **36**(5): 1698-1703.

Wood, A. J., T.-W. Lo, B. Zeitler, C. S. Pickle, E. J. Ralston, A. H. Lee, R. Amora, J. C. Miller, E. Leung and X. Meng (2011). "Targeted genome editing across species using ZFNs and TALENs." Science **333**(6040): 307-307.

Wu, B., Q. Zhang, W. Shen and J. Zhu (2008). "Anti-proliferative and chemosensitizing effects of luteolin on human gastric cancer AGS cell line." Molecular and cellular biochemistry **313**(1-2): 125-132.

Wu, J. Y., C. Y. Lin, T. W. Lin, C. F. Ken and Y. D. Wen (2007). "Curcumin affects development of zebrafish embryo." Biol Pharm Bull **30**(7): 1336-1339.

Wu, Y., F. Wang, E. A. Reece and P. Yang (2015). "Curcumin ameliorates high glucose-induced neural tube defects by suppressing cellular stress and apoptosis." American journal of obstetrics and gynecology **212**(6): 802. e801-802. e808.

Wurst, W., A. B. Auerbach and A. L. Joyner (1994). "Multiple developmental defects in Engrailed-1 mutant mice: an early mid-hindbrain deletion and patterning defects in forelimbs and sternum." Development **120**(7): 2065-2075.

Xia, Y., W. Qu, L.-N. Zhao, H. Han, X.-F. Yang, X.-F. Sun, L.-P. Hao and J. Xu (2013). "Iodine excess induces hepatic steatosis through disturbance of thyroid hormone metabolism involving oxidative stress in BALB/c mice." Biological trace element research **154**(1): 103-110.

Xiang, J., X. Fu, W. Ran, X. Chen, Z. Hang, H. Mao and Z. Wang (2013). "Expression and role of grainyhead-like 2 in gastric cancer." Medical oncology **30**(4): 714.

Xiang, J., X. Fu, W. Ran and Z. Wang (2017). "Grhl2 reduces invasion and migration through inhibition of TGFβ-induced EMT in gastric cancer." Oncogenesis **6**(1): e284-e284.

Xiang, X., Z. Deng, X. Zhuang, S. Ju, J. Mu, H. Jiang, L. Zhang, J. Yan, D. Miller and H. G. Zhang (2012). "Grhl2 determines the epithelial phenotype of breast cancers and promotes tumor progression." PLoS One **7**(12): e50781.

Xiong, K. M., R. E. Peterson and W. Heideman (2008). "Aryl hydrocarbon receptor-mediated down-regulation of sox9b causes jaw malformation in zebrafish embryos." Molecular pharmacology **74**(6): 1544-1553.

Xu, H., C. Liu, Z. Zhao, N. Gao, G. Chen, Y. Wang and J. Cui (2014). "Clinical implications of GRHL3 protein expression in breast cancer." Tumor Biology **35**(3): 1827-1831.

Xun, W., L. Shi, H. Zhou, G. Hou, T. Cao and C. Zhao (2015). "Effects of curcumin on growth performance, jejunal mucosal membrane integrity, morphology and immune status in weaned piglets challenged with enterotoxigenic Escherichia coli." International Immunopharmacology **27**(1): 46-52.

Yang, P., Z. Zhao and E. A. Reece (2008). "Activation of oxidative stress signaling that is implicated in apoptosis with a mouse model of diabetic embryopathy." American journal of obstetrics and gynecology **198**(1): 130. e131-130. e137.

Yang, S.-F., W.-E. Yang, H.-R. Chang, S.-C. Chu and Y.-S. Hsieh (2008). "Luteolin induces apoptosis in oral squamous cancer cells." Journal of dental research **87**(4): 401-406.

Yoshida, M., Y. Shimono, H. Togashi, K. Matsuzaki, J. Miyoshi, A. Mizoguchi, T. Komori and Y. Takai (2012). "Periderm cells covering palatal shelves have tight junctions and their desquamation reduces the polarity of palatal shelf epithelial cells in palatogenesis." Genes Cells **17**(6): 455-472.

Yu, Z., A. Bhandari, J. Mannik, T. Pham, X. Xu and B. Andersen (2008). "Grainyhead-like factor Get1/Grhl3 regulates formation of the epidermal leading edge during eyelid closure." Developmental Biology **319**(1): 56-67.

Yu, Z., K. K. Lin, A. Bhandari, J. A. Spencer, X. Xu, N. Wang, Z. Lu, G. N. Gill, D. R. Roop, P. Wertz and B. Andersen (2006). "The Grainyhead-like epithelial transactivator Get-1/Grhl3 regulates epidermal terminal differentiation and interacts functionally with LMO4." Dev Biol **299**(1): 122-136.

Yu, Z., J. Mannik, A. Soto, K. K. Lin and B. Andersen (2009). "The epidermal differentiation-associated Grainyhead gene Get1/Grhl3 also regulates urothelial differentiation." The EMBO journal **28**(13): 1890-1903.

Zhang, H.-Y., G.-A. Luo, Q.-L. Liang, Y. Wang, H.-H. Yang, Y.-M. Wang, X.-Y. Zheng, X.-M. Song, G. Chen and T. Zhang (2008). "Neural tube defects and disturbed maternal folate-and homocysteine-mediated one-carbon metabolism." Experimental neurology **212**(2): 515-521.

Zhao, Y., G. Yang, D. Ren, X. Zhang, Q. Yin and X. Sun (2011). "Luteolin suppresses growth and migration of human lung cancer cells." Molecular biology reports **38**(2): 1115-1119.

Zhou, H.-B., Y. Yan, Y.-N. Sun and J.-R. Zhu (2003). "Resveratrol induces apoptosis in human esophageal carcinoma cells." World Journal of Gastroenterology **9**(3): 408.

Zhou, S., Q. Dong, S. Li, J. Guo, X. Wang and G. Zhu (2009). "Developmental toxicity of cartap on zebrafish embryos." Aquatic Toxicology **95**(4): 339-346.

Zimmermann, M. B. (2012). "The effects of iodine deficiency in pregnancy and infancy." Paediatr Perinat Epidemiol **26 Suppl 1**: 108-117.

Zvelebil, M., E. Oliemuller, Q. Gao, O. Wansbury, A. Mackay, H. Kendrick, M. J. Smalley, J. S. Reis-Filho and B. A. Howard (2013). "Embryonic mammary signature subsets are activated in Brca1-/-and basal-like breast cancers." <u>Breast Cancer Research</u> **15**(2): R25.